Chapter 1
Introduction

This dissertation is based on research on two topics; (1) silsesquioxanes (SQs) based organic/inorganic hybrid beads on a chain (BoC) type polymers with SQ cages in the polymer backbones and (2) modification of silsesquioxane cages to offer semiconducting properties for optoelectronic devices and microporous materials. Section **1.1** provides basic background information about silsesquioxanes, including prior work related to studies described in this dissertation. Section **1.2** describes palladium catalyzed coupling reactions used in this work. Section **1.3** reviews the historical development, and fundamental aspects of organic photovoltaic (OPV) cells, while section **1.4** provides an overview of the research objectives and motivations for this work.

1.1. Silsesquioxanes (SQs)

The term silsesquioxanes refers to all structures with the empirical formulas $(RSiO_{1.5})_n$, where R is hydrogen or any alkyl, alkenyl, aryl groups. These compounds are extremely useful as platforms for assembling organic/inorganic hybrid materials with properties intermediate between those of ceramics and organics because these materials possess an ideal combination of a rigid, thermally stable silica core and more flexible, modifiable organic groups.[1-15] Recently, SQ derivatives have found uses in a variety of applications including in nanocomposites materials,[16-24] catalysts,[25-31] biomedical materials,[32-39] and semiconducting materials for optoelectronic devices.[40-43]

1.1.1. Nomenclatures and structures of polyhedral silsesquioxanes

The name "silsesquioxane" derives from the terms 'sil' (silicon), 'sesqui' (one and a half), and 'oxane' (oxygen), which indicate that the ratio of silicon: oxygen atoms is 1:1.5. The full IUPAC naming of silsesquioxane is complicated and burdensome, for example, the full

name of $(HSiO_{1.5})_8$ is pentacyclo[9.5.1.1^{3,9}.1^{5,15}.1^{7,13}]octasiloxane. Therefore, the compounds are more conveniently named using systematic nomenclature that gives the number of silsesquioxane links, $(SiO_{1.5})$, in the molecule and the substituents attached to the silicon atom. Accordingly, $(HSiO_{1.5})_8$ is named as octasilsesquioxane or octa(hydridosilsesquioxane).[1]

The most commonly used alternative shorthand notations come from siloxane chemistry. The letters "D", "M", "T" and "Q" refer to silicon atoms with one to four oxygen bonds respectively (Figure **1.1**) followed by numerical subscripts describing the number of silicon atoms in the molecule. These labels are often followed by numerical superscripts denoting the number of oxygen atoms that are further connected to other silicon atoms.[2,13] For example, $(HSiO_{1.5})_8$ is referred to as $(HT^3)_8$ or simply H_8T_8, having an octameric cage structure with each silicon atom connected to three oxygen atoms and H.

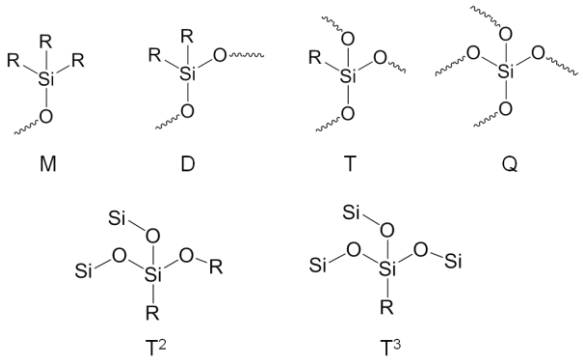

Figure 1.1. Silsesquioxane nomenclature.

Silsesquioxanes are generally prepared by hydrolysis and condensation of trifunctional silanes, $RSiX_3$, where X is normally a halide or alkoxide group. Depending on the reaction conditions, different silsesquioxanes are formed; random polymeric networks without long-range order (Figure **1.2 a**), ladder polymers (Figure **1.2 b**), incompletely condensed polyhedral species (Figure **1.2 c**) and fully condensed polyhedral species (Figure **1.2 d**).

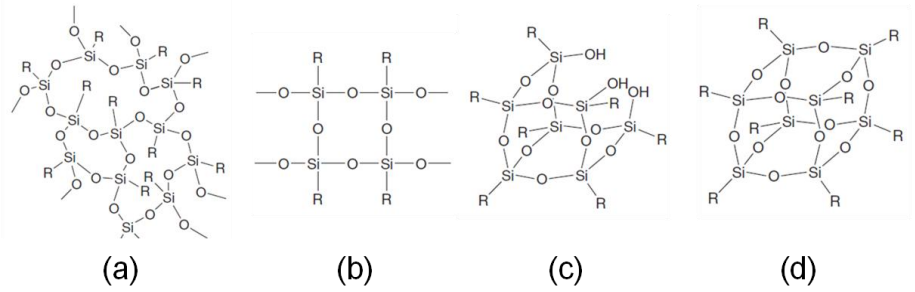

Figure 1.2. Different structures of silsesquioxanes $(RSiO_{1.5})_n$.[13]

Generally, high concentrations of $RSiX_3$ monomer favor formation of silsesquioxane polymers, while intramolecular condensation dominates in dilute reaction conditions favoring polyhedral silsesquioxanes. It is possible to manipulate the reaction to favor the formation of polyhedral clusters containing six, eight, ten or twelve silicon atoms (Figure **1.3**).[1,2,13] Typically, the most common and well-studied polyhedral SQs are octahedral clusters of the formula $(RSiO_{1.5})_8$ or T_8. Octameric silsesquioxanes are unique molecules consisting of rigid silica cores (body diagonal = 0.53 nm) with eight organic functional groups anchored to the vertices of the silica core. Moreover, the silica core and the organic groups create sphere like molecules 1-2 nm in diameter with volumes less than 2 nm^3. This defined size and structure offers opportunities as nanometer scale building blocks for a wide range of polymer nanocomposite materials.[14]

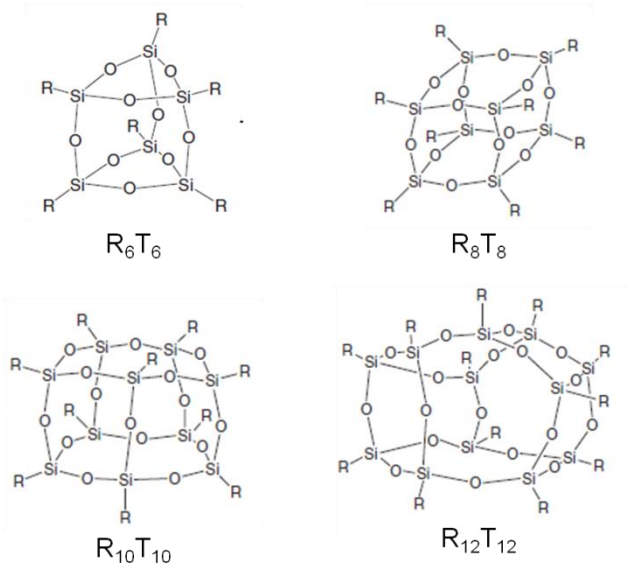

Figure 1.3. Various completely condensed polyhedral silsesquioxane cage structures.[13]

1.1.2. Synthesis of polyhedral oligosilsesquioxanes

Polyhedral oligosilsesquioxanes are formed by the following reactions; (1) Hydrolytic condensation of trifunctional monomers, $RSiX_3$ (X = alkoxy or chloride), (2) condensation of Si-functional cyclosiloxanes, $[RXSiO]_n$, (3) co-condensation of organosilicon monomers and/or oligomers of different structures and compositions, and (4) thermolysis of polysilsesquioxanes. Among these reactions, the most common method used is hydrolytic condensation of trifunctional monomers.[1]

The formation of oligosilsesquioxanes in the course of hydrolytic condensation of $RSiX_3$ is presented by the general equation (1), however, it is in reality multistep and rather complicated as seen in Scheme **1.1**.[1,15]

$$n\ RSiX_3 + 1.5n\ H_2O \rightarrow (RSiO_{1.5})_n + 3n\ HY \qquad (1)$$

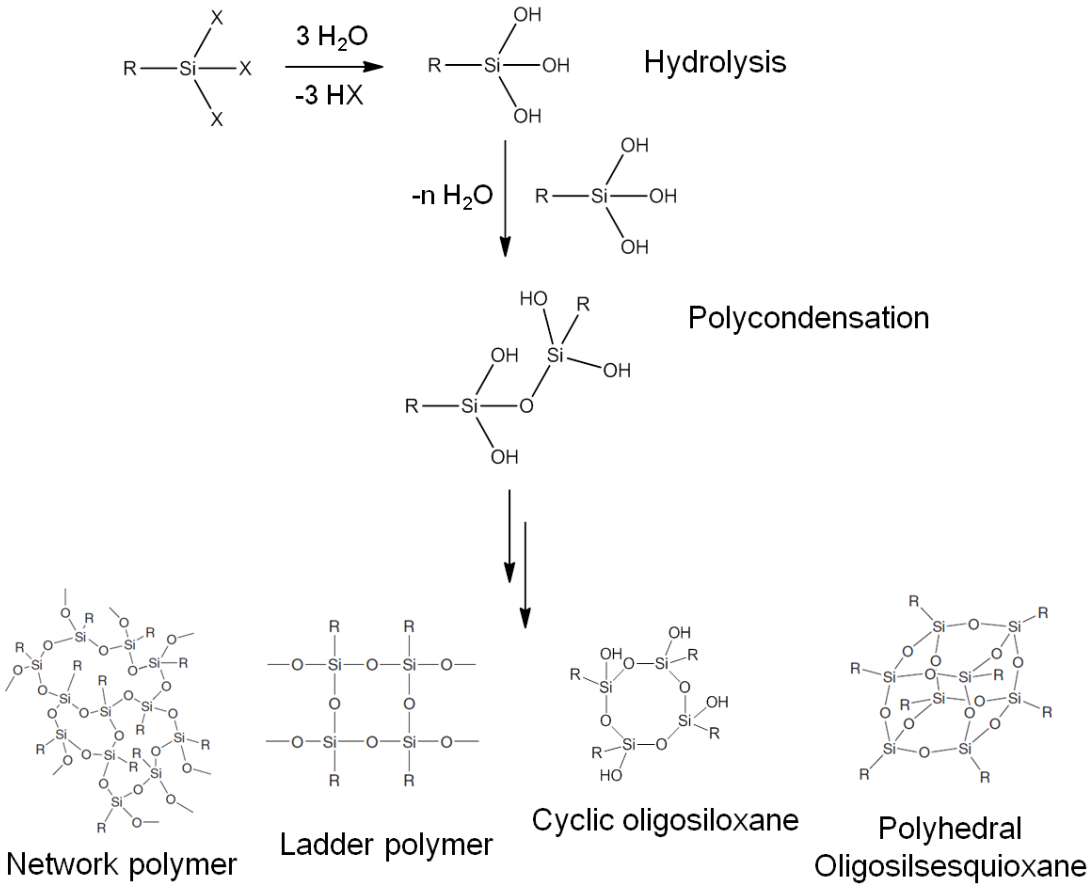

Scheme 1.1. Hydrolytic condensation reaction of $RSiX_3$.[15]

The trifunctional monomers are reactive; therefore, the synthesis of the most important oligomers is carried out in an organic solvent with the addition of water and in the presence of an appropriate acid or base catalyst. Hydrolytic condensation of trifunctional monomers leads to cross-linked three-dimensional networks, $(RSiO_{1.5})_n$. With increasing amounts of solvent, however, the corresponding condensed polycyclosiloxanes, polyhedral oligosilsesquioxanes and their derivatives form (Scheme **1.1**). The reaction rate, the degree of oligomerization, and the

yield of the polyhedral compounds depend on a host of reaction conditions such as concentration of the initial monomer, nature of solvent, character of substituent R and X groups, type of catalyst, water addition, and solubility of the polyhedral oligomers formed.[1,2,7,15] The synthesis of octaphenylsilsesquioxane (**OPS**, Ph_8T_8), which is a basic SQ molecule in this dissertation, will be discussed below for a specific example of hydrolytic condensation reaction.

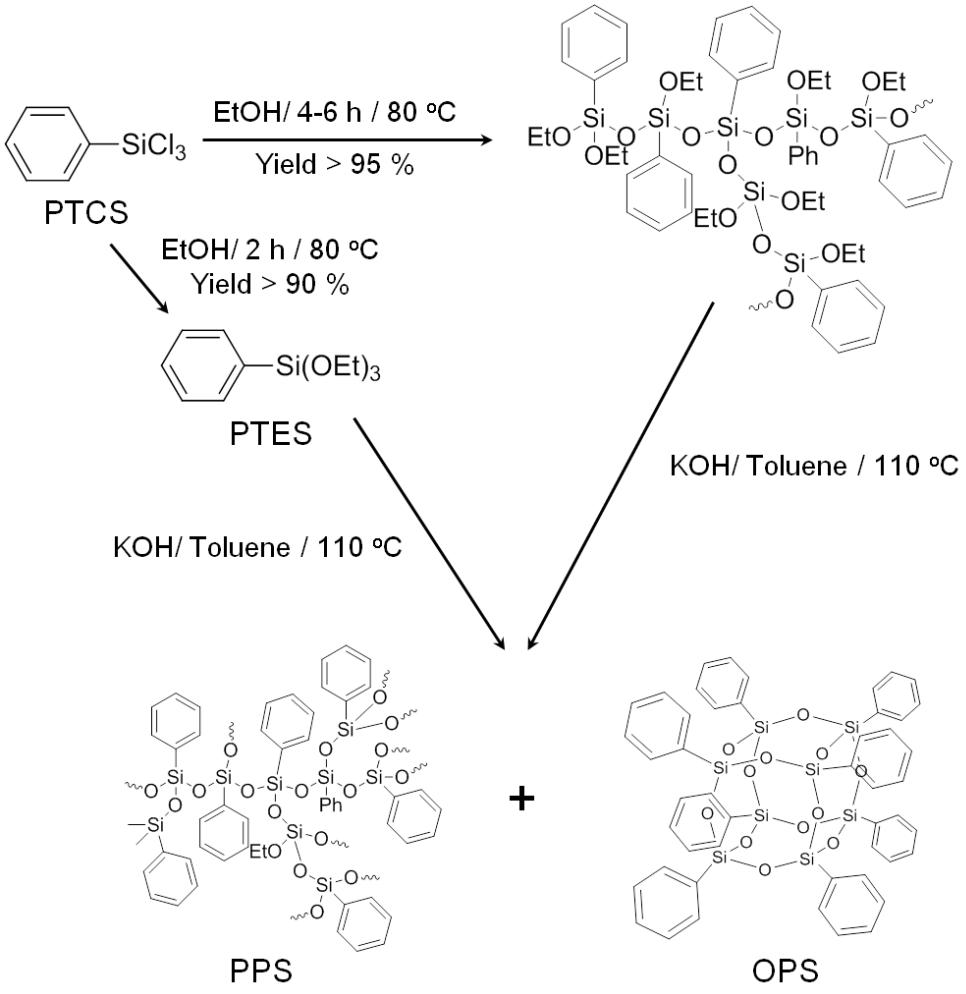

Scheme 1.2. General pathway for the synthesis of OPS.[44]

The OPS was first synthesized by Olsson in 1958 through base-catalyzed equilibration of phenyl(triethoxy)silane and its hydrolyzed oligomer at reflux.[45] Since then various efforts have been made to optimize the synthesis of OPS by modifying the reaction conditions.[46-50] However, these methods were still complex, multi-step and low-yield (9 %) process. Our group

reported simple, two-step route to high yield (> 90%) of OPS by adaptation of Brown's method[48] (Scheme **1.2**).[44]

In the first step, phenyltrichlorosilane, (PTCS, $PhSiCl_3$), is reacted with ethanol to form either the liquid monomer phenyl(triethoxy)silane, (PTES, $PhSi(OEt)_3$), or a polymeric version (polymeric PTES) depending of the reaction condition (reflux for 2 h vs. 4-6 h). Condensation of either type of PTES with catalytic amounts of KOH and minimal amounts of water in toluene provides up to 90 % yields of OPS and a polymeric phenylsilsesquioxane [$(PhSiO_{1.5})_n$, PPS] with a molecular weight of approximately 3,000 Da. The driving force for the exclusive production of OPS is its relative insolubility in toluene because equilibria exist between PTES and its condensation products. As OPS precipitates out from toluene, the system re-equilibrates to produce more OPS.

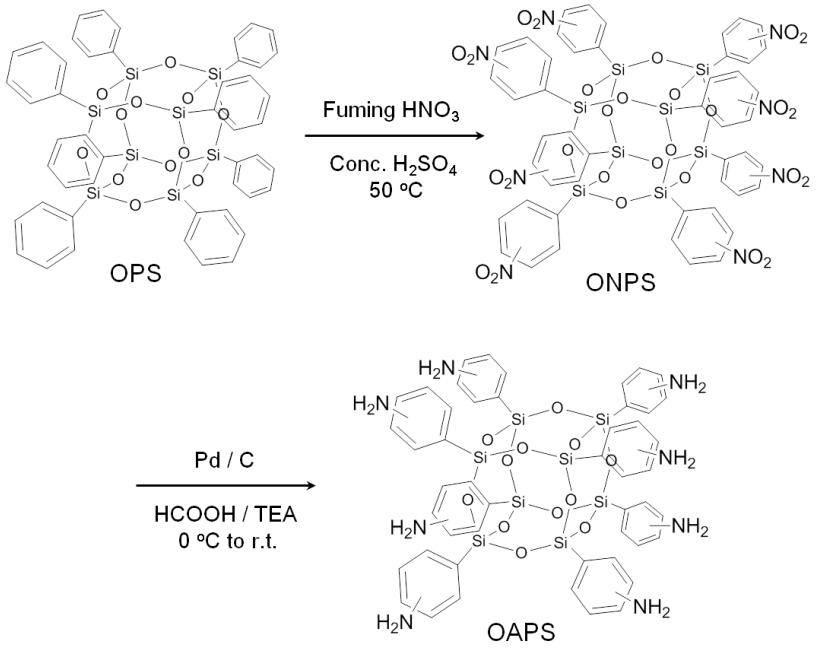

Scheme 1.3. Synthesis of ONPS and OAPS.[51]

OPS can be functionalized by electrophilic substitution to improve solubility and reactivity via various electrophilic aromatic substitution reactions, such as nitration and reduction to prepare octa(nitrophenyl)SQ (ONPS) and octa(aminophenyl)SQ (OAPS) (Scheme **1.3**)[51] and

bromination to give octa(bromophenyl)SQ (Br_xOPS) (Scheme **1.4**)[52] and iodination (I_8OPS, Scheme **1.5**).[53] The OAPS, Br_xOPS, I_8OPS are basic starting materials for this dissertation.

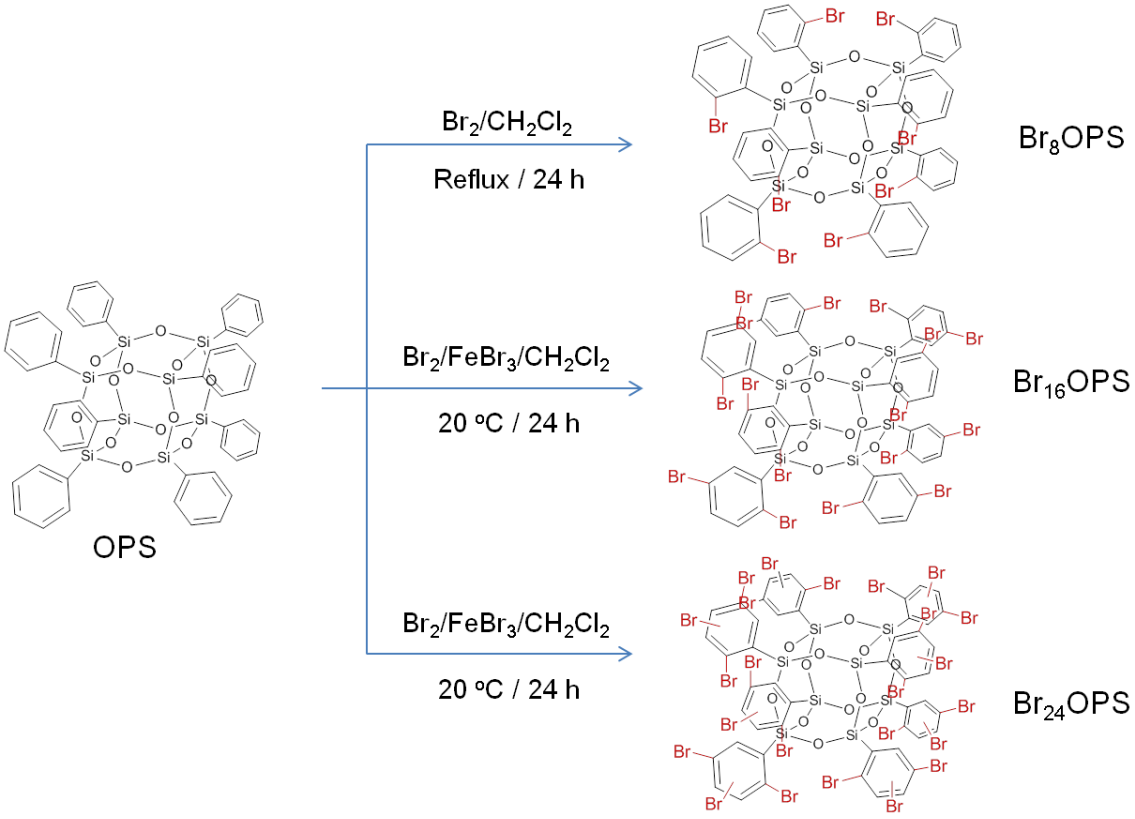

Scheme 1.4. Bromination of OPS.[52]

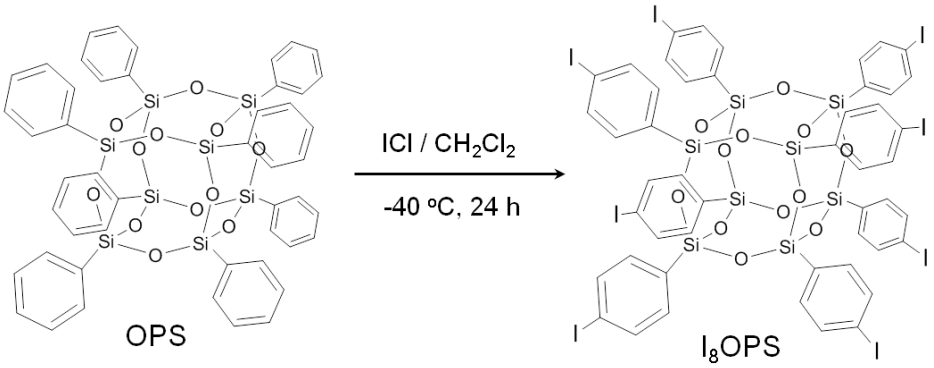

Scheme 1.5. Synthesis of I_8OPS.[53]

1.1.3. Organic/inorganic hybrid polymers containing SQs.

Organic/inorganic hybrid materials play a major role in developing high performance and high functional materials. In particular, considerable attention has concentrated on the preparation of hybrid nanocomposites using the well defined nanoscale inorganic modified agents such as clays, carbon nanotubes, graphene and polyhedral oligosilsesquioxanes (SQs).[54-62] Among these inorganic agents, SQs demonstrate unique characteristics in the construction of SQ containing hybrid polymers. SQ molecules have a definite size and structure and they can be well dispersed in a polymer even at the molecular level. In addition, the SQs' functional groups can be specifically designed to prepare one or more covalently bonded reactive functionalities suitable for polymerization, grafting, blending or other transformation.[60-62] The incorporation of SQ molecules into polymeric materials can dramatically improve their mechanical properties, thermal resistance, and surface hardening as well as reduce flammability, and viscosity during process. [63-67]

Depending on the number of SQ functional groups, three main SQ architectures can result; (a) star-like polymer, (b) cross-linked network and (c) polymers with pendant SQ cages (Figure **1.4**).[14,60-62]

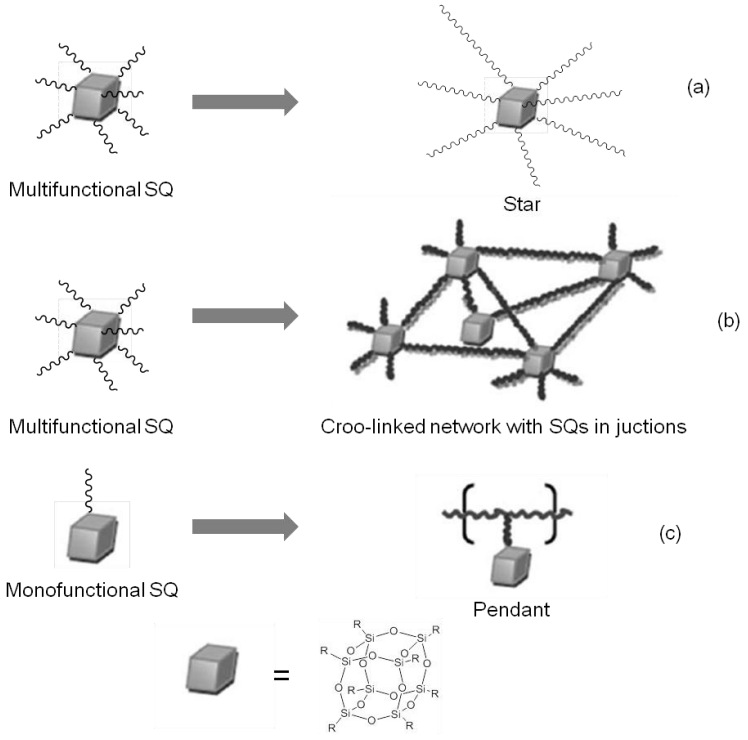

Figure 1.4. The three main types of SQ-based hybrid polymers.[62]

Star-like hybrids with SQ cores are generally prepared using functional SQs as the micro-initiator. For example, the amphiphilic star-like organic/inorganic hybrid cationic polymer was synthesized via atom transfer radical polymerization (ATRP).[68] Hydroxy functionalized silsesquioxane (octa(dimethyl-1-propanolsiloxy)silsesquioxane, SQ-OH) was first modified with 2-bromoisobutyryl bromide, which functions as a micro-initiator to initiate the polymerization of 2-(dimethyl-amino)ethylmethacrylate (DMAEMA) and give star-like polymer of SQ-*g*-PDMAEMA (Scheme **1.6**). This SQ based amphiphilic polymer is promising candidate for drug and gene delivery to cells.

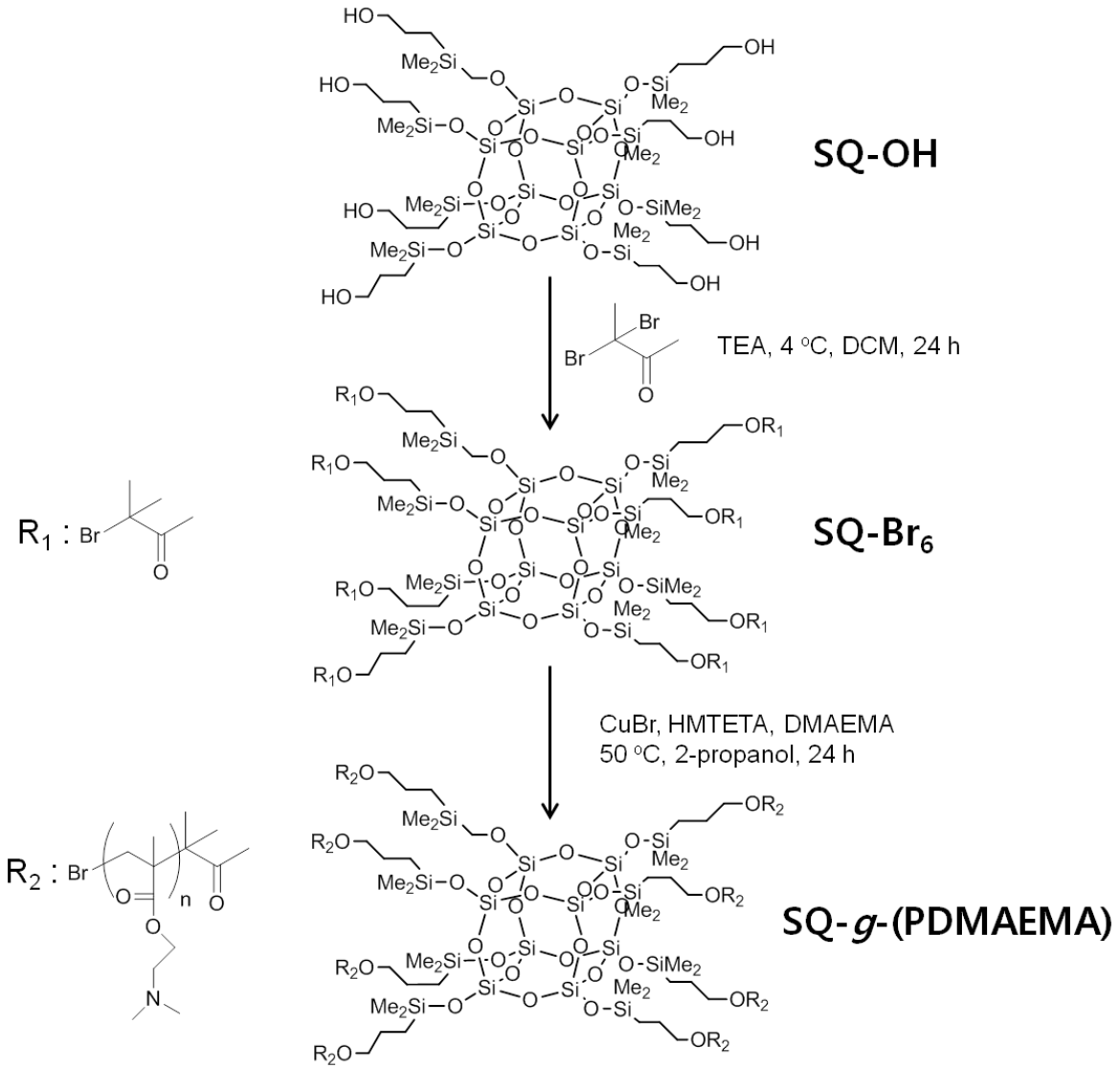

Scheme 1.6. Synthesis of SQ-*g*-PDMAEMA by ATRP.[68]

Multi-functional SQs are used as nano fillers or monomers to polymerize with organic monomers or polymers forming cross-linked hybrid networks with enhanced mechanical strength and thermal stability. Our group reported cross-linked hybrid imide and epoxy resin from octaaminophenylSQ (OAPS) (Scheme **1.7**).[69,70]

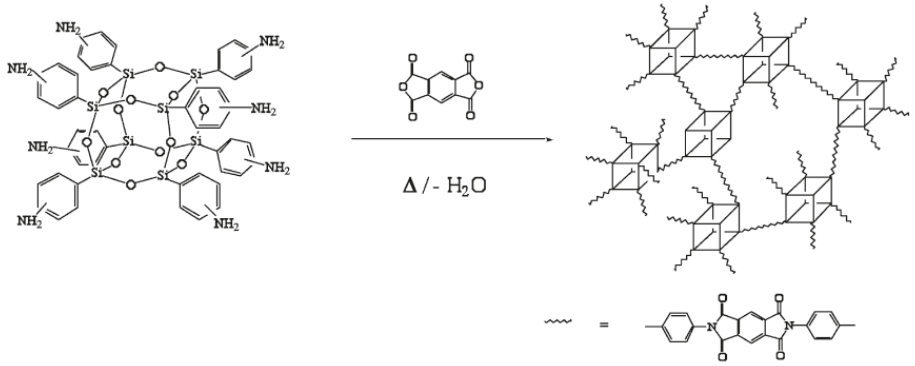

Scheme 1.7. Polyimide resin produced by the reaction of OAPS and PMDA.[69]

Another major approach to incorporating SQs into hybrid polymers is to copolymerize mono-functional SQs to attach them to the polymer backbone as pendant or end groups. Various mono-functional SQ derivatives, such as mono-methacrylate, vinyl, epoxy, and norbornyl SQs have been prepared and polymerized through many different polymerization methods including radical, condensation, ring opening polymerization.[71-75]

There are three main strategies in the preparation of monofunctional SQ molecules: (1) direct condensation of trifunctional organosilane bearing different groups; (2) substitution or addition reactions of one corner group on SQ molecules; (3) corner-capping reactions of incompletely condensed $R_7T_7(OH)_3$ molecules. Among these three approaches, corner-capping are commonly used to prepare various monofunctional SQ molecules. Scheme **1.8** provides an example of corner-capping reaction to prepare mono-methacrylate SQs and their radical polymerization.[71]

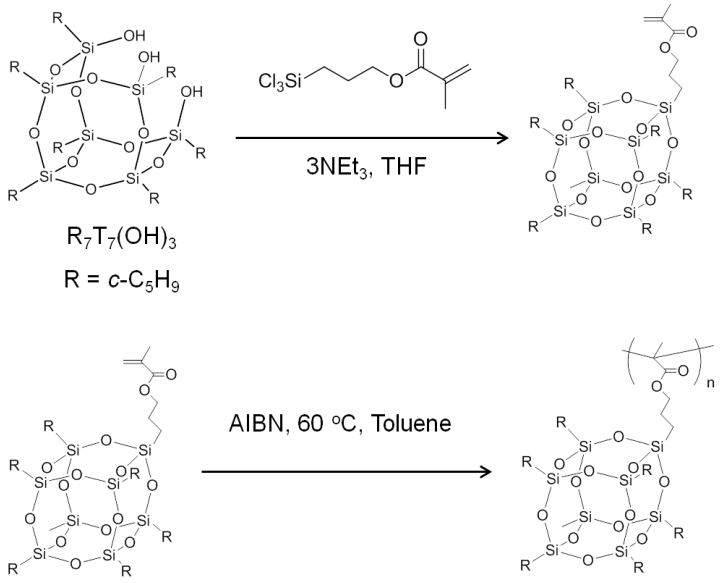

Scheme 1.8. Synthesis of mono-methacrylate by corner-capping reaction and its polymer by radical polymerization.[71]

Lastly, "beads on a chain" (BoC) polymers, SQ cages along the chain backbone, prepared via polymerization of difunctional SQs are another type of SQs incorporated organic/inorganic hybrid polymers (Scheme **1.9**). Relatively few polymers have been reported because the synthetic methods to prepare reactive difunctional SQs are rare;[76-79] however, our group recently developed a route to di- and trifunctional T_{10} and T_{12} silsesquioxane cages using F^- catalyzed exchange of functional groups between two different polysilsesquioxanes.[80]

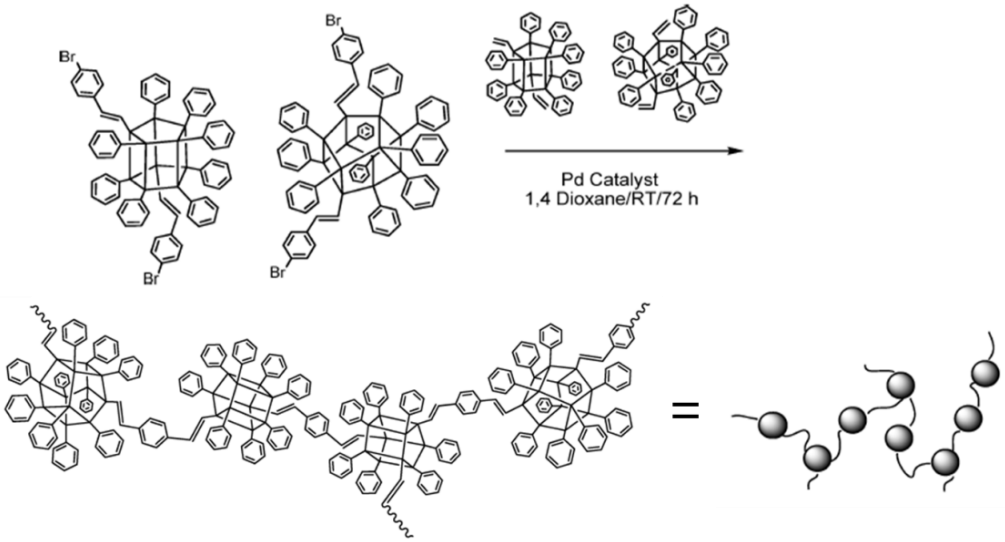

Scheme 1.9. Heck coupling of $vinyl_2Ph_x$ $T_{10/12}$ SQs with $BrStyr_2Ph_x$ $T_{10/12}$ SQs (x = 8, 10).[80]

1.1.4. Electron delocalization involving SQ core (3-D conjugation)

Conventionally, silsesquioxanes have been considered as insulators due to their silica core. Theoretical modeling studies of the cubic SQs with simple tethers such as H and alkyl groups predicted that energy gap between the highest occupied molecular orbital (HOMO) and the lowest unoccupied molecular orbital (LUMO) to be approximately 6-7 eV, which suggests that these SQs are insulators.[81-83]

However, a series of papers recently published by several research groups have shown unique photophysical properties of SQ molecules having conjugation with organic chromophores.[84,85] The absorption spectra of these molecules are similar to the small unbound molecules, but the photoluminescence spectra are red-shifted compared to the small chromophores by a significant amount. For example, Vantravers et al. reported the absorption and emission spectra of 4-vinylbiphenyl-3,5-dimethanol and SQ molecules with same molecules at their corner (Figure **1.5**). They discovered that the absorption spectrum of SQ molecules is slightly red-shifted (~ 7 nm) compared to its small molecule analogs, however, photoluminescence spectra show that the emission of SQ molecule is red-shifted by 60 nm compared with small molecule.[85]

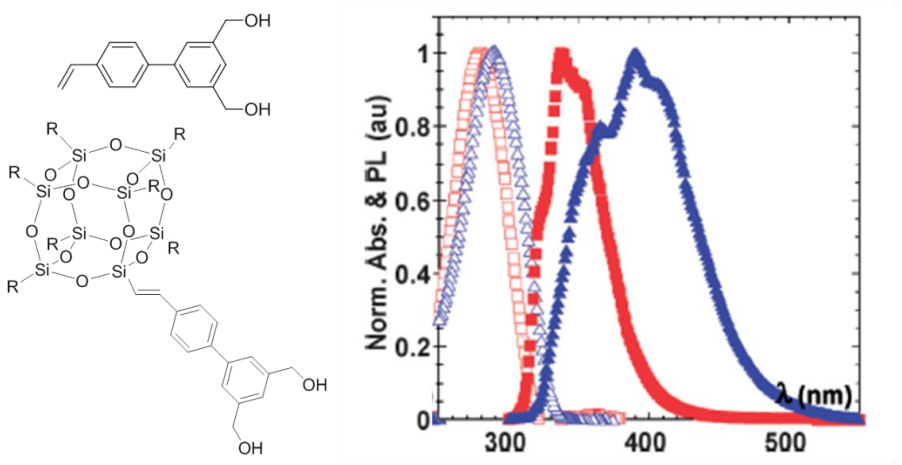

Figure 1.5. Normalized absorption (empty symbols) and photoluminescence (full symbols) spectra of 4-vinylbiphenyl-3,5-dimethanol (square) and SQ molecules (triangle).[85]

Our group has also described similar photophysical behavior for cubic SQ molecules with functionalized stilbene and vinylstilbene tethers.[15,86,87] Figure **1.6** shows that the Uv-Vis absorptions for *o*- or *p*-methylstilbeneOPSs are nearly identical to *trans*-methylstilbene as expected given the assumed insulating nature of the SQ cage.[87] However, the emission of the SQ

cages are red-shifted 60-75 nm from *trans*-methylstilbene (Figure **1.6**). This large red shift implies that the SQ molecules have longer conjugation than just the individual organic substituent on each corner.

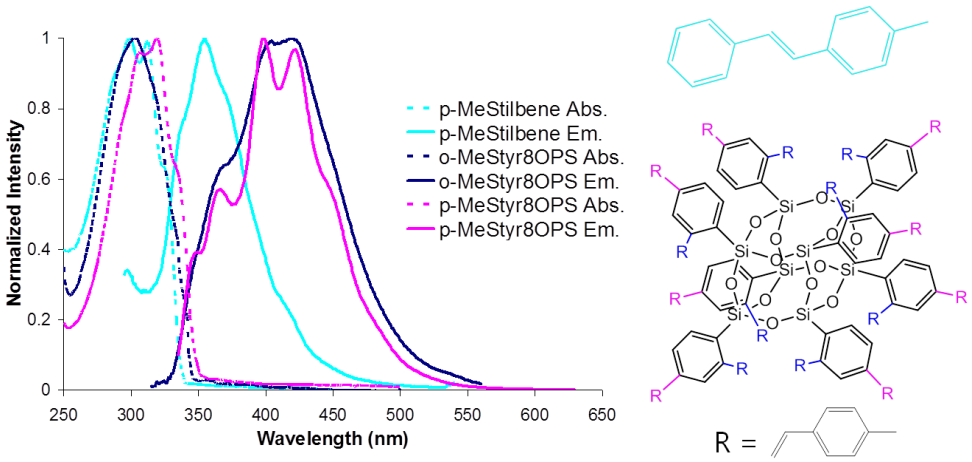

Figure 1.6. UV-Vis absorption and emission spectra of methylstilbeneOPS and *trans*-methylstilbene for comparison.[87]

Computational modeling of cubic SQs by multiple groups led to the Table **1.1** data and Figure **1.7**.[81-83, 87-89] These studies indicate that the HOMO consist of atomic orbitals of lone pair electrons of the bridging oxygens and the LUMO is a combination of atomic orbitals of the silicon, oxygen, and their substituents. Furthermore, LUMO is located in the center of SQ core with $4A_1$ symmetry (Figure **1.7**). This observation suggests that the red shift might result from extended conjugation through this 3-D LUMO.

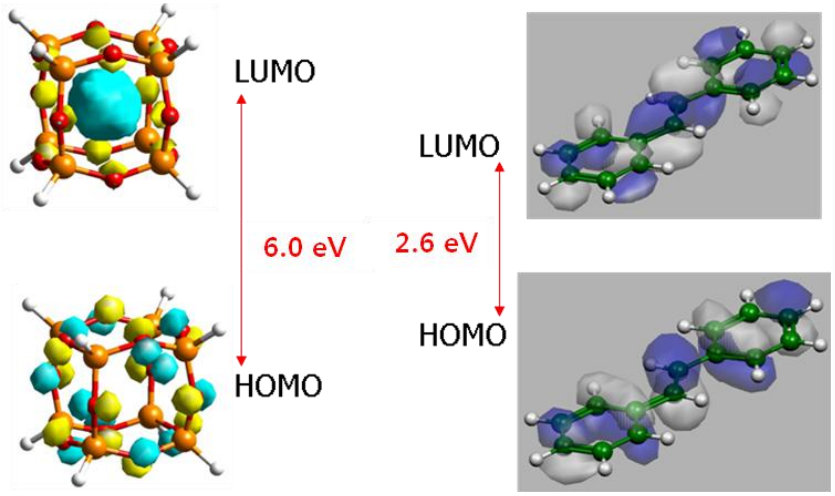

Figure 1.7. LUMO and HOMO of $[XSiO_{1.5}]_8$ and stilbene.[15, 87]

Table 1.1. DFT HOMO-LUMO calculations for various $[XSiO_{1.5}]$.[87] (all values in eV). †Measured.[89]

	$[HSiO_{1.5}]_8$	OPS	$StilSi(OSiMe_3)_3$	$Stil_1[SiO_{1.5}]_8$	$Stil_8OS$
HOMO	-7.52 (O)	-5.53	-5.16	-5.47	-4.52
Core/LUMO	-0.54 (H,Si)	-0.04	-0.21 (SiO_3)	-0.41	-0.29
Organic/LUMO		-0.86	-2.46	-2.77	-1.91
Core gap	6.98 (4.4)†	5.56	4.95	5.06	4.23
Organic gap		4.66	2.70	2.70	2.61

Theoretical modeling studies on stilbene functionalized SQs show that the HOMO of $Stil_8OS$ is the π-state of the stilbene tethers and the LUMO includes interactions between the silicon atoms and the π*-state of the stilbene tethers. The HOMO-LUMO gap for $Stil_8OS$ is estimated to be 2.6 eV (organic gap in Table **1.1**), and the gap between the HOMO and the molecular orbital inside the SQ core (core gap in Table **1.1**) is estimated to be 4.2 eV. If we consider the energy difference between calculated and measured HOMO-LUMO bandgap of H_8T_8 (4.4 eV measured vs. 6.0 eV calculated),[88, 89] then the core gap of $Stil_8OS$ could be closer to the organic tether based bandgap (organic gap). This offers another argument for electron delocalization involving the SQ core to the extent that there is a possibility of 3-D conjugation through the SQ core.

Another important observation comes from the photophysical property studies of dimethylaminostilbene functionalized siloxane (corner), cyclosiloxane (half) and cubic SQ (cubic).[87] Figure **1.8** provides chemical structures of these molecules and Table **1.2** summarize TPA and quantum efficiency data. The low photoluminescence quantum yields and structureless emission spectra of the "corner", "half" and "cubic" molecules indicate charge transfer (CT) processes, and solvatochromism studies support this behavior.[87]

Two photon absorption (TPA) studies of these molecules found that the TPA cross-section of the "corner" is 12 GM/moiety, the "half" is 8 GM/moiety and the "cubic" is 26 GM/moiety (Table **1.2**). If the charge transfer characteristics of these molecules are identical, their TPA cross-section/moiety should be identical. The fact that "cubic" molecule has the lowest photoluminescence quantum yield (Φ_f) and the highest TPA cross-section/moiety suggests that this system exhibits more efficient CT character than the fragments. The influence of the SQ core

as a whole on the photophysical behavior of the molecules is more than just a sum of the influence of the fragments.

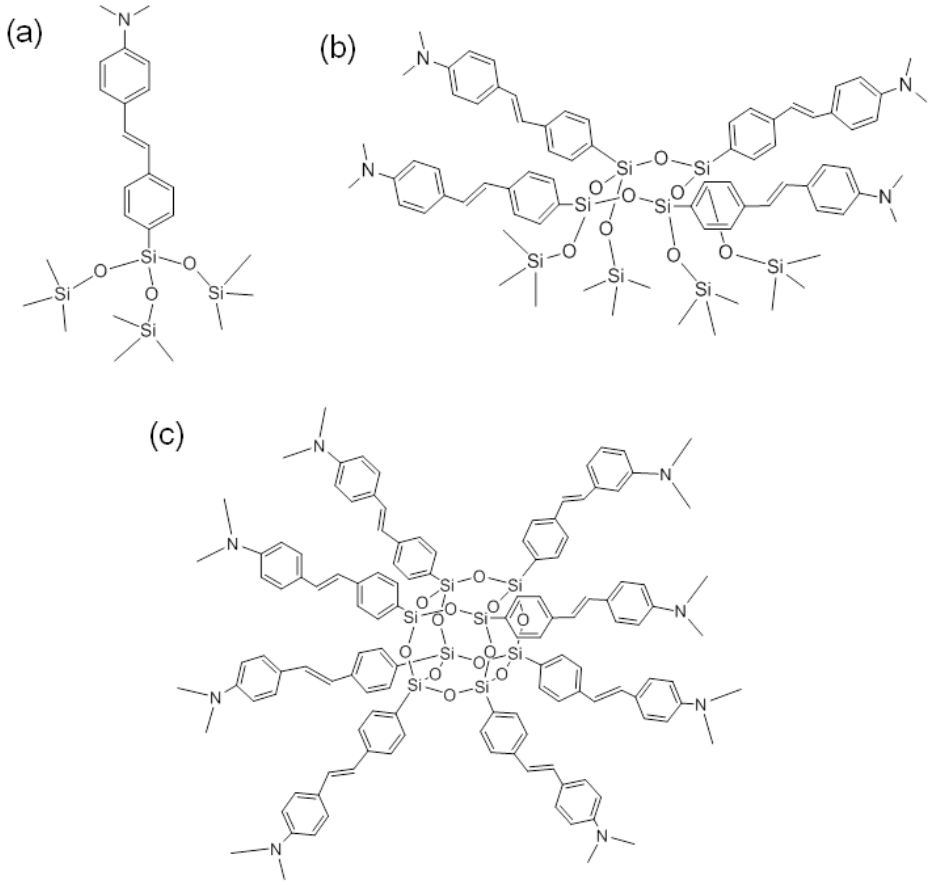

Figure 1.8. (a) Me_2NStil-corner, (b) Me_2NStil-half, and (c) Me_2NStil_8OS.[87]

Table 1.2. TPA properties of silsesquioxane derivatives and quantum efficiencies.[87]

Sample	δ (GM)	δ/moiety (GM)	λ_{max} (nm)	Φ_f
Me_2NStil-corner	12	12	780	0.08
Me_2NStil-half	30	8	790	0.09
Me_2NStil_8OS (cubic)	211	26	755	0.03

Furthermore, our group reported the photophysical properties of beads on a chain (BoC) type oligomers having divinylbenzene linkers between deca- and dodecameric SQ molecules as mentioned.[80] Their absorption and emission spectra were compared with the vinyl$Si(OEt)_3$ end capped model compounds (Figure **1.9**). Figure **1.9** shows that absorption maxima for the BoC

oligomers and model compounds are similar (~260 nm). However, the emission maximum for the BoC oligomers is red-shifted by ~60 nm from the emission maxima of the model compounds.

These results suggest that the conjugation lengths of the BoC oligomers is increased by connecting the SQs through conjugated linkers and that electronic communication occurs along the polymer chains and through the cages through the oligomer backbone. These interesting findings lead to the potential for new SQ based compounds for use in optoelectronic applications such as OLED and organic photovoltaics.

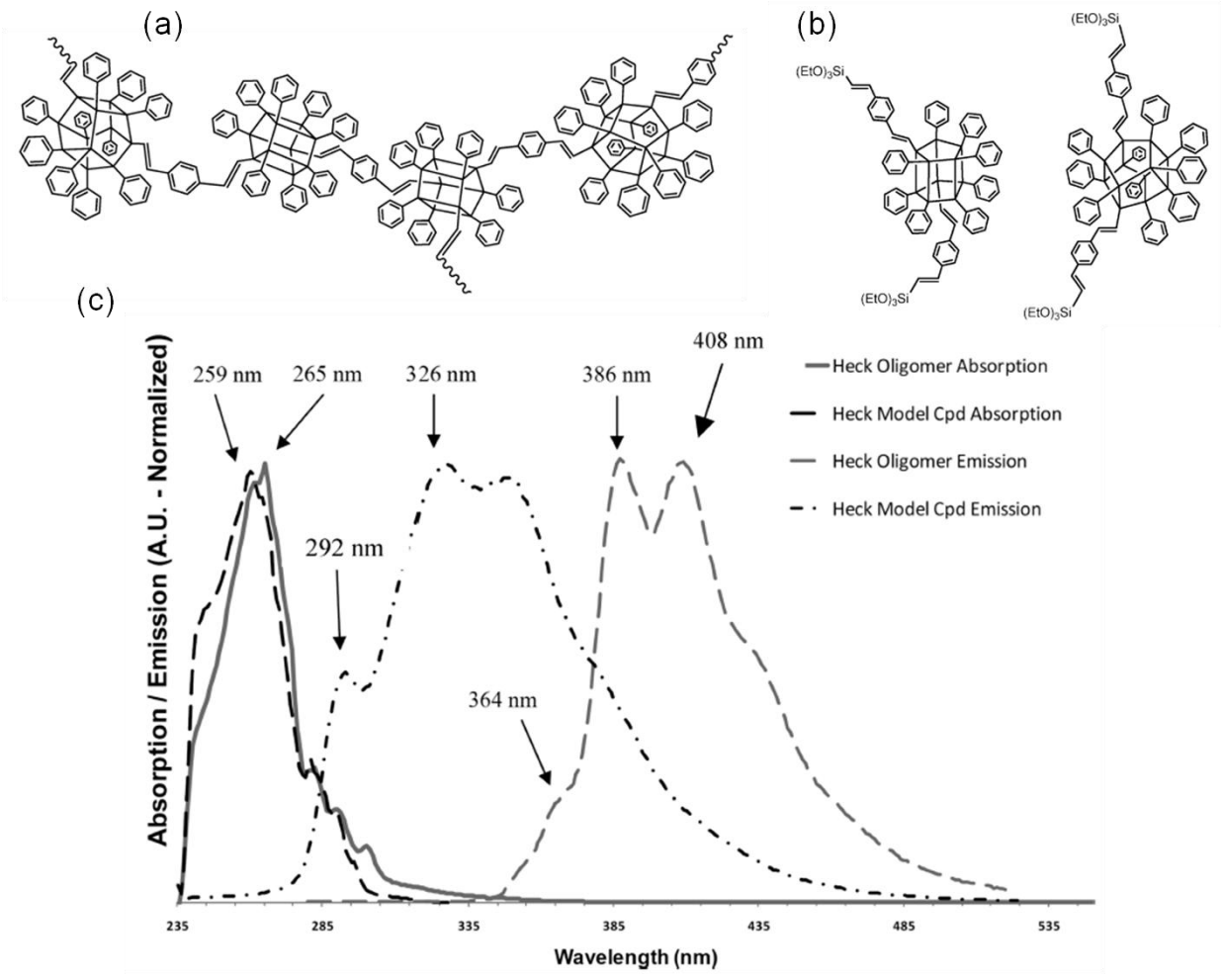

Figure 1.9. (a) SQ-based BoC oligomers, (b) $Si(OEt)_3$ end-capped model compounds and (c) Absorption and emission spectra of SQ-based BoC oligomers and model compounds.[80]

1.2. Pd catalyzed cross coupling reactions

Palladium compounds are used as a catalyst in many coupling reactions including the Heck reaction between alkenes and aryl halides,[90,91] the Suzuki reaction between aryl halides and boronic acids,[92,93] the Sonogashira coupling between aryl halides and alkynes with copper iodide as a co-catalyst,[94,95] the Stille reaction between organohalides and organotin compounds,[96,97] the Negishi coupling between organohalides and organozinc compounds.[98,99] Among them, Heck and Sonogashira coupling reactions are discussed below because these reactions are used to prepare conjugated SQ compounds in this dissertation.

1.2.1. Heck coupling

The Palladium catalyzed Heck reaction is the most efficient route for the vinylation of aryl or vinyl halides or triflates to form new C-C bonds by replacing a hydrogen atom in the alkene with a carbon substituent (Scheme **1.10**). Since the independent discovery by Mizoroki and Heck in the early 1970s,[90,91] this reaction has been intensively evolved from synthetic and mechanistic points of view. Recent developments involve the generation of chiral centers with a high degree of enantiocontrol for certain substrates using chiral ligands on palladium and the replacement of the halide with an organoboron reagent in the presence of stoichiometric reoxidant.[100]

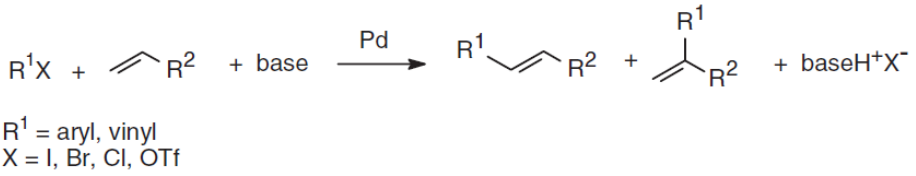

Scheme 1.10. General scheme of Heck coupling.[101]

The mechanism of Heck cross coupling is represented in Figure **1.10**.[102,103] As in most cases, the catalyst used is generated in situ, which effectively means that the first step must be reduction of the Pd (II) precursor to provide the active Pd (0) catalytic species.

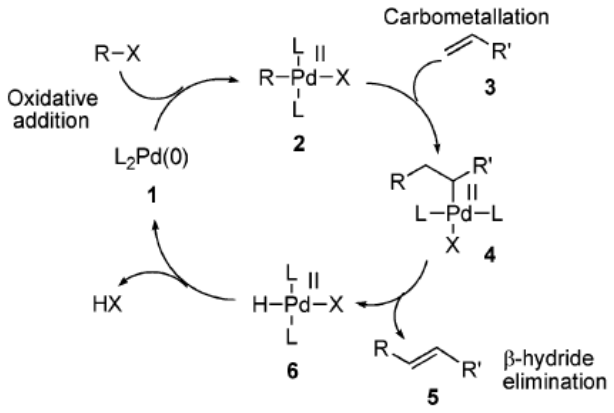

Figure 1.10. General mechanism of Heck coupling.[103]

The Pd (0) species **1** undergoing oxidative addition to generate a Pd (II) species **2**, which reacts with the olefin component **3**, possibly following initial η^2-coordination to the Pd atom. This results in a carbometallation reaction to generate Pd (II) alkyl complex **4**. Elimination of Pd hydride from complex **4** furnishes the product **5** and base assisted elimination of HX from Pd (II) complex 6 regenerates the active Pd (0) catalyst **1**.

1.2.2. Sonogashira coupling

Pd catalyzed sp^2-sp coupling between aryl or alkenyl halides or triflates and terminal alkynes has become an important method of preparing arylalkynes and conjugated enynes which are precursors for natural products, pharmaceuticals, and molecular organic materials. (Scheme **1.11**).[104,105] The two earlier studies on this topic were reported independently be Heck[106] and Cassar[107] in 1975. Both methods generally required high temperature (up to 100 ^oC). In the same year, Sonogashira reported that addition of a catalytic amount of copper (I) iodide greatly accelerates the reaction thus enabling alkynylation at room temperature.[94] Therefore, Sonogashira coupling became the most popular procedure for the alkynylation of aryl or alkenyl halides.

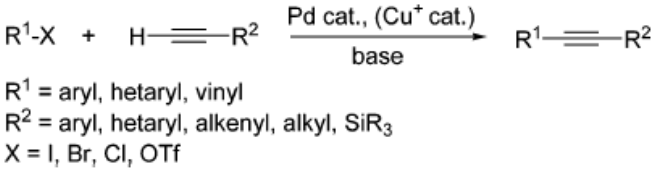

Scheme 1.11. General scheme of Sonogashira coupling.[104,105]

The copper cocatalyzed Sonogashira reaction is believed to take place through two independent catalytic cycles as shown in Figure **1.11**.[104,105] The generally accepted catalytic cycle of the Pd catalysis (the Pd-cycle) is based on an oxidation addition of R_1-X (R_1 = aryl, hetaryl, vinyl; X = I, Br, Cl, OTf) to the 14-electron $Pd(0)L_2$ formed by reduction of different Pd (II) complexes. The next step in the Pd-cycle would connect with the cycle of the copper cocatalyst (the Cu-cycle). Thus, transmetalation from the copper acetylide formed in the Cu-cycle would generate an $R^1Pd(-C{\equiv}CR^2)L_2$ species, which gives the final coupled alkyne after trans/cis isomerization and reductive elimination with regeneration of the catalyst.

In the Cu-cycle, the base, generally an amine, is supposed to abstract the acetylenic proton of the terminal alkyne, then forming a copper acetylide in the presence of the copper (I) salt. The copper acetylide continues to react with Pd intermediate during transmetalation to regenerate of the copper (I) halide.

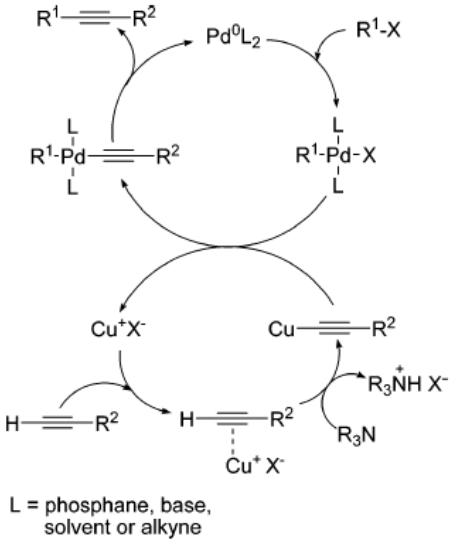

Figure 1.11. Catalytic cycle for the Sonogashira coupling.[104,105]

1.3. Organic photovoltaic (OPV) cells

Photovoltaics (PVs) harvest energy from sunlight and convert it into electrical power. This technology is one of the key solutions to the world's future global energy needs. The big drawback to current PV technologies based on inorganic materials is their high production cost. Organic photovoltaics (OPVs) are promising alternatives due to the fact that there is a potential

to fabricate them onto large areas of lightweight flexible substrates by solution processing such as spin coating, roll-to-roll printing, ink-jet printing at a low cost.[108-111] We present brief history of the development of OPV cells and their principles of operation below.

1.3.1. Brief history

The origin for organic photovoltaic (OPV) cells was the finding of dark conductivity in halogen doped organic compounds in 1954.[112] In the following years, considerable systematic research was undertaken on charge transport properties of small molecules. The first OPV cells were based on an active layer made of a single material, sandwiched between two electrodes of different work functions. Strongly coulomb bound electron-hole pairs (singlet excitons) are created by the absorption of light. As their binding energies in organic semiconductors are usually between 0.5 and 1.0 eV, the excitons must be separated to finally generate a photocurrent. To overcome the exciton binding energy, one has either to rely on the thermal energy, or dissociate the exciton at the contacts.[113] However, both processes have rather low efficiencies because temperatures are not high enough under normal operating conditions and sample thicknesses are much higher than exciton diffusion lengths. Consequently, the single layer OPV cells had power conversion efficiencies (PCE) far below 1 % for the solar spectrum.[114]

The introduction of a second organic semiconductor layer increased power conversion efficiencies of OPV cells. The first organic bilayer OPV cell was implemented by Tang.[115] The typical device configuration is shown in Figure **1.12 a**. The light is absorbed in the donor material, a hole conducting small molecule such as copper phthalocyanine. In bilayer devices, the photogenerated singlet excitons can diffuse within the donor towards the planar interface to a second layer containing the acceptor, which is usually chosen to be strongly electronegative. The acceptor material provides the energy needed for the singlet exciton to separate, as the electron goes to a state of much lower energy within the acceptor. This charge transfer dissociates the exciton, the electron moves to the acceptor material, whereas the hole remains on the donor. A prominent example for the electron acceptor material is the buckminsterfullerene (C_{60}).[116]

The difference between the electron energy of the donor and the corresponding acceptor level has to be larger than the exciton binding energy to initiate charge transfer. If the exciton reaches this donor-acceptor interface by diffusion, it is energetically favorable for the electron to

be transferred to the acceptor molecule. Because this charge transfer is very fast, within less than 50 fs in polymer-fullerene systems, compared with alternative loss mechanisms, the exciton is dissociated and the resulting charge carriers are spatially separated.[117] The bilayer OPV cells invented by Tang achieved a PCE of about 1 %.[115]

The limiting factor in this concept is that for full absorption of incident light, the layer thickness of the absorbing material must be of the order of the absorption length, approximately 100 nm. This is much more than the diffusion length of the excitons, about 10 nm. In this example, even though 100 % of incoming photons can be absorbed within the absorption layer, only 10 % reach the donor-acceptor interface and dissociate into charge carrier pairs.

To overcome this difficulty, the novel concept of bulk heterojunctions (BHJ) was introduced by Yu et al.[118] By blending donor and acceptor materials together, an interpenetrating network with a large donor-acceptor interfacial area can be achieved by controlling phase separation between the two components (Figure **1.12 b**). Bulk hetero-junctions have the advantage of being able to dissociate excitons very efficiently over the whole extent of the solar cells, thus generating electrons-hole pairs throughout in the film.

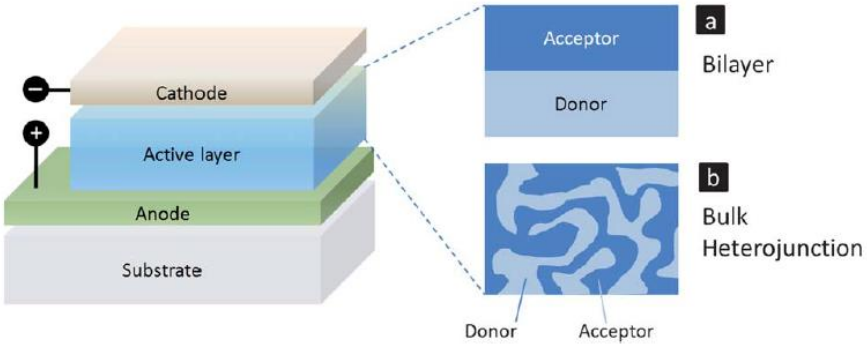

Figure 1.12. Schematic diagram of (a) a bilayer and (b) a bulk heterojunction OPVs.[110]

Good control of the morphology is important for BHJ efficiencies. The choice of solvents as well as the annealing of the OPV cells leads to a more favorable internal structure in view of the dissociation of bound electron-hole pairs and the subsequent charge transport.[119,120] Through tremendous research efforts to create novel conjugated polymers, device performance in BHJ OPV cells has increased steadily over the past decade. PCEs of over 5 % have been

achieved for the well known regioregular poly(3-hexylthiophene) (P3HT) and also for many newly developed low band gap conjugated polymers.[121- 123]

1.3.2. Operation principle of OPV cells

OPV cells typically consist of a thin active organic layers sandwiched between a high work function anode, typically transparent indium tin oxide (ITO) layer and a relatively low work function metal cathode such as aluminum and gold. The active layer is made up of two light absorbing organic semiconductors, one with an electron donating character (donor) and the other with an electron accepting character (acceptor). These semiconductors could be deposited either as two distinct layers where the donor-acceptor interface resides only between the two layers (bilayer, Figure **1.12 a**) or blended as an almost homogeneous mixture where interfacial interactions between the donor and acceptor exist throughout the blended bulk layer (bulk heterojunction, Figure **1.12 b**).[109,110]

Basically the underlying principle of a light harvesting process of OPV cells is the reverse of light emitting diodes (LEDs) and the development of the two are related. In LEDs an electron is introduced at the low-work function electrode (cathode) with the balanced introduction of a hole at the high-work function electrode (anode). At some point, the electron and the hole meet and recombine to omit light.[124,125] The reverse happens in an OPV device.

When light is absorbed in the donor, an electron is excited from the highest occupied molecular orbital (HOMO) to the lowest unoccupied molecular orbital (LUMO) forming excitons bound electron-hole pairs (Figure **1.13 i**). The excitons diffuse within the active layer and may decay back to their ground state beyond the lifetime of the exciton. Alternatively, if the exciton reaches a donor-acceptor interface within the exciton's lifetime (Figure **1.13 ii**), electrons can transfer from the LUMO of the donor to that of the acceptor and holes can transfer from the HOMO of the acceptor to that of the donor (Figure **1.13 iii**). In this state, the electron and hole on the acceptor and donor remain Coulombically bound, forming a germinated donor/acceptor pair.[126-128]

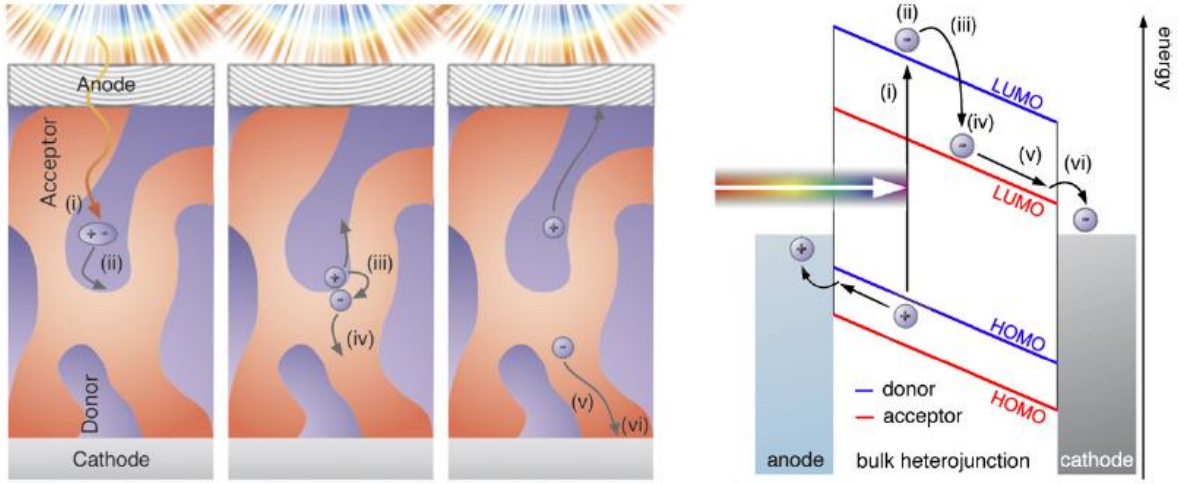

Figure 1.13. From light absorption to photocurrent in a BHJ OPV cell. Left: from a kinetic point of view, right: simplified energy diagram.[126]

This photoinduced charge transfer between donor and acceptor takes place within less than 50 fs.[126] Since all competing processes like photoluminescence (~ ns) and back transfer and thus recombination of the charge (~ µs) take place on a much larger timescale,[129,130] the charge separation process is high efficient and metastable. These possible pathways for decay of the system after excitation are compared in Figure **1.14**. As a result, photoinduced charge transfer is accompanied by strong photoluminescence quenching of the otherwise highly luminescent organic donors.[131]

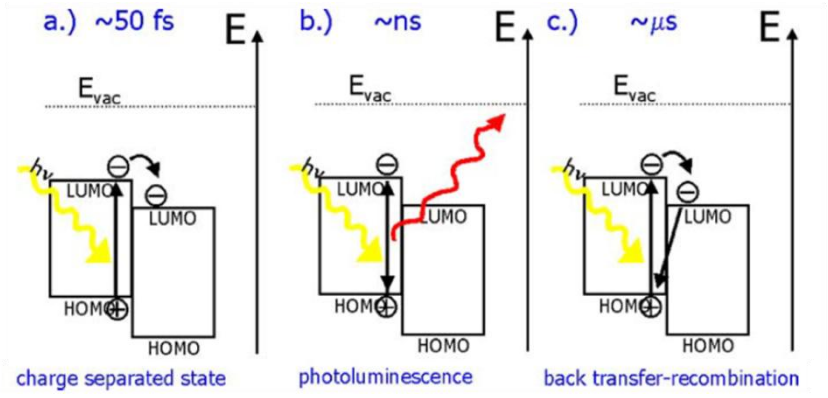

Figure 1.14. Photoinduced processes in the donor-acceptor system. (a) charge transfer, (b) photoluminescence and (c) recombination.[127]

The electron-hole pair dissociate into free hole and electron charges with the assistance of the built-in electric field that exists between the two electrodes of different work functions (Figure **1.13 iv**), then the separated charges move in opposite directions (Figure **1.13 v**) and get collected at the electrodes to drive the external circuit (Figure **1.13 iv**).

1.3.3. OPV cell parameters

The followings are important terminology for photovoltaic devices.[109,114,126] At first, it is useful to review what happens to an OPV cell in the dark and upon exposure to illumination. A graph of current (I) versus voltage (V) is a common way to illustrate the properties of solar cells (Figure **1.15**). In the dark, the *I-V* curve passes through the origin, with no potential, no current flows. However, the *I-V* curve shifts downward when the device is exposed to light.

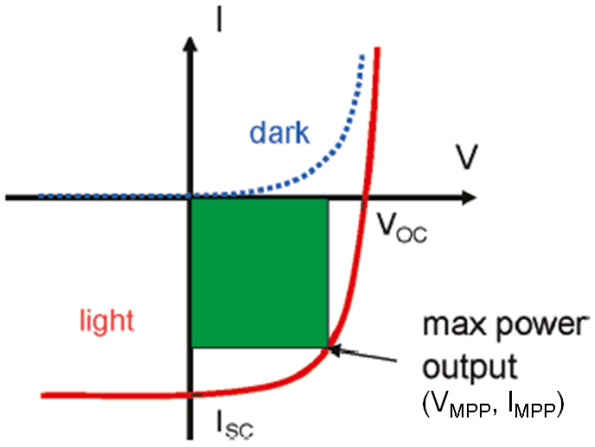

Figure 1.15. Current-voltage characteristics of an OPV cell under illumination (red) and in the dark (blue).

Air mass (AM): The path length which light takes through the atmosphere normalized to the shortest possible path length. This is denoted as 'AM(x)', where x is the inverse of the cosine of the zenith angle of the sun. Because the efficiency of a solar cell is sensitive to variation in both the power and the spectrum of the incident light, a standard spectrum and power density has been defined to facilitate an accurate comparison between solar cells measured at different times and location. The standard spectrum at the Earth's surface is AM 1.5, which means that the sun is at an angle of about 48^{o} and the intensity is commonly fixed at 100 kW/m^2.

Open circuit voltage (V_{oc}): The maximum voltage available from a solar cell and this occurs at zero current. The open-circuit voltage corresponds to the amount of forward bias on the solar cell due to the bias of the solar cell junction with the light-generated current.

Short circuit current (I_{sc}): This is the current through the solar cell when the voltage across the solar cell is zero (i.e., when the solar cell is short circuited). The short circuit current is the maximum current that a device is able to produce.

Maximum power point: The point (I_{mpp}, V_{mpp}) on the *I-V* curve where the area of the resulting rectangle is largest as illustrated as the green rectangle in the Figure **1.15**.

Fill factor (FF): This is defined as the ratio of a photovoltaic cell's actual maximum power output to its theoretical power output if both current and voltage were at their maxima, I_{sc} and V_{oc} respectively. The formula for FF in terms of the above quantities is:

$$FF = \frac{I_{mpp} V_{mpp}}{I_{sc} V_{oc}}$$

Power conversion efficiency (PCE or η_e): The ratio of energy output from the solar cell to energy input from the sun (P_{in}). P_{in} is the sum over all wavelengths and is generally fixed at 100 kW/m^2 when solar simulators are used. The formula for PCE is defined as below:

$$\eta_e = \frac{P_{out}}{P_{in}} = \frac{I_{mpp}\, V_{mpp}}{P_{in}} = \frac{FF\ I_{sc}\, V_{oc}}{P_{in}}$$

Quantum efficiency (QE): The ratio of the number of carriers collected by the solar cell to the number of photons of incident light on the solar cell. If all photons of a certain wavelength are absorbed and the resulting minority carriers are collected, then the quantum efficiency at that particular wavelength is unity. The "external" quantum efficiency of a silicon solar cell includes the effect of optical losses such as transmission and reflection. "Internal" quantum efficiency refers to the efficiency with which photons that are not reflected or transmitted out of the cell can generate collectable carriers. By measuring the reflection and transmission of a device, the external quantum efficiency can be corrected to obtain the internal quantum efficiency.

1.4. Project goals and objectives

The objectives of the work described in this dissertation are the synthesis of organic-/inorganic hybrid BoC polymers with incorporated SQs in their polymer backbone, and functionalized SQs for optoelectronic devices and nanoporous materials.

In Chapter **3**, we discuss the synthetic routes to difunctional SQs via fluoride ion catalyzed rearrangement reaction, and polymerization to prepare BoC polymers. Chapter **4** details the synthesis and photophysical properties of conjugated BoC polymers from octaiodophenylsilsesquioxane (I_8OPS). Chapter **5** describes the functionalization of deca- and dodecavinylsilsesquioxane to produce second generation compounds via cross-metathesis, and Heck coupling and its unique photophysical properties. In Chapter **6**, we describe modification of Br_{16}OPS by Heck coupling for organic photovoltaic applications. Chapter **7** gives a discussion on the synthesis of hydroxyphenyl-terminated SQs and initial studies on their use in the formation of highly cross linked polyesters. In Chapter **8**, we present an outline of potential future work based on results discussed in this dissertation.

References Cited:

1. Voronkov, M.G.; Lavrent'yev, V.I.; "Polyhedral Oligosilsesquioxanes and Their Homo Derivatives," *Top. Curr. Chem.*, **1982**, *102*, 199-236.
2. Baney, R.H.; Itoh, M.; Sakakibara, A.; Suzuki, T.; "Silsesquioxanes," *Chem. Rev.*, **1995**, *95*, 1409-1430.
3. Loy, D.A.; Shea, K.J.; "Bridged Polysilsesquioxanes. Highly Porous Hybrid Organic-Inorganic Materials," *Chem. Rev.*, **1995**, *95*, 1431-1442.
4. Calzaferri, G.; "Silsesquioxanes," in Tailor-made Silicon-Oxygen Compounds, from molecules to materials, Corriu, R. and Jutzi, P. Ed., Friedr. Vieweg & Sohn mbH, Braunshweig/Weisbaden, Germany, **1996**, pp. 149-169.
5. Lichtenhan, J.; "Silsesquioxane-based Polymers," in Polymeric Materials Encyc., Salmon, J.C. Ed., Vol. 10, CRC Press, N.Y., **1996**, pp. 7768-7777.
6. Provatas, A.; Matisons, J.G.; "Synthesis and applications of silsesquioxanes," *Trends Polym. Sci.*, **1997**, *5*, 327-333.
7. Harrison, P. G.; "Silicate cages: precursors to new materials," *J. Orgamomet. Chem.*, **1997**, *542*, 141-183.
8. Li, G.; Wang, L.; Ni, H.; Pittman, C.U.; "Polyhedral Oligomeric Silsesquioxane (POSS) Polymers and Copolymers: A Review," *J. Inorg. Organomet. Polym.*, **2001**, *11*, 123-151.

9. Duchateau, R.; "Incompletely Condensed Silsesquioxanes: Versatile Tools in Developing Silica-Supported Olefin Polymerization Catalysts," *Chem. Rev.*, **2002,** *102,* 3525-3542.
10. Abe, Y.; Gunji, T.; "Oligo- and polysiloxanes" *Prog. Polym. Sci.*, **2004**, *29*, 149-182.
11. Phillips, S.H.; Haddad, T.S.; Tomczak, S.J.; "Developments in Nanoscience: polyhedral oligomeric silsesquioxane (POSS)-polymers," *Curr. Opin. Solid State Mater. Sci*., **2004**, *8*, 21-29.
12. Laine, R.M. "Nanobuilding blocks based on the $[OSiO_{1.5}]_x$ (x = 6, 8, 10) octa-silsesquioxanes," *J. Mater. Chem*., **2005**, *15*, 3725 – 3744.
13. Lickiss, P.D.; Rataboul, F., "Fully Condensed Polyhedral Silsesquioxanes: From Synthesis to Application," *Adv. Organomet. Chem.*, **2008**, *57*, 1-116.
14. Cordes, D. B.; Lickiss, P.D.; Franck R.; "Recent Developments in the Chemistry of Cubic Polyhedral Oligosilsesquioxanes," *Chem. Rev*., **2010**, 2081–2173.
15. Laine, R.M.; Roll, M.F.; "Polyhedral Phenylsilsesquioxanes," *Macromolecules*, **2011** *44*, 1073-1220.
16. Liu, Y.; Meng, F.; Zheng, S.; "Poly(4-vinylpyridine) Nanocrosslinked by Polyhedral Oligomeric Silsesquioxane," *Macromol. Rapid Commun*., **2005**, *26*, 920-925.
17. Abad, M. J.; Barral, L.; Fasce, D. P.; Williams, R. J.; "Epoxy Networks Containing Large Mass Fractions of a Monofunctional Polyhedral Oligomeric Silsesquioxane (POSS)," *Macromolecules*, **2003**, *36*, 3128-3135.
18. Ramirez, C.; Vilarino, J. M. L.; Abad, M. J.; Barral, L.; Bouza, R.; Cano, J.; Diez, F. J.; Garcia-Garabal, S.; Lopez, J.; "Selection of a precursor of a monofunctional polyhedral oligomeric silsesquioxane reacted with aromatic diamines," *J. Appl. Polym. Sci*., **2004**, *92*, 1576-1584.
19. Kim, G. B.; Qin, H.; Fang, X.; Sun, F. C.; Mather, P. T.; "Hybrid epoxy-based thermosets based on polyhedral oligosilsesquioxane: Cure behavior and toughening mechanisms," *J. Polym. Sci., Part B: Polym. Phys*., **2003**, *41*, 3299-3313.
20. Zhang, C.; Babonneau, F.; Bonhomme, C.; Laine, R. M.; Soles, C. L.; Hristov, H. A.; Yee, A. F.; "Highly Porous Polyhedral Silsesquioxane Polymers. Synthesis and Characterization," *J. Am. Chem. Soc*., **1998**, *120*, 8380-8391.

21. Sellinger, A.; Laine, R. M.; "Silsesquioxanes as Synthetic Platforms. 3. Photocurable, Liquid Epoxides as Inorganic/Organic Hybrid Precursors," *Chem. Mater*., **1996**, *8*, 1592-1593.
22. Choi, J.; Kim, S. G.; Laine, R. M.; "Organic/Inorganic Hybrid Epoxy Nanocomposites from Aminophenylsilsesquioxanes," *Macromolecules*, **2004**, *37*, 99-109.
23. Choi, J.; Yee, A. F.; Laine, R. M.; "Organic/Inorganic Hybrid Composites from Cubic Silsesquioxanes. Epoxy Resins of Octa(dimethylsiloxyethylcyclohexylepoxide) Silsesquioxane," *Macromolecules*, **2003**, *36*, 5666-5682.
24. Takamura, N.; Viculis, L.; Zhang, C.; Laine, R. M.; "Completely discontinuous organic/ inorganic hybrid nanocomposites by self-curing of nanobuilding blocks constructed from reactions of $[HMe_2SiOSiO_{1.5}]_8$ with vinylcyclohexene," *Polym. Int*., **2007**, *56*, 1378-1391.
25. Wada, K.; Yano, K.; Kondo, T.; Mitsudo, T.; "Preparation and the catalytic activity of novel Pd nanocluster catalysts utilizing an oligosilsesquioxane ligand," *Catal. Lett*., **2006**, *112*, 63-67.
26. Feher, F. J.; Blanski, R. L.; "Olefin polymerization by vanadium-containing silsesquioxanes: synthesis of a dialkyl-oxo-vanadium(V) complex that initiates ethylene polymerization," *J. Am. Chem. Soc*., **1992**, *114*, 5886-5887.
27. Ropartz, L.; Morris, R. E.; Schwarz, G. P.; Foster, D. F.; Cole-Hamilton, D. J.; "Dendrimer-bound tertiary phosphines for alkene hydroformylation," *Inorg. Chem. Commun*., **2000**, *3*, 714-717.
28. Ropartz, L.; Foster, D. F.; Morris, R. E.; Slawin, A. M. Z.; Cole-Hamilton, D. J.; "Hydrocarbonylation reactions using alkylphosphine-containing dendrimers based on a polyhedral oligosilsesquioxane core," *J. Chem. Soc., Dalton Trans*., **2002**, 1997-2008.
29. Maschmeyer, T.; Klunduk, M. C.; Martin, C. M.; Shephard, D. S.; Thomas, J. M.; Johnson, B. F. G.; "Modelling the active sites of heterogeneous titanium-centered epoxidation catalysts with soluble silsesquioxane analogues," *Chem. Commun*., **1997**, 1847-1848.
30. Duchateau, R.; Abbenhuis, H. C. L.; van Santen, R. A.; Meetsma, A.; Theile, S. K.-H.; van Tol, M. F. H.; "Half-Sandwich Titanium Complexes Stabilized by a Novel Silsesquioxane Ligand: Soluble Model Systems for Silica-Grafted Olefin Polymerization Catalysts," *Organomet*. **1998**, *17*, 5222-5224.

31. Solans-Monfort, X.; Filhol, J.-S.; Coperet, C.; Eisenstein, O.; "Structure, spectroscopic and electronic properties of a well defined silica supported olefin metathesis catalyst, [(≡SiO)Re(≡CR)(=CHR)(CH_2R)], through DFT periodic calculations: silica is just a large siloxy ligand," *New J. Chem.*, **2006**, *30*, 842-850.
32. Kannan, R.Y.; Salacinski, H.J.; Butler, P.E.; Seifalian, A.M.; "Polyhedral Oligomeric Silsesquioxane Nanocomposites: The Next Generation Material for Biomedical Applications," *Acc. Chem. Res.*, **2005,** 38, 879-884.
33. Wu, J.; Mather, P.T.; "POSS Polymers: Physical Properties and Biomaterials Applications," *Polym. Rev.*, **2009**, 25–63.
34. McCusker, C.; Carroll, J. B.; Rotello, V. M.; "Cationic polyhedral oligomeric silsesquioxane (POSS) units as carriers for drug delivery processes," *Chem. Commun.*, **2005**, 996-998.
35. Bassindale, A. R.; Codina-Barrios, A.; Franscione, N.; Taylor, P. G.; "The use of silsesquioxane cages and phage display technology to probe silicone–protein interactions," *New J. Chem.*, **2008**, *32*, 240-246.
36. Majumdar, P.; Lee, E.; Gubbins, N.; Stafslien, S. J.; Daniels, J.; Thorson, C. J.; Chrisholm, B. J.; "Synthesis and antimicrobial activity of quaternary ammonium-functionalized POSS (Q-POSS) and polysiloxane coatings containing Q-POSS," *Polymer*, **2009**, *50*, 1124-1133.
37. Cui, L.; Zhu, L.; "Lamellar to Inverted Hexagonal Mesophase Transition in DNA Complexes with Calamitic, Discotic, and Cubic Shaped Cationic Lipids," *Langmuir*, **2006**, *22*, 5982-5985.
38. Cui, L.; Chen, D.; Zhu, L.; "Conformation Transformation Determined by Different Self-Assembled Phases in a DNA Complex with Cationic Polyhedral Oligomeric Silsesquioxane Lipid," *ACS Nano*, **2008**, *2*, 921–927.
39. Soh, M. S.; Yap, A. U. J.; Sellinger, A.; "Methacrylate and epoxy functionalized nanocomposites based on silsesquioxane cores for use in dental applications," *Eur. Polym. J.*, **2007**, *43*, 315-327.
40. Xiao, S.; Nguyen, M.; Gong, X.; Cao, Y.; Wu, H. B.; Moses, D.; Heeger, A. J.; "Stabilization of Semiconducting Polymers with Silsesquioxane," *Adv. Funct. Mater.*, **2003**, *13*, 25-29.
41. Sellinger, A.; Tamaki, R.; Laine, R. M.; Ueno, K.; Tanabe, H.; Williams, E.; Jabbour, G. E.; "Heck coupling of haloaromatics with octavinylsilsesquioxane: solution processable

nanocomposites for application in electroluminescent devices," *Chem. Commun.*, **2005**, 3700-3702.

42. Chan, K. L.; Sonar, P.; Sellinger, A.; "Cubic silsesquioxanes for use in solution processable organic light emitting diodes (OLED)," *J. Mater., Chem.*, **2009**, *19*, 9103-9120.
43. Lo, M. Y.; Zhen, C.; Lauters, M.; Jabbour, G. E.; Sellinger, A.; "Organic−Inorganic Hybrids Based on Pyrene Functionalized Octavinylsilsesquioxane Cores for Application in OLEDs," *J. Am. Chem. Soc.*, **2007**, *129*, 5808-5809.
44. Kim, S.-G.; Sulaiman, S.; Fargier, D.; Laine, R. M.; "Octaphenyloctasilsesquioxane and Polyphenylsilsesquioxane for Nanocomposite," In *Materials Syntheses. A Practical Guide*; Schubert, U.; Husing, N.; Laine, R. M.; Eds.,; Springer-Verlag: Wien, 2008, pp. 179-191.
45. Olsson, K.; "Improved Preparation of Octakis(alkylsilsesquioxanes)," *Ark. Kemi*, **1958**, *13*, 367-378.
46. Olsson, K; Growall, C; "Octa(arylsilsesquioxanes), (ArSi)8O12 I. Phenyl, 4-Toyl, and 1-Naphtyl Compounds," *Ark. Kemi*, **1961**, *17*, 529-540.
47. Brown Jr., J. F.; Vogt, L. H.; Prescott, P. I.; "Preparation and Characterization of the Lower Equilibrated Phenylsilsesquioxanes," *J. Am. Chem. Soc.*, **1964**, *86*, 1120-1125.
48. Brown Jr., J. F.; "The Polycondensation of Phenylsilanetriol," *J. Am. Chem. Soc.*, **1965**, *87*, 4317-4324.
49. Bassindale, A. R.; Liu, Z.; MacKinnon, I. A.; Taylor, P. G.; Yang, Y.; Light, M. E.; Horton, P. N.; Jursthouse, M. B.; "A Higher Yielding Route for T8 Silsesquioxane Cages and X-Ray Crystal Structures of Some Novel Spherosilicates," *Dalton Trans.*, **2003**, 2945-2949.
50. Dare, E. O.; Liu, L.-K.; Peng, J.; "Modified Procedure for Improved Synthesis of Some Octameric Silsesquioxanes via Hydrolytic Polycondensation in the Presence of Amberlite Ion-Exchange Resins," *Dalton Trans.*, **2006**, 3668-3671.
51. Tamaki, R.; Tanaka, Y.; Asuncion, M. Z.; Choi, J.; Laine, R. M.; "Octa(aminophenyl)silsesquioxane as a Nanoconstruction Site," *J. Am. Chem. Soc.*, **2001**, *123*, 12416-12417.
52. Roll, M. F.; Mathur, P.; Takahashi, K.; Kampf, J. W.; Laine, R. M.; "$[PhSiO_{1.5}]_8$ promotes self-bromination to produce $[o\text{-}BrPhSiO_{1.5}]_8$: further bromination gives crystalline [2,5-

$Br_2PhSiO_{1.5}]_8$ with a density of 2.32 g cm^{-3} and a calculated refractive index of 1.7 or the tetraicosa bromo compound $[Br_3PhSiO_{1.5}]_8$," *J. Mater. Chem.*, **2011**, *21*, 11167-11176.

53. Roll, M. F.; Asuncion, M. Z.; Kampf, J. W.; Laine, R. M.; "*para*-Octaiodophenyl-silsesquioxane, $[p\text{-}IC_6H_4SiO_{1.5}]_8$, a Nearly Perfect Nano-Building Block," *ACS Nano*, **2008**, *2*, 320-326.
54. Kickelbick, G; "Concepts for the incorporation of inorganic building blocks into organic polymers on a nanoscale," *Prog. Polym. Sci*., **2003**, *28*, 83-114.
55. Pyun, J.; Matyjaszewski, K.; "Synthesis of Nanocomposite Organic/Inorganic Hybrid Materials Using Controlled/"Living" Radical Polymerization," *Chem. Mater*., **2001**, *13*, 3436-3448.
56. Althues, H.; Henie, J.; Kaskel, S.; "Functional inorganic nanofillers for transparent polymers," *Chem. Soc. Rev*., **2007**, *36*, 1454-1465.
57. Kuilla, T.; Bhadra, S.; Yao, D; Kim, N. H.; Bose, S.; Lee, J. H.; "Recent advances in graphene based polymer composites," *Prog. Polym. Sci*., **2010**, *35*, 1350-1375.
58. Pavlidou, S.; Papaspyrides, C. D.; "A review on polymer–layered silicate nanocomposites," *Prog. Polym. Sci*., **2008**, *33*, 1119-1198.
59. Wang, C. C.; Guo, Z. X.; Fu, S. K.; Wu, W.; Zhu, D. B.; "Polymers containing fullerene or carbon nanotube structures," *Prog. Polym. Sci*., **2004**, *29*, 1079-1141.
60. Kuo, S.-W.; Chang, F.-C.; "POSS related polymer nanocomposites," *Prog. Polym. Sci*., **2011**, *36*, 1649-1696.
61. Zhang, W.; Muller, A. H. E.; "Architecture, self-assembly and properties of well-defined hybrid polymers based on polyhedral oligomeric silsesquioxane (POSS)," *Prog. Polym. Sci*., **2013**, *38*, 1121-1162.
62. Wang, F.; Lu, X.; He, C.; "Some recent developments of polyhedral oligomeric silsesquioxane (POSS)-based polymeric materials," *J. Mater. Chem*., **2011**, *21*, 2775-2782.
63. Liu, L.; Hu, Y.; Song, L.; Nazare, S.; He, S.; Hull, R.; "Combustion and thermal properties of OctaTMA-POSS/PS composites," *J. Mater, Sci*, **2007**, *42*, 4325-4333.
64. Leu, C.-M.; Chang, Y.-T.; Wei, K.-H.; "Synthesis and Dielectric Properties of Polyimide-Tethered Polyhedral Oligomeric Silsesquioxane (POSS) Nanocomposites via POSS-diamine," *Macromolecules*, **2003**, *36*, 9122-9127.

65. Huang, J.; Xiao, Y.; Mya, K. Y.; Liu, X.; He, C.; Dai, J.; Siow, Y. P.; "Thermomechanical properties of polyimide-epoxy nanocomposites from cubic silsesquioxane epoxides," *J. Mater. Chem.*, **2004**, *14*, 2858-2863.
66. Froehlich, J. D.; Young, R.; Nakamura, T.; Ohmori, Y.; Li, S.; Mochizuki, A.; Lauters, M.; Jabbour, G. E.; "Synthesis of Multi-Functional POSS Emitters for OLED Applications," *Chem. Mater.*, **2007**, *19*, 4991-4997.
67. Madbouly, S. A.; Otaigbe, J. U.; Nanda, A. K.; Wicks, D. A.; "Rheological Behavior of POSS/Polyurethane−Urea Nanocomposite Films Prepared by Homogeneous Solution Polymerization in Aqueous Dispersions," *Macromolecules*, **2007**, *40*, 4982-4991.
68. Loh, X. J.; Zhang, Z.-X.; Mya, K. Y.; Wu, Y.-L.; He, C.; Li, J.; "Efficient gene delivery with paclitaxel-loaded DNA-hybrid polyplexes based on cationic polyhedral oligomeric silsesquioxanes," *J. Mater. Chem.*, 2010, **20**, 10634-10642.
69. Choi, J. W.; Tamaki, R.; Kim, S. G.; Laine, R. M.; "Organic/Inorganic Imide Nanocomposites from Aminophenylsilsesquioxanes," *Chem. Mater.*, **2003**, *15*, 3365-3375.
70. Sulaiman, S.; Brick, C. M.; De Sana, C. M.; Katzenstein, J. M.; Laine, R. M.; Basheer, R. A.; "Tailoring the Global Properties of Nanocomposites. Epoxy Resins with Very Low Coefficients of Thermal Expansion," *Macromolecules*, **2006**, *39*, 5167-5169.
71. Lichtenhan, J. D.; Otonari, Y. A.; Carr, M. J.; "Linear Hybrid Polymer Building Blocks: Methacrylate-Functionalized Polyhedral Oligomeric Silsesquioxane Monomers and Polymers," *Macromolecules*, **1995**, *28*, 8435-8437.
72. Tsuchida, A.; Bolln, C.; Sernetz, F. G.; Frey, H.; Mulhaupt, R.; "Ethene and Propene Copolymers Containing Silsesquioxane Side Groups," *Macromolecules*, **1997**, *30*, 2818-2814.
73. Mather, P. T.; Jeon, H. G.; Romo-Uribe, A. : Haddad, T. S.; Lichtenhan, J. D.; "Mechanical Relaxation and Microstructure of Poly(norbornyl-POSS) Copolymers," *Macromolecules*, **1999**, *32*, 1194-1203.
74. Leu, C. M.; Chang, T. Y.; Wei, K. H.; "Synthesis and Dielectric Properties of Polyimide-Tethered Polyhedral Oligomeric Silsesquioxane (POSS) Nanocomposites via POSS-diamine," *Macromolecules*, **2003**, *36*, 9122-9127.
75. Constable, G. S.; Lesser, A. J.; Coughlin, E. B.; "Morphological and Mechanical Evaluation of Hybrid Organic−Inorganic Thermoset Copolymers of Dicyclopentadiene and Mono- or

Tris(norbornenyl)-Substituted Polyhedral Oligomeric Silsesquioxanes," *Macromolecules*, **2004**, *37*, 1276-1282.

76. Lichtenhan, J. D.; Vu, N. Q.; Carter, J. A.; Gilman, J. W.; Feher, F. J.; "Silsesquioxane Siloxane Copolymers from Polyhedral Silsesquioxanes," *Macromolecules*, **1993**, *26*, 2141-2142.
77. Seino, M.; Hayakawa, T.; Ishida, Y.; Kakimoto, M.; Watanabe, K.; Oikawa, H.; "Hydrosilylation polymerization of double-decker-shaped silsesquioxane having hydrosilane with diynes," *Macromolecules*, **2006**, *39*, 3473-3475.
78. Li,Z.; Kawakami, Y.; "Formation of incompletely condensed oligosilsesquioxanes by hydrolysis of completely condensed POSS via reshuffling," *Chem. Lett*., **2008**, *37*, 804-805.
79. Hoque, M. A.; Kakihana, Y.; Shinker, S.; Kawakami, Y.; "Polysiloxanes with Periodically Distributed Isomeric Double-Decker Silsesquioxane in the Main Chain," *Macromolecules*, **2009**, *42*, 3309-3315.
80. Asuncion, M. Z.; Laine, R. M.; "Fluoride Rearrangement Reactions of Polyphenyl- and Polyvinylsilsesquioxanes as a Facile Route to Mixed Functional Phenyl, Vinyl T_{10} and T_{12} Silsesquioxanes," *J. Am. Chem. Soc*., **2010**, *132*, 3723-3736.
81. Xiang, K. H.; Pandey, R.; Pernisz, U. C.; Freeman, C.; "Theoretical Study of Structural and Electronic Properties of H-Silsesquioxanes," *J. Phys. Chem. B*, **1998**, *102*, 8704-8711.
82. Lin, T.; He, C.; Xiao, Y.; "Theoretical Studies of Monosubstituted and Higher Phenyl-Substituted Octahydrosilsesquioxane," *J. Phys. Chem. B*, **2003**, *107*, 13788-13792.
83. Mattori, M.; Mogi, K.; Sakai, Y.; Isobe, T.; "Studies on the Trapping and Detrapping Transition States of Atomic Hydrogen in Octasilsesquioxane Using the Density Functional Theory B3LYP Method," *J. Phys. Chem. A*, **2000**, *104*, 10868-10872.
84. Andre, P.; Cheng, G.; Ruseckas, A.; van Mourik, T.; Fruchtl, H.; Crayston, J. A.; Morris, R. E.; Cole-Hamilton, D.; Samuel, I. D. W.; "Hybrid Dendritic Molecule with Confined Chromophore Architecture to Tune Fluorescence Efficiency," *J. Phys. Chem. B*, **2008**, *112*, 16382-16392.
85. Vautravers. N. R.; Andre, P.; Cole-Hamilton, D.; "Fluorescence Activation of a Polyhedral Oligomeric Silsesquioxane in the Presence of Reducing Agents," *J. Mater. Chem*., **2009**, *19*, 4545-4550.

86. Sulaiman, S.; Bhaskar, A.; Zhang, J.; Guda, R.; Goodson III, T.; Laine, R. M.; "Molecules with Perfect Cubic Symmetry as Nanobuilding Blocks for 3-D Assemblies. Elaboration of Octavinylsilsesquioxane. Unusual Luminescence Shifts May Indicate Extended Conjugation Involving the Silsesquioxane Core," *Chem. Mater*., **2008**, *20*, 5563-5573.
87. R. M. Laine, S. Sulaiman, C. Brick, M. Roll, R. Tamaki, M. Z. Asuncion, M. Neurock, J. S. Filhol, C. Y. Lee, J. Zhang, T. Goodson III, M. Ronchi, M. Pizzotti, S. C. Rand, and Y. Li, "Synthesis and Photophysical Properties of Stilbeneoctasilsesquioxanes. Emission Behavior Coupled with Theoretical Modeling Studies Suggest a 3-D Excited State Involving the Silica Core," *J. Am. Chem. Soc*., **2010**, *132*, 3708.
88. Ossadnik, C.; Veprek, S.; Marsmann, H. C.; Rikowski, E.; "Photoluminescent Properties of Substituted Silsesquioxanes of the Composition $R_n(SiO_{1.5})_n$," *Monatsch. Chem*., **1999**, *130*, 55-68.
89. Azinovic, D.; Cai, J.; Eggs, C.; Konig, H.; Marsmann, H. C.; "Photoluminescence from silsesquioxanes $R_8(SiO_{1.5})_8$," *J. Luminescence*, **2002**, *97*, 40-50.
90. Mizoroki, T,; Mori, K.; Ozaki, A.; "Arylation of Olefin with Aryl Iodide Catalyzed by Palladium," *Bull. Chem. Soc. Jpn*., **1971**, *44*, 581.
91. Heck, R. F.; Nolley, J. P.; "Palladium-catalyzed vinylic hydrogen substitution reactions with aryl, benzyl, and styryl halides," *J. Org. Chem*., **1972**, *37*, 2320-2322.
92. Miyaura, N.; Yamada, K.; Suzuki, A.; "A new stereospecific cross-coupling by the palladium-catalyzed reaction of 1-alkenylboranes with 1-alkenyl or 1-alkynyl halides," *Tetrahedron Lett*., **1979**, *20*, 3437-3440.
93. Miyaura, N.; Suzuki, A.; "Stereoselective synthesis of arylated (*E*)-alkenes by the reaction of alk-1-enylboranes with aryl halides in the presence of palladium catalyst," *J. Chem. Soc., Chem. Commun*., **1979**, 866-867.
94. Sonogashira, K.; Tohda, Y.; Hagihara, N.; "A convenient synthesis of acetylenes: catalytic substitutions of acetylenic hydrogen with bromoalkenes, iodoarenes and bromopyridines," *Tetrahedron Lett*., **1975**, *16*, 4467-4470.
95. Sonogashira, K.; "Development of Pd–Cu catalyzed cross-coupling of terminal acetylenes with sp^2-carbon halides," *J. Organomet. Chem*., **2002**, *653*, 46-49.

96. Milstein, D.; Stille, J. K.; "A general, selective, and facile method for ketone synthesis from acid chlorides and organotin compounds catalyzed by palladium," *J. Am. Chem. Soc*., **1978**, *100*, 3636-3638.
97. Milstein, D.; Stille, J. K.; "Palladium-catalyzed coupling of tetraorganotin compounds with aryl and benzyl halides. Synthetic utility and mechanism," *J. Am. Chem. Soc*., **1979**, *101*, 4992-4998.
98. Negishi, E.; Baba, S.; "Novel stereoselective alkenyl–aryl coupling *via* nickel-catalysed reaction of alkenylanes with aryl halides," *J. Chem. Soc., Chem. Commun*., **1976**, 596-597.
99. Baba, S.; Negishi, E.; "A novel stereospecific alkenyl-alkenyl cross-coupling by a palladium- or nickel-catalyzed reaction of alkenylalanes with alkenyl halides," *J. Am. Chem. Soc*., **1976**, *98*, 6729-6731.
100. Du, X.; Suguro, M.; Hirabayashi, K.; Mori, A.; "Mizoroki−Heck Type Reaction of Organoboron Reagents with Alkenes and Alkynes. A Pd(II)-Catalyzed Pathway with $Cu(OAc)_2$ as an Oxidant," *Org. Lett*., **2001**, *3*, 3313-3316.
101. De, Meijere, A.; Meyer, F. E.; "Fine Feathers Make Fine Birds: The Heck Reaction in Modern Garb," *Angew. Chem. Int. Ed. Engl*., **1994**, *33*, 2379-2411.
102. Knowles, J. P.; Whiting, A.; "The Heck-Mizoroki cross-coupling reaction: a mechanistic perspective," *Org. Biomol. Chem*., **2007**, *5*, 31-44.
103. Beletskaya, I. P.; Cheprakov, A. V.; "The Heck Reaction as a Sharpening Stone of Palladium Catalysis," *Chem. Rev*., **2000**, *100*, 3009-3066.
104. Chinchilla, R.; Najera, C.; "The sonogashira Reaction: A Booming Methodology in Synthetic Organic Chemistry," *Chem. Rev*., **2007**, *107*, 874-922.
105. Chinchilla, R.; Najera, C.; "Recent advances in Sonogashira Reactions," *Chem. Soc. Rev*., **2011**,*40*, 5084-5121.
106. Diek, H. A.; Heck, R. F.; "Palladium catalyzed synthesis of aryl, heterocyclic and vinylic acetylene derivatives," *J. Organomet. Chem*., **1975**, *93*, 259-263.
107. Cassar, L.; "Synthesis of aryl- and vinyl-substituted acetylene derivatives by the use of nickel and palladium complexes," *J. Organomet. Chem*., **1975**, *93*, 253-257.

108. Li, G.; Shrotriya, V.; Huang, J. S.; Yao, Y.; Moriarty, T.; Emery, K.; Yang, Y.; "High-efficiency solution processable polymer photovoltaic cells by self-organization of polymer blends," *Nat. Mater*., **2005**, *4*, 864-868.
109. Brabec, C. J.; Sariciftci, N. S.; Hummenlen, J. C.; "Plastic Solar Cells," *Adv. Funct. Mater*., **2001**, *11*, 15-26.
110. Gunes, S.; Neugebauer, H.; Sariciftci, N. S.; "Conjugated Polymer-Based Organic Solar Cells," *Chem. Rev.*, **2007**, *107*, 1324-1338.
111. Krebs, F. C.; "Fabrication and processing of polymer solar cells: A review of printing and coating techniques," *Sol. Energy Mater. Sol. Cells*, **2009**, *93*, 394-412.
112. Akamatsu, H.; Inokuchi, H.; Matsunaga, Y.; "Electrical conductivity of the perylene-bromine complex," *Nature*, **1954**, *173*, 168-169.
113. Hertel, D.; Baessler, H.; "Photoconduction in Amorphous Organic Solids," *Chem. Phys. Chem*., **2008**, *9*, 666-688.
114. Chamberlain, G. A.; "Organic solar cells: a review," *Solar Cells*, **1983**, *8*, 47-83.
115. Tang, C. W.; "Two-layer organic photovoltaic cell," *Appl. Phys. Lett*., **1986**, *44*, 183-185
116. Smalley, R. H.; "Discovering the fullerenes," *Rev. Mod. Phys*., **1997**, *69*, 723-730.
117. Sariciftci, N. S.; Smilowitz, L.; Heeger, A. J.; Wudl, F.; "Photoinduced Electron Transfer from a Conducting Polymer to Buckminsterfullerene," *Science*, **1992**, *258*, 1474-1476.
118. Yu, G.; Gao, J.; Hummelen, J. C.; Wudl, F.; Heeger, A. J.; "Polymer Photovoltaic Cells: Enhanced Efficiencies via a Network of Internal Donor-Acceptor Heterojunctions," *Science*, **1995**, *270*, 1789-1791.
119. Shaheen, S. E.; Brabec, C. J.; Sariciftci, N. S.; "2.5% efficient organic plastic solar cells," *Apply. Phys. Lett*., **2001**, *78*, 841-843.
120. Padinger, F.; Rittberger, R. S.; Sariciftci, N. S.; "Effects of Postproduction Treatment on Plastic Solar Cells," *Adv. Funct. Mater*., **2003**, *13*, 85-88.
121. Peet, J.; Kim, J. Y.; Coates, N. E.; Ma, W. L.; Moses, D.; Heeger, A. J.; Bazan, G. C.; "Efficiency enhancement in low-bandgap polymer solar cells by processing with alkane dithiols," *Nature Mater*., **2007**, *6*, 497-500.

122. Park, S. H.; Roy, A.; Beaupre, S.; Cho, S.; Coates, N.; Moon, J. S.; Moses, D.; Leclerc, M.; Lee, K.; Heeger, A. J.; "Bulk heterojunction solar cells with internal quantum efficiency approaching 100%," *Nature Photon.*, **2009**, *3*, 297-U5.
123. Green, M. A.; Emery K.; Hishikawa, Y.; Warta, W.; "Solar cell efficiency tables (version 35)," *Prog. Photovolt.*, **2010**, *18*, 144-150.
124. Burroughes, J. H.; Bradley, D. D. C.; Brown, A. R.; Marks, R. N.; Mackay, K.; Friend, R. H.; Burns, P. L.; Holmes, A. B.; "Light-emitting diodes based on conjugated polymers," *Nature*, **1990**, *347*, 593-541.
125. Greenham, N. C.; Moratti, S. C.; Mradley, D. D. C.; Friend, R. H.; Holmes, A. B.; "Efficient light-emitting diodes based on polymers with high electron affinities," *Nature*, **1993**, *365*, 628-630.
126. Deibel, C.; Dyakonov, V.; "Polymer-fullerene bulk heterojunction solar cells," *Rep. Prog. Phys.*, **2010**, *73*, 096401.
127. Spanggaard, H.; Krebs, F. C.; "A brief history of the development of organic and polymeric photovoltaics," *Sol. Energy Mater. Sol. Cells*, **2004**, *83*, 125-146.
128. Brabec, C. J.; Zerza, G.; Cerullo, G.; Silvestri, S. D.; Luzzati, S.; Hummelen, J. C.; Sariciftci, S.; "Tracing photoinduced electron transfer process in conjugated polymer/fullerene bulk heterojunctions in real time," *Chem. Phys. Lett.*, **2001**, *340*, 232-236.
129. Montanari, I.; Nogueira, A. F.; Nelson, J.; Durrant, J. R.; Winder, C.; Loi, M. A.; Sariciftci, N. S.; Brabec, C. J.; "Transient optical studies of charge recombination dynamics in a polymer/fullerene composite at room temperature," *Appl. Phys. Lett.*, **2002**, *81*, 3001-3003.
130. Nogueira, A. F.; Montari, I.; Nelson, J.; Durrant, J. R.; Winder, C.; Sariciftci, N. S.; Brabec, C. J.; "Charge recombination in conjugated polymer/fullerene blended films studied by transient absorption Spectroscopy," *J. Phys. Chem. B*, **2003**, *107*, 1567-1573.
131. Hoppe, H.; Niggemann, M.; Winder, C.; Kraut, J.; Hiesgen, R.; Hinsch, A.; Meissner, D.; Sariciftci, N. S.; "Nanoscale morphology of conjugated polymer/fullerene-based bulk-heterojunction solar cells," *Adv. Funct. Mater.*, **2004**, *14*, 1005-1011.

Chapter 2

Experimental Techniques and Syntheses

2.1. Materials

Octaphenylsilsesquioxane [$(C_6H_5SiO_{1.5})_8$, OPS], octaaminophenylsilsesquioxane [$(NH_2C_6H_4SiO1_{.5})_8$, OAPS], octaiodophenylsilsesquioxane (I_8OPS), Octavinylsilsesquioxane (OVS) and polyvinylsilsesquioxane (PVS) were prepared using literature methods[1-5] or received as gifts from Mayaterials Inc. Octa(2,5-dibromophenyl)silsesquioxane (Br_{16}OPS) was synthesized by bromination of octaphenylsilsesquioxane (OPS) using previously reported methods.[6]

Diglycidyl ether of bisphenol A (DGEBA) (DER 331, MW 372) was purchased from Dow Chemical Corp. (Midland, MI). Tris(triphenylphosphine)CuI was prepared using literature method.[7]

Methylene chloride (CH_2Cl_2) was purchased from Fisher and distilled from CaH_2 under N_2 prior to use. Tetrahydrofuran (THF) and 1,4-dioxane was distilled from sodium benzophenone ketyl under N_2 prior to use. All other chemicals were purchased from Fisher or Aldrich and used as received. All other chemicals were purchased from Aldrich or Fisher and used as received. All manipulations were performed under nitrogen unless otherwise stated.

2.2. Analytical Techniques

Gel permeation chromatography (GPC)

All GPC analyses were done on a Waters 440 system equipped with Waters Styragel columns (7.8 x 300, HT 0.5, 2, 3, 4) with RI detection using Optilab DSP interferometric refractometer and THF as solvent. The system was calibrated using polystyrene standards and toluene as reference. Analyses were performed using PL Caliber 7.04 software (Polymer Labs, Shropshire UK).

Matrix-assisted laser desorption/time-of-flight spectrometry

MALDI-ToF was done on a Micromass TofSpec-2E equipped with a 337 nm nitrogen laser in positive-ion reflection mode using poly(ethylene glycol) as calibration standard, dithranol as matrix, and $AgNO_3$ as ion source. Sample was prepared by mixing solution of 5 parts matrix (10 mg/mL in THF), 5 parts sample (1 mg/mL in THF), and 1 part of $AgNO_3$ (2.5 mg/mL in water) and blotting the mixture on the target plate.

NMR analyses

All ^1H were run in DMSO on a Varian INOVA 500 spectrometer. ^1H-NMR spectra were collected at 500 MHz using a 7998.4 Hz spectral width, a relaxation delay of 0.5s, a pulse width of 45˚, 65 k data points, and TMS (0.00ppm) as an internal reference.

Diffuse reflectance Fourier-transform infrared spectroscopy (DRIFTS)

IR spectra were recorded on a Nicolet 6700 Series FTIR spectrometer (Thermo Fisher Scientific, Inc., Madison, WI). Optical grade, random cuttings of KBr (International Crystal Laboratories, Garfield, NJ) were ground, with 1.0 wt % of the sample to be analyzed. For DRIFT analyses, samples were packed firmly and leveled off at the upper edge to provide a smooth surface. The FTIR sample chamber was flushed continuously with N_2 prior to data acquisition in the range 4000-400 cm^{-1} with a precision of ± 4 cm^{-1}.

Thermalgravimetric analyses (TGA)

Thermal stabilities of materials under N_2 or air were examined using a 2960 simultaneous DTA-TGA (TA Instruments, Inc., New Castle, DE). Samples (5-10 mg) were loaded in alumina pans and ramped to 1000 ℃ while heating at 5 ℃/min in N_2 or air flow rates of 60 mL/min.

UV-Vis spectrometry

UV-vis measurements were recorded on an Agilent (model 8341) spectrophotometer using spectrophotometric grade dried THF as solvent. Concentrations were typically 10^{-6}-10^{-7} M, to give absorption maxima of approximately 50% for a 0.5 cm path length.

Photoluminescence spectrometry

Photoluminescence measurements were obtained on a Horiba Fluoromax-2 fluorimeter in THF. The compounds were studied at their respective maximum absorption wavelengths. Samples from UV-vis measurements were diluted to ~10^{-7} M, in order to reduce the likelihood of excimer formation and fluorimeter detector saturation.

Photoluminescence quantum yields (Φ_{PL})

Φ_{PL} was determined by comparison between a standard and the sample.[8] Each sample was compared for Φ_{PL} with Bis-MSB (1,4-bis(2-methylstyryl)benzene) at different wavelengths, in order to account for the most similar concentration between standard and sample. The solutions were diluted to provide three sets of concentrations with absorptions ranging from 0.01-0.04, to reduce fluorimeter saturation and excimer formation. The total area of emission for each sample and the standard was calculated by first subtracting out the background signal, and then calculating the area. The experiments were repeated at least two times, and averaged. To obtain the best accuracy, the slope of a plot of emission versus absorption was determined and calculated according to the equation;

$$\Phi_{PL}\,(x) = \left(\frac{A_s}{A_x}\right)\left(\frac{F_x}{F_s}\right)\left(\frac{n_x}{n_s}\right)^2 \Phi_{PL}(s)$$

where Φ_{PL} is the quantum yield, A is the absorption at the excitation wavelength, F is the total integrated emission, and n is the refractive index of the solution, which due to low concentration, can be approximated as the refractive index of the solvent. Subscripts x and s refer to the sample and reference respectively. These measurements may have some error (±1%) due to the sensitivity of the fluorescence spectrophotometer and other environmental conditions.

Two-photon studies

Two-Photon Excited Fluorescence Measurements

To measure the TPA cross sections, we followed the two-photon excited fluorescence (TPEF) method.[9] A 10^{-5} M solution of Coumarin-307 in methanol or Bis-MSB in cyclohexane was used as reference. The laser used for the study was a SpectraPhysics Mai Tai diode-pumped

mode-locked Ti: sapphire laser. The laser wavelength was varied from 760 nm to 820 nm, with an average band-width of ~30 nm, with a ~100 fs pulse, with 650 nm wavelengths achieved by using a SpectraPhysics OPAL and beam-doubling system pumped at 775 nm. The input power from the laser was varied by using a polarizer. An iris was placed prior to the polarizer in order to ensure a circular beam. The beam from the polarizer was focused on the sample cell (quartz cuvette, 0.5 cm path length) using a lens with a focal length of 11.5 cm. The fluorescence was collected in a direction perpendicular to the incident beam. A 2.54 cm focal length plano-convex lens was used to direct the collected fluorescence into a monochromator. The output from the monochromator was coupled to a photomultiplier tube. The photons were converted into counts by a photon-counting unit. A logarithmic plot between collected fluorescence photons and input intensity gave a slope of 2, ensuring a quadratic dependence between the same.[10] The intercept enabled us to calculate the TPA cross-section from the action cross-section by multiplying by the fluorescence quantum yield of the sample.

2.3. Syntheses

2.3.1. Beads on a Chain (BoC) polymers formed from $[NH_2PhSiO_{1.5}]_x[PhSiO_{1.5}]_{10-x}$ and $[NH_2PhSiO_{1.5}]_x[PhSiO_{1.5}]_{12-x}$ mixtures (x = 2-4)

Synthesis of $[NH_2PhSiO_{1.5}]_x[PhSiO_{1.5}]_{10/12-x}$ (x = 2-4)

To an oven-dried, 100 ml Schlenk flask under N_2, equipped with a magnetic bar was added 0.27 g (0.24 mmol) of OAPS and 0.73 g (0.47 mmol) of OPS. THF (20 ml) was added by syringe followed by 0.036 mL (0.036 mmol, 5.0 mol % OPS and OAPS) of 95 % tetra-*n*-butyl ammonium fluoride (TBAF) solution (1.0 M in THF). The mixture was stirred at room temperature for 72 h and any unreacted OPS was removed by filtration in N_2. Calcium chloride powder ($CaCl_2$, 0.6 g) was added to the filterate and the mixture stirred at room temperature for 2 h. After filtering again, solvent was dried *in vacuo* providing 0.85 g of a dark brown solid equal to an 85 % yield. This solid was purified by column chromatography on silica. The product was eluted using an 8:2 ratio of methylene chloride:hexane followed by THF (column yield: 30 %). Characterization data: ^{1}H-NMR (DMSO, δ ppm): 4.5-5.5 (br, -NH_2), 6.5-8.0 (br, Ar-*H*). FTIR (cm^{-1}): 3380 (νN-H), 3230-2840 (νC-H, aromatic), 1594, 1430 (νC=C, aromatic), 1131 (νSi-O).

MALDI-ToF: *m/z*= 1171 [$AgSi_8O_{12}(C_6H_5)_6(NH_2C_6H_4)_2$], 1324 [$Si_{10}O_{15}(C_6H_5)_8(NH_2C_6H_4)_2$], 1340 [$Si_{10}O_{15}(C_6H_5)_7(NH_2C_6H_4)_3$], 1430 [$AgSi_{10}O_{15}(C_6H_5)_8(NH_2C_6H_4)_2$], 1444 [$AgSi_{10}O_{15}$-$(C_6H_5)_7(NH_2C_6H_4)_3$], 1583 [$Si_{12}O_{18}(C_6H_5)_{10}(NH_2C_6H_4)_2$], 1599 [$Si_{12}O_{18}(C_6H_5)_9(NH_2C_6H_4)_3$], 1171 [$AgSi_{12}O_{18}(C_6H_5)_{10}(NH_2C_6H_4)_2$] amu (Table **3.5**). GPC(found): M_n = 1250; M_w = 1290; PDI = 1.04. TGA (air, 1000 ℃): found = 45.1 %; $T_{d5\%}$= 450 ℃.

Polymerization of $[NH_2PhSiO_{1.5}]_x[PhSiO_{1.5}]_{10/12-x}$ (x = 2-4) with DGEBA

To a dry 25 mL round bottom flask equipped with magnetic stirrer $[NH_2PhSiO_{1.5}]_x$-$[PhSiO_{1.5}]_{10/12-x}$ (x = 2-4) were added (1.0 g, 2.0 mmol of NH_2PH) and DGEBA (0.30 g, 0.81 mmol, 1.6 mmol of epoxy group). The flask was evacuated and flushed three times with N_2. 1,4-dioxane (10 mL) was added via syringe. The reaction mixture was stirred at 90 ℃ for 24 h and monitored by GPC. Thereafter the reaction mixture was precipitated into 150 mL MeOH. The precipitated products were collected and dried *in vacuo* to give a brown powder (0.95 g, 73 %). The product was further purified by selective dissolution in THF. Thus, 0.5 g of product was added to 10 ml THF and stirred 2 h at room temperature. The solution was filtered and filtrate was precipitated in 100 ml of methanol (low molecular weight polymer, 0.21 g, 40 %). The insoluble polymer was collected and 10 ml of THF was again added. This solution was sonicated for 6 h at 60 ^oC then filtered and the filtrate precipitated in 100 ml of methanol (high molecular weight polymer, 0.15 g, 30 %). *Note that to avoid formation of highly crosslinked products only 80 mol % epoxy is added*. Characterization data: ^{1}H-NMR (DMSO, δ ppm): 1.2 (br, -C*H*$_3$), 3.5-4.3 (br, ArC*H*$_2$C*H*$_2$C*H*OHC*H*$_2$), 4.7-5.6 (br, -N*H*), 6.0-7.9 (br, Ar-*H*). FTIR (cm^{-1}): 3500 (νN-H), 3100-2800 (νC-H, aromatic), 1595 (νC=C, aromatic), 1250 (νC-O), 1131 (νSi-O). GPC (found): M_n = 9,000; M_w = 74,000,000; PDI = 8,000. TGA (air, 1000 ℃): found = 33.0 %; $T_{d5\%}$ = 280℃.

2.3.2. Synthesis and characterization of conjugated BoC polymers from octaiodophenyl-silsesquioxane (I_8OPS)

Polymerization of I_8OPS and divinylbenzene (DVB) (**Polymer I**)

To an oven dried 100 mL Schlenk flask under N_2 was added 1.0 g (0.49 mmol) of I_8OPS, 40 mg (0.08 mmol) of $Pd[P(t\text{-}Bu)_3]_2$ and 36 mg (0.04 mmol) of $Pd_2(dba)_3$. 1,4-dioxane (20 mL) was added by syringe, followed by 0.9 mL (4.3 mmol) of NCy_2Me and 20 μL (0.14 mmol) of

DVB. The mixture was heated with stirring at 60 ^{o}C under N_2. After 24 h, an additional 5 μL (0.04 mmol) of DVB was added and stirring was continued for another 24 h, followed by cooling to ambient. The reaction mixture was then filtered through 1 cm Celite and precipitate into 150 mL of methanol.

The resulting solid was filtered off, redissolved in 10 mL THF, filtered through another 1 cm Celite column to remove remaining Pd particles and reprecipitated into 150 mL methanol. The product was further purified by column chromatography (silica, THF). The resulting solid was vacuum dried for 6 h at 80 ^{o}C, giving 0.65 g (65 % yield). Characterization data: ^{1}H-NMR (DMSO, δ ppm): 8.2-6.5 (br, Ar-*H*), FTIR (cm^{-1}): 3028 (νC-H, aromatics), 1598 (νC=C), 1134 (νSi-O), GPC: Mn = 9 K, Mw = 27 K, PDI = 2.9. TGA (air, 1000 ℃): found = 27.4 %, calc. = 25.1 %, $T_{d5\%}$ = 300 ℃.

General Heck reaction of **Polymer I (Polymers II-IV)**

To a oven dried 100 mL Schlenk flask under N_2 was added 1.0 g of **Polymer I**, 30 mg (0.06 mmol) of Pd[P(*t*-Bu)$_3$]$_2$ and 27 mg (0.03 mmol) of $Pd_2(dba)_3$. 1,4-dioxane (20 mL) was added by syringe, followed by 0.6 mL (2.9 mmol) of NCy_2Me and 9.0 mmol of R-styrene. The mixture was heated with stirring at 60 ^{o}C under N_2 for 72 h and then quenched by filtering through a 1 cm Celite. The solution was precipitated into 150 mL methanol and filtered. The solid was further purified by column chromatography to remove low molecular weight monomeric SQs as above.

Heck reaction of **Polymer I** and styrene (**Polymer II**)

Polymer **I** and styrene (1.1 mL) were allowed to react according to the above general procedure. The solid was further purified by column chromatography (silica, 1:1 of methylene chloride:hexane). The resulting solid was vacuum dried for 4 h and was obtained as a white solid (0.7 g, 54 % yield). Characterization data: ^{1}H-NMR (DMSO, δ ppm): 8.2-6.5 (br, Ar-*H*), FTIR (cm^{-1}): 3024 (νC-H, aromatic), 1600 (νC=C), 1131 (νSi-O), GPC: Mn = 17 K, Mw = 37 K, PDI = 2.2. TGA (air, 1000 ℃): found = 29.4 %, calc. = 27.1 %, $T_{d5\%}$ = 300 ℃.

Heck reaction of **Polymer I** and vinylanisole (**Polymer III**)

Polymer **I** and *p*-vinylanisole (1.2 mL) were allowed to react according to the above general procedure. The solid was further purified by column chromatography (silica, 2:1 of methylene chloride:hexane). The resulting solid was vacuum dried for 4 h and was obtained as a white solid (0.68 g, 48 % yield). Characterization data: ^{1}H-NMR (DMSO, δ ppm): 8.2-6.5 (br, Ar-*H*), 3.7 (s, C*H*$_3$). FTIR (cm^{-1}): 3023 (νC-H, aromatic), 2931 (νC-H, alkane), 1597 (νC=C), 1250 (νC-O), 1131 (νSi-O), GPC: Mn = 24 K, Mw = 54 K, PDI = 2.2. TGA (air, 1000 ℃): found = 25.7 %, calc. = 24.6 %, $T_{d5\%}$ = 355 ℃.

Heck reaction of **Polymer I** and vinylaniline (**Polymer IV**)

Polymer **I** and *p*-vinylaniline (1.0 mL) were allowed to react according to the above general procedure. The solid was further purified by column chromatography (silica, 5:1 of THF:hexane). The resulting solid was vacuum dried for 4 h and was obtained as a yellowish solid (0.62 g, 48 % yield). Characterization data: ^{1}H-NMR (DMSO, δ ppm): 8.2-6.5 (br, Ar-*H*), 5.3 (br, N*H*$_2$). FTIR (cm^{-1}): 3381 (νN-H), 3023 (νC-H aromatic), 2929 (νC-H, alkane), 1618 (νC=C), 1130 (νSi-O), GPC: M_n = 21 K, M_w = 31 K, PDI = 1.5. TGA (air, 1000 ℃): found = 27.4 %, calc. = 25.8 %, $T_{d5\%}$ = 370 ℃.

General procedure for the preparation of diiodophenyl SQs (**Monomers A, B and C**)

To an oven dried 100 mL Schlenk flask under N_2 was added 1.0 g (0.49 mmol) of I_8OPS, 40 mg (0.08 mmol) of Pd[P(*t*-Bu)$_3$]$_2$ and 36 mg (0.04 mmol) of Pd$_2$(dba)$_3$. 1,4-dioxane (20 mL) was added by syringe, followed by 0.9 mL (4.3 mmol) of NCy$_2$Me and 2.9 mmol (6 eq.) of *p*-R-styrene. The mixture was heated with stirring at 60 ^{o}C under N_2 for 72 h and then quenched by filtering through 1 cm Celite. The solution was precipitated into 150 mL methanol and filtered. The solid was used for polymerization without further purification.

(I-Ph)$_2$(stilbene)$_6$ T_8 SQ (Monomer **A**)

I_8OPS and styrene (0.4 mL) were allowed to react according to the above general procedure. The resulting solid was vacuum dried for 4 h and was obtained as a white solid (1.22 g, 87 % yield). Characterization data: ^{1}H-NMR (DMSO, δ ppm): 8.0-6.5 (br, Ar-*H*, -C*H*=C*H*-),

FTIR (cm^{-1}): 3024 (νC-H, aromatic), 1574 (νC=C), 1132 (νSi-O), GPC: M_n = 1,870, M_w = 1,900, PDI = 1.01, TGA (air, 1000 ℃): found = 25.5 %, calc. = 25.3 %, $T_{d5\%}$ = 390 ℃.

(I-Ph)$_2$(methoxystilbene)$_6$ T_8 SQ (Monomer **B**)

I_8OPS and *p*-vinylanisole (0.4 mL) were allowed to react according to the above general procedure. The resulting solid was vacuum dried for 4 h and was obtained as a white solid (1.13 g, 81 % yield). Characterization data: ^{1}H-NMR (DMSO, δ ppm): 8.2-6.5 (br, Ar-*H*, -C*H*=C*H*-), 3.7 (s, -OCH_3). FTIR (cm^{-1}): 3029 (νC-H, aromatic), 2931 (νC-H, alkane), 1596 (νC=C), 1251 (νC-O), 1132 (νSi-O). GPC: M_n = 2,050, M_w = 2,090, PDI = 1.02, TGA (air, 1000 ℃): found = 23.2 %, calc. = 23.1 %, $T_{d5\%}$ = 315 ℃.

(I-Ph)$_2$(aminostilbene)$_6$ T_8 SQ (Monomer **C**)

I_8OPS and *p*-vinylaniline (0.35 mL) were allowed to react according to the above general procedure. The resulting solid was vacuum dried for 4 h providing a yellow solid (1.05 g, 78 % yield). Characterization data: ^{1}H-NMR (DMSO, δ ppm): 8.0-6.8 (br, Ar-*H*), 6.6 (br, -C*H*=C*H*-), 5.4 (br, NH_2). FTIR (cm^{-1}): 3383 (νN-H), 3025 (νC-H, aromatic), 1594 (νC=C), 1131 (νSi-O), GPC: M_n = 2,190, M_w = 2,260, PDI = 1.03, TGA (air, 1000 ℃): found = 24.6 %, calc. = 24.2 %, $T_{d5\%}$ = 395 ℃.

General Polymerization of diiodophenyl SQ and divinylbenzene (DVB) (**Polymers V-VIII**)

To an oven dried 100 mL Schlenk flask under N_2 was added 1.0 g diiodophenyl SQ, 10 mg (0.02 mmol) of Pd[P(*t*-Bu)$_3$]$_2$ and 10 mg (0.01 mmol) of Pd_2(dba)$_3$. 1,4-dioxane (20 mL) was added by syringe, followed by 0.2 mL (1.0 mmol) of NCy_2Me and 35 μL (0.25 mmol) of DVB. The mixture was heated with stirring at 60 ^{o}C under N_2. After 24 h, an additional 15 μL (0.12 mmol) of DVB was added and stirring was continued for another 24 h, followed by cooling to ambient. The reaction mixture was then filtered through a 1 cm Celite and precipitate into 150 mL of methanol. The resulting solid was filtered off, redissolved in 10 mL THF, filtered through another 1 cm Celite column to remove remaining Pd particles and reprecipitated into 150 mL methanol. The product was further purified by column chromatography.

Polymerization of (I-Ph)$_2$(stilbene)$_6$ T_8 SQ and DVB (**Polymer V**)

(I-Ph)$_2$(stilbene)$_6$ T_8 SQ was allowed to react according to the above general procedure. The solid was further purified by column chromatography (silica, 2:1 of methylene chloride:hexane). The resulting solid was vacuum dried for 4 h and was obtained as a white solid (0.52 g, 51 % yield). Characterization data: ^{1}H-NMR (DMSO, δ ppm): 8.2-6.5 (br, Ar-*H*, -C*H*=C*H*-). FTIR (cm^{-1}): 3024 (νC-H), 1600 (νC=C), 1132 (νSi-O), GPC: Mn = 12 K, Mw = 20 K, PDI = 1.7. TGA (air, 1000 ℃): found = 28.2 %, calc. = 27.1 %, $T_{d5\%}$ = 370 ℃.

Polymerization of (I-Ph)$_2$(methoxystilbene)$_6$ T_8 SQ and DVB (**Polymer VI**)

(I-Ph)$_2$(methoxystilbene)$_6$ T_8 SQ was allowed to react according to the above general procedure. The solid was further purified by column chromatography (silica, 2:1 of methylene chloride:hexane). The resulting solid was vacuum dried for 4 h and was obtained as a white solid (0.55 g, 56 % yield). Characterization data: ^{1}H-NMR (DMSO, δ ppm): 8.2-6.5 (br, Ar-*H*, -C*H*=C*H*-), 3.7 (s, -OCH_3). FTIR (cm^{-1}): 3022 (νC-H, aromatic), 2931 (νC-H, alkane), 1597 (νC=C), 1251 (νC-O), 1130 (νSi-O), GPC: M_n = 30 K, M_w = 72 K, PDI = 2.4. TGA (air, 1000 ℃): found = 25.6 %, calc. = 24.6 %, $T_{d5\%}$ = 320 ℃.

Polymerization of (I-Ph)$_2$(aminostilbene)$_6$ T_8 SQ and DVB (**Polymer VII**)

(I-Ph)$_2$(aminostilbene)$_6$ T_8 SQ was allowed to react according to the above general procedure. The solid was further purified by column chromatography (silica, 1:5 of hexane:THF). The resulting solid was vacuum dried for 4 h giving a white solid (0.43, 44 % yield). Characterization data: ^{1}H-NMR (DMSO, δ ppm): 8.0-6.6 (br, Ar-*H*, -C*H*=C*H*-), 5.3 (br, NH_2). FTIR (cm^{-1}): 3383 (νN-H), 3021 (νC-H, aromatic), 2961 (νC-H, alkane), 1595 (νC=C), 1130 (νSi-O), GPC: M_n = 22 K, M_w = 30 K, PDI = 1.4. TGA (air, 1000 ℃): found = 26.7 %, calc = 25.8 %, $T_{d5\%}$ = 300 ℃.

Copolymerization of (I-Ph)$_2$(methoxystilbene)$_6$ T_8 SQ and (I-Ph)$_2$(aminostilbene)$_6$ T_8 SQ and DVB (**Polymer VIII**)

0.5 g of (I-Ph)$_2$(methoxystilbene)$_6$ T_8 SQ and 0.5 g of (I-Ph)$_2$(aminostilbene)$_6$ T_8 SQ were allowed to react according to the above general procedure. The solid was further purified

by column chromatography (silica, 1:2 of hexane:THF). The resulting solid was vacuum dried for 4 h giving a white solid (0.47 g, 48 % yield). Characterization data: ^{1}H-NMR (DMSO, δ ppm): 8.0-6.6 (br, Ar-*H*, -C*H*=C*H*-), 5.3 (br, NH_2), 3.7 (s, -OCH_3). FTIR (cm^{-1}): 3383 (νN-H), 3022 (νC-H, aromatic), 1596 (νC=C), 1251 (νC-O), 1131 (νSi-O), GPC: Mn = 8 K, Mw = 21 K, PDI = 2.7. TGA (air, 1000 ℃): found = 25.8 %, calc. = 25.2 %, $T_{d5\%}$ = 310 ℃.

General Polymerization of diiodophenyl SQ and 1,4-diethynyl benzene (DEB) (**Polymers IX-XII**)

To an oven dried 100 mL Schlenk flask under N_2 was added 1.0 g diiodophenyl SQ, 10 mg (0.02 mmol) of Pd[P(*t*-Bu)$_3$]$_2$, 10 mg (0.01 mmol) of $Pd_2(dba)_3$ and 68 mg (0.07 mmol) of Tris(triphenylphosphine)CuI. 1,4-dioxane (20 mL) was added by syringe, followed by 0.2 mL (1.0 mmol) of NCy_2Me and 50 μL (0.50 mmol) of DEB solution in 1,4-dioxane (0.1 g/mL). The mixture was heated with stirring at 60 ^{o}C under N_2. After 24 h, an additional 20 μL (0.20 mmol) of DEB solution was added and stirring was continued for another 24 h, followed by cooling to ambient. The reaction mixture was then filtered through a 1 cm Celite and precipitate into 150 mL of methanol then the resulting solid was filtered off. The product was further purified by column chromatography.

Polymerization of (I-Ph)$_2$(stilbene)$_6$ T_8 SQ and DEB (**Polymer IX**)

(I-Ph)$_2$(stilbene)$_6$ T_8 SQ was allowed to react according to the above general procedure. The solid was further purified by column chromatography (silica, 2:1 of methylene chloride: hexane). The resulting solid was vacuum dried for 4 h and was obtained as a white solid (0.52 g, 51 % yield). Characterization data: ^{1}H-NMR (DMSO, δ ppm): 8.2-6.5 (br, Ar-*H*, -C*H*=C*H*-). FTIR (cm^{-1}): 3024 (νC-H, aromatic), 1599 (νC=C), 1130 (νSi-O), GPC: M_n = 16 K, M_w = 27 K, PDI = 1.7. TGA (air, 1000 ℃): found = 28.1 %, calc. = 27.2 %, $T_{d5\%}$ = 370 ℃.

Polymerization of (I-Ph)$_2$(methoxystilbene)$_6$ T_8 SQ and DEB (**Polymer X**)

(I-Ph)$_2$(methoxy-stilbene)$_6$ T_8 SQ was allowed to react according to the above general procedure. The solid was further purified by column chromatography (silica, 2:1 of methylene chloride:hexane). The resulting solid was vacuum dried for 4 h and was obtained as a white solid

(0.55 g, 54 % yield). Characterization data: ^{1}H-NMR (DMSO, δ ppm): 8.2-6.5 (br, Ar-*H*, -C*H*=C*H*-), 3.7 (s, -OCH_3). FTIR (cm^{-1}): 3024 (νC-H, aromatic), 2931 (νC-H, alkane), 1597 (νC=C), 1251 (νC-O), 1130 (νSi-O), GPC: Mn = 16 K, Mw = 20 K, PDI = 1.3. TGA (air, 1000 ℃): found = 24.3 %, calc. = 24.7 %, $T_{d5\%}$ = 300 ℃.

Polymerization of (I-Ph)$_2$(aminostilbene)$_6$ T_8 SQ and DEB (**Polymer XI**)

(I-Ph)$_2$(*p*-aminostilbene)$_6$ T_8 SQ was reacted according to the above general procedure. The solid was further purified by column chromatography (silica, 1:5 of hexane:THF). The resulting solid was vacuum dried for 4 h and was obtained as a white solid (0.40, 39 % yield). Characterization data: ^{1}H-NMR (DMSO, δ ppm): 8.0-6.3 (br, Ar-*H*, -C*H*=C*H*-), 5.3 (br, NH_2). FTIR (cm^{-1}): 3381 (νN-H), 3022 (νC-H, aromatic), 2961 (νC-H, alkane), 1595 (νC=C), 1131 (νSi-O), GPC: M_n = 10 K, M_w = 19 K, PDI = 1.9. TGA (air, 1000 ℃): found = 26.7 %, calc. = 25.9 %, $T_{d5\%}$ = 330 ℃.

Copolymerization of (I-Ph)$_2$(methoxystilbene)$_6$ T_8 SQ and (I-Ph)$_2$(aminostilbene)$_6$ T_8 SQ and DEB (**Polymer XII**)

0.5 g of (I-Ph)$_2$(methoxystilbene)$_6$ T_8 SQ and 0.5 g of (I-Ph)$_2$(amino-stilbene)$_6$ T_8 SQ was reacted according to the above general procedure. The solid was further purified by column chromatography (silica, 1:2 of hexane:THF). The resulting solid was vacuum dried for 4 h giving a white solid (0.47 g, 48 % yield). Characterization data: ^{1}H-NMR (DMSO, δ ppm): 8.0-6.6 (br, Ar-*H*, -C*H*=C*H*-), 5.3 (br, NH_2), 3.7 (s, -OCH_3). FTIR (cm^{-1}): 3381 (νN-H), 3027 (νC-H, aromatic), 1595 (νC=C), 1250 (νC-O), 1130 (νSi-O), GPC: M_n = 9 K, M_w = 22 K, PDI = 2.5. TGA (air, 1000 ℃): found = 25.5 %, calc. = 25.3 %, $T_{d5\%}$ = 340 ℃.

2.3.3. Synthesis and characterization of second generation (GEN2) derivatives by functionalization of vinyl $T_{10/12}$ silsesquioxanes

Synthesis of Vinyl$_x$ (x = 10, 12 and 14) T_{10}, T_{12} and T_{14} SQs

PVS (95 g, 1.2 mol) was placed in a 5 L round bottom flask equipped with magnetic stirrer. 4.0 L THF was added to the flask. PVS was insoluble in THF at this stage. To the

suspension of PVS in THF, 2.0 mL of 1.0 M TBAF (2.0 mmol) was added dropwise. PVS started to dissolve to THF and became a homogeneous solution in a few hours. The solution was stirred further 72 h at room temperature. To quench the reaction, $CaCl_2$ (100 g, 0.9 mol) was added and stirred an additional 5 h. $CaCl_2$ was then filtered off and THF was removed from the filtrate under reduced pressure. The solid residue was washed with 100 mL deionized water for three times until the chloride ion was not detected by the $AgNO_3$ test. The product was collected and dried in vacuo to give a white powder (93g, 98% with respect to the initial mass of PVS). Characterization data: MALDI-ToF: *m*/*z* (Ag^+ adduct) = 829 [$AgSi_9O_{14}H_1(C_2H_3)_9$], 899 [$AgSi_{10}O_{15}(C_2H_3)_{10}$], 988 [$AgSi_{11}O_{17}H_1(C_2H_3)_{11}$], 1057 [$AgSi_{12}O_{18}(C_2H_3)_{12}$], 1216 [$AgSi_{14}O_{21}$-$(C_2H_3)_{14}$] amu. GPC (found): M_n = 790; M_w = 828; PDI = 1.05.

Gen 1 via Heck Chemistry

General reaction of vinyl$_x$ (x = 10, 12 and 14) T_{10}, T_{12} and T_{14} SQs

A dry 50 mL round bottom Schlenk flask under N_2 was charged with Pd[P(*t*-Bu_3)]$_2$ (194 mg, 0.38 mmol). 1,4-Dioxane (10 mL) was added and the mixture was stirred at room temperature, resulting in a homogeneous orange solution. Bromo-compounds (14.3 mmol), NCy_2Me (4.0 mL, 19.0 mmol) and vinylT_{10}/T_{12} (1.0 g, 12.7 mmol vinyl group, solution in 2 mL of dioxane) were then added successively via syringe. The resulting solution was allowed to stir at room temperature for 72 h. The solution became light-brown in color, and white amine hydrochloride salt precipitates were observed. The solution was stirred further at 60 ℃ for 48 h to complete the reaction. The reaction mixture was cooled to ambient and filtered through 2 cm Celite to remove precipitates. The catalyst was quenched and product coincidentally precipitated into 200 mL of methanol. The products were isolated by filtration and dried *in vacuo* to give a powder characterized by methods described below. Tabulated characterization data are presented in the text (Table **5.1**).

Double Heck addition reactions of vinyl$_{10/12}$SQs

A dry 50 mL round bottom Schlenk flask under N_2 was charged with Pd[P(*t*-Bu_3)]$_2$ (97 mg, 0.19 mmol). 1,4-Dioxane (10 mL) was added and the mixture stirred at room temperature, resulting in a homogeneous orange solution. Bromo-compounds (14.3 mmol), NCy_2Me (4.0 mL,

19.0 mmol) and vinyl $T_{10/12}$-silsesquioxane (0.5 g, 6.3 mmol vinyl group, solution in 2 mL of dioxane) were then added successively via syringe. The resulting solution was allowed to stir at 90 ℃ for 24 h. The solution turned canary-yellow, and white amine hydrochloride salt precipitates formed. The catalyst was quenched and product coincidentally precipitated into 200 mL of methanol. The products were filtered off and dried *in vacuo* to give a powder characterized by the methods described below. Tabulated characterization data are presented in the text (Table **5.1**).

Gen1 via Metathesis

To a dry 25 mL Schlenk flask under N_2 was added 0.40 g (5.1 mmol of vinyl group) of vinyl$T_{10/12}$ and 21.0 mg (0.026 mmol, 0.5 mol %) of first generation Grubbs catalyst. Dry CH_2Cl_2 (6 mL) was added by syringe followed by *p*-R-styrene (7.56 mmol). The mixture was stirred at 40 ^oC for 72 h and then quenched in 200 mL of methanol. The solution was filtered and the powder was further purified by column chromatography (THF/hexane eluent mixtures system). Tabulated characterization data are presented in the text (Table **5.2**).

General Heck reaction of *p*-BrStyrenyl $T_{10/12}$ SQs (GEN2 compounds)

To a dry 50 mL Schlenk flask under N_2 was added 0.50 g (2.1 mmol of Br) of *p*-BrStyrenyl$T_{10/12}$, 19 mg (0.04 mmol, 2 mol %) of $Pd[P(t\text{-}Bu)_3]_2$, and 18 mg (0.02 mmol, 1 mol %) of $Pd_2(dba)_3$. Dry 1,4-dioxane (10 mL) was added by syringe, followed by NCy_2Me (2.11 mmol, 0.45 mL) and *p*-R-styrene (6.4 mmol). The resulting solution was allowed to stir at room temperature for 72 h. The reaction mixture was filtered through 1 cm Celite to remove ammonium chloride precipitate. The solution was then quenched by precipitation into 200 mL of methanol and filtered. The isolated solid was redissolved in 10 mL of THF and filtered again through a 2 cm Celite to remove any remaining Pd particles and reprecipitated into 200 mL of methanol. The solution was filtered and the powder was further purified by column chromatography. The characterization data are presented in tabular form in the text (Table **5.3**).

2.3.4. Functionalization of Br_{16}OPS for bulk heterojunction (BHJ) organic photovoltaics

General Heck coupling of Br_{16}OPS

To a dry 25 mL Schlenk flask under N_2 was added 1.0 g of Br_{16}OPS (7.0 mmol of Br), 71 mg (0.14 mmol) of $Pd[P(t\text{-}Bu)_3]_2$, 64 mg (0.07 mmol) of $Pd_2(dba)_3$. 1,4-dioxane (10 ml) was then added by syringe followed by NCy_2Me (1.6 ml, 7.7 mmol) and R-styrene (20.9 mmol, 3 eq. of Br). The mixture was stirred at 70 ^oC for 48 h and then quenched by filtering through 1 cm Celite. The solution was then precipitated into 200 mL of methanol and filtered. The isolated solid was redissolved in 10 mL of THF and filtered again through a 1 cm Celite to remove any remaining Pd particles and reprecipitated into 200 mL of methanol. The solution was filtered and the powder was dried in vacuo at 60 ^oC for 4 h.

$5FStyr_{16}$OPS (**I**): pentafluoro(5F)styrene = 2.9 mL; Yield = 90 %; GPC: M_n = 3310, M_w = 3380, PDI = 1.02; TGA (air, 1000 ^oC): Found = 0 %, Calculated = 11.7 %, $T_{d5\%}$ = 285 ^oC.

$CNStyr_{16}$OPS (**II**): 4-cyanostyrene = 2.7 mL; Yield = 90 %; GPC: M_n = 3490, M_w = 3600, PDI = 1.03; TGA (air, 1000 ^oC): Found = 15.4 %, Calculated = 15.7 %, $T_{d5\%}$ = 270 ^oC.

General 2nd Heck coupling of $5FStyr_{16}$OPS with 4-bromotriphenylamine (**III**)

To a dry 25 mL Schlenk flask under N_2 was added 0.50 g (1.0 mmol) of $5FStyr_{16}$OPS, 60 mg (0.12 mmol) of $Pd[P(t\text{-}Bu)_3]_2$, 54 mg (0.06 mmol) of $Pd_2(dba)_3$ and 1.9 g (5.8 mmol, 6 eq. of SQs) of 4-bromotriphenylamine. 1,4-dioxane (5 ml) was then added by syringe followed by NCy_2Me (1.4 ml, 6.4 mmol). The mixture was stirred at 70 ^oC for 48 h and then quenched by filtering through 1 cm Celite. The solution was then precipitated into 200 mL of methanol and filtered. The isolated solid was redissolved in 10 mL of THF and filtered again through a 1 cm Celite to remove any remaining Pd particles and reprecipitated into 200 mL of methanol. The solution was filtered and the powder was dried in vacuo at 60 ^oC for 4 h. Characterization data: Yield = 90 %; GPC: M_n = 4220, M_w = 4430, PDI = 1.05; TGA (air, 1000 ^oC): Found = 6.9 %, Calculated = 6.8 %, $T_{d5\%}$ = 280 ^oC.

General 2nd Heck coupling of CNStyr$_{16}$OPS with 4-bromotriphenylamine (**IV**)

To a dry 25 mL Schlenk flask under N_2 was added 0.50 g (1.3 mmol) of CNStyr$_{16}$OPS, 80 mg (0.16 mmol) of Pd[P(*t*-Bu)$_3$]$_2$, 72 mg (0.08 mmol) of $Pd_2(dba)_3$ and 2.5 g (7.8 mmol, 6 eq. of SQs) of 4-bromotriphenylamine. 1,4-dioxane (5 ml) was then added by syringe followed by NCy_2Me (1.8 ml, 8.6 mmol). The mixture was stirred at 70 ^oC for 48 h and then quenched by filtering through 1 cm Celite. The solution was then precipitated into 200 mL of methanol and filtered. The isolated solid was redissolved in 10 mL of THF and filtered again through a 1 cm Celite to remove any remaining Pd particles and reprecipitated into 200 mL of methanol. The solution was filtered and the powder was dried in vacuo at 60 ^oC for 4 h. Characterization data: Yield = 90 %; GPC: M_n = 4400, M_w = 4490, PDI = 1.02; TGA (air, 1000 ^oC): Found = 9.9 %, Calculated = 9.6 %, $T_{d5\%}$ = 270 ^oC.

2.3.5. Synthesis and characterization of hydroxyl terminated silsesquioxanes and their use for cross-linked polyesters

General metathesis reactions of vinyl T_8 (OVS) and $T_{10/12}$ SQs

To a dry 250 mL Schlenk flask under N_2 was added 4.0 g (9.60 mmol) of vinyl SQ and 63.0 mg (0.08 mmol) of first generation Grubbs catalyst. Dry CH_2Cl_2 (60 mL) was added by syringe followed by 11.6 g (113 mmol) of *p*-acetoxystyrene. The mixture was stirred for 168 h at 40℃ and conversion of starting materials was monitored via MALDI-ToF. The solution was quenched by precipitation into 500 mL of hexane and then filtered. The resulting solid was vacuum dried for 4 h and was obtained as a white solid. The product was further purified by column chromatography to remove residual catalyst. (silica, 1:4 hexane:THF).

Metathesis reactions of OVS (GEN1 *p*-acetoxy T_8 SQ)

OVS and *p*-acetoxystyrene were allowed to react according to the above general procedure (8.3 g, 80.0 % yield). Characterization data: ^{1}H-NMR (DMSO, δ ppm): 2.3 (s, 3H, -C*H*$_3$), 6.4 (d, H, J = 20 Hz, Si-C*H*=CH-), 7.1 (d, 2H, J = 26 Hz, Ar-*H*), 7.3 (t, H, J = 20 Hz, Si-CH=C*H*-), 7.5 (d, 2H, J = 48 Hz, Ar-*H*). ^{13}C-NMR ($CDCl_3$, δ ppm): 21.2 (-*C*H$_3$), 119.1 (Si-C=*C*-), 121.9 (Ar -*C*H), 128.0 (Ar -*C*H), 135.1 (Si-*C*=C-), 147.6 (Ar *C*-C), 151.2 (Ar *C*-O), 169.4 (*C*=O). MALDI-ToF: *m/z* (Ag^+ adduct) = 1813.47 [$Ag(SiO_{1.5})_8(C_8H_6)_8(C_2H_3O_2)_8$]. FTIR (cm^{-1}):

1096 (νSi-O), 1203 (νC-O), 1603 (νC=C), 1505 (νSi-C), 1763 (νC=O), GPC: Mn = 2070, Mw = 2150, PDI = 1.04. TGA (air, 1000 ℃): found = 27.9 %, calc. = 28.2 %, $T_{d5\%}$ = 345 ℃.

Metathesis reactions of vinyl $T_{10/12}$ SQ (GEN1 *p*-acetoxy $T_{10/12}$ SQ)

Vinyl $T_{10/12}$ SQ and *p*-acetoxystyrene were allowed to react according to the above general procedure using 6.0 g of vinyl $T_{10/12}$ SQ, 94.5 mg of first generation Grubbs catalyst, and 17.4 mL of *p*-acetoxystyrene (13.6 g, 84.1 % yield). Characterization data: ^{1}H-NMR (DMSO, δ ppm): 2.3 (s, 3H, -C*H*$_3$), 6.4 (d, H, J = 20 Hz, Si-C*H*=CH-), 7.1 (d, 2H, J = 8 Hz, Ar-H), 7.3 (d, H, J = 20 Hz, Si-CH=C*H*-), 7.5 (d, 2H, J = 8 Hz, Ar-H). ^{13}C-NMR ($CDCl_3$, δ ppm): 21.2 (-*C*H$_3$), 117.5 (Si-C=*C*-), 121.9 (Ar -*C*H), 128.0 (Ar -*C*H), 135.1 (Si-*C*=C-), 148.2 (Ar *C*-C), 151.2 (Ar *C*-O), 169.4 (*C*=O). MALDI-ToF: *m/z* (Ag^+ adduct) = 2240.37 [$Ag(SiO_{1.5})_{10}(C_8H_6)_{10}(C_2H_3O_2)_{10}$], 2666.67 [$Ag(SiO_{1.5})_{12}(C_8H_6)_{12}(C_2H_3O_2)_{12}$]. FTIR ($cm^{-1}$): 1117 (νSi-O), 1205 (νC-O), 1505 (νSi-C), 1603 (νC=C), 1763 (νC=O), GPC: Mn = 2500, Mw = 2560, PDI = 1.02. TGA (air, 1000 ℃): found = 28.4 %, calc. = 28.2 %, $T_{d5\%}$ = 345 ℃.

General Heck reaction converting *p*-BrStyrenyl T_8 and $T_{10/12}$ SQ to *p*-acetoxy GEN2

To a dry 50 mL Schlenk flask under N_2 was added 1.0 g (4.28 mmol of Br) of *p*-BrStyrenylSQ, 43.70 mg bis(tri-tert-butylphosphine) palladium catalyst, and 39.15 mg tris(dibenzylideneacetone)-dipalladium catalyst. Dry 1, 4-dioxane (20 mL) was added via syringe followed by 0.61 mL (2.24 mmol) of N-methyldicyclohexylamine, and 1.96 mL (8.88 mmol) of *p*-acetoxystyrene. The mixture was stirred at room temperature for 72 hours and then quenched by filtering through 1 cm Celite. The solution was then precipitated into 200 mL methanol and filtered. The resulting solid was vacuum dried for 4 h and was obtained as a yellow solid. The product was further purified by column chromatography to remove residual Pd catalyst. (silica, 1:2 of hexane:THF).

Heck coupling reactions of *p*-BrStyrenyl T_8 SQ (GEN2 *p*-acetoxy T_8 SQ)

p-BrStyrenyl T_8 SQ and *p*-acetoxystyrene were allowed to react according to the above general procedure (1.25 g, 93 % yield). Characterization data: ^{1}H-NMR (DMSO, δ ppm): 2.3 (s, 3H, -C*H*$_3$), 6.5 (d, H, J = 20 Hz, Si-C*H*=CH-), 7.3-7.6 (m, 11H, Ar-*H*, Si-CH=C*H*-, Ar-C*H*=C*H*-

Ar). ^{13}C-NMR ($CDCl_3$, δ ppm): 21.2 (-*C*H_3), 117.2 (Si-C=*C*-), 121.9 (Ar -*C*H), 126.9 (Ar -*C*H), 127.5 (Ar -*C*H), 128.3 (Ar –*C*H=*C*H-Ar), 135.1 (Si-*C*=C-), 136.7 (Ar *C*-C), 138.0 (Ar *C*-C), 148.9 (Ar *C*-C), 150.2 (Ar *C*-O), 169.5 (*C*=O). MALDI-ToF: *m/z* (Ag+ adduct) = 2629.59 $[Ag(SiO_{1.5})_8(C_8H_6)_{16}(C_2H_3O_2)_8]$. FTIR ($cm^{-1}$): 1095 (νSi-O), 1202 (νC-O), 1510 (νSi-C), 1598 (νC=C), 1760 (νC=O), GPC: Mn = 4080, Mw = 4240, PDI = 1.04. TGA (air, 1000 ℃): found = 19.2 %, calc. = 19.1 %, $T_{d5\%}$ = 335 ℃.

Heck coupling reactions of *p*-BrStyrenyl $T_{10/12}$ SQ (GEN2 *p*-acetoxy $T_{10/12}$ SQ)

p-BrStyrenyl T_{10}/T_{12} SQ and *p*-acetoxystyrene were allowed to react according to the above general procedure (1.2 g, 89 % yield). Characterization data: ^{1}H-NMR (DMSO, δ ppm): 2.3 (s, 3H, -C*H*$_3$), 6.5 (m, H, Si-C*H*=CH-), 7.0-7.6 (m, 11H, Ar-*H*, Si-CH=C*H*-, Ar-C*H*=C*H*-Ar). ^{13}C-NMR ($CDCl_3$, δ ppm): 21.2 (-*C*H_3), 117.2 (Si-C=*C*-), 121.9 (Ar -*C*H), 126.9 (Ar -*C*H), 127.5 (Ar -*C*H), 128.3 (Ar –*C*H=*C*H-Ar), 135.1 (Si-*C*=C-), 136.7 (Ar *C*-C), 138.0 (Ar *C*-C), 148.9 (Ar *C*-C), 150.2 (Ar *C*-O), 169.5 (*C*=O). MALDI-ToF: *m/z* (Ag^+ adduct) = 3261.0 $[Ag(SiO_{1.5})_{10}(C_8H_6)_{20}(C_2H_3O_2)_{10}]$, 3891.3 $[Ag(SiO_{1.5})_{12}(C_8H_6)_{24}$-$(C_2H_3O_2)_{12}]$. FTIR ($cm^{-1}$): 1009 (νSi-O), 1202 (νC-O), 1510 (νSi-C), 1598 (νC=C), 1759 (νC=O), GPC: Mn = 4130, Mw = 4270, PDI = 1.03. TGA (air, 1000 ℃): found = 19.5 %, calc. = 19.1 %, $T_{d5\%}$ = 305 ℃.

General hydrolysis reaction to prepare *p*-hydroxySQs

To a dry 50 mL Schlenk Flask under N_2 was added 0.50 g (2.34 mmol for GEN1 compounds and 1.59 mmol for GEN2 compounds) *p*-acetoxy SQ and 12.5 mL of THF. 0.2 mL of 37 % HCl Solution and 0.5 mL of deionized water was added to the reaction by syringe and the reaction flask was wrapped in aluminum foil to limit light promoted oxidation. The reaction was stirred at room temperature and monitored by disappearance of the C=O peak using FTIR. The reaction was neutralized using saturated $NaHCO_3$ and the product was extracted using methylene chloride. The solution was then dried over Na_2SO_4 and evaporated by vacuum to give a white solid as product and stored in the refrigerator.

Hydrolysis reactions of GEN1 *p*-acetoxy T_8 SQ (GEN1 *p*-hydroxy T_8 SQ)

GEN1 *p*-acetoxy T_8 SQ was allowed to react according to the above general procedure. The resulting solid was vacuum dried for 4 h and was obtained as a white solid (0.33 g, 82.2 % yield). Characterization data: ^{1}H-NMR (DMSO, δ ppm): 6.2 (d, H, J = 20 Hz, Si-C*H*=CH-), 6.7 (d, 2H, J = 26 Hz, Ar-*H*), 7.1 (t, H, J = 20 Hz, Si-CH=C*H*-), 7.3 (d, 2H, J = 48 Hz, Ar-*H*), 9.8 (s, H, -O*H*). MALDI-ToF: *m/z* (Ag+ adduct) = 1477.47 $[Ag(SiO_{1.5})_8(C_8H_6)_8(OH)_8]$, 1519.48 $[Ag(SiO_{1.5})_8(C_8H_6)_8(OH)_7\text{-}(C_2H_3O_2)_1]$. FTIR ($cm^{-1}$): 1112 (νSi-O), 1510 (νSi-C), 1606 (νC=C), 3326 (νO-H), GPC: Mn = 2000, Mw = 2030, PDI = 1.01. TGA (air, 1000 ℃): found = 34.6 %, calc. = 35.1 %, $T_{d5\%}$ = 235 ℃.

Hydrolysis reactions of GEN1 *p*-acetoxy $T_{10/12}$ SQ (GEN1 *p*-hydroxy $T_{10/12}$ SQ)

GEN1 acetoxy $T_{10/12}$ SQ was allowed to react according to the above general procedure. The resulting solid was vacuum dried for 4 h and was obtained as a white solid (0.32 g, 79.7 % yield). Characterization data: ^{1}H-NMR (DMSO, δ ppm): 6.2 (d, H, J = 20 Hz, Si-C*H*=CH-), 6.7 (d, 2H, J = 8 Hz, Ar-H), 7.1 (d, H, J = 20 Hz, Si-CH=C*H*-), 7.3 (d, 2H, J = 8 Hz, Ar-H), 9.7 (s, H, -O*H*). MALDI-ToF: *m/z* (Ag^+ adduct) = 1819.44 $[Ag(SiO_{1.5})_{10}(C_8H_6)_{10}(OH)_{10}]$, 2162.48 $[Ag(SiO_{1.5})_{12}(C_8H_6)_{12}(OH)_{12}]$. FTIR ($cm^{-1}$): 1115 (νSi-O), 1511 (νSi-C), 1605 (νC=C), 3328 (νO-H), GPC: Mn = 2240, Mw = 2300, PDI = 1.03. TGA (air, 1000 ℃): found = 34.4 %, calc. = 35.1 %, $T_{d5\%}$ = 280 ℃.

Hydrolysis reactions of GEN2 *p*-acetoxy T_8 SQ (GEN2 *p*-hydroxy T_8 SQ)

GEN2 *p*-acetoxy T_8 SQ was allowed to react according to the above general procedure. The resulting solid was vacuum dried for 4 h and was obtained as a white solid (0.35 g, 80.8 % yield). Characterization data: ^{1}H-NMR (DMSO, δ ppm) 6.7-7.6 (m, 12H, Si-C*H*=CH-, Ar-*H*, Si-CH=C*H*-, Ar-C*H*=C*H*-Ar), 9.6 (s, H, -O*H*). MALDI-ToF: *m/z* (Ag+ adduct) = 2293.10 $[Ag(SiO_{1.5})_8(C_8H_6)_{16}(OH)_8]$. FTIR ($cm^{-1}$): 1097 (νSi-O), 1513 (νSi-C), 1597 (νC=C), 2962 (νO-H), GPC: Mn = 3410, Mw = 3560, PDI = 1.04. TGA (air, 1000 ℃): found = 22.2 %, calc. = 22.0 %, $T_{d5\%}$ = 360 ℃.

Hydrolysis reactions of GEN2 *p*-acetoxy $T_{10/12}$ SQ (GEN2 *p*-hydroxy $T_{10/12}$ SQ)

GEN2 acetoxy $T_{10/12}$ SQ was allowed to react according to the above general procedure. The resulting solid was vacuum dried for 4 h and was obtained as a white solid (0.36 g, 83.1 % yield). Characterization data: ^{1}H-NMR (DMSO, δ ppm): 6.5-7.8 (m, 12H, Si-C*H*=CH-, Ar-*H*, Si-CH=C*H*-, Ar-C*H*=C*H*-Ar), 9.6 (s, H, -O*H*). FTIR (cm^{-1}): 1115 (νSi-O), 1514 (νSi-C), 1597 (νC=C), 3022 (νO-H), GPC: Mn = 3490, Mw = 3590, PDI = 1.03. TGA (air, 1000 ℃): found = 22.3 %, calc. = 22.0 %, $T_{d5\%}$ = 345 ℃.

General polyesterification reaction of *p*-hydroxySQs and adipoyl chloride

To a dry 10 mL Schlenk flask under N_2 was added 0.50 g (2.92 mmol for GEN1 compounds and 1.83 for GEN2 compounds) of *p*-hydroxySQ, 3 mL of 1,4-dioxane, and 0.42 mL (3.07 mmol for GEN1 compounds, 1.92 mmol for GEN2 compounds) of adipoyl chloride. 0.81 mL (5.8 mmol) of triethylamine diluted in 3 mL of 1,4-dioxane was added dropwise to the reaction, which formed a white-yellow precipitate. The reaction was stirred at 40 ℃ for 1 hour and was then filtered. The solid was then stirred with deionized water for 1 hour at room temperature to dissolve any remaining acid and filtered again.

Polyesterification reactions of GEN1 *p*-hydroxy T_8 SQ (GEN1 T_8 polymer SQ)

GEN1 hydroxy T_8 SQ was allowed to react according to the above general procedure with a yield of 0.36 g, 72.0 % yield. Characterization data: FTIR (cm^{-1}): 1119 (νSi-O), 1504 (νSi-C), 1602 (νC=C), 1758 (νC=O), 1292, 1361, 2947 (C-H). TGA (air, 1000 ℃): found = 19.4%, $T_{d5\%}$ = 230 ℃.

Polyesterification reactions of GEN1 *p*-hydroxy $T_{10.12}$ SQ (GEN1 $T_{10/12}$ polymer SQ)

GEN1 hydroxy $T_{10/12}$ SQ was allowed to react according to the above general procedure with a yield of 0.33 g, 66.0 % yield. Characterization data: FTIR (cm^{-1}): 1119 (νSi-O), 1505 (νSi-C), 1603 (νC=C), 1758 (νC=O), 1360, 2954 (C-H). TGA (air, 1000 ℃): found = 20.6%, $T_{d5\%}$ = 240 ℃.

Polyesterification reactions of GEN2 *p*-hydroxy T_8 SQ (GEN2 T_8 polymer SQ)

GEN2 hydroxy T_8 SQ was allowed to react according to the above general procedure with a yield of 0.37 g, 74.0 % yield. Characterization data: FTIR (cm^{-1}): 1116 (νSi-O), 1511 (νSi-C), 1598 (νC=C), 1738 (νC=O), 1261, 1359, 2961 (C-H). TGA (air, 1000 ℃): found = 22.0 %, $T_{d5\%}$ = 210 ℃.

Polyesterification reactions of GEN2 *p*-hydroxy $T_{10/12}$ SQ (GEN2 $T_{10/12}$ polymer SQ)

GEN2 hydroxy $T_{10/12}$ SQ was allowed to react according to the above general procedure using 0.15 g (0.55 mmol) of GEN2 hydroxy $T_{10/12}$ SQ, 0.13 mL (0.55 mmol) of adipoyl chloride, and 0.24 mL (x mmol) of triethylamine with a yield of 0.16 g, 106.7 % yield. Characterization data: FTIR (cm^{-1}): 1122 (νSi-O), 1511 (νSi-C), 1598 (νC=C), 1755 (νC=O), 1358 (νC-H). TGA (air, 1000 ℃): found = 10.1 %, $T_{d5\%}$ = 230 ℃.

References Cited:

1. Kim, S.-G.; Sulaiman, S.; Fargier, D.; Laine, R. M.; "Octaphenyloctasilsesquioxane and Polyphenylsilsesquioxane for Nanocomposite," In *Materials Syntheses. A Practical Guide*; Schubert, U.; Husing, N.; Laine, R. M.; Eds.,; Springer-Verlag: Wien, 2008, pp. 179-191.
2. Tamaki, R.; Tanaka, Y.; Asuncion, M. Z.; Choi, J.; Laine, R. M.; "Octa(aminophenyl)-silsesquioxane as a Nanoconstruction Site," *J. Am. Chem. Soc*., **2001**, *123*, 12416-12417.
3. Roll, M.F.; Asuncion, M.Z.; Kampf, J.; Laine, R.M.; "*para*-Octaiodophenylsilsesquioxane, $[p\text{-}IC_6H_4SiO_{1.5}]_8$, a Nearly perfect Nono-building block." *ACS Nano*, **2008**, *2*, 320-326.
4. Ronchi, M.; Sulaiman, S.; Boston, N. R.; Laine, R. M.; "Fluoride catalyzed rearrangements of polysilsesquioxanes, mixed Me,Vinyl T_8, Me, Vinyl T_{10} and T_{12} cages," *Applied Organometallic Chemistry*, **2010**, *24*, 551–557.
5. Harrison, P. G.; Hall, C.; "Preparation and characterization of octasilsesquioxane cage monomers," *Main Group Met. Chem*., **1997**, *8*, 515-529.
6. Roll, M. F.; Mathur, P.; Takahashi, K.; Kampf, J. W.; Laine, R. M.; "$[PhSiO_{1.5}]_8$ promotes self-bromination to produce $[o\text{-}BrPhSiO_{1.5}]_8$: further bromination gives crystalline $[2,5\text{-}Br_2PhSiO_{1.5}]_8$ with a density of 2.32 g cm^{-3} and a calculated refractive index of 1.7 or the tetraicosa bromo compound $[Br_3PhSiO_{1.5}]_8$," *J. Mater. Chem*., **2011**, *21*, 11167-11176.

7. Fife, D.J.; Moore, W.M.; Morse, K.W.; "Solution equilibria of tertiary phosphine complexes of copper(I) halides," *Inorg. Chem.*, **1984**, *23*, 1684-1691.
8. Maciejewski, A.; Steer, R. P. "Spectral and photophysical properties of 9,10-diphenylanthracene in perfluoro-n-hexane: the influence of solute—solvent interactions," *J. Photochem.***1986**, *35*, 59-69.
9. Xu, C.; Webb, W. W. "Measurement of two-photon excitation cross sections of molecular fluorophores with data from 690 to 1050 nm." *J. Opt. Soc. Am. B.* **1996**, *13*, 481-491.
10. Bhaskar, A.; Ramakrishna, G.; Lu, Z.; Twieg, R.; Hales, J. M.; Hagan, D. J.; Van Stryland, E.; Goodson, T. "Investigation of Two-Photon Absorption Properties in Branched Alkene and Alkyne Chromophores." *J. Am. Chem. Soc.* **2006**, *128*, 11840-111849.

Chapter 3

Beads on a Chain (BoC) polymers formed from $[NH_2PhSiO_{1.5}]_x[PhSiO_{1.5}]_{10-x}$ and $[NH_2PhSiO_{1.5}]_x[PhSiO_{1.5}]_{12-x}$ mixtures (x = 2-4)

Published in Macromolecules, **2011**, *44*, pp. 7263-7272

Abstract

We recently reported that catalytic amounts of F^- cause rapid rearrangement of silsesquioxane (SQ) T_8 cages in THF at room temperature. These rearrangements lead primarily to the T_{10} and T_{12} cages as long as the F^- is trapped for example using $CaCl_2$ to form insoluble CaF_2 in situ. In this report, we use this approach to make di- and tri-aminophenyl, phenyl silsesquioxane T_{10} and T_{12} mixtures; $(NH_2Ph)_xPh_{10-x/12-x}(SiO_{1.5})_{10/12}$. Thereafter, we isolate the fraction that consists primarily of x = 2-4 via column chromatography. We then explore the reaction of this fraction (fraction 3) with the diglycidyl ether of bisphenol A (DGEBA) to form a soluble epoxy resin wherein the cage SQs is contained in the chain backbone. We call these products beads on a chain (BoC) polymers. The use of 1:1 mole ratios of [epoxide]:[NH_2Ph] of DGEBA and $[NH_2PhSiO_{1.5}]_x[PhSiO_{1.5}]_{10/12-x}$ (x = 2-4) leads to insoluble products. However, the reaction of 0.8:1 mole ratio of [epoxide]:[NH_2Ph] provides a soluble but bimodal distribution of products (after 24 h reaction at 90℃ in THF). The low MW component is much more soluble in THF than the higher MW component allowing simple separation. The low MW polymer has a M_n of 6k Da with a PDI of 1.6. The higher MW material has a M_n of 21m Da with a PDI of 21.

Both components offer similar ceramic yields (to SiO_2) of 32±1% indicating that the relative content of cages is identical. They also exhibit very similar FTIR spectra suggesting that

they are the same material. Two explanations are possible for the bimodal size distribution. One is that the positioning of the NH_2 groups on the cage leads to cyclic trimers given that the average monomer unit will mass ≈ 1700-1900 Da, which represents the low MW fraction. Alternately and more likely, the higher molecular weight component consists of di- and triamino functionalities such that in the growing chain, once the first two amine groups on the cage react, the third group is likely sterically protected. Thus, only late in the reaction will the quantities of the third group exceed those of the diamino components allowing a slow tertiary functionalization and likely some degree of cross-linking to occur. That this happens is suggested by the much poorer solubility of the higher MW materials as well as the very large PDI. These studies serve as a model for other possible studies targeting BoC polymers.

3.1. Introduction

There is recent, intense interest in the use of silsesquioxane (SQ) cages as nanobuilding blocks for the synthesis and processing of nanocomposite materials and as sites for attaching multiple types of functionalities for diverse applications as witnessed by the publication of 17 reviews over the past 30 years, with the majority published in the last 10 years.[1-17] Despite the now thousands of articles and patents concerning SQs, the number of papers that describe the synthesis and properties of SQs as part of a polymer backbone is limited to just a few studies.[18-24] Some examples of difunctional silsesquioxane monomers and what we propose to call "beads on a chain" (BoC) polymers are those shown in Schemes **3.1** and **3.2**.[24]

In part, this problem arises because until now it has been difficult to synthesize SQs with just two or three functional groups on the cage that would permit their copolymerization with other monomer units. Most SQs or POSS compounds currently described in the literature either have only one or 8, 16 or even 24 functional groups or functional group equivalents attached to the cage vertices.[1-17,25-27] However, the opportunity to synthesize di- and tri-functional SQs, especially in T_{10} and T_{12} cages and BoC polymers therefrom now exists.[28]

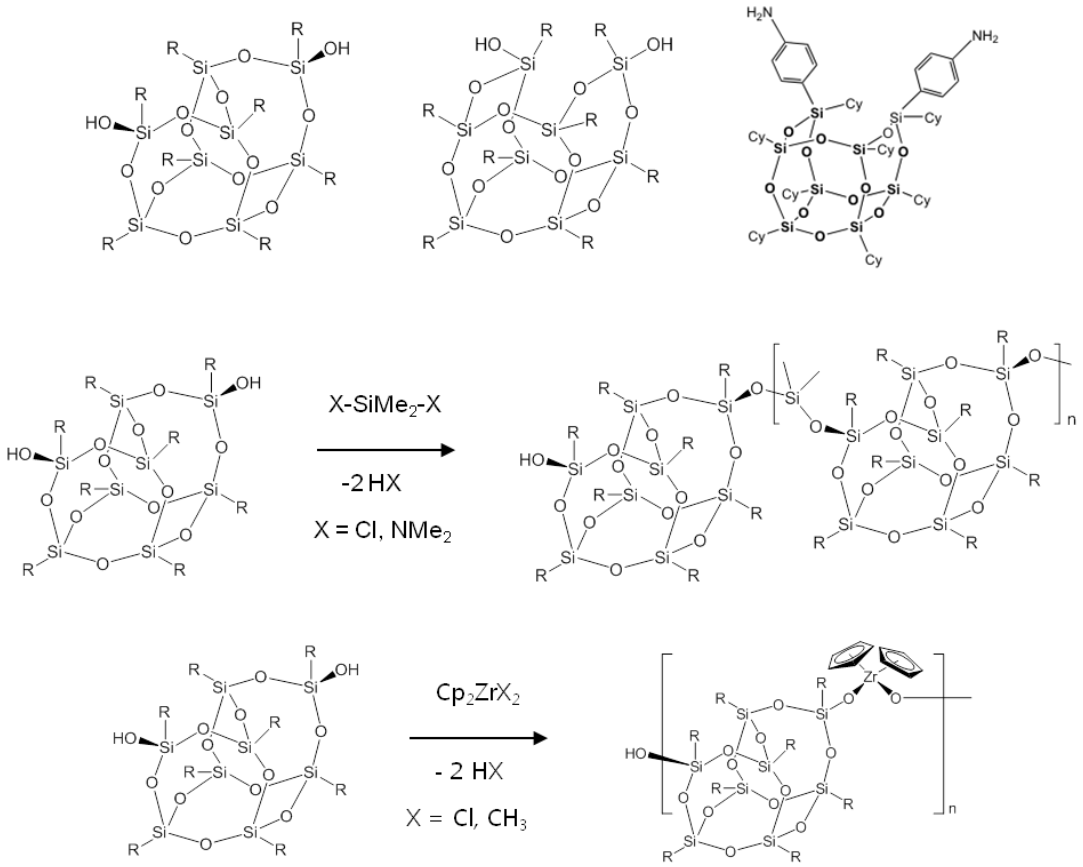

Scheme 3.1. Examples of Difunctional SQs and examples of polymerization via Si-OH bonds of "beads on a chain" (BoC) polymers (R= Cy = cyclohexyl).[24]

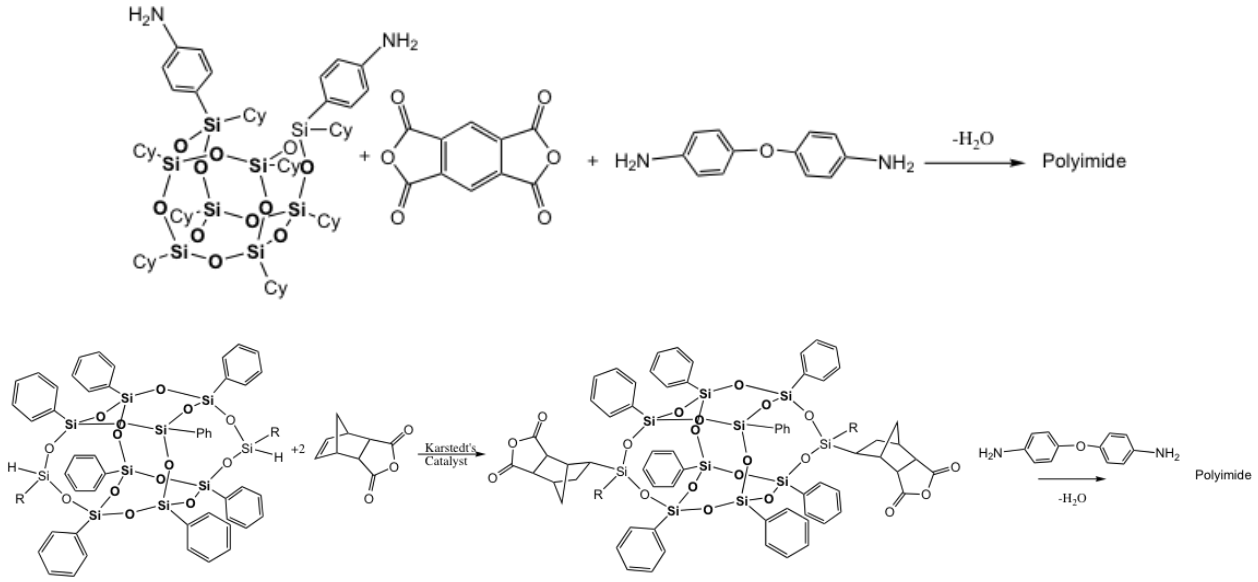

Scheme 3.2. Polymerization of difunctional SQs to BoC polyimides.[18-23]

We recently described using F^- in the form of tBu_4NF to catalyze the rapid equilibration of functional groups between two types of polysilsesquioxanes or from SQ resins in THF at room temperature to form T_{10} and T_{12} mixed functional SQs as suggested in Scheme **3**.[28-30]

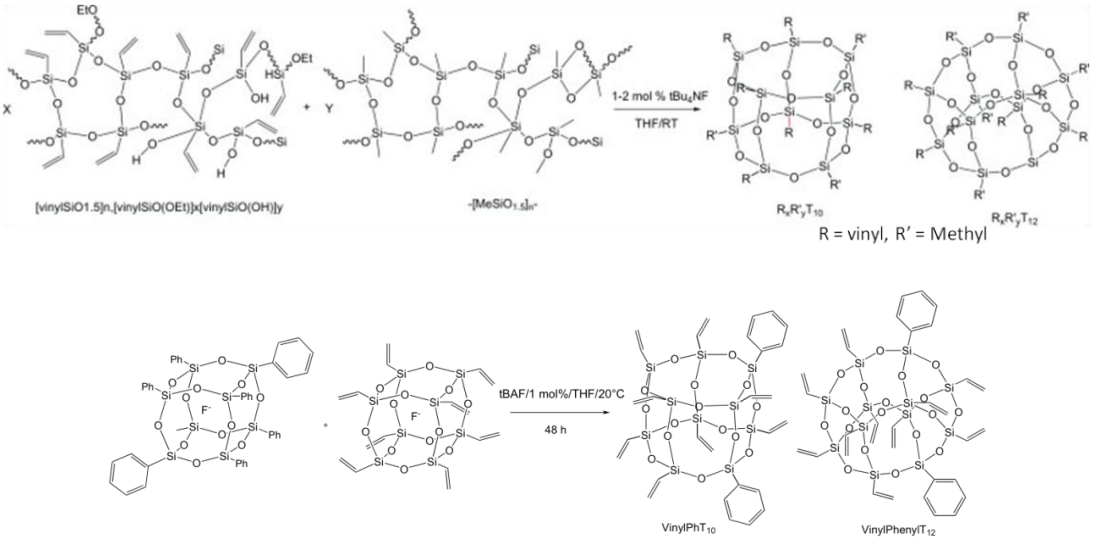

Scheme 3.3. F^- catalyzed formation of T_{10} and T_{12} SQs from polymeric SQ resins or T_8 cages.

We report here an extension of this method to the synthesis of di- and triarylamine cages targeting the synthesis of BoC polymers that represent new classes of curing agents for epoxy resins, and possible comonomers for the synthesis of polyamides and polyimides. One key objective is to take advantage of the robust nature of SQs to develop families of high temperature stable, soluble and processable BoC polymer systems.

3.2. Results and Discussion

Based on our experience with the Scheme **3.3** vinyl/phenyl SQ equilibration studies, we began with efforts to identify an OPS:OAPS ratio that would provide statistically controllable mixtures of cages, as seen in Scheme **3.4**.

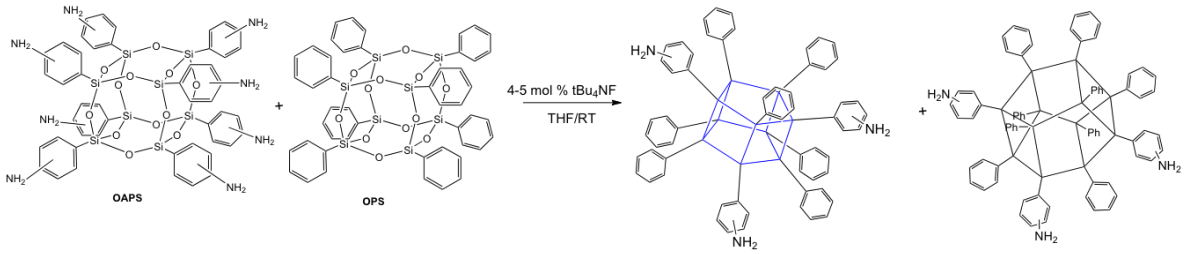

Scheme 3.4. Synthesis of $[NH_2PhSiO_{1.5}]_x[PhSiO_{1.5}]_{10/12-x}$ (x = 2-4) from OAPS and OPS.

In the following sections, we first discuss the synthesis of mixtures of di- and tri functional T_{10} and T_{12} aminophenyl SQs and their characterization. We then describe their reactions with the diglycidyl ether of bisphenol A (DGEBA) and the characterization of the resulting polymer. We present here studies designed to provide a basic aromatic amine model for BoC syntheses of related epoxy resins systems and for future amidation and imidation studies.

3.2.1. Synthesis of $[NH_2PhSiO_{1.5}]_x[PhSiO_{1.5}]_{10/12-x}$ (x = 2-4)

Based on our first two studies,[28,29] we explored the catalytic rearrangement of OPS/OAPS mixtures with TBAF targeting di- and tri-amino SQs per Scheme **3.4**. Figure **3.1** and Table **3.1** provide MALDI-ToF data for a 3:1 mole ratio following 72 h of reaction.

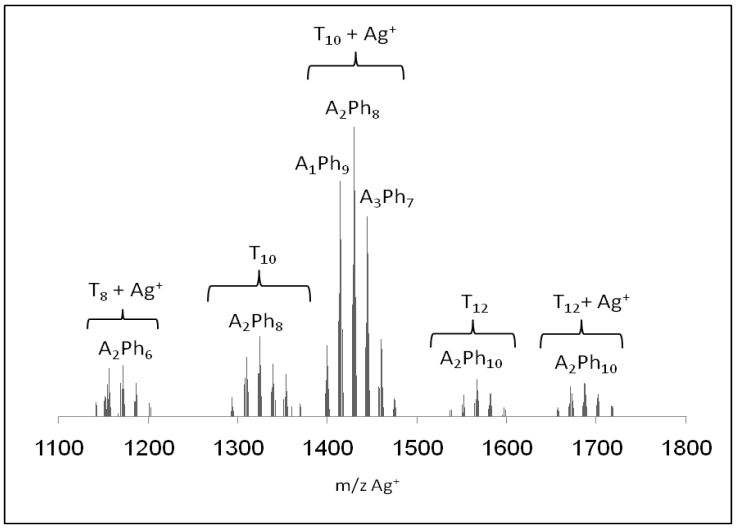

Figure 3.1. MALDI-ToF spectrum of 3:1 OPS:OAPS reaction with TBAF (RT/72 h).

The Figure **3.1** spectrum shows a mixture of the T_8, T_{10} and T_{12} cages (major product is T_{10}) with aminophenyl group contents ranging from 0 ~ 5 but with ≈ 20 % quantities of unsubstituted SQs. The OPS:OAPS ratios were varied to optimize diaminophenyl contents, per Table **3.2**. In the case of 4:1 of OPS:OAPS reaction, the main products are monoaminophenyl SQ compounds. Although the 2.5:1 of OPS:OAPS reaction shows diaminophenyl SQ compounds as the main product like the 3:1 of OPS:OAPS reaction, the relative peak intensities of triaminophenyl SQ compounds in the MALDI are higher than for 3:1 of OPS:OAPS. Given that triaminophenyl SQ compounds could form cross link points during the polymerization that

would be difficult to separate from diaminophenyl SQ compounds by column chromatography due to their very similar chemical structures and properties (e.g. polarity, solubility). Thus, we decided to use the 3:1 of OPS:OAPS ratio as an optimum.

Table 3.1. MALDI-ToF data for 3:1 of OPS:OAPS reaction with TBAF. †

Most Common Isotope	Found (Da)	Calc. (Da)	Relative Peak Intensities (%)
$(C_6H_5)_8(SiO_{1.5})_8$ (+ Ag^+)	1140.8	1141.4	5
$(NH_2C_6H_4)_1(C_6H_5)_7(SiO_{1.5})_8$ (+ Ag^+)	1155.9	1156.5	17
$(NH_2C_6H_4)_2(C_6H_5)_6(SiO_{1.5})_8$ (+ Ag^+)	1170.8	1171.5	18
$(NH_2C_6H_4)_3(C_6H_5)_5(SiO_{1.5})_8$ (+ Ag^+)	1185.9	1186.5	12
$(C_6H_5)_{10}(SiO_{1.5})_{10}$	1292.7	1291.8	7
$(NH_2C_6H_4)_1(C_6H_5)_9(SiO_{1.5})_{10}$	1308.7	1307.8	21
$(NH_2C_6H_4)_2(C_6H_5)_8(SiO_{1.5})_{10}$	1323.7	1323.8	28
$(NH_2C_6H_4)_3(C_6H_5)_7(SiO_{1.5})_{10}$	1338.7	1339.9	18
$(C_6H_5)_{10}(SiO_{1.5})_{10}$ (+ Ag^+)	1398.6	1399.8	25
$(NH_2C_6H_4)_1(C_6H_5)_9(SiO_{1.5})_9$ (+ Ag^+)	1413.6	1414.8	81
$(NH_2C_6H_4)_2(C_6H_5)_8(SiO_{1.5})_8$ (+ Ag^+)	1428.6	1429.8	100
$(NH_2C_6H_4)_3(C_6H_5)_8(SiO_{1.5})_7$ (+ Ag^+)	1443.6	1444.8	69
$(C_6H_5)_{12}(SiO_{1.5})_{12}$	1551.5	1551.2	4
$(NH_2C_6H_4)_1(C_6H_5)_{11}(SiO_{1.5})_{12}$	1566.5	1566.2	8
$(NH_2C_6H_4)_2(C_6H_5)_{10}(SiO_{1.5})_{12}$	1581.5	1582.2	13
$(NH_2C_6H_4)_3(C_6H_5)_9(SiO_{1.5})_{12}$	1598.4	1598.2	8
$(C_6H_5)_{12}(SiO_{1.5})_{12}$ (+ Ag^+)	1567.4	1568.2	3
$(NH_2C_6H_4)_1(C_6H_5)_{11}(SiO_{1.5})_{12}$ (+ Ag^+)	1672.3	1673.2	11
$(NH_2C_6H_4)_2(C_6H_5)_{10}(SiO_{1.5})_{12}$ (+ Ag^+)	1687.4	1688.2	12
$(NH_2C_6H_4)_3(C_6H_5)_9(SiO_{1.5})_{12}$ (+ Ag^+)	1702.4	1703.2	8

†Error in reported intensities is ± 5%

Because the unsubstituted SQs are relatively insoluble, we chose to recover the soluble products via column chromatography (see Experimental) and thereafter isolate the mono- and diamino components as a prelude to synthesizing a "linear" polymer. Because we have no way of

knowing the exact placement of the amino groups on the phenyl rings (*p:m:o* ratios are 1:1:0[16]) and the amino group positions on the T_{10} and T_{12} cages are unknown, the concept of linear is not really correct but offers the simplest descriptor.

Table 3.2. MALDI-ToF peak intensities for several ratio of OPS:OAPS reaction with TBAF.[†]

Most Common Isotope	2.5 : 1	3 : 1	4 : 1
$(C_6H_5)_8(SiO_{1.5})_8$ (+ Ag^+)	4	5	20
$(NH_2C_6H_4)_1(C_6H_5)_7(SiO_{1.5})_8$ (+ Ag^+)	16	17	17
$(NH_2C_6H_4)_2(C_6H_5)_6(SiO_{1.5})_8$ (+ Ag^+)	22	18	13
$(NH_2C_6H_4)_3(C_6H_5)_5(SiO_{1.5})_8$ (+ Ag^+)	14	12	5
$(C_6H_5)_{10}(SiO_{1.5})_{10}$	9	7	18
$(NH_2C_6H_4)_1(C_6H_5)_9(SiO_{1.5})_{10}$	31	21	19
$(NH_2C_6H_4)_2(C_6H_5)_8(SiO_{1.5})_{10}$	50	28	40
$(NH_2C_6H_4)_3(C_6H_5)_7(SiO_{1.5})_{10}$	40	18	15
$(C_6H_5)_{10}(SiO_{1.5})_{10}$ (+ Ag^+)	17	25	70
$(NH_2C_6H_4)_1(C_6H_5)_9(SiO_{1.5})_{10}$ (+ Ag^+)	69	81	100
$(NH_2C_6H_4)_2(C_6H_5)_8(SiO_{1.5})_{10}$ (+ Ag^+)	100	100	91
$(NH_2C_6H_4)_3(C_6H_5)_7(SiO_{1.5})_{10}$ (+ Ag^+)	87	69	42
$(C_6H_5)_{12}(SiO_{1.5})_{12}$	11	4	5
$(NH_2C_6H_4)_1(C_6H_5)_{11}(SiO_{1.5})_{12}$	18	8	20
$(NH_2C_6H_4)_2(C_6H_5)_{10}(SiO_{1.5})_{12}$	17	13	16
$(NH_2C_6H_4)_3(C_6H_5)_9(SiO_{1.5})_{12}$	7	8	3
$(C_6H_5)_{12}(SiO_{1.5})_{12}$ (+ Ag^+)	-	3	2
$(NH_2C_6H_4)_1(C_6H_5)_{11}(SiO_{1.5})_{12}$ (+ Ag^+)	7	11	7
$(NH_2C_6H_4)_2(C_6H_5)_{10}(SiO_{1.5})_{12}$ (+ Ag^+)	11	12	7
$(NH_2C_6H_4)_3(C_6H_5)_9(SiO_{1.5})_{12}$ (+ Ag^+)	12	8	3

[†]Error in reported intensities is ± 5%

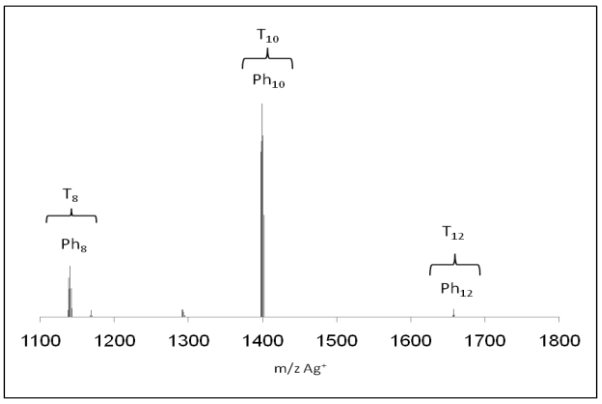

Figure 3.2. MALDI-ToF of Fraction 1.

Elution using dichloromethane:hexane (8:2) gave fractions 1 (R_f value: 0.9) and 2 (R_f value: 0.6) separate from the original crude, dark brown mixture. After Fraction 2 eluted, the elution solvent was changed to THF to obtain Fraction 3. The MALDI-ToF of Fractions 1, 2 and 3 are shown in Figures **3.2-3.4** respectively.

Table 3.3. MALDI-ToF data (Ag^+ Adduct) for Fraction 1.[†]

Most Common Isotope	Found (Da)	Calculated (Da)	Relative Peak Intensity (%)
$(C_6H_5)_8(SiO_{1.5})_8$	1141.0	1141.4	24
$(C_6H_5)_{10}(SiO_{1.5})_{10}$	1399.1	1399.8	100
$(C_6H_5)_{12}(SiO_{1.5})_{12}$	1657.6	1658.2	4

[†]Error in reported intensities is ± 5%

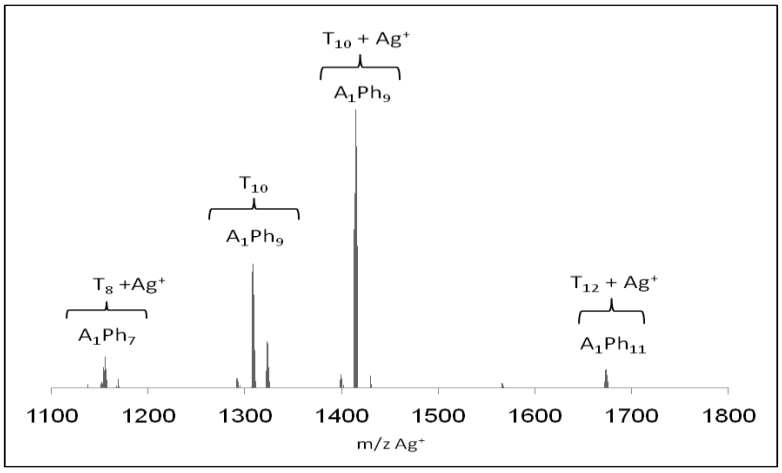

Figure 3.3. MALDI-ToF of Fraction 2.

Table 3.4. MALDI-ToF data (Ag^+ Adduct) for Fraction 2.[†]

Most Common Isotope	Found (Da)	Calculated (Da)	Relative Peak Intensity (%)
$(NH_2C_6H_4)_1(C_6H_5)_7(SiO_{1.5})_8$ (+ Ag^+)	1156.9	1156.5	11
$(NH_2C_6H_4)_1(C_6H_5)_9(SiO_{1.5})_{10}$	1308.0	1307.8	45
$(NH_2C_6H_4)_2(C_6H_5)_8(SiO_{1.5})_{10}$	1323.1	1323.8	17
$(NH_2C_6H_4)_1(C_6H_5)_9(SiO_{1.5})_{10}$ (+ Ag^+)	1414.9	1414.8	100
$(NH_2C_6H_4)_1(C_6H_5)_{11}(SiO_{1.5})_{12}$ (+ Ag^+)	1672.9	1673.2	7

[†]Error in reported intensities is ± 5%

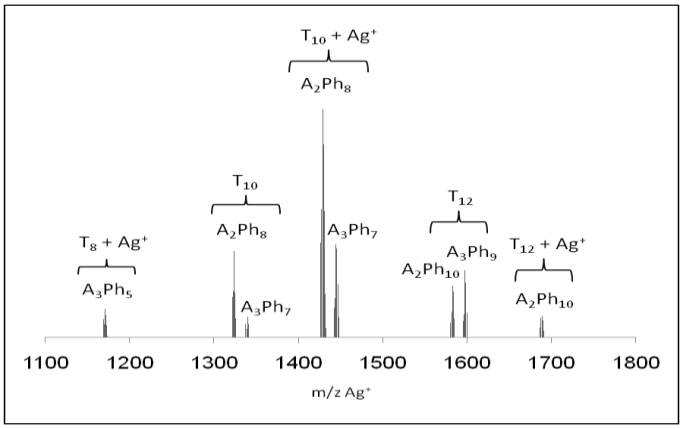

Figure 3.4. MALDI-ToF of Fraction 3.

MALDI-ToF spectra show that Fraction 1 consists of a mixture of OPS and dPS (decaphenyl SQ). Fraction 2 is mostly mono-aminophenyl SQ (T_{10}) whereas Fraction 3 is a mixture of the desired di-aminophenyl SQs (T_{10} and T_{12}) and Tri-aminophenyl SQ (T_8). It is important to note that MALDI intensity data often does not provide a direct quantification of the species present as the intensities relate to the facility with which the individual components ionize. Thus, these data are best considered as being qualitatively similar to the actual isomer compositions.

Table 3.5. MALDI-ToF data (Ag^+ Adduct) for Fraction 3.[†]

Most Common Isotope	Found (Da)	Calculated (Da)	Relative Peak Intensity (%)
$(NH_2C_6H_4)_2(C_6H_5)_6(SiO_{1.5})_8$ (+ Ag^+)	1170.8	1171.5	13
$(NH_2C_6H_4)_2(C_6H_5)_8(SiO_{1.5})_{10}$	1323.6	1323.8	38
$(NH_2C_6H_4)_3(C_6H_5)_7(SiO_{1.5})_{10}$	1339.6	1339.9	9
$(NH_2C_6H_4)_2(C_6H_5)_8(SiO_{1.5})_{10}$ (+ Ag^+)	1429.5	1429.8	100
$(NH_2C_6H_4)_3(C_6H_5)_7(SiO_{1.5})_{10}$ (+ Ag^+)	1443.6	1444.8	40
$(NH_2C_6H_4)_2(C_6H_5)_{10}(SiO_{1.5})_{12}$	1582.5	1582.2	22
$(NH_2C_6H_4)_3(C_6H_5)_9(SiO_{1.5})_{12}$	1598.5	1598.2	29
$(NH_2C_6H_4)_2(C_6H_5)_{10}(SiO_{1.5})_{12}$ (+ Ag^+)	1687.4	1688.2	9

[†]Error in reported intensities is ± 5%

The TGAs of fraction 3, OPS and OAPS in air are shown in Figure **3.5**. The TGA of fraction 3 reveals high thermal stability (T_d = 450 ^oC) and a ceramic yield to SiO_2 of 45.2 % (Table **3.6**). The ceramic yield indicates that the ratio of aminophenyl to phenyl groups is 27:73. This ratio can be used to calculate an 8.8:1 phenyl:amine proton ratio matching the 8.3:1 integration of Figure **3.6**.

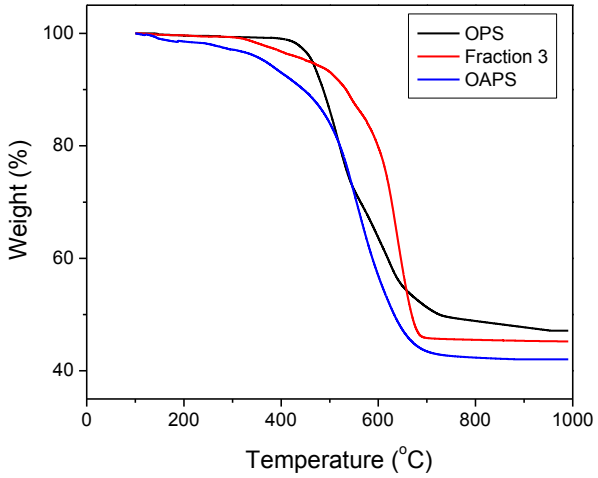

Figure 3.5. TGA of $[NH_2PhSiO_{1.5}]_x[PhSiO_{1.5}]_{10/12-x}$ (x = 2-4) (Fraction 3) and OPS, OAPS for comparison.

Table 3.6. Decomposition temperatures ($T_{d5\%}$) and ceramic yields of $[NH_2PhSiO_{1.5}]_x$-$[PhSiO_{1.5}]_{10/12-x}$ (x = 2-4) (Fraction 3) and starting materials for comparison. (air/10 ^oC/min to 1000 ^oC). Theoretical ceramic yields for compounds detected by MALDI are given for reference.

Compound	$T_{d5\%}$ (°C)	Ceramic Yield (%)	Theoretical Ceramic Yield (%)
OPS	465	47.1	46.5
OAPS	360	42.0	41.7
Fraction 3	450	45.2	

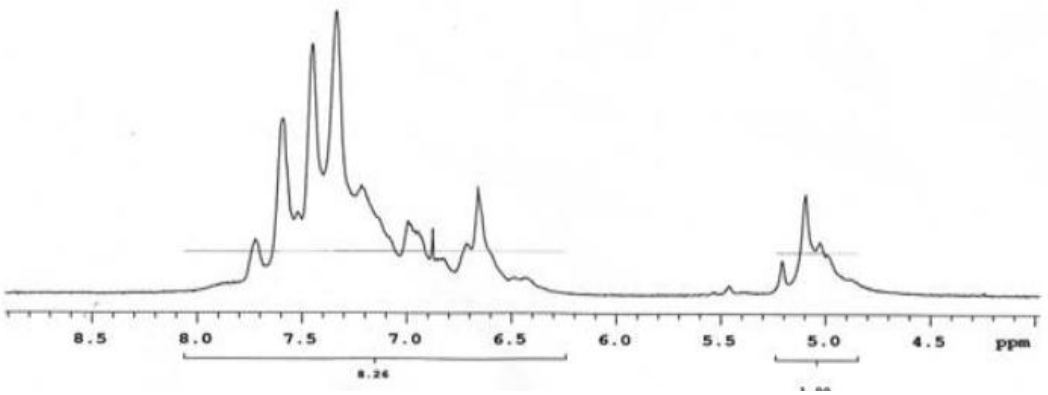

Figure 3.6. ^{1}H-NMR of $[NH_2PhSiO_{1.5}]_x[PhSiO_{1.5}]_{10/12-x}$ (x = 2-4) (Fraction 3) in DMSO-d_6.

Figure **3.7** provides GPC data (THF) for the starting compounds, the crude reaction mixture and Fraction 3. Table **3.5** provides relevant molecular weights and polydispersities for the same materials. The molecular weights are measured against polystyrene standards and are always lower than the estimated values because of the spherical nature of the SQs.

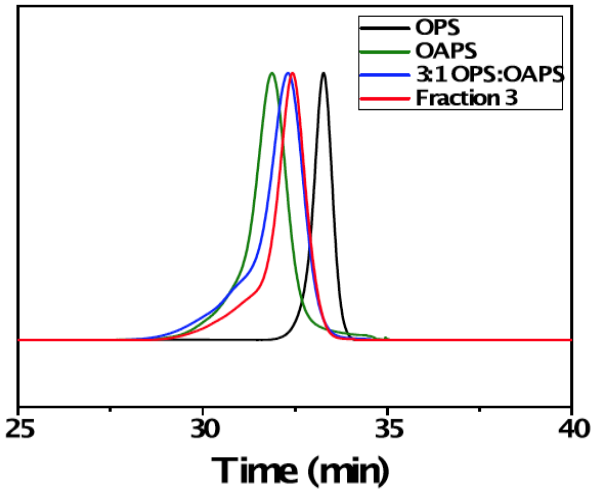

Figure 3.7. GPC (THF) of the starting compounds, the crude reaction mixture and Fraction 3.

Table 3.7. GPC determined molecular weights and polydispersities of Figure **7** components.

	t_R (min)	M_n	M_w	PDI
OPS	33.3	940	945	1.01
OAPS	31.9	1450	1490	1.03
3:1 OPS:OAPS reaction product	32.3	1330	1410	1.06
Fraction 3	32.5	1250	1290	1.04

3.2.2. Polymerization of $[NH_2PhSiO_{1.5}]_x[PhSiO_{1.5}]_{10/12-x}$ (x = 2-4) and DGEBA

Fraction 3 consisting primarily of $[NH_2PhSiO_{1.5}]_x[PhSiO_{1.5}]_{10/12-x}$ (x = 2-4) was reacted with DGEBA in effort to form a BoC polymer per Scheme **3.5**.

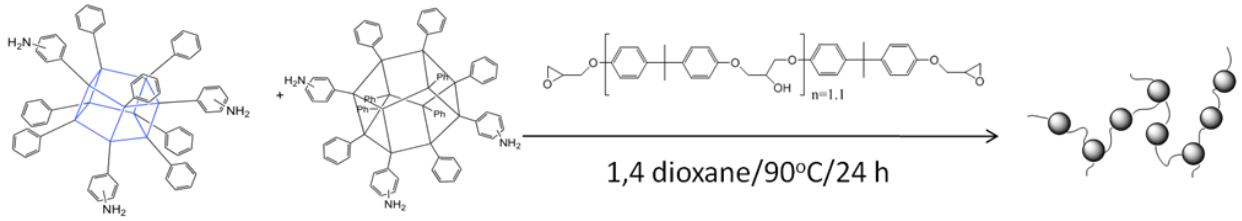

Scheme 3.5. BoC polymerization of $[NH_2PhSiO_{1.5}]_x[PhSiO_{1.5}]_{10/12-x}$ (x = 2-4) with DGEBA.

In this polymerization, when DGEBA was added at 1:1 mole ratio of [epoxy]:[amine], insoluble cross-linked polymer was observed to form as might be expected given that fraction 3 includes tri-amino functionalized cages. Therefore, the amount of DGEBA and reaction time were adjusted eliminate formation of insoluble. By trial and error, we found that a 0.8:1 ratio of [epoxy]:[amine] provided a soluble high molecular weight polymer. Thus Figure **3.8** provides GPC traces following the polymerization process with time. Initially, only low MW oligomers are observed until the last 3 h of reaction.

At 24 h of reaction time, the synthesized BoC polymers are soluble in THF and exhibit a bimodal molecular weight distribution by GPC as seen in Figures **3.8** and **3.9**. The bimodal components can be purified by precipitation using solubility differences. The low molecular weight (MW) polymers dissolve easily in THF on stirring for 2 h at ambient. In contrast, the high MW polymers must be sonicated dissolve. Figure **3.9** records the GPC traces for the mixture of

fraction 3 and DGEBA, the as-formed BoC polymer, and its fractional dissolution products (see Experimental).

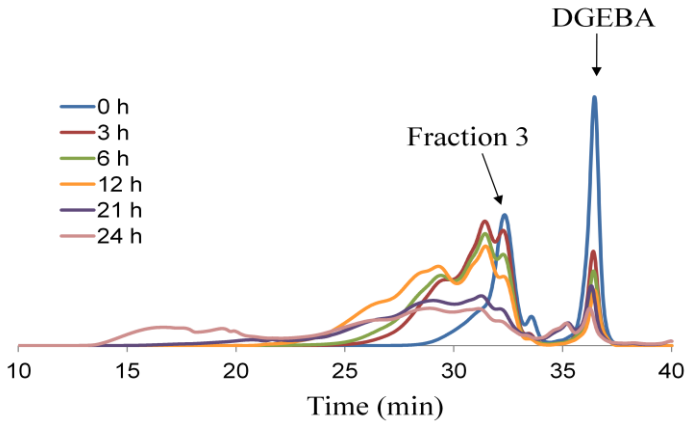

Figure 3.8. Progress of fraction 3 and DGEBA polymerization, monitored by GPC.

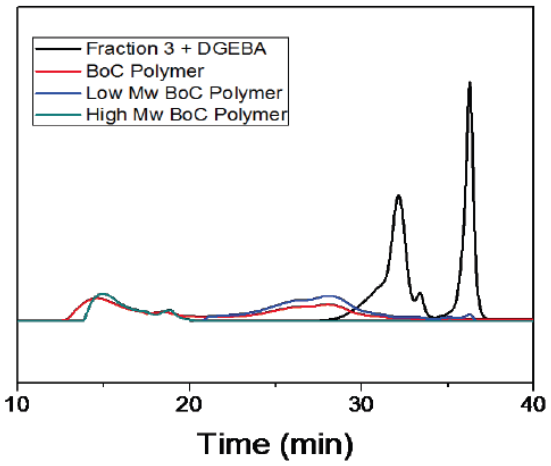

Figure 3.9. GPC trace of fraction 3 and DGEBA mixture, BoC polymer after 24 h, separated low and high molecular weight BoC polymers.

Table 3.8. GPC determined molecular weights and polydispersities of Figure **3.9** components.

	M_n	M_w	PDI
BoC polymer	9k	74m	8000
Low Mw polymer	6k	10k	1.6
High Mw polymer	12.6m	270m	21

The formation of a bimodal size distribution can be explained in several ways. First it is important to note that although fraction 3 consists of both di- and triamino- cages, the exact position of amino groups on the "spherical" surface of the cages is unknown. It is possible that some of these groups are adjacent to each other. Thus, one could envision that epoxy reactions will lead to compounds wherein it is possible to form cyclomers. If the average MW of the monomer unit is of the order of 1700-1900 Da, then one can envision a cyclic with three repeat units in it.

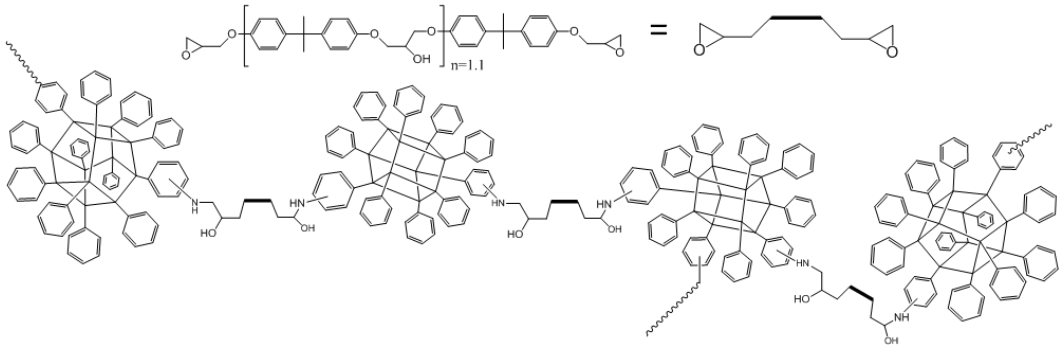

Figure 3.10. General Epoxy coupling reaction.

Alternately, the epoxy reaction of Figure **3.10** will first produce "linear" oligomers where some of the cages will have a third NH_2- group. One can envision that after two epoxy linkages form, this third NH_2- may be sufficiently sterically encumbered as to be much less reactive. At some point, as amine functionalities react, those left will be these encumbered sites. Eventually, they can be expected to react. This process will produce branches and or cross-links between shorter chains leading to very non-linear but higher MW species and/or species with several links between shorter chains. One might then suggest that the "interior" of these species will be less accessible to solvent resulting in quite different behavior to a common solvent. This seems most likely given the propensity to form insoluble materials at a 1:1 mole ratio of epoxy to amine as used traditionally.

While all species are soluble in the original reaction solution at 90 ℃, on precipitation only the low MW species are readily soluble in cold THF. The higher MW polymer only dissolved when heated to ≈ 60 ℃ and encouraged to dissolve via sonication. These aspects suggest difficult in solvating "interior" components supporting the above speculation.

In efforts to understand the structure of the BoC products, we briefly explored ^{1}H NMR characterization. Thus Figure **3.11** provides the NMR of BoC polymer, the starting DGEBA oligomer. The integration ratio of amino to phenyl proton of fraction 3 and BoC polymer changes from 1:10.8 to 1:11.9. Also, the alkyl proton (Ha, Hd) peaks broadened, as might be expected, after polymerization. These mean the DGEBAs are incorporated in the BoC polymers.

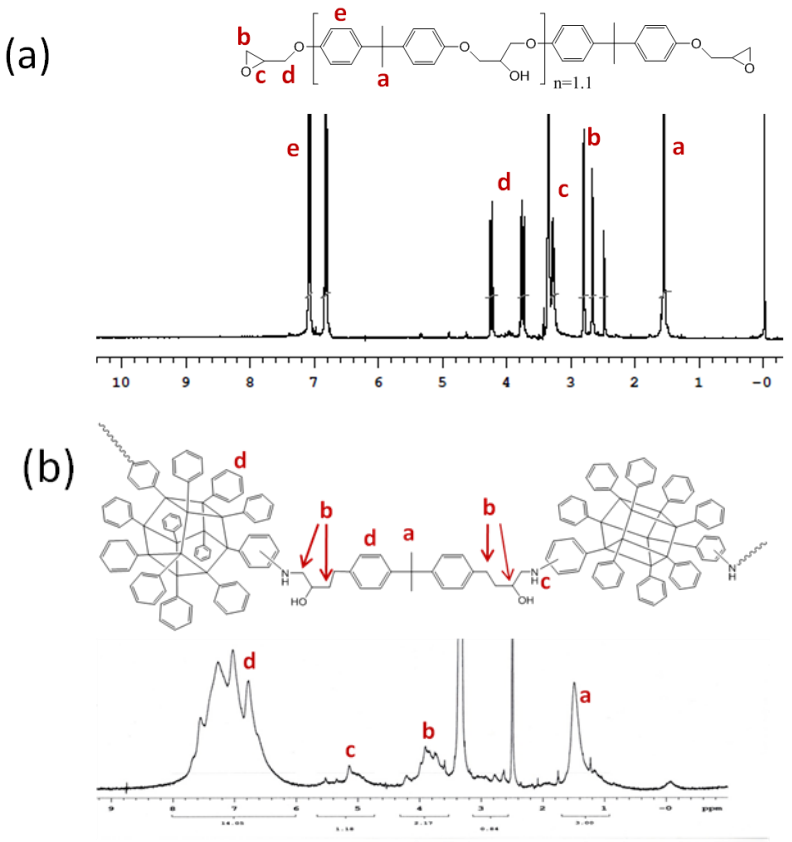

Figure 3.11. ^{1}H-NMR for (a) DGEBA, and (b) BoC polymer in DMSO-d_6.

Complementary IR studies are presented in Figure **3.12**. In general, the FTIR of the high MW and low MW fractions are quite similar with a slight broadening in the High MW materials at 1050 cm^{-1} in a region attributable to νC-O. Otherwise the FTIRs are as expected for these compounds based on our previous work.[31]

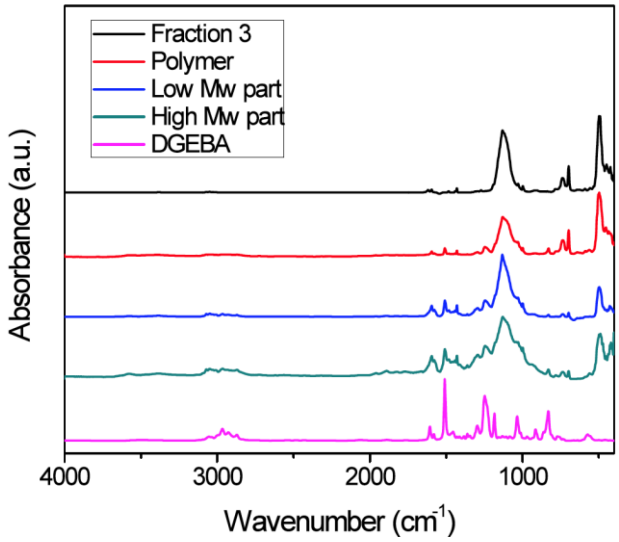

Figure 3.12. IR spectra of monomers and synthesized polymers for comparison.

Figure **3.13** shows TGAs of BoC polymer and starting materials. Table **3.9** shows $T_{5\%}$ for the high and low MW polymers to be 320-330℃ in air as expected from previously published studies on OAP/DEGBA nanocomposites.[31] The ceramic yields for both systems are 32±1 % respectively.

The lower ceramic yield found for the BoC polymer compared to fraction 3 arises because the polymer incorporates DGEBA which dilutes the total silica mass.

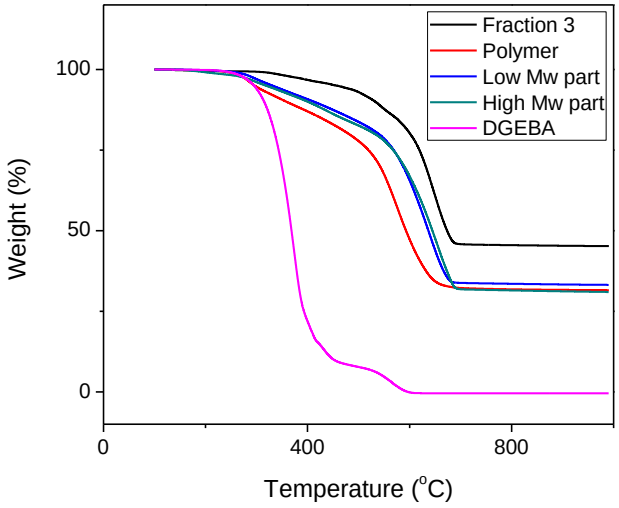

Figure 3.13. TGA of the synthesized polymer and starting materials for comparison in air (10℃/min).

Table 3.9. Decomposition temperatures ($T_{d5\%}$, $T_{d50\%}$) and ceramic yields of synthesized polymers and starting materials for comparison (air, 10 ^{o}C/min to 1000 ^{o}C).

Compound	$T_{d5\%}$(^{o}C)	$T_{d50\%}$ (^{o}C)	Ceramic Yield (%)	Theoretical Ceramic Yield (%)
DGEBA	295	370	0.0	
Fraction 3	450	670	45.2	
BoC Polymer	300	595	31.6	34.7
High Mw part	320	645	31.0	
Low Mw part	330	635	33.2	

DSC studies shown in Figure **3.14** suggest an initial Tg for both the low and high MW components at ≈ 125 ℃ which disappear in the second cycle likely as a result of extended cross-linking.

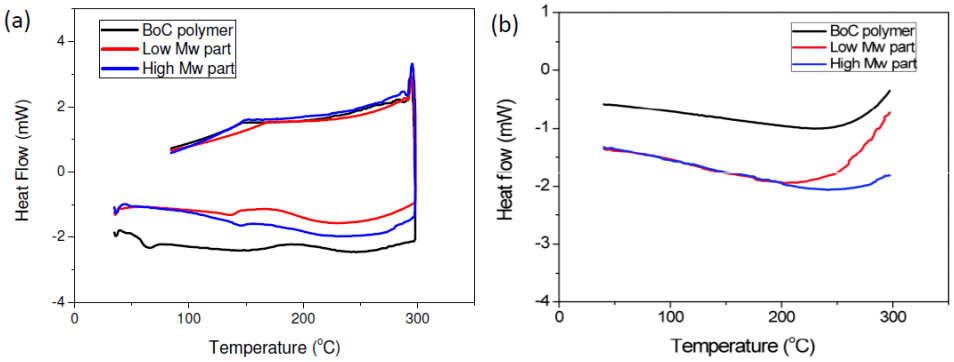

Figure 3.14. (a) First (b) Second DSC of BoC polymer, high Mw part and low Mw part.

3.3. Conclusions

We find that it is quite possible to develop routes to BoC epoxy resin systems that are soluble and processable if one is careful to control the amine:epoxy ratios. The accompanying paper provides a parallel approach wherein an alkyl amine group is used in place of an aromatic amine, extending the generality of this approach. In future papers, we plan to present mechanical properties data as shown in the accompanying paper and also to extend the current studies to amides and imides. Finally, it is important to recognize that the insolubles from this system may be redissolved by addition of more OPS and a catalytic amount of fluoride ion making these systems recyclable.

References Cited:

1. Voronkov, M.G.; Lavrent'yev, V.I.; "Polyhedral Oligosilsesquioxanes and Their Homo Derivatives," *Top. Curr. Chem*., **1982**, *102*, 199-236.
2. Baney, R.H.; Itoh, M.; Sakakibara, A.; Suzuki, T.; "Silsesquioxanes," *Chem. Rev*., **1995**, *95*, 1409-1430.
3. Loy, D.A.; Shea, K.J.; "Bridged Polysilsesquioxanes. Highly Porous Hybrid Organic-Inorganic Materials," *Chem. Rev*., **1995**, *95*, 1431-1442.
4. Calzaferri, G.; "Silsesquioxanes," in Tailor-made Silicon-Oxygen Compounds, from molecules to materials, Corriu, R. and Jutzi, P. Ed., Friedr. Vieweg & Sohn mbH, Braunshweig/Weisbaden, Germany, **1996**, pp. 149-169.
5. Lichtenhan, J.; "Silsesquioxane-based Polymers," in Polymeric Materials Encyc., Salmon, J.C. Ed., Vol. 10, CRC Press, N.Y., **1996**, pp. 7768-7777.
6. Provatas, A.; Matisons, J.G.; "Synthesis and applications of silsesquioxanes," *Trends Polym. Sci*., **1997**, *5*, 327-333.
7. Li, G.; Wang, L.; Ni, H.; Pittman, C.U.; "Polyhedral Oligomeric Silsesquioxane (POSS) Polymers and Copolymers: A Review," *J. Inorg. Organomet. Polym.*, **2001**, *11*, 123-151.
8. Duchateau, R.; "Incompletely Condensed Silsesquioxanes: Versatile Tools in Developing Silica-Supported Olefin Polymerization Catalysts," *Chem. Rev.*, **2002,** *102*, 3525-3542.
9. Abe, Y.; Gunji, T.; "Oligo- and polysiloxanes" *Prog. Polym. Sci.*, **2004**, *29*, 149-182.
10. Phillips, S H.; Haddad, T. S.; Tomczak, S. J.; "Developments in nanoscience: polyhedral oligomeric silsesquioxane (POSS)-polymers," *Curr. Opin. Solid State Mater. Sci*., **2004**, *8*, 21-29.
11. Laine, R. M.; "Nanobuilding blocks based on the $[OSiO_{1.5}]_x$ (x = 6, 8, 10) octasilsesquioxanes," *J. Mater. Chem*., **2005**, *15*, 3725-3744.
12. Lickiss, P. D.; Rataboul, F.; "Fully Condensed Polyhedral Oligosilsesquioxanes (POSS): From Synthesis to Application," *Adv. Organomet. Chem*., **2008**, *57*, 1-116.
13. Chan, K. L.; Sonar, P.; Sellinger, A.; "Cubic silsesquioxanes for use in solution processable organic light emitting diodes (OLED)," *J. Mater. Chem*., **2009**, *19*, 9103-9120.

14. Kannan, R. Y.; Salacinski, H. J.; Butler, P. E.; Seifalian, A. M.; "Polyhedral oligomeric silsesquioxane nanocomposites: The next generation material for biomedical applications," *Acc. Chem. Res.*, **2005**, *38*, 879-884.
15. Cordes, D. B.; Lickiss, P. D.; Franck, R.; "Recent Developments in the Chemistry of Cubic Polyhedral Oligosilsesquioxanes," *Chem. Rev.*, **2010**, *10*, 2081-2173.
16. Laine, R. M.; Roll, M. F.; "Polyhedral Phenylsilsesquioxanes," *Macromolecules*, **2011**, *44*, 1073-1109.
17. Wu, J.; Mather, P. T.; "POSS Polymers: Physical Properties and Biomaterials Applications," *Polym. Rev.*, **2009**, *49*, 25-63.
18. Li, Z.; Kawakami, Y.; "Formation of incompletely condensed oligosilsesquioxanes by hydrolysis of completely condensed POSS via reshuffling," *Chem. Lett.*, **2008**, *37*, 804-805.
19. Morimoto, Y.; Watanabe, K.; Ootake, N.; Inagaki, J. Yoshida, K.; Ohguma, K.; "Silsesquioxane Derivatives and Process or Production Therefore," U. S. Patent Application 20040249103A1 Sept. 2002.
20. Seino, M.; Hayakawa, T.; Ishida, Y.; Kakimoto, M.; Watanabe, K.; Oikawa, H. "Hydrosilylation Polymerization of Double-Decker-Shaped Silsesquioxane Having Hydrosilane with Diynes," *Macromolecules*, **2006**, *39*, 3473-3475.
21. Yoshida, K.; Hattori, T.; Ootake, N.; Tanaka, R.; Matsumoto, H.; "Silsesquioxane-Based Polymers: Synthesis of Phenylsilsesquioxanes with Double-Decker Structure and Their Polymers," in Silicon Based Polymers, Ganachaud, F.; Boileau. S.; Boury, B. eds Springer Netherlands **2008**, pp. 205-211.
22. Hoque, Md. A.; Kakihana, Y.; Shinke, S.; Kawakami, Y.; "Polysiloxanes with Periodically Distributed Isomeric Double-Decker Silsesquioxane in the Main Chain," *Macromolecules*, **2009**, *42*, 3309-3315.
23. Wu, S.; Hayakawa, T.; Kikuchi, R.; Grunzinger, S. J.; Kakimoto, M.; Oikawa, H.; "Synthesis and Characterization of Semiaromatic Polyimides Containing POSS in Main Chain Derived from Double-Decker-Shaped Silsesquioxane," *Macromolecules*, **2007**, 40, 5698-5705.

24. Lichtenhan, J. D.; Vu, N. Q.; Carter, J. A.; Gilman, J.W.; Feher, F.J.; "Silsesquioxane-siloxane copolymers from polyhedral silsesquioxanes," *Macromolecules,* **1993**, *26* 2141–2142.

25. Takahashi, K.; Sulaiman, S.; Katzenstein, J. M.; Snoblen, S.; Laine, R. M.; "New Aminophenylsilsesquioxanes, Synthesis, Properties and Epoxy Nanocomposites," *Aust. J. Chem.*, **2006**, *59*, 564-570.

26. Roll, M. F.; Mathur, P.; Takahashi, K.; Kampf, J. W.; Laine, R. M.; "$[PhSiO_{1.5}]_8$ promotes self-bromination to produce $[o\text{-}BrPhSiO_{1.5}]_8$: further bromination gives crystalline $[2,5\text{-}Br_2PhSiO_{1.5}]_8$ with a density of 2.32 g cm^{-3} and a calculated refractive index of 1.7 or the tetraicosa bromo compound $[Br_3PhSiO_{1.5}]_8$," *J. Mater. Chem.*, **2011**, *21*, 11167-11176.

27. Sulaiman, S.; Zhang, J.; Goodson III, T.; Laine, R. M.; "Synthesis, characterization and photophysical properties of polyfunctional phenylsilsesquioxanes: $[o\text{-}RPhSiO_{1.5}]_8$, $[2,5\text{-}R_2PhSiO_{1.5}]_8$, and $[R_3PhSiO_{1.5}]_8$. Compounds with the highest number of functional units/unit volume," *J. Mater. Chem.*, **2011**, *21*, 11177-11187.

28. Asucion, M. Z.; Laine, R.M. "Fluoride Rearrangement Reactions of Polyphenyl- and Polyvinylsilsesquioxanes as a Facile Route to Mixed Functional Phenyl, Vinyl T_{10} and T_{12} Silsesquioxanes," *J. Am. Chem. Soc.*, **2010**, *132*, 3723-3736.

29. Ronchi, M.; Sulaiman, S.; Boston, N. R.; Laine, R. M.; "Fluoride catalyzed rearrangements of polysilsesquioxanes, mixed Me, vinyl T_8, Me, vinyl T_{10} and T_{12} cages," *Appl. Organometal. Chem.* **2009**, *24*, 551-557.

30. Samthong, C.; Laine R. M.; Somwangthanaroj, A.; "Synthesis and characterization of organic/inorganic epoxy nanocomposites from poly(aminopropyl/phenyl)-silsesquioxanes," *J. Appl. Polym. Sci.*, **2013**, *128*, 3601-3608.

31. Tamaki, R.; Tanaka, Y.; Asuncion, M. Z.; Choi, J.; Laine, R. M. "Octa(aminophenyl)-silsesquioxane as a Nanoconstruction Site," *J. Am. Chem. Soc.* **2001** *123*, 12416-12417.

Chapter 4

Synthesis and characterization of conjugated BoC polymers from Octaiodophenylsilsesquioxane (I_8OPS)

Published in Macromolecules, vol. 46, pp 7580-7590, 2013

Abstract

The general objectives of the work reported here and in accompanying papers are to identify optimal tools for the synthesis of silsesquioxane (SQ) based BoC oligomers and polymers; especially those that show 3-D, through chain (cage) conjugation in the excited state. Here we first examine the utility of polymerizing octa(iodophenyl)silsesquioxane (I_8OPS) with divinylbenzene (DVB) using Heck catalytic cross coupling as baseline systems for BoCs with model dendrons. Thereafter, we functionalize the remaining IPh groups by cross coupling with 4-$MeOC_6H_4CH=CH_2$ or 4-$NH_2C_6H_4CH=CH_2$. As an alternate approach, we first functionalize (*p*-$IPhSiO_{1.5}$)$_8$ with 4-$MeOC_6H_4CH=CH_2$ or 4-$NH_2C_6H_4CH=CH_2$ by catalytic cross coupling such that only an average of two iodophenyls remain and then polymerized with DVB or 1,4-diethynylbenzne (DEB). This latter approach permits synthesis of copolymers as demonstrated using 1:1 mixtures of the two SQs with R = NH_2 or OMe.

Here we assess the utility of two different routes to conjugated BoC polymers. Investigation of the UV-vis absorption and emission properties of these BoCs indicates the DVB polymers exhibit no emission red-shifts because a significant portion of the DVB used is the 1,3 isomer. However, the DEB polymers reveal ~40 nm red-shifts and charge transfer (CT) behavior, suggesting electronic interactions between SQ cages through the conjugated, bridging moieties. DEB copolymers with R = NH_2- and MeOStilbene functional groups on the cages show red

shifts intermediate between the red shifts of the simple homopolymeric materials, rather than independent emissions from both units as would obtain with a physical mixture again supporting electronic communication along the polymer chains *and through the cages* via the conjugated linkers.

4.1. Introduction

Polyhedral silsesquioxanes (SQs), $[RSiO_{1.5}]_{8,10,12}$ (R = alkyl, alkenyl, alkynyl, aryl, R'Me_2SiO, etc) have received considerable recent attention because of their: (1) robust nature due in part to the silica core; (2) potential to be functionalized up to 24 times in one or two steps; (3) ease of purification, (4) potential to be assembled nanometer by nanometer into 3-D nanostructures (nanocomposites) because of their high symmetry and small size (1.2-1.6 nm dia.), (5) ability to undergo functional group exchange under mild conditions promoted by F^-, and (6) potential to offer 3-D conjugation in the excited state.[2-22]

We recently developed a route to di- and trifunctional T_{10} and T_{12} silsesquioxane cages using F^- catalyzed exchange of functional groups between two different polysilsesquioxanes (1)[1] and/or T_8 systems (2).[23] We have used this approach to synthesize the first "beads on a chain" or BoC oligomers finding that the use of conjugated linkers resulted in large red shifts in emission compared to model compounds leading to the conclusion that some form of 3-D conjugation occurs in the excited state that involves both the cages and the conjugated linker.

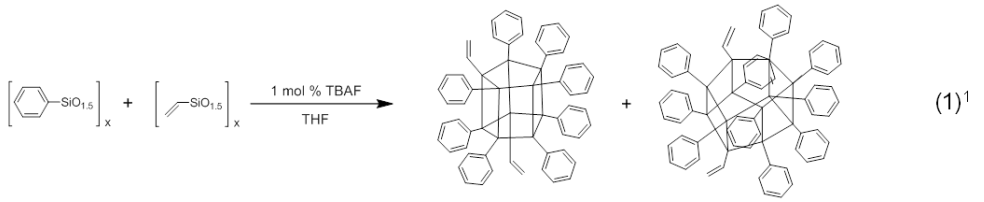

(1)[1]

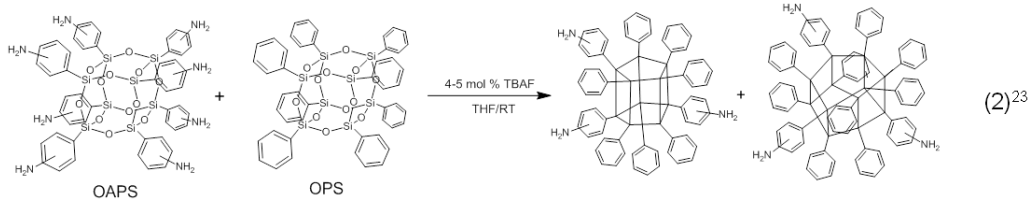

(2)[23]

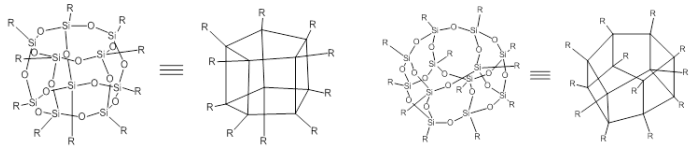

Electron delocalization through SQ cores and via conjugated linkers could offer potentially new organic/inorganic hybrid semiconducting materials and or systems that could serve as components in OLEDs and photovoltaic devices. This then provides the motivation to develop sets of synthetic tools for the synthesis of other BoC oligomers and polymers. Additional motivation arises because of the recent interest in the synthesis of dendronized polymer systems.[24-26]

A number of other groups have used ring opening methods to produce difunctional SQs and then gone on to produce polymeric systems with the cage in the backbone leading to several brief examples of BoC polymers.[27, 28] In these previous efforts, the resulting BoC polymers were unfunctionalized.

In this paper, we concentrate on the use of Heck and Sonogashira catalytic cross coupling to access a variety of conjugated BoC systems starting from octa(iodophenyl)SQ (I_8OPS), [*p*-IPhSi$O_{1.5}$]$_8$. In a complementary study reported coincidentally, we explore the use of ADMET metathesis and "reverse" Heck cross coupling with brominated organic linkers as additional synthetic routes to BoC systems.[29]

The first step in our efforts began with exploration of routes to BoCs with the potential to serve as a basis set for making highly functionalized BoC systems for multiple applications per reaction (3). A further objective was to generate more examples of BoCs that offer 3-D conjugation in the excited state to probe the general nature of these unusual systems.

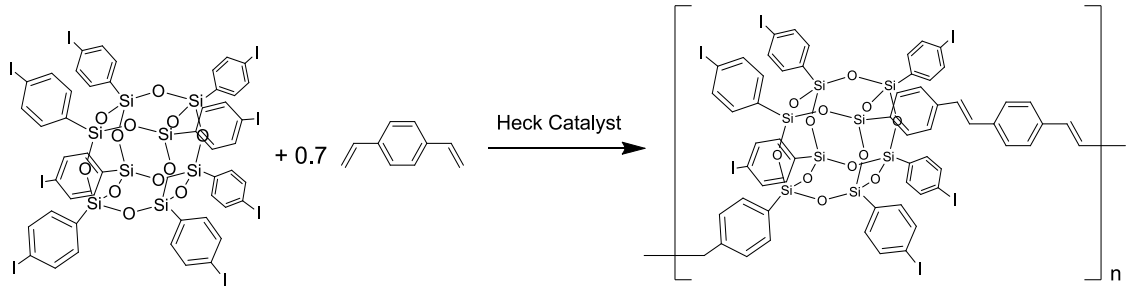

(3)

4.2. Results and Discussion

The objectives of this study were to develop synthetic tools that can be used to make highly functionalized or dendronized BoC oligomers and polymers. We are particularly interested in exploring how the introduction of conjugated linkers affects the emissive behavior

of these materials with the idea of finding multiple new examples that offer what we believe is 3-D conjugation in the excited state.

In the following sections, we describe two different synthetic routes to conjugated silsesquioxane BoC oligomers and polymers. A complementary paper discusses two additional synthetic routes to the same materials.[29] First, we explore the polymerization of I_8OPS via Heck coupling with divinylbenzene (DVB) and its further functionalization with *p*-R-styrene compounds via a second Heck coupling. Next, we discuss the synthesis of di- and triiodophenyl SQs through partial Heck coupling of I_8OPS with *p*-R-styrene, followed by polymerization with DVB and 1,4-diethynylbenzene (DEB) using Heck and Sonogashira coupling methods. Thereafter we discuss the photophysical properties of synthesized BoC polymers, the di- and triiodophenyl SQs and their copolymers with DVB and DEB. These systems represent the first models mapping structure-property relationships in highly dendronized BoCs. In a second complementary paper we describe one example of a more extensively conjugated linker and other approaches to BoC systems.[29]

4.2.1. Synthesis of BoC polymers from I_8OPS and DVB

Our initial work centered on reacting I_8OPS with DVB using Heck coupling to form BoC polymers per reaction (3). We find that the amount and method of addition of DVB are critical to preparing soluble polymers because all eight iodide groups can react to form crosslinked, insoluble polymers. After trial and error, we found that high molecular weight, soluble polymers were obtained when 0.7 eq. of DVB was added incrementally (see Chapter **2**). The synthesized polymers include low molecular weight SQs, therefore, these polymers were further purified via column chromatography prior to model dendronization studies. Also, these polymers show very broad molecular weight distributions (Figure **4.1**) as might be expected because single I_8OPS molecules are statistically likely to react with more than one DVB as discussed just below.

Even though the polymer **I** in reaction (3) and Scheme **4.1** described as a linear polymer, however, the actual chemical structure we expect is branch polymer with kink points because more than one DVB can coupled with I_8OPS and the coupling position is not controllable (Figure **4.2**).

Heck coupling of polymer **I** and *p*-R-styrene was attempted in initial efforts to demonstrate their potential to be modified via traditional Heck, Sonogashira, Stille, and Suzuki coupling chemistries (Scheme **4.1**). As mentioned earlier, the general structure of synthesized polymer **II-IV** is not linear but the structure described in Figure **4.2**. The chemical structure of polymers in Scheme **4.1** is simplified for clarity.

Figure **4.3** provides the GPC traces of polymers **I**–**IV** after purification via column chromatography. The GPC results show, as expected, that the introduction of styrenyl groups in polymer **I** increases the molecular weight.

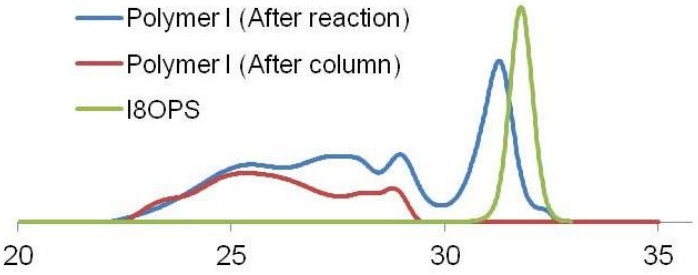

Figure 4.1. GPC trace of I_8OPS and polymer **I** before and after purification for comparison.

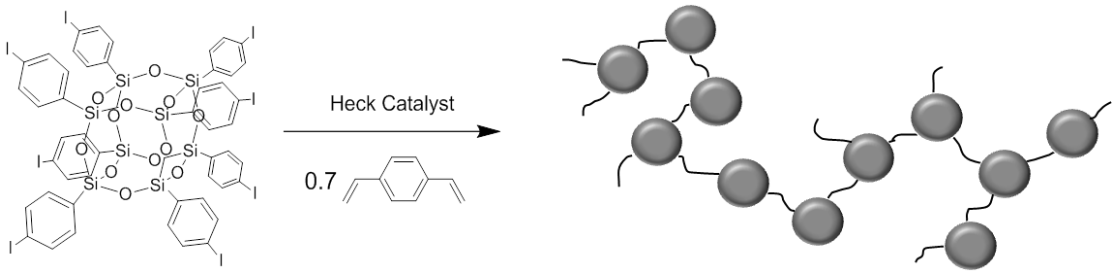

Figure 4.2. General BoC structure of Polymer **I**.

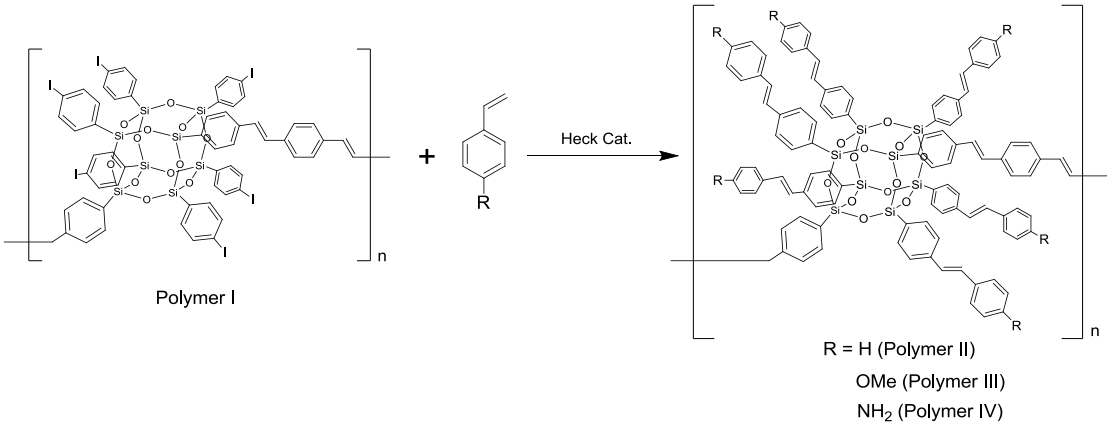

Scheme 4.1. Heck coupling of polymer **I**.

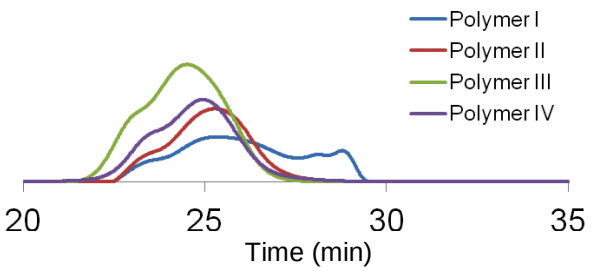

Figure 4.3. GPC traces for polymers **I**–**IV** after purification.

Polymers **II**–**IV** were characterized by FTIR (Figure **S-4**), ^{1}H-NMR (Figure **S-5**), and TGA (Figure **S-6**, Table **1**). Polymers **III** and **IV** showed characteristic methoxy (νC-O, 1250 cm^{-1}) and amino (νN-H, 3381 cm^{-1}) bands in FTIR. ^{1}H-NMR spectra also exhibit characteristic peaks at 3.7 (OCH_3, polymer **III**) and 5.3 (NH_2, polymer **IV**) ppm.

The found ceramic yields (CYs) for polymers **I-IV** that are about 1 wt % higher than the theoretical value; calculated based on perfectly linear polymer structures as illustrated in reaction (3) and Scheme **4.1** (Table **4.1**). The more iodo groups replace by DVB, the higher the ceramic yield because the molar mass of two iodine atoms is higher than one linking DVB (254 vs. 130). It is important at this juncture to note that CYs vary by ±0.2 % in repeated runs; although the resulting ceramic is white indicating complete oxidation of organics. Given that the Table **4.1** found CYs are about 1 wt % higher means that some fraction of the remaining iodo groups may also have reacted with DVB.

One reasonable alternative is that during Heck coupling, in the catalytic cycle, some "Pd-H" species is generated that reduces C-I aromatic bonds to C-H bonds leading to higher than calculated ceramic yields. This is a well-known side reaction in Heck cross coupling studies especially with iodo species.[30,31] We view this as a more reasonable explanation for the higher ceramic yields observed in this system rather than the above suggested reaction with additional DVB.

These results prompted our efforts to develop routes to BoCs with more regular structures as discussed just below. Nonetheless it is worthwhile noting that the TGA data indicate that these compounds have good to excellent thermal stabilities (> 300 ^{o}C) in air.

Table 4.1. Characterization data for polymers **I** - **IV**.

	GPC				TGA		
	M_n (KDa)	M_w (KDa)	PDI	DP	C.Y (wt %) (Found)	C.Y. (wt %) (Theory)	$T_{d(5\%)}$ (^oC)
Polymer **I**	9	27	2.9	6 ~ 18	26.4	25.1	300
Polymer **II**	17	37	2.2	9 ~ 19	28.1	27.1	300
Polymer **III**	24	54	2.2	11 ~ 26	25.5	24.6	355
Polymer **IV**	21	31	1.5	10 ~ 14	26.9	25.8	370

4.2.2. Synthesis of BoC polymers from diiodophenyl SQ monomers

As noted just above, the direct Heck coupling of I_8OPS with DVB is sensitive to the amount and method of addition of DVB. Moreover, the modification of the remaining iodo groups of synthesized BoC polymers (polymer **I**) is anticipated to be somewhat more difficult as coupling can be anticipated to be hindered in the polymer compared with the starting I_8OPS. Therefore, we assessed an alternate route that is initiated by first preparing di- and tri-iodo monomers via partial Heck coupling of I_8OPS with *p*-R-styrene.

4.2.2.1. Preparation of di- and triiodophenyl SQ

The title compounds were synthesized as illustrated in Scheme **2**. The chemical structure of monomer **A**, **B** and **C** in Scheme **2** provided one of isomers of diiodophenyl SQs for clarity. As discussed below, actual chemical composition of monomers are mixture of mono-, di- and triiodophenyl SQs. Moreover, di-, and triiodophenyl SQs are mixture of structural isomers because the substitution pattern of *p*-R-styrene around the SQ cube is random.

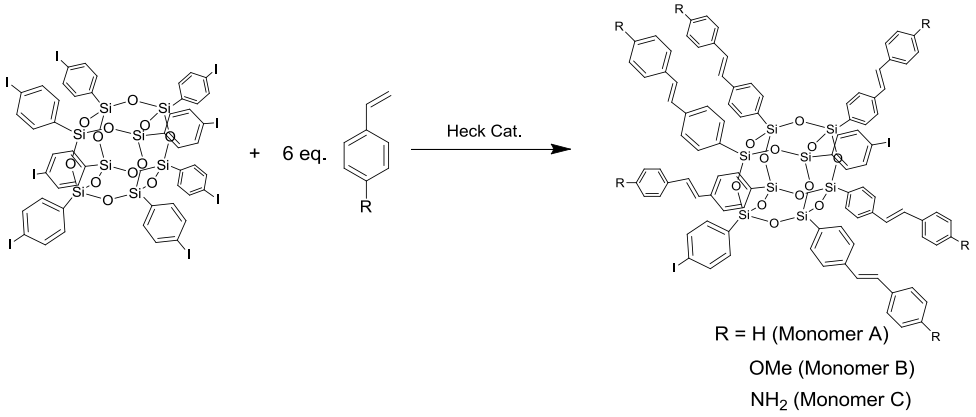

Scheme 4.2. Synthesis of monomers **A**, **B** and **C**.

The monomers were characterized by GPC (Figure **A1.1**), TGA (Figure **4.4**, Table **4.2**), MALDI-ToF (Figure **4.5**, Table **4.3**), ^{1}H-NMR and IR (Figure **A1.2**, **A1.3**). Figure **4.4** shows the TGAs of I_8OPS and monomers **A**, **B** and **C** in air. The theoretical ceramic yields for each monomer were calculated assuming perfect di-iodophenyl SQs. The found CYs match the theoretical values indicating that the average number of iodo groups per SQ cages is two (Table **4.2**). This means that it is possible to control the average degree of functionalization.

These results are supported by ^{1}H-NMR (Figure **S-3**). The calculated ratio of phenyl and vinyl protons to methyl protons in monomer **B** is 34:9 which corresponds to the integration, 33.2:9. For monomer **C**, the expected phenyl:vinyl:amino proton ratios (14:3:3) matches well with the measured peak ratios of 15:3:3.

Table 4.2. Characterization data for monomers **A** – **C** and I_8OPS.

	GPC			TGA		
	Mn (Da)	Mw (Da)	PDI	CY (%) (Found)	CY (%) (Theory)	$T_{d(5\%)}$ (^{o}C)
I_8OPS	1,450	1,490	1.01	23.6	23.6	400
Monomer **A**	1,870	1,900	1.01	25.5	25.3	390
Monomer **B**	2,050	2,090	1.02	23.2	23.1	315
Monomer **C**	2,190	2,260	1.03	24.6	24.2	395

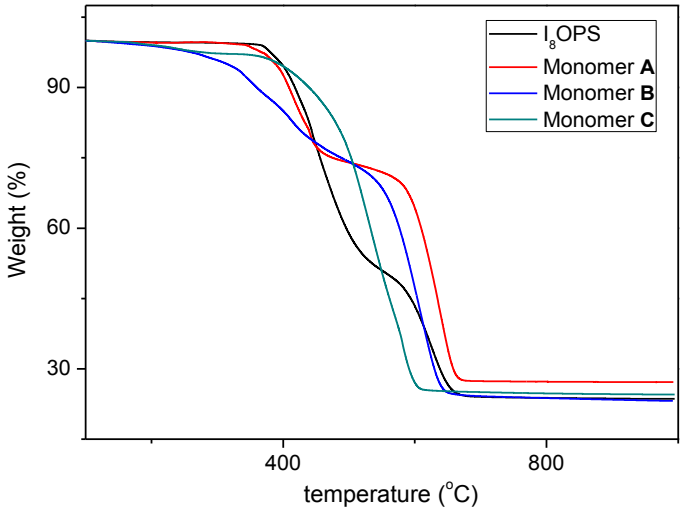

Figure 4.4. TGA of monomers **A**, **B** and **C** and I_8OPS for comparison (air, 10°C/min).

The MALDI-ToF data (Figure **4.4**, Table **4.3**) show that monomers **A** and **B** consist of a mixture of the desired di-iodophenyl SQ and mono and tri-iodophenyl SQs. Monomer **C** does not ionize under the experimental conditions used. Because these monomers include trifunctional SQs, DVB and/or DEB were added incrementally to prevent formation of insoluble, highly crosslinked polymers (see Chapter **2**). It is important to note that MALDI intensity data often does not provide a direct quantification of the species present because the intensities relate to the facility with which the individual components ionize. Thus, these data are best considered as qualitatively similar to the actual isomer compositions (see reference 29 where MALDI data vs. CY are compared).

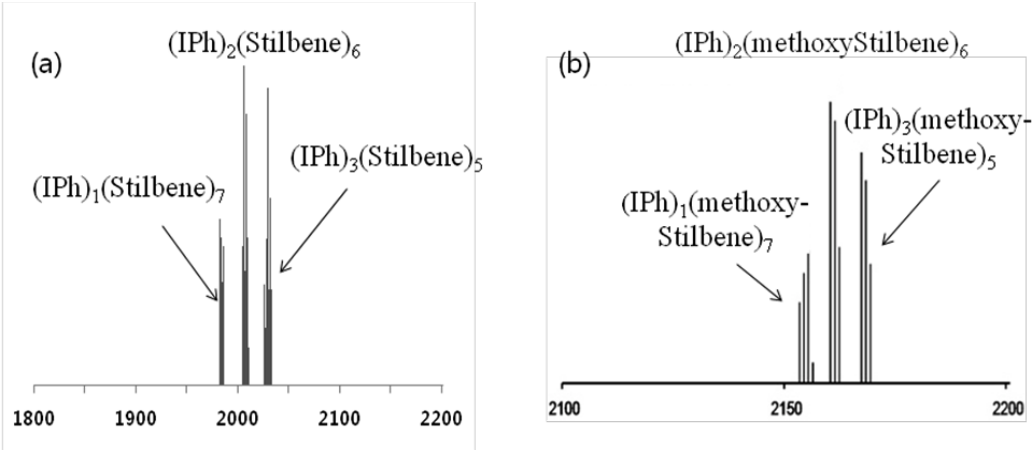

Figure 4.5. MALDI-ToF for (a) Monomer **A** and (b) **B**.

Table 4.3. MALDI-ToF data for Monomer **A** and **B**.[†]

Most Common Isotope	Found (Da)	Calculated (Da)	Relative Peak Intensity (%)
$(I\text{-}C_6H_4)_1(stilbene)_7(SiO_{1.5})_8$	1981.7	1982.2	52
$(I\text{-}C_6H_4)_2(stilbene)_6(SiO_{1.5})_8$	2005.8	2006.0	100
$(I\text{-}C_6H_4)_3(stilbene)_5(SiO_{1.5})_8$	2029.4	2029.7	87
$(I\text{-}C_6H_4)_1(OMestilbene)_7(SiO_{1.5})_8$	2154.3	2154.8	39
$(I\text{-}C_6H_4)_2(OMestilbene)_6(SiO_{1.5})_8$	2160.6	2161.1	100
$(I\text{-}C_6H_4)_3(OMestilbene)_5(SiO_{1.5})_8$	2166.7	2167.3	82

[†]Error in reported intensities is ± 5%

4.2.2.2. Polymerization of diiodophenyl SQs with DVB

The di- and triiodophenyl SQs (monomers **A**, **B** and **C**) were reacted with DVB using Heck coupling per Scheme **4.3**. One advantage of this approach is its potential for forming copolymers. To demonstrate this potential, a copolymer of monomers **B** and **C** (1:1 ratio) was synthesized (polymer **VIII**). As mentioned already, the synthesized polymer **V-VIII** is not linear polymer as shown in scheme **4.3** but the structure could be a branch polymer as described in Figure **4.2** because the monomers are mixture of di- and triiodophenyl SQs. The chemical structure of polymers in Scheme **4.3** is simplified for clarity.

Figure **4.6** and Table **4.4** provide characterization data for the synthesized polymers. The CYs are well matched with the theoretical values unlike the polymers **II** – **IV** even though in principle these polymers have same chemical structure. This approach allows us to also escape the process that leads to loss of iodo groups as noted above.

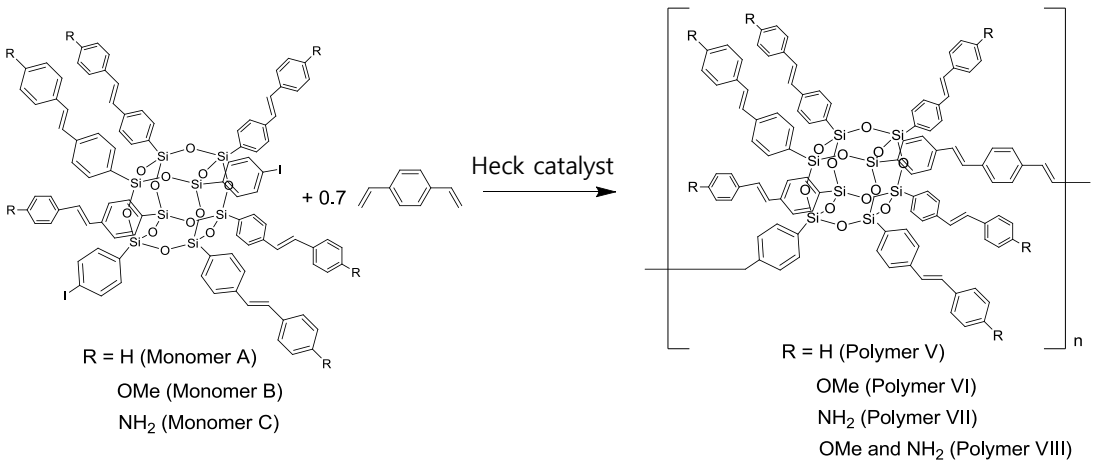

Scheme 4.3. Polymerization of diiodophenyl SQs and DVB via Heck coupling.

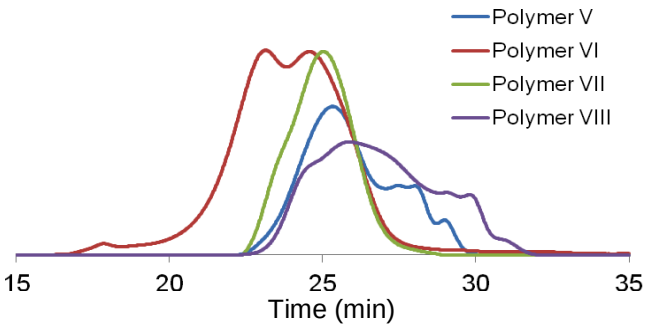

Figure 4.6. GPC traces for Polymers **V-VIII**.

Table 4.4. Characterization data for polymers **V** - **VIII**.

	GPC				TGA		
	Mn (KDa)	Mw (KDa)	PDI	DP	CY (%) (Found)	CY (%) (Theory)	$T_{d(5\%)}$ (^{o}C)
Polymer **V**	12	20	1.7	6 ~ 10	27.4	27.1	370
Polymer **VI**	30	72	2.4	14 ~ 34	25.0	24.6	320
Polymer **VII**	22	30	1.4	10 ~ 13	26.1	25.8	300
Polymer **VIII**	8	21	2.7	4 ~ 10	25.5	25.2	310

Polymers **VI**-**VIII** exhibit characteristic FTIR and ^{1}H-NMR spectra (Figure **A1.4**, **A1.5**). In particular, polymer **VIII** exhibits both methoxy and amino peaks indicating successful copolymerization. The photophysical properties of these polymers support this contention and are discussed below.

4.2.2.3. Polymerization of diiodophenyl SQs with 1,4-diethynylbenzene (DEB)

As discussed below, the absence of an emission red shift in the DVB polymers observed when using a starting material that was 75 % 1,3-DVB prompted us to explore the use of 1,4-diethynylbenzene, DEB. Conjugated BoC polymers were synthesized via Sonogashira cross coupling of monomers **A**-**C** with DEB per Scheme **4.4**. A copolymer of monomers **B** and **C** (1:1 ratio) was also synthesized (polymer **XII**). As mentioned already, the chemical structure of synthesized polymer **IX**-**XII** is not linear as provided in scheme **4.4** but the actual structure could be a branch polymer (Figure **4.2**). The chemical structure of polymers in Scheme **4.4** is simplified for clarity.

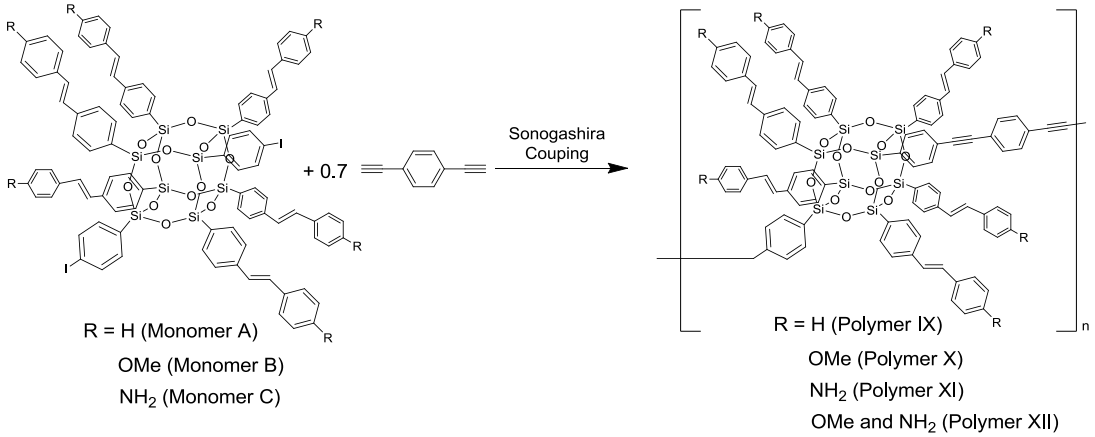

Scheme 4.4. Polymerization of diiodophenylSQs and DEB via Sonogashira coupling.

The Figure **4.7** and Table **4.5** characterization data indicate that the DEB polymers have lower molecular weights than the DVB polymers. This likely arises because the triple bonds of the linker allow fewer degrees of freedom thereby reducing the solubility of the resulting DEB oligomers and polymers.

In general, the FTIR, ^{1}H-NMR, TGA spectra (Figure **A1.4**, **A1.5**, **A1.6**) are all in agreement with those expected for the isolated polymers. Their photophysical properties are discussed below.

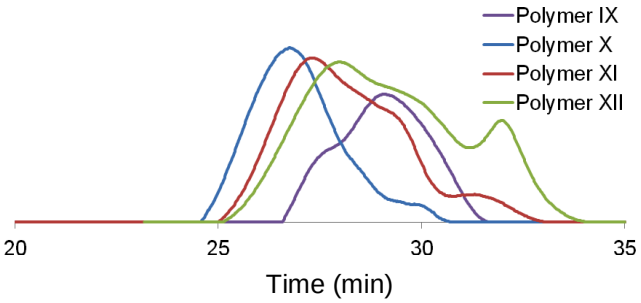

Figure 4.7. GPC traces for Polymers **IX-XII**.

Table 4.5. Characterization data for polymers **IX - XII**.

	GPC				TGA		
	Mn (KDa)	Mw (KDa)	PDI	DP	CY (%) (Found)	CY (%) (Theory)	$T_{d(5\%)}$ (^{o}C)
Polymer **IX**	16	27	1.7	8 ~ 14	28.1	27.2	370
Polymer **X**	16	20	1.3	8 ~ 10	24.3	24.7	300
Polymer **XI**	10	19	1.9	5 ~ 8	26.7	25.9	330
Polymer **XII**	9	22	2.5	4 ~ 10	25.5	25.3	340

4.2.3. Photophysical properties.

Figure **4.8** depicts the general structures of the DVB and DEB polymers. Figure **4.9** provides their UV-vis absorption and emission spectra and those for the corresponding monomers (THF). Their spectral data are summarized in Table **4.6**. The UV-vis absorption maxima of all the polymers are identical to the corresponding monomers and are very similar to our previous reports for the T_8[19,20] or $T_{10/12}$[21] or BoC SQs.[1]

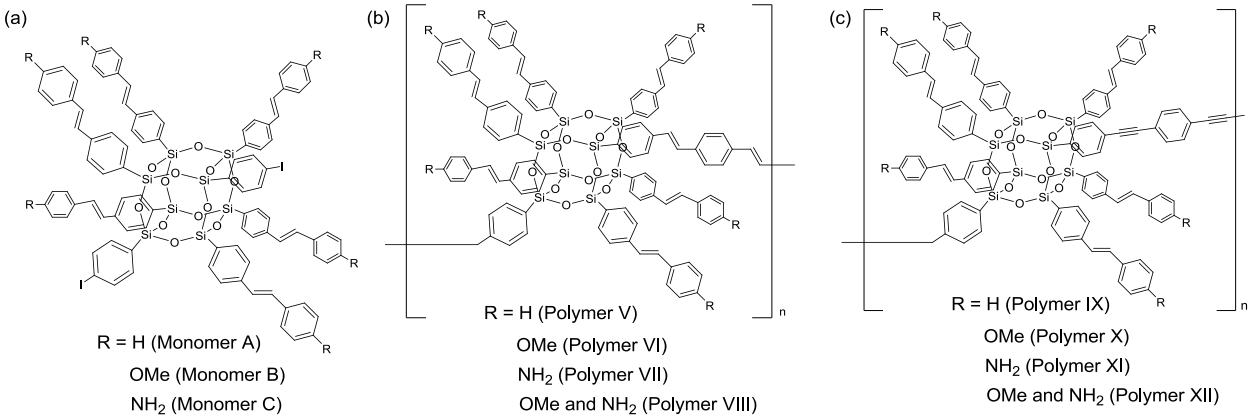

Figure 4.8. Proposed structures of (a) monomers, (b) DVB polymers and (c) DEV polymers.

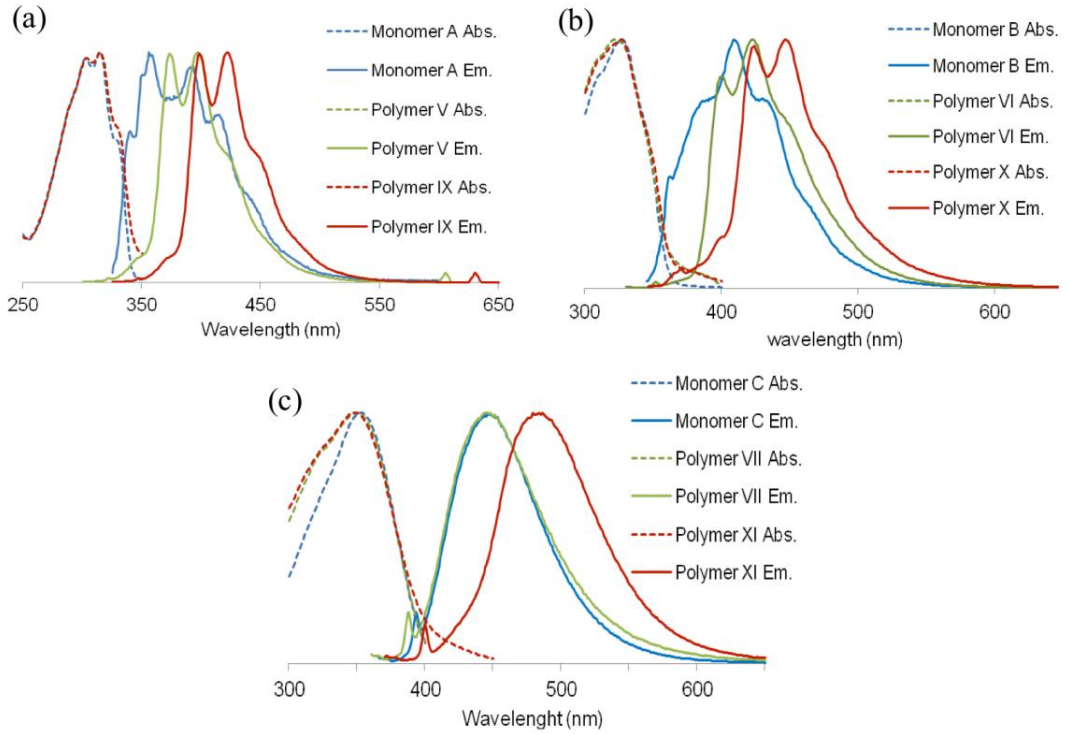

Figure 4.9. UV-vis and emission spectra of monomer, DVB polymer, DEB polymer in THF for comparison. (a) R=H, (b) R=OMe, (c) R=NH_2.

Table 4.6. Spectral data for monomers, DVB and DEB polymers.

	R	UV λ_{max} (nm) (± 2 nm)	PL λ_{max} (nm) (± 2 nm)	Φ_{PL} (%)
Monomers	Monomer **A** (H)[a]	315	359, 391	11
	Monomer **B** (OMe)[a]	327	409	12
	Monomer **C** (NH_2)[a]	353	446	6
DVB polymers	Polymer **V** (H)[a]	315	375, 397	23
	Polymer **VI** (OMe)[a]	321	422	19
	Polymer **VII** (NH_2)[a]	350	443	2
	Polymer **VIII** (OMe, NH_2)[a]	324	425	4
DEB polymers	Polymer **IX** (H)[a]	315	400, 423	12
	Polymer **X** (OMe)[a]	327	447	5
	Polymer **XI** (NH_2)[a]	350	484	1
	Polymer **XI** (NH_2)[b]	351	497	
	Polymer **XII** (OMe, NH_2)[a]	327	464	1
	Polymer **XII** (OMe, NH_2)[b]	330	479	

[a] in THF, [b] in Acetonitrile.

The DVB polymer emission spectra show less than 10 nm red shifts (R = H, OMe) or no shift (R = NH_2) compared with their respective monomers. This result indicates that there is no or very little electronic interaction between the SQ cages as might be anticipated because our source of DVB consists of a mixture of 1,3- (75 %) and 1,4-DVB (25 %) isomers.

Because 1,3-DVB does not offer conjugation in either the ground or excited states and presence of just 25 % 1,4-DVB greatly limits the opportunity to extend conjugation. These results support the fact that the red shifts observed previously[22] require conjugation through the linkers between the cages. Furthermore, overall, it seems that all forms of cages studied to date exhibit what we term 3-D excited state conjugation through cages via the conjugated linkers.

In contrast, the DEB polymer emission spectra show significant (~40 nm) red shifts compared with their respective monomers. This suggests 3-D electron delocalization in the excited state and conjugation that extends through the SQ cages and through the conjugated linker as seen in previously and in the two accompanying papers.[29]

Figure **4.10** provides the UV-vis and emission spectra for the copolymer of monomer **B** (methoxystilbene) and monomer **C** (aminostilbene), and their homopolymers for comparison. In

the case of the DVB polymers, the copolymer spectrum looks like a physical mixture of each homopolymer. As mentioned just above, conjugation in the DVB polymers is severely limited due to the high proportion of the 1,3-DVB isomer used in their syntheses. However, the maximum emission of the DEB copolymer (λ_{max}: 464±2 nm) is between that of the two homopolymers (λ_{max}: 447±2 and 484±2 nm). *This suggests that the lowest unoccupied molecular orbital (LUMO) of the copolymer reflects communication between each type of SQ through the conjugated tether*.

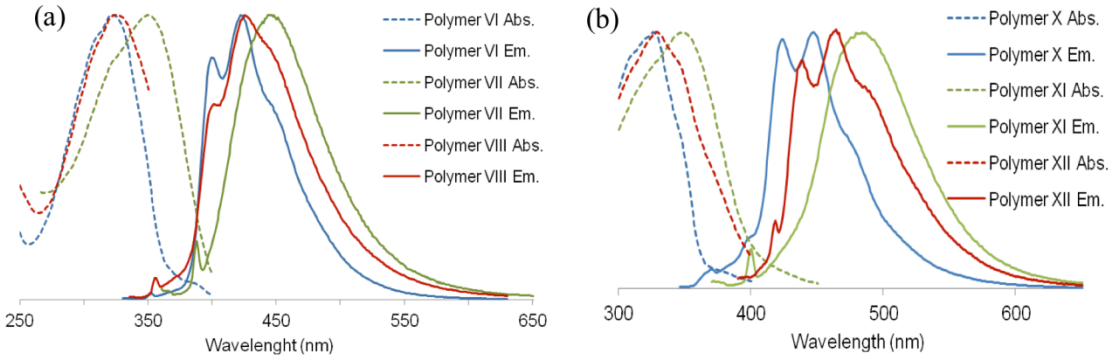

Figure 4.10. UV-vis and emission spectra of methoxystilbene polymers, aminostilbene polymers and their copolymers in THF for comparison. (a) DVB polymers, (b) DEB polymers.

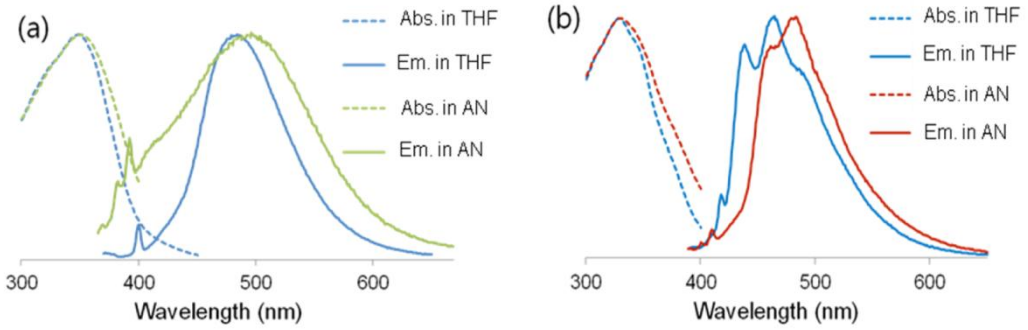

Figure 4.11. UV-vis and emission spectra of (a) Polymer XI, (b) Polymer XII in two good solvents (THF, AN).

To investigate the potential for charge transfer (CT) behavior in the DEB aminostilbeneSQ polymers, as seen in simple aminostilbenevinyl SQ compounds,[19-21] the solvent polarity effects on emission of polymers **XI** (homopolymer) and **XII** (copolymer) were explored. Figure **4.11**

provides the UV-vis and PL spectra for Polymers **XI** and **XII** in THF and acetonitrile (AN). Both polymers show ~ 15 nm red shifts in the more polar solvent, AN, than in the THF. Even though the red shift is less than in the *4*-aminostilbenevinylT_8 (25 nm) and $T_{10/12}$ (30 nm) SQs, [22-24] DEB polymers having 4-aminostilbene groups also show CT stabilization. As a final comment, the emission quantum yields seen in Table **4.6** are in line with what we have seen previously and are typical of stilbene moieties on and off SQ cages.[19-21]

4.3. Conclusions

This report details the synthesis and characterization of sets of non-conjugated (DVB) and conjugated (DEB) BoC polymers and copolymers derived from I_8OPS. We have explored two different synthetic routes, changing the reaction sequence of I_8OPS functionalization and linking each SQ via Heck or Sonogashira cross coupling with DVB or DEB. We have begun to explore the photophysical properties of these BoC polymers. Even though DVB polymers show no or very little conjugation because of the high density of 1,3-DVB linkers, the DEB polymers exhibit significant red shifts (~40 nm) in emission spectra compared with their corresponding monomers suggesting electron delocalization through the conjugated SQ cages.

Thus the DVB polymers and copolymers that do not offer conjugation between SQ cages, offer a negative proof for our continuing argument that when conjugation exists the observed red shifts support the presence of delocalization within and between cages. Moreover, the fact that the emission spectra of the DEB copolymers are an average of each homopolymer rather than a sum of the two individual homopolymers indicates communication between the two different SQ cages. Furthermore, BoC polymers having *p*-aminostilbene group exhibit charge transfer (CT) stabilization. These unique photophysical properties offer potential for new organic/inorganic hybrid semiconducting materials.

Finally, it is important to note that the compounds, oligomers and polymers prepared here do not offer conjugation in the ground state and should not be compared with typical organic polymers where π-π interactions in the ground state can greatly affect the HOMO energies. Consequently, these new materials will differ quite significantly from all organic systems and should not be compared with them. However, we do find that the introduction of

9,9'-dimethylfluorene linkers does offer a first example where there appears to be conjugation in the ground state as discussed in a complementary paper.[29]

References Cites:

1. Voronkov, M.G.; Lavrent'yev, V.I.; "Polyhedral Oligosilsesquioxanes and Their Homo Derivatives," *Top. Curr. Chem*., **1982**, *102*, 199-236.
2. Baney, R.H.; Itoh, M.; Sakakibara, A.; Suzuki, T.; "Silsesquioxanes," *Chem. Rev*., **1995**, *95*, 1409-1430.
3. Loy, D.A.; Shea, K.J.; "Bridged Polysilsesquioxanes. Highly Porous Hybrid Organic-Inorganic Materials," *Chem. Rev*., **1995**, *95*, 1431-1442.
4. Calzaferri, G.; "Silsesquioxanes," in Tailor-made Silicon-Oxygen Compounds, from molecules to materials, Corriu, R. and Jutzi, P. Ed., Friedr. Vieweg & Sohn mbH, Braunshweig/Weisbaden, Germany, **1996**, pp. 149-169.
5. Lichtenhan, J.; "Silsesquioxane-based Polymers," in Polymeric Materials Encyc., Salmon, J.C. Ed., Vol. 10, CRC Press, N.Y., **1996**, pp. 7768-7777.
6. Provatas, A.; Matisons, J.G.; "Synthesis and applications of silsesquioxanes," *Trends Polym. Sci*., **1997**, *5*, 327-333.
7. Li, G.; Wang, L.; Ni, H.; Pittman, C.U.; "Polyhedral Oligomeric Silsesquioxane (POSS) Polymers and Copolymers: A Review," *J. Inorg. Organomet. Polym.*, **2001**, *11*, 123-151.
8. Duchateau, R.; "Incompletely Condensed Silsesquioxanes: Versatile Tools in Developing Silica-Supported Olefin Polymerization Catalysts," *Chem. Rev.*, **2002,** *102*, 3525-3542.
9. Abe, Y.; Gunji, T.; "Oligo- and polysiloxanes" *Prog. Polym. Sci*., **2004**, *29*, 149-182.
10. Phillips, S H.; Haddad, T. S.; Tomczak, S. J.; "Developments in nanoscience: polyhedral oligomeric silsesquioxane (POSS)-polymers," *Curr. Opin. Solid State Mater. Sci*., **2004**, *8*, 21-29.
11. Kannan, R. Y.; Salacinski, H. J.; Butler, P. E.; Seifalian, A. M.; "Polyhedral oligomeric silsesquioxane nanocomposites: The next generation material for biomedical applications," *Acc. Chem. Res*., **2005**, *38*, 879-884.
12. Laine, R. M.; "Nanobuilding blocks based on the $[OSiO_{1.5}]_x$ (x = 6, 8, 10) octasilsesquioxanes," *J. Mater. Chem*., **2005**, *15*, 3725-3744.

13. Lickiss, P. D.; Rataboul, F.; "Fully Condensed Polyhedral Oligosilsesquioxanes (POSS): From Synthesis to Application," *Adv. Organomet. Chem.*, **2008**, *57*, 1-116.
14. Chan, K. L.; Sonar, P.; Sellinger, A.; "Cubic silsesquioxanes for use in solution processable organic light emitting diodes (OLED)," *J. Mater. Chem.*, **2009**, *19*, 9103-9120.
15. Wu, J.; Mather, P. T.; "POSS Polymers: Physical Properties and Biomaterials Applications," *Polym. Rev.*, **2009**, *49*, 25-63.
16. Cordes, D. B.; Lickiss, P. D.; Franck, R.; "Recent Developments in the Chemistry of Cubic Polyhedral Oligosilsesquioxanes," *Chem. Rev.*, **2010**, *10*, 2081-2173.
17. Laine, R. M.; Roll, M. F.; "Polyhedral Phenylsilsesquioxanes," *Macromolecules*, **2011**, *44*, 1073-1109.
18. Sulaiman, S.; Bhaskar, A.; Zhang, J.; Guda, R.; Goodson, T.; Laine, R. M.; "Molecules with Perfect Cubic Symmetry as Nanobuilding Blocks for 3-D Assemblies. Elaboration of Octavinylsilsesquioxane. Unusual Luminescence Shifts May Indicate Extended Conjugation Involving the Silsesquioxane Core," *Chem. Mater.*, **2008**, *20*, 5563-5573.
19. Laine, R. M.; Sulaiman, S.; Brick, C.; Roll, M.; Tamaki, R.; Asuncion M. Z.; Neurock, M.; Filhol, J.-S.; Lee, C.-Y.; Zhang, J.; Goodson, T.; Ronchi, M.; Pizzotti, M.; Rand, S. C.; Li, Y.; "Synthesis and Photophysical Properties of Stilbeneoctasilsesquioxanes. Emission Behavior Coupled with Theoretical Modeling Studies Suggest a 3-D Excited State Involving the Silica Core," *J. Am. Chem. Soc.*, **2010**, *132*, 3708-3722.
20. Jung, J. H.; Furgal, J.; Goodson, T.; Mizumo, T.; Schwartz, M.; Chou, K.; Vonet, J.-F.; Laine, R. M.; "3-D Molecular Mixtures of Catalytically Functionalized $[vinylSiO_{1.5}]_{10}/[vinylSiO_{1.5}]_{12}$. Photophysical Characterization of Second Generation Derivatives," *Chem. Mater.*, **2012**, *24*, 1883-1895.
21. Furgal, J.C.; Jung, J.H.; Goodson, T.; Laine, R.M. "Analyzing Structure-Photophysical Property Relationships of Isolated T_8, T_{10}, and T_{12} Stilbenevinyl Silsesquioxanes: Evidence for "Red-Edge" Fluorescence Effects and 3D Excited State Charge Delocalization." *J. Am. Chem. Soc.*, **2013**, *135*, 12259-12269.
22. Asuncion, M.Z.; Laine, R.M.; "Fluoride Rearrangement Reactions of Polyphenyl- and Polyvinylsilsesquioxanes as a Facile Route to Mixed Functional Phenyl, Vinyl T-10 and T-12 Silsesquioxanes," *J. Am. Chem. Soc.*, **2010**, *132*, 3723-3736.

23. Jung, J.H.; Laine, R.M.; "Beads on a Chain (BoC) Polymers Formed from the Reaction of $NH_2PhSiO_{1.5}]_{(x)}[PhSiO_{1.5}]_{(10-x)}$ and $[NH_2PhSiO_{1.5}]_{(x)}[PhSiO_{1.5}]_{(12-x)}$ Mixtures (x=2-4) with the Diglycidyl Ether of Bisphenol A," *Macromolecules*, **2011**, *44*, 7263-7272.
24. Frauenrath, H.; "Dendronized polymers–building a new bridge from molecules to nanoscopic objects," *Prog. Polym. Sci*., **2005**, *30*, 325-384.
25. Schluter, A. D.; Rabe, J. P.; "Dendronized polymers: Synthesis, Characterization, assembly at interfaces, and manipulation," *Angew. Chem. Int. Ed*., **2000**, *39*, 864-883.
26. Zhang, A.; Shu, L.; Bo, Z.; Schluter, D.; "Dendronized polymers: Recent progress in synthesis," *Macromol. Chem. Phys*., **2003**, *204*, 328-339.
27. Li, Z.; Kawakami, Y.; "Formation of Incompletely Condensed Oligosilsesquioxanes by Hydrolysis of Completely Condensed POSS via Reshuffling," *Chem. Lett*., **2008**, *37*, 804-805.
28. Lichtenhan, J. D.; Vu, N. Q.; Carter, J. A.; Gilman, J. W.; Feher, F. J.; "Silsesquioxane-Siloxane copolymers from polyhedral silsesquioxanes," *Macromolecules*, **1993**, *26*, 2141-2142.
29. Furgal, J. C.; Jung, J. H.; Clark, S.; Goodson III, T.; Laine, R. M.; "Beads on a Chain (BoC) Phenylsilsesquioxane (SQ) Polymers via F^- Catalyzed Rearrangements and ADMET or Reverse Heck Cross-coupling Reactions: Through Chain, Extended Conjugation in 3-D with Potential for Dendronization," *Macromolecules*, **2013**, *46*, 7591-7604.
30. Knowles, J. P.; Whiting, A.; "The Heck-Mizoroki cross-coupling reaction: a mechanistic perspective." *Org. Biomol. Chem*., **2007**, *5*, 31-44.
31. Jutand, A.; "Mechanism of the Mizoroki-Heck reaction," in The Mizoroki-Heck reaction, Oestreich, M. eds., John Wiley & Sons, **2009**, pp 1-50.

Chapter 5

Synthesis and characterization of second generation (GEN2) derivatives by functionalization of vinyl $T_{10/12}$ silsesquioxanes

Published in Chemistry of Materials, **2012**, *24*, pp. 1883-1895

Abstract

Fluoride ion catalyzed rearrangement of –[vinyl$SiO_{1.5}]_n$- oligomers and polymers in THF provides essentially quantitative conversion to mixtures of the 3-D cage compounds [vinyl$SiO_{1.5}]_{10}$ and [vinyl$SiO_{1.5}]_{12}$ with small amounts of the [vinyl$SiO_{1.5}]_{14}$ cage. These mixtures are easily transformed into their respective styrenyl analogs by metathesis with *p*-R-styrene to give 100 % conversion to the Generation 1 (GEN1) compounds [*p*-R-styrenyl$SiO_{1.5}]_{10/12}$. The R = Br compounds are then easily modified by Heck coupling with *p*-R-styrene in > 90 % yields and ≈ 100 % conversion to the Generation 2 (GEN2) compounds [*p*-R-stilbenevinyl$SiO_{1.5}]_{10/12}$. These studies were designed to map structure-photophysical properties in these 3-D molecules with the goal of finding replacements for C_{60} and C_{70} electron acceptor compounds currently in use in most organic photovoltaics. Photophysical characterization indicates that the GEN2 compounds have average band gaps that are slightly smaller than their T_8 analogs. However, the C_6F_5 derivative offers blue shifted absorption with a very red shifted emission in contrast to the blue emission shift that was expected coincident with the absorption blue shift.

Initial cyclic voltammetry studies suggest that the GEN2 C_6F_5 derivative has HOMO-LUMO energies that may, through further modification, provide energy levels that meet our target objectives. In addition, solvent studies targeting absorption and emission behavior find emission behavior in poor solvents for R = H, Me, MeO that suggests some form of aggregation. This aggregation red-shift of emission perhaps arises from partial interdigitation of *p*-R-stilbenevinyl groups. Because these molecules are three dimensional; moieties opposite the

points of interdigitation emit as they do in good solvents leading to emissions that broadened greatly. Furthermore, because we have previously observed what appears to be 3-D conjugation in the excited state, these results suggest the potential to promote charge transport in three dimensions perhaps similar to C_{60}/C_{70}. Alternately, these same materials may serve as novel emitters for light emitting diodes.

5.1. Introduction

Silsesquioxane (SQ) cage chemistry has recently received a great deal of attention because of the many benefits that can be derived from SQs' potential to offer high degrees of functionalization coupled with thermal stabilities improved by the heat capacity inherent in their silica cores and their high solubility in multiple organic solvents allowing ease of purification. To date this area of research has been the subject of some 17 reviews.[1-17] Most of these reviews focus on the chemistry of the octahedral compounds $[RSiO_{1.5}]_8$ (where R = R'$SiMe_2O$ and R/R' = alkyl, aryl, alkenyl, alkynyl, etc.).

Research by Bassindale et al.,[18-20] Rikowski et al.,[21] and Mabry, Bowers et al.[22] described the influence of various bases on the formation of SQ cages with some evidence suggesting F^- catalytically scrambles the R groups. In recent work, we demonstrated that this route provides an excellent method of making mixed functional cages; not mixed functional $[R^1SiO_{1.5}]_{8-x}[R^2SiO_{1.5}]_x$ but $[R^1SiO_{1.5}]_{10-x}[R^2SiO_{1.5}]_x$ and $[R^1SiO_{1.5}]_{12-x}[R^2SiO_{1.5}]_x$ cages almost exclusively.[23-25] Most recently we learned to make large quantities of $[vinylSiO_{1.5}]_{10/12}$ mixtures from the T resin, $[vinylSiO_{1.5}]_x$.[24]

Previously, we reported using $[vinylSiO_{1.5}]_8$ to synthesize $[p\text{-}RStrylSiO_{1.5}]_8$ where R = H, Me, MeO, Br, NH_2 and the corresponding stilbenevinylSQs, $[RStilCH{=}CH_2SiO_{1.5}]_8$.[26,27] We also characterized their photophysical properties in detail as these materials appear to exhibit some form of conjugation in the excited state.[24,26] A further motivation comes from work of Sellinger et al.,[28] who describe Heck cross-coupling of $[vinylSiO_{1.5}]_8$ with organic moieties conjugated to the SQ silica cage. The resulting compounds offer exceptional improvements in their electron and hole transport properties when used as components in organic light emitting diodes (OLED) compared with simple organics as reviewed recently.[14]

In this report, we continue efforts to expand our knowledge of the photophysical properties of these systems as potential new components in the development of OLEDs but also as highly stable, easily modified and robust components for hybrid photovoltaics. In particular, our long term goal is to find materials that can replace components such as the C_{60} and C_{70} fullerenes (e.g. PCBM) currently used in many hybrid photovoltaics given their very high cost and potential toxicity especially as singlet oxygen generators.[29,30] In this vein, we report here efforts to functionalize $[vinylSiO_{1.5}]_{10/12}$ via reaction scheme **5.1**, **5.2** and **5.3**.

More specifically, our objective in the current studies is to map the photophysical properties especially of the GEN2 compounds of reaction scheme **5.3** to compare the effects (if any) of the larger cage sizes on emissive behavior, two photon cross-sections and also on their HOMO-LUMO energies via cyclic voltammetry for the reasons mentioned just above. We use the term "map" because the properties of these types of 3-D molecules are for the most part unknown and consequently, we must develop a detailed understanding of many of their properties as a prelude to learning to tailor their properties to meet our stated objectives.

As we will see below, for some types of functionalization, the photophysical behavior observed differs very little from the T_8 compounds; however, for others there is a considerable difference. Indeed the C_6F_5 derivatives offer novel behavior that for the present is inexplicable.

5.2. Results and Discussion

In the following sections we first discuss our synthetic approaches to generating $T_{10/12}$ compounds with very high degrees of functionalization and thereafter their photophysical properties. Because both sets of compounds have very similar chemical and physical properties we have not found simple methods of separating the T_{10} from the T_{12} compounds. Thus, at the outset it is important to realize that these compounds can be considered to be relatively well-defined oligomers rather than discrete molecular species although the distinction may seem small. Consequently, we are exploring average properties though the differences may not be particularly great. Also note that in the current studies we see small amounts of T_{14} compounds. The exact structure of this component is unknown but sees Baney and Itoh.[2]

As seen with the T_8 compounds, we are able to install layers of organic functionality starting from the silica cage out. In a future paper, we will develop routes to the further

functionalization of the GEN2 compounds developed here, to produce GEN3 compounds that come closer to meeting our stated objectives. Because our starting points for the compounds made here are vinyl functionalized species, two pathways can be explored for further modification; Heck or metathesis cross-coupling. Sellinger et al.[14,28] report using Heck coupling to mono- and partially di-functionalize $[vinylSiO_{1.5}]_8$. Using their work as the starting point, we explored the use of Heck coupling to synthesize mono- (S) and di- (D) functionalized $vinylT_{10/12}$ (Scheme **5.1**).

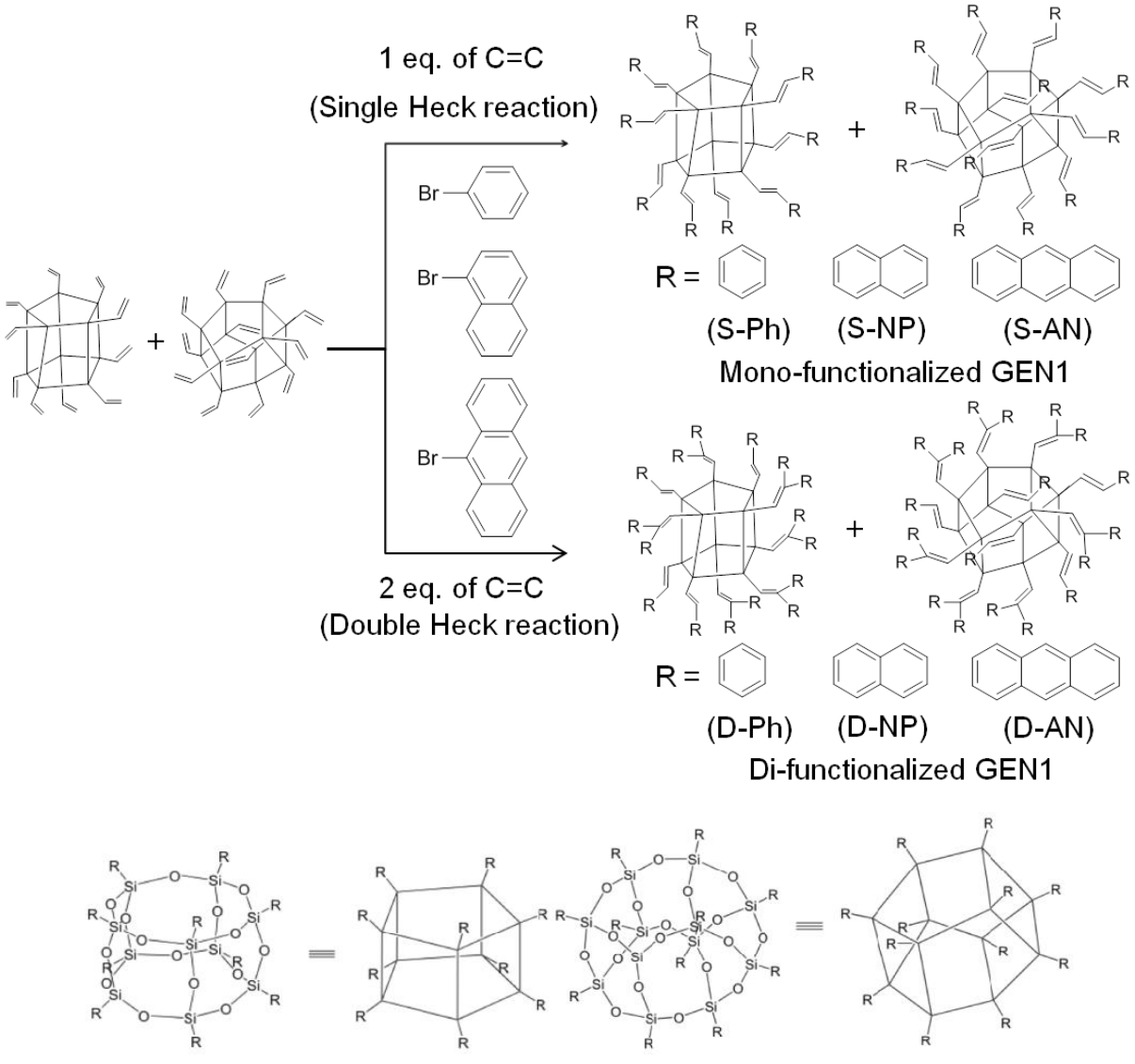

Scheme 5.1. Heck coupling reaction of $vinylT_{10/12}$ (GEN1).

Table **5.1** summarizes our findings indicating that with the exception of anthracene, functionalization, even with efforts to limit coupling to mono-functionalization, gave significant di-functionalization. Furthermore, under the conditions used, it was not possible to obtain complete di-functionalization as also reported by Sellinger et al.[28] albeit for the vinylT_8.

Table 5.1. Characterization of GEN 1 Mono (S) and Double (D) Heck coupling compounds (NP = Naphthalene, An = Anthracene).

	TGA				m/z (Ag^+ adduct)				GPC	
R group	Ceramic yield (%)		Ave. Substit.	$T_{d5\%}$ ^oC	T_{10}		T_{12}		M_n	PDI
	found	Calc.			MALDI		MALDI			
Vinyl	75.4	75.9	--	240	900.0	899.2	1056.0	1057.5	950	1.03
S-Ph	34.8	38.7	1.2	420	1890.4	Ph_{13}	2124.4	Ph_{14}	1550	1.05
D-Ph	29.7	26.0	1.6	385	2350.0	Ph_{19}	2660.4	Ph_{21}	1590	1.07
S-NP	27.3	29.3	1.1	480	2286.3	NP_{11}	2696.4	NP_{13}	1620	1.07
D-NP	21.4	18.1	1.6	455	3050.8	NP_{17}	3460.2	NP_{19}	1700	1.08
S-AN	23.1	23.5	1.0	445	2661.5	AN_{10}	3171.3	AN_{12}	1820	1.08
D-AN	23.6	14.7	1.0	445	2661.8	AN_{10}	3171.8	AN_{12}	1890	1.17

In contrast to the Heck coupling reactions, the metathesis products give analyses (Table **5.2**) expected for 100 % cross-coupling and mono-functionalization (Scheme **5.2**). As such, and in particular, the *p*-bromophenyl derivative was scaled to 10 g quantities to serve as the starting point for all GEN2 compounds (Scheme **5.3**).

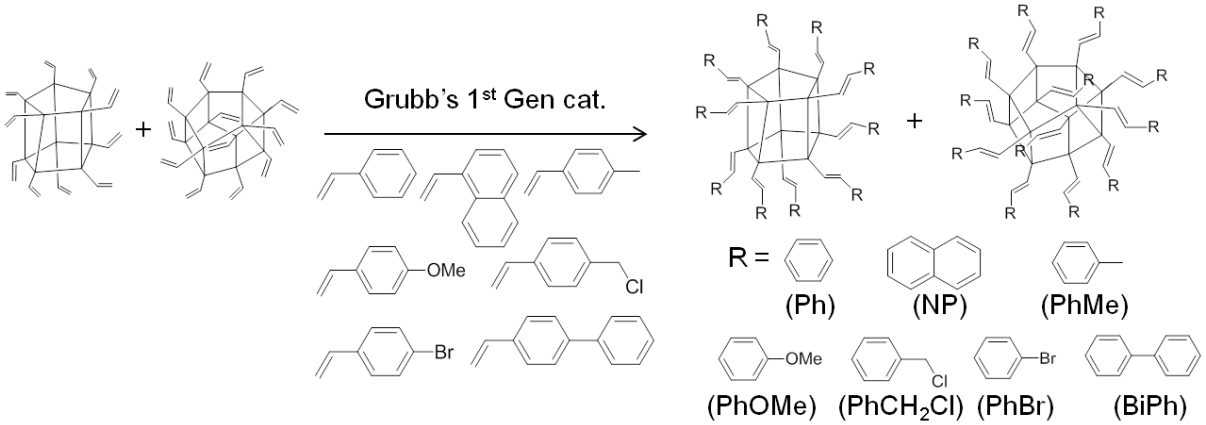

Scheme 5.2. Metathesis reaction of vinyl$T_{10/12}$ (GEN1).

Table 5.2. Characterization of GEN1 materials produced by metathesis (NP = naphthalene).

	TGA				m/z (Ag^+ adduct)				GPC	
R group	Ceramic yield (%)		Ave. Subst.	$T_{d5\%}$ ^oC	T_{10}		T_{12}		M_n	PDI
	actual	calc			MALDI	Calc.	MALDI	Calc.		
Ph	38.8	38.7	1.0	430	1659.0	1660.7	1970.0	1971.3	1540	1.06
NP	28.7	29.3	1.0	415	2164.0	2161.3	2574.8	2572.0	1650	1.05
PhMe	35.8	35.5	1.0	330	1800.9	1801.0	2140.0	2139.6	1600	1.04
PhOMe	31.9	32.4	1.0	395	1960.4	1961.0	2332.0	2331.6	1630	1.03
$PhCH_2Cl$	30.7	29.5	1.0	340	2144.7	2145.4	2552.0	2552.9	1860	1.04
BrPh	25.0	25.7	1.0	335	2452.0	2449.7	2920.3	2918.1	1830	1.06
BiPh	25.4	26.0	1.0	340	2422.1	2421.7	2885.7	2884.5	2150	1.04

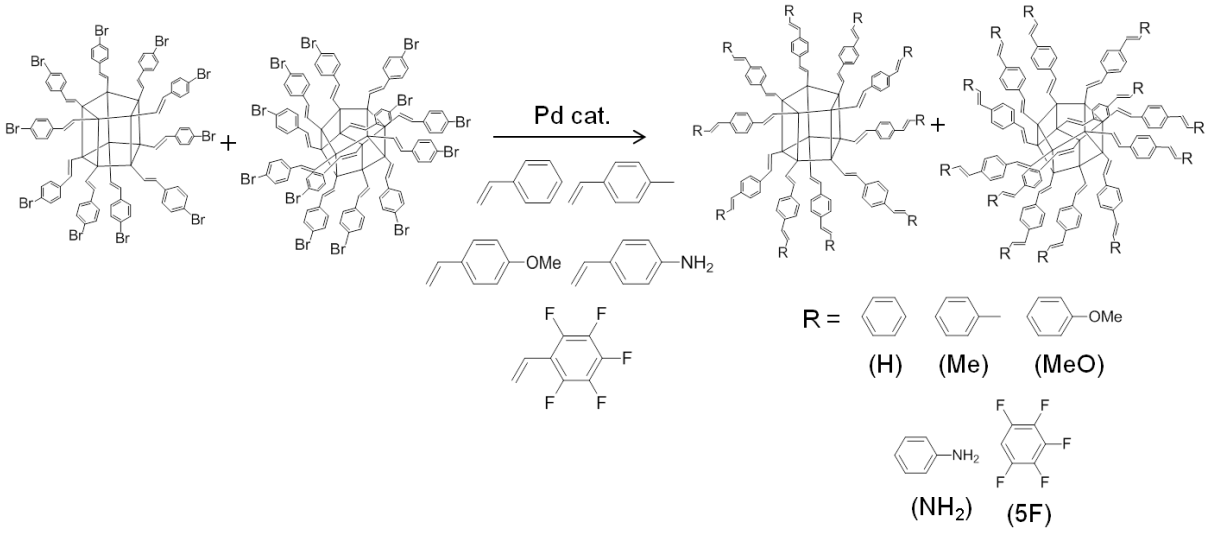

Scheme 5.3. Heck coupling reaction of *p*-BrStyrenyl$T_{10/12}$ (GEN2).

Table 5.3. Characterization of GEN2 compounds.

	TGA				m/z (Ag^+ adduct)				GPC	
R'	CY (%)		Ave. Subst.	$T_{d5\%}$ ^oC	T_{10}		T_{12}		M_n	PDI
	Found	Calc.			MALDI	Calc.	MALDI	Calc.		
H	23.3	23.4	1.0	390	2680.7	2681.5	3195.1	3196.2	3200	1.04
Me	21.5	22.1	1.0	385	2820.1	2821.7	3362.8	3364.5	3500	1.03
MeO	20.9	20.9	1.0	350	2981.0	2981.7	3555.2	3556.5	3530	1.04
NH_2	22.1	22.6	1.0	390	2832.3	2831.6	3376.9	3376.4	4100	1.03
5F	17.0	17.3	1.0	345	3581.6	3581.0	4276.4	4275.6	4140	1.05

In general the TGA, MALDI and GPC data are all in agreement with those expected for the compounds isolated. It should be noted that the calculated ceramic yields (CY) in Table **5.1**, are those calculated for the average degree of substitution as determined by the MALDI data and not theoretical values for single and di-substitution.

It is also important to note that the MALDI intensity data used to calculate the average degree of substitution depend on the ease of ionization of each particular species. While these are not necessarily the same for given degrees of substitution, they are viewed as being qualitatively the same. Consequently, there may be some error in the average degree of substitution observed which may account for some slight discrepancies in the CY data.

It should also be noted that because all the SQ compounds described here are three dimensional and are roughly spherical in nature compared with 2-D molecules, they occupy different hydrodynamic volumes than what might be expected for oligomers of similar atomic mass. Therefore, the polystyrene standards used to calibrate the GPC, will not give calculated M_n values representative of the actual SQ molecular masses.

Figure **5.1** provides two representative spectra for GEN1 *p*-MeOStyrenylSQ and GEN2 for C_6F_5stilbenevinylSQ. The cage structure is maintained throughout the syntheses as witnessed by the strong νSi-O bands near 1100 cm^{-1}, aside from this specific band, the remaining IR bands are typical of those found in aromatic compounds. As such, Tables **A2.1** and **A2.2** list all of the respective IR bands of the compounds synthesized as described in the experimental.

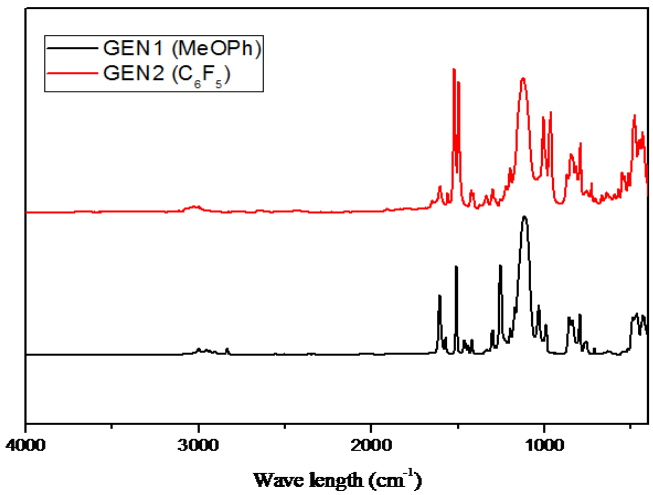

Figure 5.1. Representative FTIR for GEN1 *p*-MeOStyrenylSQ and GEN2 C_6F_5 stilbenevinylSQ.

GPC data for GEN1 and GEN2 SQs are given in Tables **5.1-3**. Figure **5.2** provides representative GPC chromatograms for vinylSQ, styrenylSQs (GEN1) made by different methods and stilbenevinylSQ (GEN2). These materials show narrow molecular weight distributions, indicating that they retain their cage structures. Note that the three different styrenylSQs show the same retention times, even though they have different numbers of phenyl groups, because SQ cages are rigid and spherical molecules of approximately the same hydrodynamic radii.

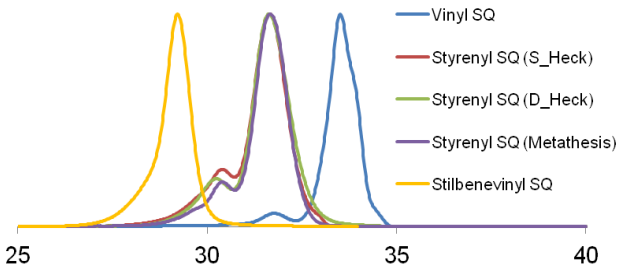

Figure 5.2.GPC traces of vinylSQ and styrenylSQs (different reaction conditions) and stilbenevinylSQ (GEN2).

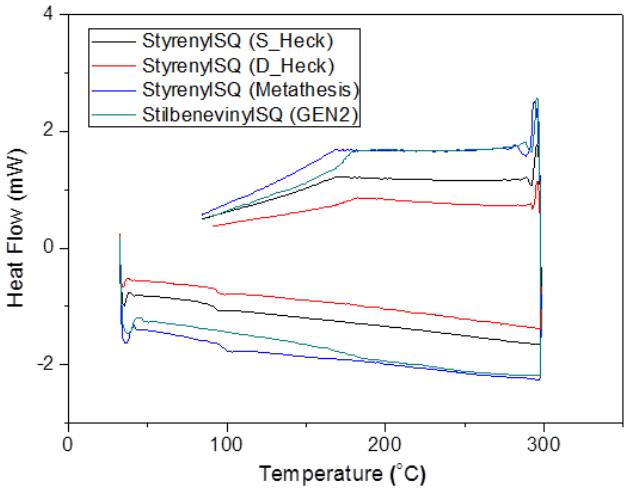

Figure 5.3. DSC traces of selected styrenylSQs and stilbenevinylSQ (GEN2), second scan.

Figure **5.3** shows representative DSC traces of GEN1 StyrenylSQs and GEN2 stilbenevinylSQs. As seen in Figure **5.3**, GEN1 compounds present endotherms indicative of melting near 100 ^{o}C for the second scan. Hot stage optical microscopy also shows that these

materials melt over a 100-120 ^{o}C range as might be expected for $T_{10/12}$ mixtures. However, the GEN2 compounds do not show melting behavior in the DSC and decompose at temperatures >200 ^{o}C. Table **A2.3** lists the melting points of the GEN1 compounds synthesized as described in the experimental.

Photophysical studies

The following work is divided into two sections, steady state spectroscopy and two-photon absorption measurements.

Steady-State Spectroscopy

Figures **5.4-6** provide absorption and emission spectra (THF) for selected GEN1 compounds with the data shown in Tables **5.4** and **5.5**. The absorption spectra for both the single and double Heck phenyl and naphthalene compounds exhibit distinct band structure, with absorption maxima being nearly the same for both single and double Heck derivatives. These values are λ_{max} = 254±2 vs. 258±2 nm for the phenyls respectively, and λ_{max} = 302±2 nm for both naphthalenes. Furthermore, the doubly functionalized compound emission spectra are slightly red-shifted as might be expected for cross-conjugated moieties due to slightly extended excited state conjugation. Both the single and double Heck phenyl and naphthalene compounds give similar spectra respectively.

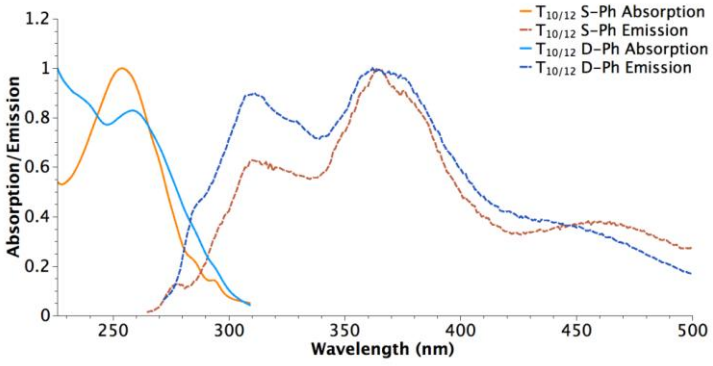

Figure 5.4. UV-vis absorption and PL spectra for GEN1 $T_{10/12}$ R = S-Ph, and D-Ph (THF).

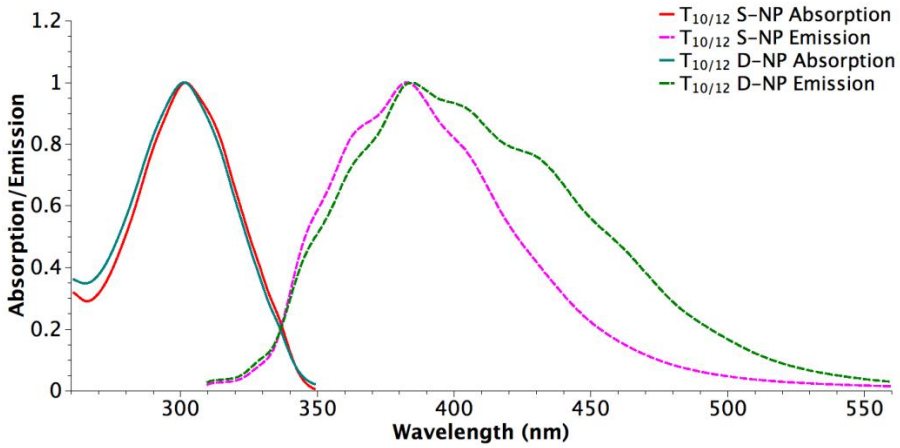

Figure 5.5. UV-vis absorption and PL spectra of GEN1 $T_{10/12}$ R = S-NP and D-NP (THF).

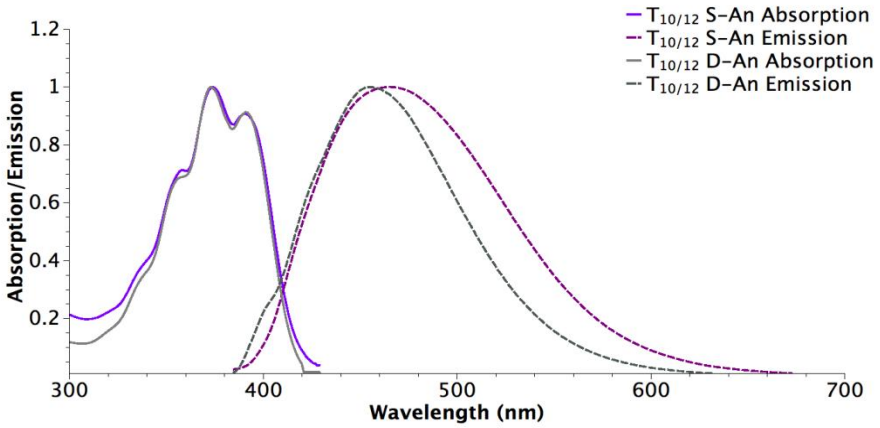

Figure 5.6. UV-vis absorption and PL spectra of GEN1 $T_{10/12}$ R = S-An and D-An (THF).

Table 5.4. Absorption and Emission Maxima for GEN1 compounds.

	Absorption(nm)	Emission(nm)	Stokes Shift (cm^{-1})
$T_{10/12}$ R = S-Ph	254	310, 364	7112
$T_{10/12}$ R = D-Ph	258	311, 362	6501
$T_{10/12}$ R = S-NP	302	384	7071
$T_{10/12}$ R = D-NP	302	386	7206
$T_{10/12}$ R = S-An	374	465	4135
$T_{10/12}$ R = D-An	374	455	3663

Table 5.5. Photophysical data for GEN1 compounds.

	$\Phi_{PL(x)}$	Cross-section per Chromophore δ(GM) at 795 nm
$T_{10/12}$ R = S-Ph	0.03	-
$T_{10/12}$ R = S-NP	0.03	~0.01
$T_{10/12}$ R = S-An	0.13	~0.001

In contrast, while mono functionalized anthracene offers the most red-shifted absorption at ~374±2 nm and emission at λ_{max} = 465±2 nm. Its emission is featureless possibly resulting from charge transfer or from an averaging of the emission signals. All of the absorption and emission spectra were taken at concentrations of 10^{-6} to 10^{-7} molar where formation of excimers/exciplexes between two cages is unlikely. However, it is possible that internal excimers form. Zhang et al. report formation of T-type excimers on zinc (II) acetate w/N,N'-Bis(anthracen-9-ylmethyl)propane-1,3-diamine ligands, which give broad emission bands similar to those found here, suggesting the possibility of internal T-type excimer formation on the cages.[30] We believe this is not occurring as the individual moieties are almost 90 ° apart on the surface of the cage and even with some rotation are unlikely to be able to approach each other.

A comparison between the molar extinction coefficients of S-anthracene and D-anthracene, of $4.2x10^4$ $M^{-1}cm^{-1}$ and $4.8x10^4$ $M^{-1}cm^{-1}$ respectively reveals just a slight increase in absorption efficiency of the doubly substituted versus the singly substituted. This is consistent with the double and single species both being approximately only singly substituted. As a comparison, the D-naphthalene showed an increase in molar extinction coefficient compared to that of S-naphthalene, $9.6x10^4$ $M^{-1}cm^{-1}$ and $1.0x10^4$ $M^{-1}cm^{-1}$ respectively, evidence of increased substitution as seen in Table **5.1**, which gives a substitution of 1.2 for the S-and 1.6 for the D-naphthalene.

The calculated fluorescent quantum yield (QY) was 13% for S-anthracene. This contrasts with a literature QY for vinylanthracene linked to aliphatic carbons of 80%.[32] The lower than expected QY for the S-anthracene system may arise because of a photoinduced electron transfer (PET) fluorescence quenching process, which may also be evident in the solvent

study of the S-anthraceneSQ.[33] The S-anthracene QY is ≈ 2% in acetonitrile, likely arising from non-radiative decay enhanced by the smaller, more polar acetonitrile solvent.

In general the Stokes shift differences between the mono- and di-substituted compounds are small, with no general trends observed for the GEN1 compounds.

The lack of structure in the anthracene systems prompted us to examine the effects of solvent polarity on emission behavior with the intent of enhancing CT behavior if it existed. Thereafter we decided that it would be wise to explore the effects of good, bad and polar or nonpolar solvents on the photophysical behavior of several of our GEN2 compounds.

For the anthracene moieties, there is a noticeable solvent effect for emission on going from 95:5% of acetonitrile:THF to the less polar THF solvent. This was studied by dilution with THF from the 95% acetonitrile sample, with a 25% reduction in concentration and amount of acetonitrile per measurement as shown in Figure **5.7**. The emission spectrum shifts from λ_{max} = 492±2 nm in acetonitrile to λ_{max} = 465±2 nm in THF, with ~25% reduction in intensity with each dilution of THF.

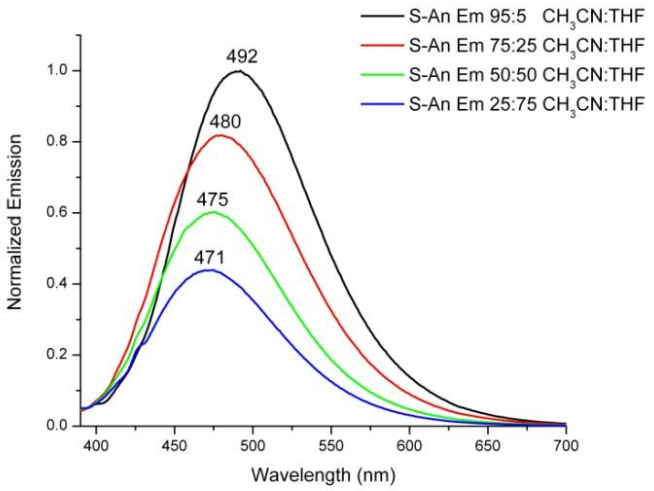

Figure 5.7. Solvent study of GEN1 $T_{10/12}$ R = S-An by sequential dilution with THF to reduce the amount of acetonitrile and the overall concentration.

In contrast, samples prepared with equimolar concentrations with different ratios of acetonitrile:THF evinced no shifts at all; although fluorescence quenching was notable with a decrease in intensity on going from THF to acetonitrile. We suggest that this arises due to differences in solvent interactions with the chromophore (Figure **5.8**), as noted just above. As

acetonitrile concentration increases, a second band appears $\lambda_{max} \approx 415 \pm 2$ nm and the emission becomes more structured as was originally expected. This emission is similar to that expected for vinylanthracene.[31]

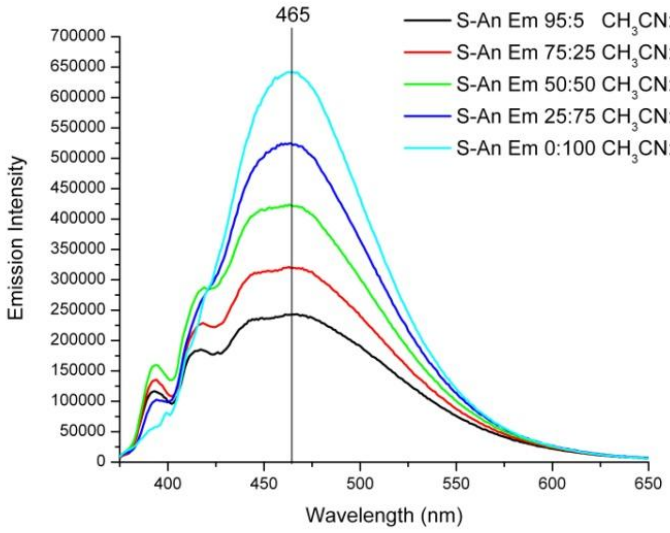

Figure 5.8. GEN1 $T_{10/12}$ R = S-An emission spectra at different acetonitrile:THF ratios (1 μM).

Further analysis in hexane:THF mixtures shows a similar trend, with higher hexane concentrations giving the lowest intensities, and THF the highest (Figure **A1.1**). The spectra show slight blue shifts with increased hexane concentration, attributable to poorer solvation, though the general shape and intensity trends are similar to those of acetonitrile.

Figures **5.9** and **5.10** show GEN2 compound absorption and emission behavior (THF) with the data tabulated in Table **5.6**. In keeping with what is generally expected, aromatic rings with more polar substituents, (e.g. R = NH_2, OMe), are red-shifted compared to less polar substituents, (e.g. R = H, Me). In part this arises from a switch from π-π* transitions dominating the photophysical properties to charge transfer (CT) behavior as seen in the T_8 GEN2 systems.[26,27]

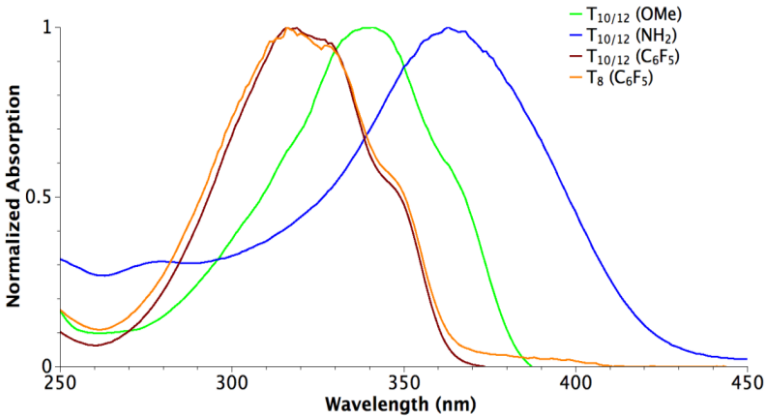

Figure 5.9. UV-vis absorption spectra of selected GEN2 R-stilbenevinylSQs in THF.

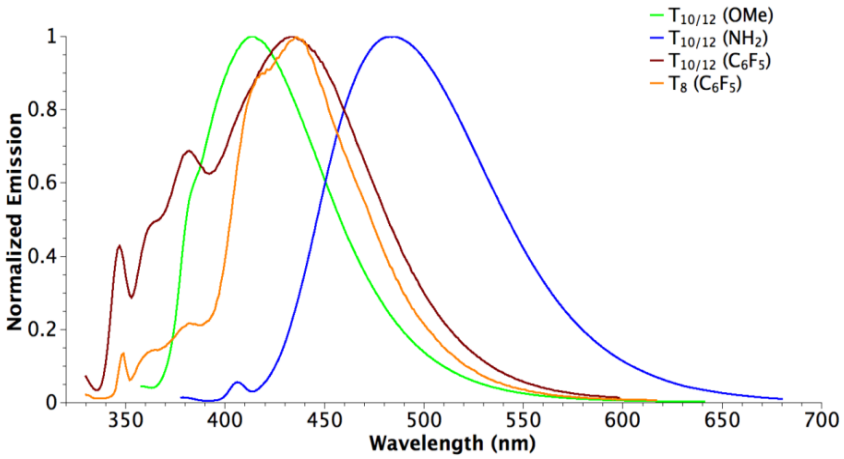

Figure 5.10. PL emission spectra of selected GEN2 R-stilbenevinylSQ compounds in THF.

Table 5.6. Absorption and Emission Maxima for GEN2 compounds.

$T_{10/12}R$ =	Absorption (±2 nm)	Emission (±2 nm)	Stokes Shift (cm^{-1})	Φ_{PLx}
H	333	387	3988	0.2
Me	333	393	4316	0.1
OMe	343	418	5402	0.07
NH_2	363	483	7056	0.07
C_6F_5	316	445	9173	0.01
$T_8C_6F_5$	317	434	8504	0.03

The UV/Vis and PL spectra for 4-aminostilbenevinyl $T_{10/12}$ SQ were also examined as a function of the solvents acetonitrile, THF and cyclohexane as seen in Figure **5.11** and Table **5.7**. As expected, acetonitrile with 5% THF added to improve solubility leads to a 32 nm red-shift compared to THF alone because of CT stabilization in the more polar solvent. The absorption spectra for all three solvents are essentially the same, with cyclohexane with 5% THF and THF samples having identical emissions.

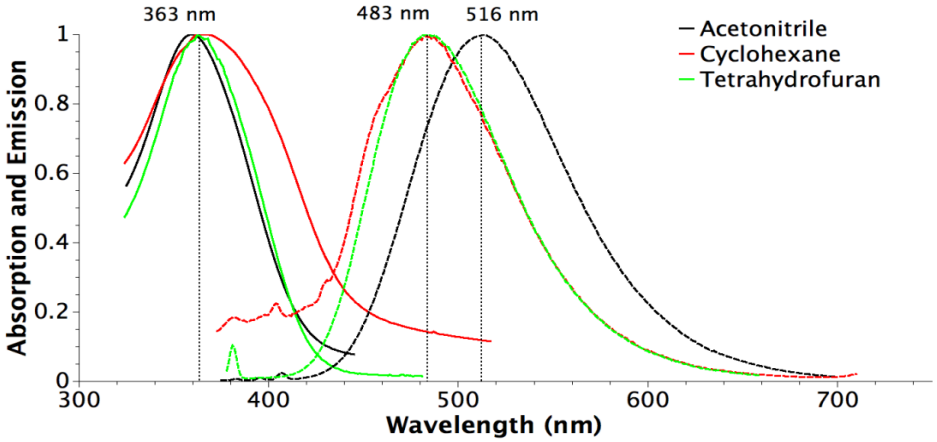

Figure 5.11. UV/vis absorption and PL spectrum of $T_{10/12}$ 4-aminostilbenevinylSQ.

Table 5.7. UV/vis absorption and PL for $T_{10/12}$ 4-aminostilbenevinylSQ as a function of solvent.

	Absorption (± 2 nm)	Emission (± 2 nm)
Acetonitrile (5% THF)	363	516
Cyclohexane (5% THF)	365	483
THF	363	483

The absorption of 4-aminostilbenevinyl $T_{10/12}$ SQ in THF, acetonitrile and cyclohexane reveals a $\lambda_{max} \approx 363 \pm 2$ nm within error limits the same as the $\lambda_{max} \approx 360 \pm 2$ nm seen for the T_8 analog.[26,27] In THF, both the T_8 and $T_{10/12}$ systems exhibit featureless emissions at $\lambda_{max} \approx 486 \pm 2$ nm. In acetonitrile, the T_8 analog exhibits a structureless emission at $\lambda_{max} \approx 507 \pm 2$ nm, whereas the $T_{10/12}$ system emits at 517±2 nm. We believe that this slight red-shift for the $T_{10/12}$ system is real compared to the emissions in THF. One possible interpretation is that the average band gap for the mixture is slightly lower in energy than that for the T_8 compound. One might expect some

change in band gap if the cages interact electronically with the organic functional groups as we have suggested elsewhere.[26,27] In this instance, this behavior would suggest the larger GEN2 cages have slightly smaller band gaps.

The most unusual compound, however, is the GEN2 $T_{10/12}$ R = C_6F_5 derivative. This compound exhibits a λ_{max} of absorption that is blue-shifted from 333 ± 2 nm for R = H to 316 ± 2 nm, see Table **5.6** and Figure **5.9**. This shift is anticipated based on the electron withdrawing character of C_6F_5. However, the emission is red-shifted to a λ_{max} of 443 ± 2nm which is even greater than the R = OMe analog with (Figure **5.10**). This is surprising since one would expect that the emission would also be blue-shifted. The Stokes shift at 9173 $cm^{-1}$is the largest of any GEN2 compounds. The source of this exceptional red-shift is unclear at present, but clearly indicative of the unusual photophysical properties in these systems.

Another important difference between the T_8 and $T_{10/12}$ amino systems resides in the emission quantum efficiencies (Φ_{PLx}) compared against the standard Bis-MSB [1,4-bis(2-methylstyryl)benzene] (Φ_{PLx}= 95%). The Φ_{PLx} of the GEN2 T_8 R = NH_2 is somewhat lower $\Phi_{PL(x)}$ than the GEN2 $T_{10/12}$ R = NH_2 compounds, 5% vs. 7% respectively, which is significant in the calculation of the two-photon cross-section discussed below. All GEN2 $T_{10/12}$ compounds except the R = NH_2 have slightly lower $\Phi_{PL(x)}$ than their T_8 counterparts.

The molar extinction coefficients (ε)/chromophore for these compounds are T_8 $3.43x10^4$ $M^{-1}cm^{-1}$ and $T_{10/12}$ $3.64x10^4$ $M^{-1}cm^{-1}$, suggesting that increasing the chromophore density in the same volume does not influence overall absorption. The somewhat lower $\Phi_{PL(x)}$ probably arises from some self-absorption but this again is not particularly significant. The molar extinction coefficients are all listed in Table **A2.4**.

The effects of solvation on the UV/vis and PL spectra for $T_{10/12}$ stilbenevinylSQ were assessed in THF, acetonitrile, and hexane, with spectra shown in Figure **5.12, 5.13** and **A2.2** respectively, with emission λ_{max} data given in Table **5.8**. This study compared the effects of solvent on both solubility and potential charge transfer properties.

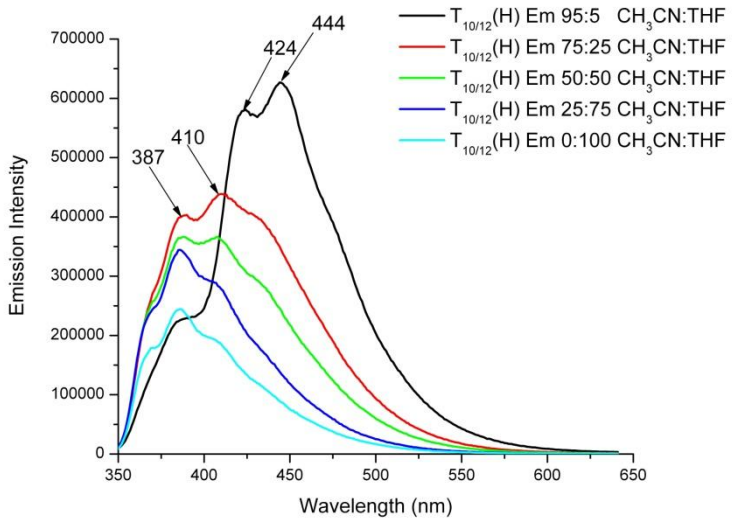

Figure 5.12. Emission studies of $T_{10/12}$ stilbenevinylSQ in acetonitrile/THF mixtures (serial dilution study)

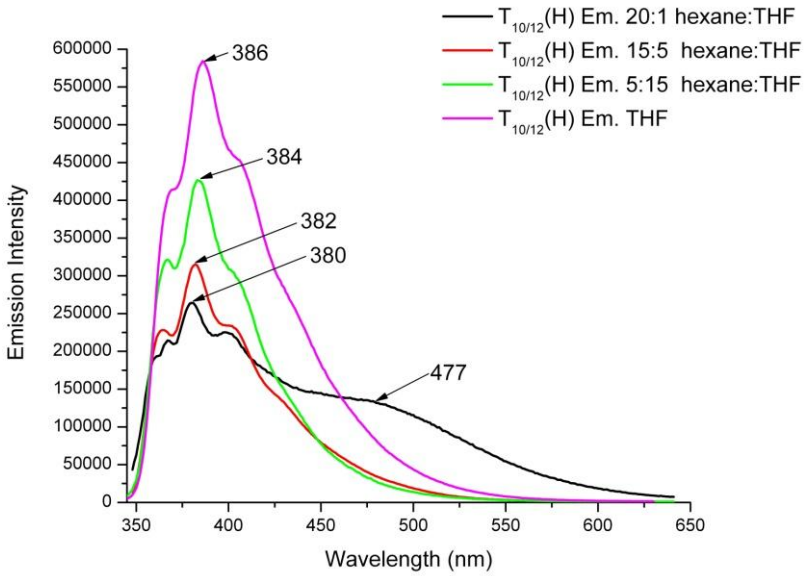

Figure 5.13. Emission studies of $T_{10/12}$ stilbenevinylSQ in hexane/THF at constant 0.86 μM concentration.

Table 5.8. Emission (nm) of T_8 and $T_{10/12}$ stilbenevinylSQs (± 2 nm) in acetonitrile:THF.

Acetonitrile:THF	95:5	75:25	50:50	25:75	0:100
$T_{10/12}$ R = H^S	444	410	410	387	387
$T_{10/12}$ R = Me^S	402	-	398	394	393
T_8 R = H^S	386	-	384	-	385
T_8 stilbene^S	357	-	358	358	358
$T_{10/12}$ R = H^C	387				

(S) = Serial Dilution study, (C) = Constant concentration study.

A comparison of λ_{max} for $T_{10/12}$ stilbenevinylSQ in 95:5 of acetonitrile:THF vs. THF shows a 57-nm red shift (444 ± 2 nm) from THF (387 ± 2 nm) as a function of acetonitrile content, Figure **5.12**. In these studies, a single concentration was made (0.86 μM) in 95:5 acetonitrile:THF, which was successively diluted with acetonitrile, eventually to ~0 % acetonitrile. The fluorescence intensity diminishes on moving to pure THF as expected with dilution. One possible explanation for this shift in emission is that acetonitrile promotes CT behavior; however, the band structure is retained contradicting this explanation. Additional solvent effect studies were then run to further explore this effect.

In the first one, $T_{10/12}$ stilbenevinylSQ at constant 0.86 μM concentration provides a somewhat different trend. Figure **A2.2** shows that at constant concentrations, the lowest intensities are observed in 95:5 of acetonitrile:THF and the most intense in THF. However, there are no changes in λ_{max}, suggesting that the Figure **5.12** shifts arise as a result of poorer solvent interactions.

Consequently, we decided to move to emission studies with poorer solvents as seen in Figures **5.13** and **5.14**. Figure **5.13** shows that at 20:1 of hexane:THF a new peak appears at 477±2 nm. The breadth of the peak suggests aggregation.[34] However, at higher THF concentrations this "aggregate peak" disappears as solubility improves. It is important to note that the original emission band is still present but slightly blue-shifted compared with the THF sample. An explanation for this blue shift is discussed below. While intriguing, the Figure **5.13** data represent a single data point. Thus, additional studies were run at different hexane:THF ratios closer to the 20:1 value in Figure **5.13**. Thus at 10:1, 20:1 and 30:1 ratios of hexane:THF at three concentrations, 0.85, 0.43 and 0.28 μM respectively, we again see (Figure **5.14**) the

apparent formation of aggregates with a $\lambda_{max} \approx 492$ nm. The original THF emission centered at $\lambda_{max} \approx 379$ nm appears to be of almost equal intensity.

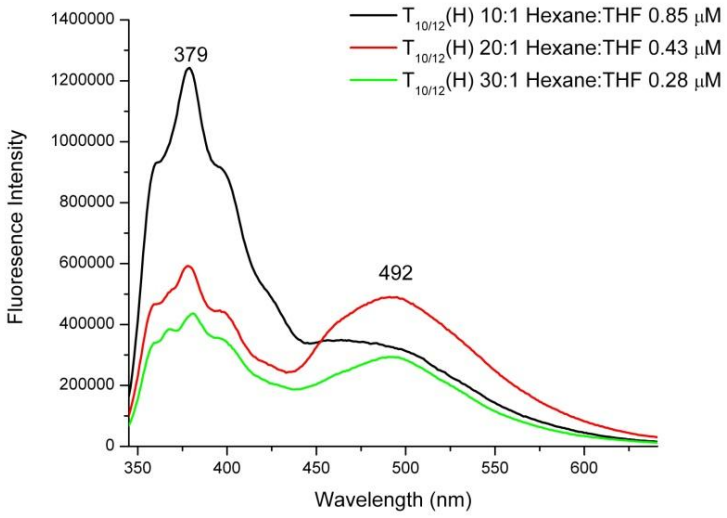

Figure 5.14. $T_{10/12}$ stilbenevinylSQ emission in 10:1, 20:1 and 30:1 of hexane:THF at various concentrations, suggesting "aggregate" formation.

A final study, run in MeOH (Figure **5.15**), shows the same behavior, although the ratio of intensities now favors the 492 nm peak. The fact that two poor solvents at both ends of the "spectrum," hexane and MeOH, bring about formation of the same red shifted, featureless emission.

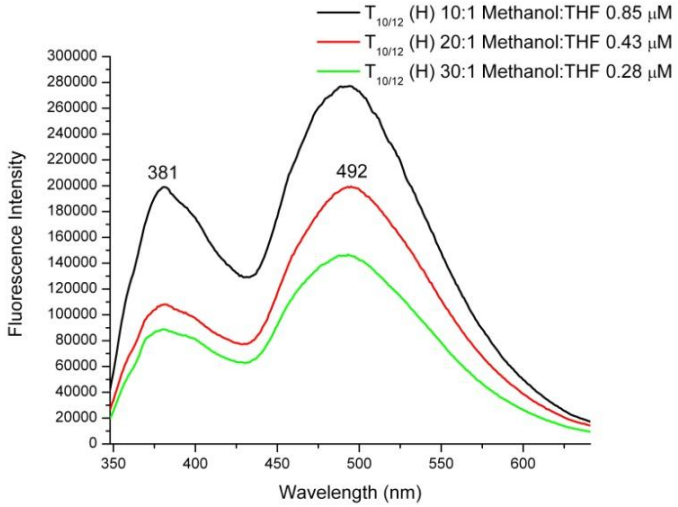

Figure 5.15. Emission spectra of $T_{10/12}$ stilbenevinylSQ in 10:1, 20:1 and 30:1 of MeOH:THF at various concentrations, showing "aggregate" formation.

The simplest explanation is that an interdigitated excimer forms such as suggested in Figure **5.16**, though the interdigitation may be more complex and involve multiple cages. It can be seen that the 3-D nature of the compounds will greatly limit the degree of overlap between two cages. Given that the same emissions are exhibited in two very different but poor solvents seems to support this conclusion. A further conclusion can be drawn based on the observation of emission from the original moieties, albeit blue shifted.

Interdigitation is first likely to occur between two cages across a narrow set of moieties in a "face-to-face" conformation; thus, moieties opposite the point(s) of interdigitation will retain their emissive behavior. If we then suggest that there is a real electronic interaction between the moieties on the original cages and the cage itself as we have described elsewhere;[24,26,27] then removing the interdigitated moieties from the overall electronic structure would diminish this interaction leading to the observed blue shift.

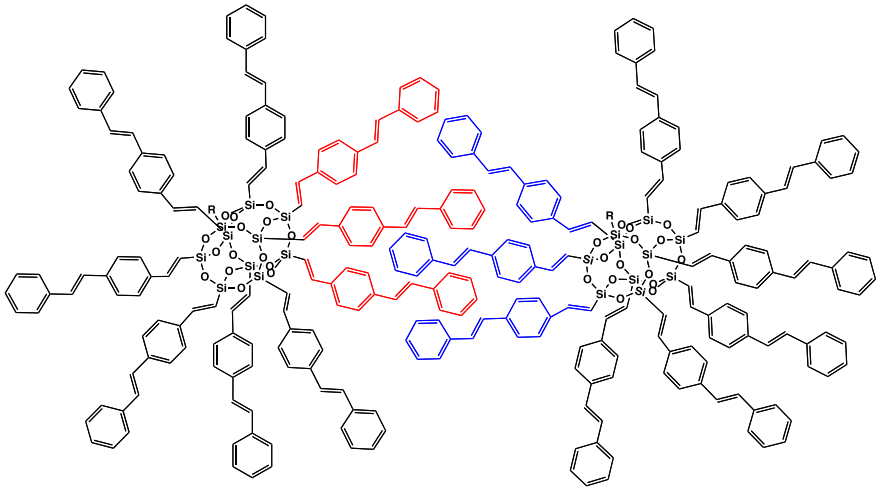

Figure 5.16. Possible aggregation or exciplex formation between two GEN2 stilbenevinylSQs.

While this behavior is reminiscent of emissions from solid state aggregate materials,[35] there is an aspect of these emissions that may have some import with respect to our above stated objectives. One possible benefit from this type of interaction is that emission now extends from approximately 350 nm out to 550 nm suggesting the potential for a single system to become a white light emitter with further functionalization and optimization of processing. It is important to add that we have seen evidence that suggests 3-D conjugation in the excited state.[24,26,27] As such, it may be that some types of aggregates will offer hole and electron transport properties

that are superior to 2-D aromatics.[36-41] The potential for such behavior may already exist as reviewed recently by Sellinger et al.[14] Clearly more work needs to be done here, but the potential appears to exist for some very novel materials and photophysics.

As a further extension of the above studies, we examined the effects of solvents on the emissive behavior of T_8 stilbenevinylSQs finding no effect in acetonitrile:THF mixtures, see Table **5.8**. We also extended our studies to $T_8/T_{10/12}$ mixtures in MeOH:THF (Figure **A2.9**) finding that some interactions are observed as noted in Table **5.9** with much reduced red shifts for T_8 vs. $T_{10/12}$ that suggests weaker aggregation. One possible explanation is that while the $T_{10/12}$ cages are slightly larger, they offer smaller angles between chromophores (~72° T_{10}, ~60° T_{12} vs. ~90° T_8) perhaps leading to stronger interactions when interdigitation occurs, stabilizing such species. This seems probable given that the T_8 cages by themselves do not exhibit interdigitation in poor solvents but do when mixed with the $T_{10/12}$ cages. Consequently, one can suggest that the smaller angles offer better opportunities to form stable interdigitated systems pointing a possible design criterion for further studies on these phenomena.

Table 5.9. Emission (nm) of T_8 and $T_{10/12}$ stilbenevinylSQs (± 2 nm) in hexane:THF or MeOH:THF of varying concentrations.

Hexane:THF	10:1	20:1	30:1	Aggregate λ_{max}
Concentration (μM)	0.85	0.43	0.28	--
$T_{10/12}$ R = H	379	379	379	492
T_8 R = H^S	380	380	380	-
Methanol:THF	10:1	20:1	30:1	Aggregate λ_{max}
Concentration (μM)	1.1	0.55	0.36	--
$T_{10/12}$ R = H	381	381	381	492
T_8 R = H	384	384	384	420/442

Finally, we also explored the effects of solvents on the emissive behavior of other $T_{10/12}$ *p*-stilbenevinylSQs as seen in Table **5.10**. The only clear cases for aggregation are for the R = Me and R = OMe compounds which exhibit shifts from an average $\lambda_{max} \approx 390$ nm ±5 nm (Me) 405±5 nm R = OMe in hexane:THF mixtures to $\lambda_{max} \approx 460/454$ R = Me/OMe nm in MeOH:THF at 20:1 (Figures **A2.4-A2.7**). Note that no temperature dependence was observed for R = Me

emission as seen in Figure **A2.5**. No evidence of excimer formation was seen for the anthracene derivatives (Figure **A2.8**).

Table 5.10. Emission (nm) of T_8 and $T_{10/12}$ stilbenevinylSQs (± 2 nm) in hexane:THF or MeOH:THF at constant concentrations, (*)= "Aggregate".

Hexane:THF	20:1	15:5	5:15	0:100
$T_{10/12}$ R = H	380 (477)*	382	384	386
$T_{10/12}$ R = Me	385	390	393	395
$T_{10/12}$ R = OMe	402	396	406	413
T_8 R = H	380	381	384	385
$T_{10/12}$ R = S-An	452	456	458	464
Methanol:THF	20:1			
$T_{10/12}$ R = H	379 (492)*			
$T_{10/12}$ R = Me	460			
$T_{10/12}$ R = OMe	454			
T_8 R = H	384 (420/442)*			
$T_{10/12}$ R = S-An	456			

It is now well recognized that ordering of molecules in π-π stacking ensembles (e.g. J and H aggregates) provide structures that allow control and fine tuning of electron and/or hole (exciton) transport properties. In turn, this control permits their employ in multiple important applications ranging from dye sensitization in photography to electrochromic and electroluminescent to organic photovoltaic to non-linear optical devices, etc.[35-41]

In general, most molecules that exhibit strong π-π stacking interactions are relatively planar and aromatic. To the best of our knowledge, no one has explored the effects of such interactions in 3-D molecules. We believe that the above results may be of value in developing new components for both OLEDs and/or organic photovoltaics if properly explored.

Two-Photon Absorption Measurements (TPA)

TPA cross-sections were determined for selected GEN1 and GEN2 compounds. The GEN1 compounds do not exhibit any TPA properties (Table **5.5**) as might be expected since they do not contain polarizable groups necessary to obtaining high TPA cross-sections. The double Heck and the phenyl compounds were not studied since the double Heck had similar

functionalization to the single products, and the phenyl absorption band at 254 nm made it difficult to study by our TPEF method.

TPA cross-sections for selected GEN2 compounds are plotted as a function of wavelength and are shown in Figure **5.17**, with results given in Table **5.11**. The cross-section values per chromophore are given in Table **5.12**. Full plots for each SQ are given in Figure **A2.10**. TPA values can provide a measure of the degree of enhanced absorption per chromophore and coupling between donor and acceptor regions,[42,43] leading to some measure of understanding of the potential photocurrent of photovoltaic devices that might incorporate these compounds as components. [26,27]

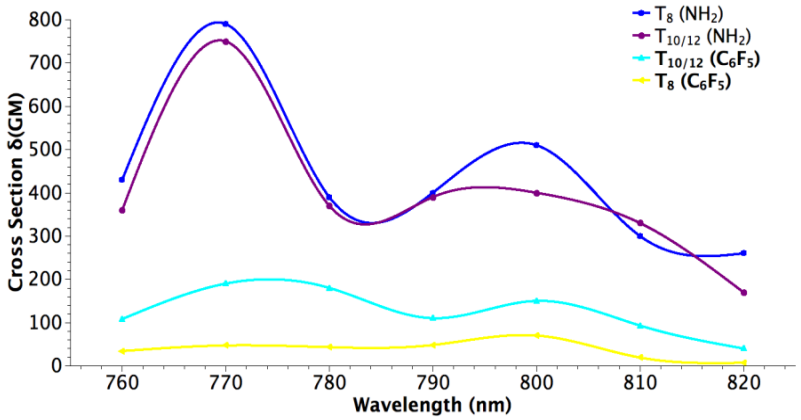

Figure 5.17. Two-photon absorption spectra of selected GEN2 compounds in THF.

Table 5.11. Two-photon studies of GEN2 compounds with respective cross-sections given.

Two-photon cross section in δ (GM) (10^{-50} cm^4 s $photon^{-1}$)								
SQ	650	760	770	780	790	800	810	820
$T_{10/12}$ R = H	4	-	8	7	5	6	4	0.3
$T_{10/12}$ R = Me	12	-	10	9	6	7	5	8
$T_{10/12}$ R = OMe	33	-	18	21	19	23	16	5
$T_{10/12}$ R = NH_2	80	360	750	370	390	400	330	170
$T_{10/12}$ R=C_6F_5	110	108	190	180	110	150	93	40
T_8 R = NH_2	-	430	790	390	400	510	300	260
T_8 R = C_6F_5	-	34	47	43	48	70	19	7

Table 5.12. Two-photon laser wavelengths studied and respective cross-section per chromophore on GEN2 SQs.

SQ	Wavelength (± 2 nm)	Cross-section/Chromophore δ(GM)
$T_{10/12}$ R = H	770	~1
$T_{10/12}$ R = Me	650	~1
$T_{10/12}$ R = OMe	650	3
T_8 R = NH_2	770	100
$T_{10/12}$ R = NH_2	770	68
T_8 R = C_6F_5	800	9
$T_{10/12}$ R = C_6F_5	770	17

The data presented here suggest that the TPA cross-sections for the GEN2 $T_{10/12}$ increase with conjugation and electron donating ability of the R-substituent on the chromophore. Thus on changing from R=H to NH_2 results in an 800 fold increase in cross-section per cage. It is important to note that measured TPA cross-sections depend on the fluorescence quantum efficiency (ϕ_{PL}) as these values are part of the cross-section calculation, which uses an "action cross-section" (based on fluorescence comparison with a standard), which is then multiplied by the quantum yield to give the corrected value based on the fluorescence efficiency.[44,45,] A 1 % difference in ϕ_{PL} can affect the cross-section by as much as 100 GM. This is particularly evident when comparing the difference between the previously published results on the T_8 cages and these new larger cages.[26,27]

If the T_8 and $T_{10/12}$ R = NH_2 substituted cages are compared (those with the highest cross sections), it is interesting to note that due to the lower quantum yield of the T_8 species, the cross-section at 770 nm is higher than that for $T_{10/12}$, 100 GM vs. 68 GM respectively per chromophore. These values may arise as a consequence of different cage geometries, which orient the chromophores differently by angle and proximity to one another leading to changes in fluorescence efficiency. Interestingly, the maximum cross-section arises from a lower energy excitation (770 nm) than expected from the single photon absorption (363 nm), suggesting that we are accessing a lower energy state.

The maximum TPA would be expected to exist around 725 nm or double the one photon absorption, which may be the case, but do to limits in instrumentally accessible wavelengths,

was not explored. Since a lower energy state can be accessed, this may explain the large Stokes shift in the single photon fluorescence through relaxation before emission. Since the T_8 cage is more symmetrical than the $T_{10/12}$ cages, it can be rationalized that the chromophore orientations may change fluorescence properties.[26,27] SQs in general give enhanced TPA cross-sections compared to single chromophores due to the enhanced dipole-moment term from the electrophilic nature of the cage.[26,42,43,46]

The TPA analyses for the R = C_6F_5 species are not as expected. Figure **A2.10** and Table **5.11** compare the cross-sections between the T_8 and $T_{10/12}$ R = C_6F_5 compounds. The corss-section values per chromophore are 9 GM for the T_8 and 17 GM for the $T_{10/12}$. These findings are surprising given the strong electron withdrawing character of the substituent.[26,27] If we assume that for the R = NH_2 compounds the cage acts as a strong electron withdrawing center enabling CT behavior in these systems, the introduction of R = C_6F_5 should provide two withdrawing sites competing for the electron populating the excited state. Such a situation should reduce the CT behavior significantly leading to lower TPA cross-sections, which is contrary to what is found. Recognizing that the TPA data for the R = C_6F_5 moiety is well below that of the R = NH_2 substituted GEN2 compounds it is still surprising to see any TPA cross-section values at all. This again may relate to the emission red shift for which we have no explanation as yet.

Cyclic Voltammetry

In order to probe the HOMO-LUMO levels in this first set of GEN2 compounds, we conducted cyclic voltammetry studies in films cast from dichlorobenzene as discussed in the experimental section. These studies are viewed as a qualitative analysis of the redox behavior of these molecules. Figure **5.18** provides an overview of the data measured, a representative CV of the GEN2 pentafluorophenyl SQ is shown as Figure **A2.11**.

The literature suggests that a potential replacement for PCBM derivatives should have a LUMO that is actually somewhat higher than -4.2 eV, preferably in the -3.8 to -3.4 eV in order to optimize V_{oc}.[47-49] Thus, in view of our current efforts, we must reduce the LUMO of one of the above compounds to this range to perhaps realize our goals. This is notwithstanding the obvious need to learn to process good devices with these new compounds, which still may be a difficult task. As we will see in future papers the R = C_6F_5 derivatives offer the best opportunity to access these target properties.[50]

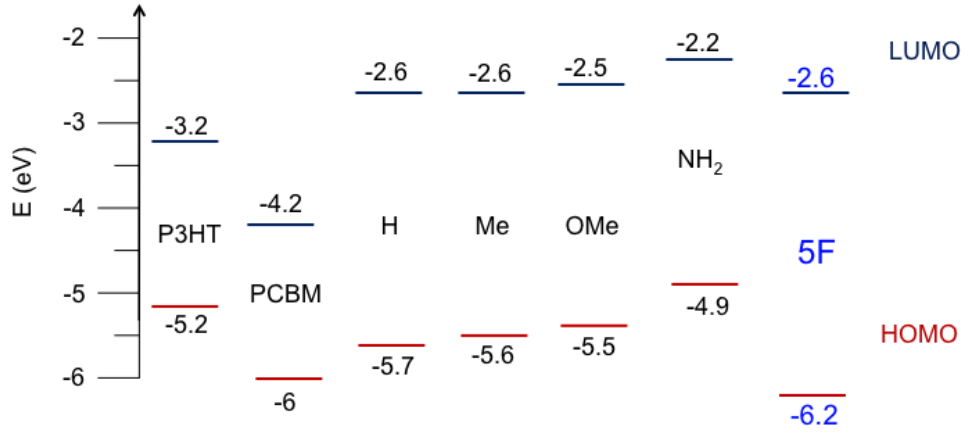

Figure 5.18. Cyclic voltammetry studies of GEN2 compounds, with published data for P3HT (poly-3-hexylthiophene) and PCBM ([6,6]-phenyl-C_{61}-butyric acid methyl ester) added.

5.3. Conclusions

Our stated objective in this work was to synthesize and then map the photophysical properties of sets of three dimensional molecules derived from vinylT_{10}SQ and vinylT_{12}SQ mixtures as GEN1 and GEN2 compounds. These mapping studies are considered as a first step in exploring their potential utility as components on organic electronic and photonic materials. As we anticipated, based on early studies of the vinylT_8SQs the synthesized compounds were all quite soluble in multiple organic solvents and easily purified by traditional methods. Although a mixture is used, the analytical results indicate that it is possible to obtain 100 % conversions to target GEN1 and then GEN2 products.

The photophysical behavior of these compounds is mostly similar to that of the T_8 compounds with some clear exceptions. In particular the $T_{10/12}$ systems are able to interdigitate in poor solvents exhibiting behavior that appears to indicate aggregation. Given their 3-D structures, this aggregation appears to be 3-D in nature and most likely differs considerable from aggregates formed from traditional organic molecules.

The photophysical data suggest that the mixed $T_{10/12}$ systems have slightly smaller band gaps than those measured for the T_8 analogs. Furthermore, they show a higher propensity to interdigitate perhaps because of the slightly larger cage sizes. However, TPA data suggest slightly lower cross-sections except for the C_6F_5 compounds, which offer much unexpected properties.

Given our previous finding of the existence of conjugation through the center of the cage for these types of systems in the excited state, the aggregation data suggest some novel potential for 3-D hole/electron transport properties perhaps reminiscent of fullerene type compounds and with further modification allowing their use in place of fullerene PCBM derivatives in photovoltaic devices as we will show in the next manuscript in this series.

References Cited:

1. Voronkov, M.G.; Lavrent'yev, V.I.; "Polyhedral Oligosilsesquioxanes and Their Homo Derivatives," *Top. Curr. Chem*., **1982**, *102*, 199-236.
2. Baney, R.H.; Itoh, M.; Sakakibara, A.; Suzuki, T.; "Silsesquioxanes," *Chem. Rev*., **1995**, *95*, 1409-1430.
3. Loy, D.A.; Shea, K.J.; "Bridged Polysilsesquioxanes. Highly Porous Hybrid Organic-Inorganic Materials," *Chem. Rev*., **1995**, *95*, 1431-1442.
4. Calzaferri, G.; "Silsesquioxanes," in Tailor-made Silicon-Oxygen Compounds, from molecules to materials, Corriu, R. and Jutzi, P. Ed., Friedr. Vieweg & Sohn mbH, Braunshweig/Weisbaden, Germany, **1996**, pp. 149-169.
5. Lichtenhan, J.; "Silsesquioxane-based Polymers," in Polymeric Materials Encyc., Salmon, J.C. Ed., Vol. 10, CRC Press, N.Y., **1996**, pp. 7768-7777.
6. Provatas, A.; Matisons, J.G.; "Synthesis and applications of silsesquioxanes," *Trends Polym. Sci*., **1997**, *5*, 327-333.
7. Li, G.; Wang, L.; Ni, H.; Pittman, C.U.; "Polyhedral Oligomeric Silsesquioxane (POSS) Polymers and Copolymers: A Review," *J. Inorg. Organomet. Polym.*, **2001**, *11*, 123-151.
8. Duchateau, R.; "Incompletely Condensed Silsesquioxanes: Versatile Tools in Developing Silica-Supported Olefin Polymerization Catalysts," *Chem. Rev.*, **2002,** *102*, 3525-3542.
9. Abe, Y.; Gunji, T.; "Oligo- and polysiloxanes" *Prog. Polym. Sci.*, **2004**, *29*, 149-182.
10. Phillips, S H.; Haddad, T. S.; Tomczak, S. J.; "Developments in nanoscience: polyhedral oligomeric silsesquioxane (POSS)-polymers," *Curr. Opin. Solid State Mater. Sci*., **2004**, *8*, 21-29.

11. Kannan, R. Y.; Salacinski, H. J.; Butler, P. E.; Seifalian, A. M.; "Polyhedral oligomeric silsesquioxane nanocomposites: The next generation material for biomedical applications," *Acc. Chem. Res.*, **2005**, *38*, 879-884.
12. Laine, R. M.; "Nanobuilding blocks based on the $[OSiO_{1.5}]_x$ (x = 6, 8, 10) octasilsesquioxanes," *J. Mater. Chem.*, **2005**, *15*, 3725-3744.
13. Lickiss, P. D.; Rataboul, F.; "Fully Condensed Polyhedral Oligosilsesquioxanes (POSS): From Synthesis to Application," *Adv. Organomet. Chem.*, **2008**, *57*, 1-116.
14. Chan, K. L.; Sonar, P.; Sellinger, A.; "Cubic silsesquioxanes for use in solution processable organic light emitting diodes (OLED)," *J. Mater. Chem.*, **2009**, *19*, 9103-9120.
15. Wu, J.; Mather, P. T.; "POSS Polymers: Physical Properties and Biomaterials Applications," *Polym. Rev.*, **2009**, *49*, 25-63.
16. Cordes, D. B.; Lickiss, P. D.; Franck, R.; "Recent Developments in the Chemistry of Cubic Polyhedral Oligosilsesquioxanes," *Chem. Rev.*, **2010**, *10*, 2081-2173.
17. Laine, R. M.; Roll, M. F.; "Polyhedral Phenylsilsesquioxanes," *Macromolecules*, **2011**, *44*, 1073-1109.
18. Bassindale, A. R.; Liu, Z.; MacKinnon, I. A.; Taylor, P. G.; Yang, Y.; Light, M. E.; Horton, P. N.; Hursthouse, M. B.; "A higher yielding route for T_8 silsesquioxane cages and X-ray crystal structures of some novel spherosilicates," *Dalton Trans.*, **2003**, 2945-2949.
19. Bassindale, A. R.; Pourny, M.; Taylor, P. G.; Hursthouse, M. B.; Light, M. E.; "Fluoride-ion encapsulation within a silsesquioxane cage," *Angew. Chem. Int. Ed.*, **2003**, *42*, 3488-3490.
20. Bassindale, A. R.; Parker, D. J.; Pourny, M.; Taylor, P. G.; Horton, P. N.; Hursthouse, M. B.; "Fluoride ion entrapment in octasilsesquioxane cages as models for ion entrapment in zeolites. Further examples, X-ray crystal structure studies, and investigations into how and why they may be formed," *Organometallics*, **2004**, *23*, 4400-4405.
21. Rikowski, E.; Marsmann, H. C.; "Cage-rearrangement of silsesquioxanes," *Polyhedron*, **1997**, *16*, 3357-3361.
22. Anderson, S. E.; Bodzin, D. J.; Bodzin, D. J.; Haddad, T. S.; Boatz, J. A.; Mabry, J. M.; C. Mitchell, M. T. Bowers, "Structural Investigation of Encapsulated Fluoride in Polyhedral

Oligomeric Silsesquioxane Cages Using Ion Mobility Mass Spectrometry and Molecular Mechanics," *Chem. Mater*., **2008**, *20*, 4299-4309.

23. Ronchi, M.; Sulaiman, S.; Boston, N. R.; Laine, R. M.; "Fluoride catalyzed rearrangements of polysilsesquioxanes, mixed Me, Vinyl T_8, Me, Vinyl T_{10} and T_{12} cages," *Applied Organometal. Chem.*, **2010**, *24*, 551-557.
24. Asuncion, M. Z.; Laine, R.M. "Fluoride Rearrangement Reactions of Polyphenyl- and Polyvinylsilsesquioxanes as a Facile Route to Mixed Functional Phenyl, Vinyl T_{10} and T_{12} Silsesquioxanes," *J. Am. Chem. Soc.*, **2010**, *132*, 3723-3736.
25. Jung, J. H.; Laine, R.M. "Beads on a chain (BOC) polymers formed from the reaction of $NH_2PhSiO_{1.5}]_x[PhSiO_{1.5}]_{10-x}$ and $[NH_2PhSiO_{1.5}]_x[PhSiO_{1.5}]_{12-x}$ mixtures (x = 2-4) with the diglycidyl ether of bisphenol A," *Macromolecules*, **2011**, *44*, 7263-7272.
26. Sulaiman, S.; Brick, C.; Roll, M.; Bhaskar, A.; Goodson, T.; Zhang, J.; Laine, R. M. "Molecules with Perfect Cubic Symmetry as Nanobuilding Blocks for 3-D Assemblies. Elaboration of Octavinylsilsesquioxane. Unusual Luminescence Shifts May Indicate Extended Conjugation Involving the Silsesquioxane Core." *Chem. Mater.*, **2008**, *20*, 5563-5573.
27. Laine, R. M.; Sulaiman, S.; Brick, C.; Roll, M.; Tamaki, R.; Asuncion, M. Z.; Neurock, M.; Filhol, J.-S.; Lee, C.-Y.; Zhang, J.; Goodson, T.; Ronchi, M.; Pizzotti, M.; Rand, S. C.; Li, Y. "Synthesis and Photophysical Properties of Stilbeneoctasilsesquioxanes. Emission Behavior Coupled with Theoretical Modeling Studies Suggest a 3-D Excited State Involving the Silica Core." *J. Am. Chem. Soc.*, **2010**, *132*, 3708-3722.
28. Sellinger, A.; Tamaki, R.; Laine, R.M.; Ueno, K.; Tanabe, H.; Williams, E.; Jabbour, G.E. "Heck Coupling of Haloaromatics with Octavinylsilsesquioxane: Solution Processable Nanocomposites for application in electroluminescent devices," *Chem. Commun.*, **2005,** 3700-3702.
29. Usenko, C. Y.; Harper, S. L.; Tanguay, R. L.; *"In vivo* evaluation of carbon fullerene toxicity using embryonic zebrafish," *Carbon*, **2007**, *45* 1891-1898.
30. Sera, N.; Tokiwa, H.; Miyata, N. "Mutagenicity of the fullerene C^{60}-generated singlet oxygen dependent formation of lipid peroxides," *Carcinogenesis*, **1996**, *17*, 2163-2169.

31. Zhang, G.; Yang, G.; Wang, S.; Chen, Q.; Ma, J.S., "A Highly Fluorescent Anthracene-Containing Hybrid Material Exhibiting Tunable Blue–Green Emission Based on the Formation of an Unusual "T-Shaped" Excimer (pages 3630–3635)," *Chem. Eur. J.*, **2007**, *13*, 3630-3635.
32. Bonneau, R.; Carmichael, I.; Hug, H.G. "Molar Absorption Coefficients of Transient Species in Solution." *Pure* & *Appl. Chem.*, **1991**, *63*, 289-299.
33. Eaton, D. F.; "Reference Materials for Fluorescence Measurement" *Pure* & *Appl. Chem.*, **1988**, *60*, 1107-1114.
34. Jenekhe, S. A.; Osaheni, J. A. "Excimers and Exciplexes of Conjugated Polymers," *Science*, **1994**, *265*, 765-768.
35. Bolton, O.; Lee, K.; Kim, H.-J.; Lin, K. Y.; Kim, J.; "Activating efficient phosphorescence from purely organic materials by crystal design," *Nature Chem.*, **2011** *3*, 205-210 and references therein.
36. Cariati, E.; Macchi, R.; Roberto, D.; Ugo, R.; Galli, S.; Masciocchi, N.; Sironi; A., "Sequential Self-Organization of Silver(I) Layered Materials with Strong SHG by J Aggregation and Intercalation of Organic Nonlinear Optical Chromophores through Mechanochemical Synthesis," *Chem. Mater.*, **2007**, *19*, 3704-3711.
37. Arai, Y.; Segawa, H.; "Cl^- Complexation Induced H- and J-Aggregation of *meso*-Tetrakis(4-sulfonatothienyl)porphyrin Diacid in Aqueous Solution" *J. Phys. Chem. B*, **2011**, *115*, 7773–7780.
38. Yi, J.; Chen, Z.; Xiang, J.; Zhang, F.; "Photocontrollable J-Aggregation of a Diarylethene–Phthalocyanine Hybrid and Its Aggregation-Stabilized Photochromic Behavior," *Langmuir*, **2011**, *27*, 8061-8066.
39. Slavnova, T. D.; Chibisov, A. K.; Görner, H.; "Kinetics of Salt-Induced J-aggregation of Cyanine Dyes," *J. Phys. Chem. A* **2005,** *109*, 4758-4765.
40. Chaudhuri, D.; Li, D.; Che, Y.; Shafran, E.;. Gerton, J. M.; Zang, L.; Lupton, J. M.; "Enhancing Long-Range Exciton Guiding in Molecular Nanowires by H-Aggregation Lifetime Engineering," *Nano Lett.*, **2011**, *11*, 488-492.

41. Deng, Y.; Li, Y.; Wang, X.; "Colloidal Sphere Formation, H-Aggregation, and Photoresponsive Properties of an Amphiphilic Random Copolymer Bearing Branched Azo Side Chains," *Macromolecules*, **2006**, *39*, 6590-6598.
42. Ramakrishna, G.; Bhaskar, A.; Goodson, T. G. "Ultrafast Excited State Relaxation Dynamics of Branched Donor-π-Acceptor Chromophore: Evidence of a Charge-Delocalized State," *J. Phys. Chem. B*, **2006**, *110*, 20872.; Haley, J. E.; Krein, D. M.; Monahan, J. L.; Burke, A. R.; McLean, D. G.; Slagle, J. E.; Fratini, A.; Cooper, T. M. "Photophysical Properties of a Series of Electron-Donating and -Withdrawing Platinum Acetylide Two-Photon Chromophores." *J. Phys. Chem. A*, **2010**, *115*, 265-273.
43. Varnavski, O.; Yan, X.; Mongin, O.; Blanchard-Desce, M.; Goodson, T. "Strongly Interacting Organic Conjugated Dendrimers with Enhanced Two-Photon Absorption." *J. Phys. Chem. C.*, **2006**, *111*, 149-162.
44. Maciejewski A.; Steer, R. P. "Spectral and photophysical properties of 9,10-diphenylanthracene in perfluoro-n-hexane: the influence of solute—solvent interactions," *J. Photochem.*, **1986**, *35*, 59-69.
45. Xu, C.; Webb, W. W. "Measurement of two-photon excitation cross sections of molecular fluorophores with data from 690 to 1050 nm." *J. Opt. Soc. Am. B.*, **1996**, *13*, 481-491.
46. Goodson III, T.; "Optical Excitations in Organic Dendrimers Investigated by Time-Resolved and Nonlinear Optical Spectroscopy."*Acc. Chem. Res.*, **2005**, *38*, 99-107.
47. Kim, K-H.; Kang, H.; Nam, S. Y.; Jung, J.; Kim, P. S.; Cho, C-H.; Lee, C.; Yoon, S. C.; Kim, B. J. "Facile Synthesis of o-Xylenyl Fullerene Multiadducts for High Open Circuit Voltage and Efficient Polymer Solar Cells," *Chem. Mater*., **2011**, 23, 5090-5095.
48. He, Y.; Chen, H.-Y.; Hou, J.; Li, Y.; "Indene-C60 Bisadduct: A New Acceptor for High-Performance Polymer Solar Cells," *J. Am. Chem. Soc*., **2010** *132*, 1377-1382.
49. Lenes, M.; Wetzelaer, G-J. A. H.; Kooistra, F. B.; Veenstra, S. C.; Hummelen, J. C.; Blom; P. W. M. "Fullerene Bisadducts for Enhanced Open-Circuit Voltages and Efficiencies in Polymer Solar Cells," *Adv. Mater.*, **2008**, *20* 2116-2119.
50. Jung, J. H.; Furgal, J.; Goodson, T.; Laine, R. M.; unpublished work.

Chapter 6

Functionalization of Br_{16}OPS for bulk heterojunction (BHJ) organic photovoltaics (OPV)

With contributions from Mr. Jojo Amonoo and Mr. David Bilby (Materials Science and Engineering Department, University of Michigan) for fabrication and evaluation of OPV cells

Abstract

The objective of this work is to develop new acceptor materials based on functionalized silsesquioxanes (SQs) for bulk heterojunction (BHJ) organic photovoltaics (OPV). Octa(2,5-dibromophenyl)silsesquioxane (Br_{16}OPS) is functionalized by Heck coupling with penta-fluorostyrene and 4-cyanostyrene ($5FSty_{16}$OPS, $CNSty_{16}$OPS) and 4-bromotriphenylamine ($5FSty_{16}$-TPA OPS, $CNSty_{16}$-TPA OPS) in effort to control the highest occupied molecular orbital (HOMO) and the lowest unoccupied molecular orbital (LUMO) energies. These compounds are characterized by ^{1}H-NMR, FTIR, TGA and MALDI-ToF. The LUMO energy levels of these functionalized Br_{16}OPS are measured by cyclic voltammetry and offer optimal values of -3.6 eV. The photophysical data for triphenylamine (TPA) incorporated SQs indicate charge transfer (CT) behavior through electron push-full structures of typical donors and acceptors. Nevertheless, a BHJ device of $5FSty_{16}$OPS and P3HT showed poor performance with a power conversion efficiency (PCE) of 0.0007 ± 0.0005 %, partial substitution of PCBM by $5FSty_{16}$OPS retains OPV performance of reference cell which is fabricated with mixture of P3HT and PCBM (4.1 %) if the content of $5FSty_{16}$OPS is less than 15 %. Although the influence of $5FSty_{16}$OPS on OPV performance is unclear at present, this result implies that there must be an interaction between SQs and P3HT or PCBM.

6.1. Introduction

Fullerenes and their derivatives, in particular [6,6]-phenyl C_{61} or C_{71} butyric acid methyl esters (PCBMs), are the most widely used acceptors in organic photovoltaics (OPV) field because (1) they exhibit ultrafast (~ 50 fs) photoinduced electron transfer from donor semiconducting polymers (2) their triply degenerate LUMO enables it to be reduced by up to six electrons, which reflects its unique stabilization of negative charge, and (3) they show high electron mobilities (up to 6 cm^2/Vs) even in composites.[1-6] However, they have disadvantages such as weak absorption in the visible region that limits light harvesting, and a low-energy LUMO that results in lower open circuit voltages (V_{oc}) as well as high costs of production.[7-9] Therefore, many research groups are trying to develop new acceptors based on other structural platforms like conjugated polymer acceptors or n-type small molecules.[10-12]

Recently, our group reported that polyhedral silsesquioxanes (SQs), $[RSiO_{1.5}]_{8,10,12}$, with various conjugated organic groups offer charge delocalization through 3-D conjugation in the excited state, tunable bandgaps, high absorption as well as extensive charge transfer behavior.[14-17] These properties coupled with ease of synthesis and functional group variation suggest significant potential for optoelectronic applications. For example, significant advances have been made in incorporating SQ cages into organic light emitting materials.[18-20] However, only a few reports describe electronically active silica and siloxane nanoparticles, not silsesquioxanes, for photovoltaic applications. [21, 22]

An objective of the work reported here was to develop a hybrid non-fullerene acceptor materials based on SQs to substitute for PCBM. When designing a new acceptor, it is critical to control LUMO energy levels because the acceptor LUMO must be sufficiently below the donor LUMO to allow efficient electron transfer.[11, 12] In Chapter **5**, we showed that the LUMO energy of *p*-R-stilbenevinyl-functionalized SQs (GEN2) are higher than the LUMO of poly(3-hexylthiophene)s, P3HTs, electron donor, thus, we need other types of SQs functionalized with electron withdrawing groups.

Our group recently developed a synthetic route to very pure $[o\text{-}BrPhSiO_{1.5}]_8$ (Br_8OPS), $[2,5\text{-}Br_2PhSiO_{1.5}]_8$ ($Br_{16}OPS$), and $[Br_3PhSiO_{1.5}]_8$ ($Br_{24}OPS$) and demonstrated the potential to introduce 8, 16 or 24 functional groups in the same volume (Scheme **6.1**).[13, 23] Furthermore, these functional groups are expected to offer extended conjugation through the central phenyl ring and

the center of the SQ cages. Therefore, in this study, we have developed synthetic routes to introduce high densities of electron withdrawing groups into the SQs based on Br_{16}OPS to control the LUMOs of SQs and to explore their potential applicability as acceptors for OPV devices.

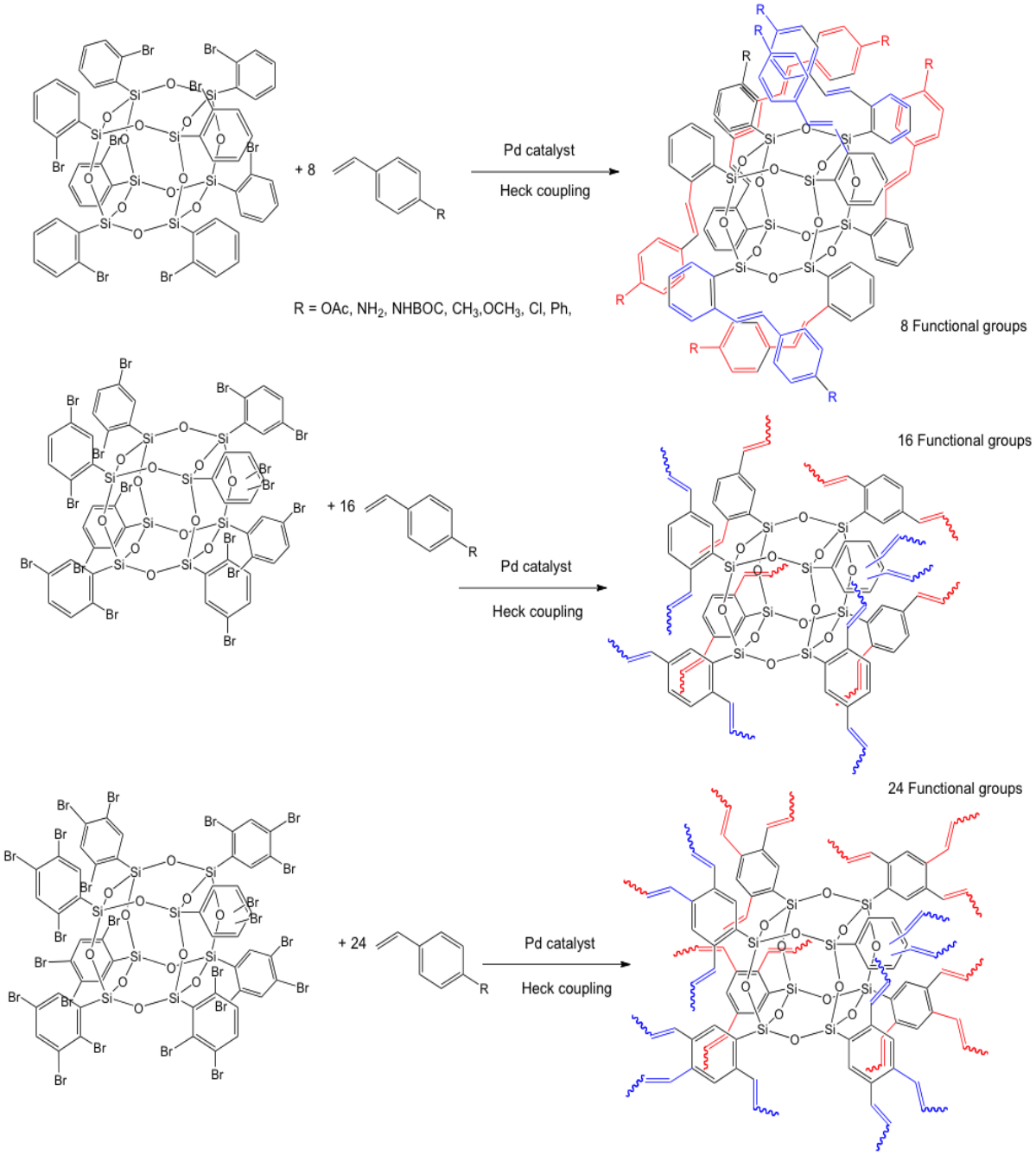

Scheme 6.1. Heck coupling of *o*-Br_8OPS, 2,5-Br_{16}OPS and Br_{24}OPS.[13]

6.2. Results and Discussion

In the following sections, we discuss the synthesis and characterization of various Br_{16}OPS derivatives prepared by Heck cross-coupling reactions. We then discuss their photophysical properties and thereafter device performance in organic photovoltaic (OPV) cells fabricated using $5FSty_{16}$OPS as an electron acceptor.

6.2.1. Synthesis and characterization of functionalized $[2,5\text{-}Br_2PhSiO_{1.5}]_8$ (Br_{16}OPS) derivatives

At first, Br_{16}OPS is functionalized by Heck coupling with pentafluorostyrene and 4-cyanostyrene to control LUMO energy levels (Scheme **6.2**). These reactions were run under more vigorous reaction conditions (higher concentration of styrene compounds and elevated temperature) compared with our previous work using BrStyrenylOS (see Chapter **2**) due to the steric hindrance of *ortho*-Br groups.[13]

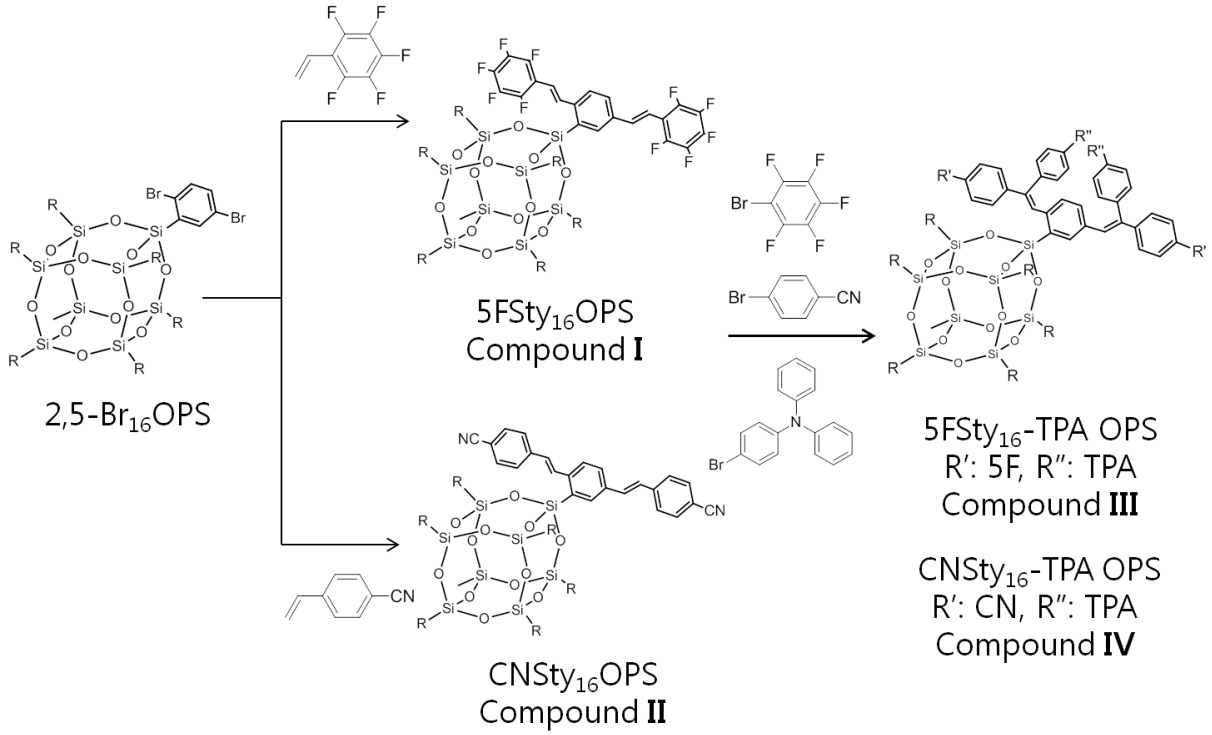

Scheme 6.2. Functionalization of $[2,5\text{-}Br_2PhSiO_{1.5}]_8$ (Br_{16}OPS).

Table 6.1. Characterization of compounds **I** - **IV**.

SQs	GPC			TGA			
	Mn	Mw	PDI	CY	Theo. CY	$T_{d5\%}$(°C)	# of TPA
Br_{16}OPS	2920	2950	1.01	20.2 %	20.9 %	310	-
$5FSty_{16}$OPS (**I**)	3310	3380	1.02	0 %	11.7 %	285	-
$CNSty_{16}$OPS (**II**)	3490	3600	1.03	15.4 %	15.7 %	270	-
$5FSty_{16}$-TPA OPS (**III**)	4220	4430	1.05	6.9 %	6.8 %	280	12
$CNSty_{16}$-TPA OPS (**IV**)	4400	4490	1.02	9.9 %	9.6 %	270	8

The synthesized Heck products, $5FSty_{16}$OPS (compound **I**) and $CNSty_{16}$OPS (compound **II**), are further functionalized through a second Heck coupling with bromopentafluorobenzene or 4-bromobenzonitrile to incorporate more electron withdrawing groups or with 4-bromotriphenylamine to introduce an electron donating group to control HOMO and LUMO energy levels of SQs. Surprisingly, the only electron donating group, triphenylamine (TPA), is successfully incorporated via second Heck cross-coupling ($5FSty_{16}$-TPA OPS, compound **III** and $CNSty_{16}$-TPA OPS, compound **IV**), even though the TPA group is bulkier than the electron withdrawing groups. These compounds are characterized by FTIR, GPC, TGA and MALDI-ToF. The characterization data are summarized in Table **6.1**.

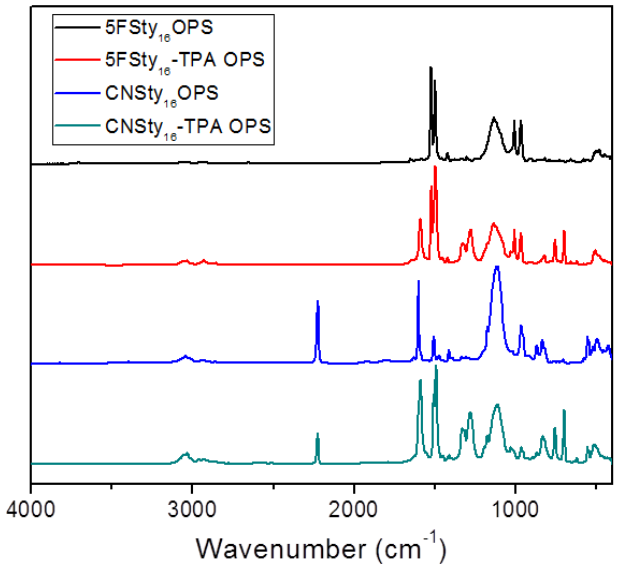

Figure 6.1. FTIR spectra of compounds **I** - **IV**.

The FTIR spectrum show characteristic peaks νC-F (1500 and 1520 cm^{-1}) of compound **I** and νC≡N (2200 cm^{-1}) of compound **II** respectively (Fig **6.1**). After introduction of the TPA group, new νC-N of aromatic amine peaks appear at 1330, 1280 cm^{-1}.

Figure **6.2** provides MALDI-ToF spectra of Br_{16}OPS and compound **I**. Although Br_{16}OPS are purified multiple times by recrystallization, small amounts of other brominated species such as Br_{15}OPS and Br_{17}OPS are present in this compound. It should be noted that the number of Br groups, 16 is calculated based on the ceramic yield (Table **6.1**), and reflects an average of the actual numbers of Br groups present per SQs. The MALDI-ToF spectrum of compound **I** confirms the complete conversion of Br. No MALDI-ToF data were obtained for other compounds probably because they are unstable under the UV laser of MALDI-ToF. Thus, the conversion of Br groups of compound **II** and the average number of incorporated TPA groups of compound **III**, **IV** are determined by TGA ceramic yield.

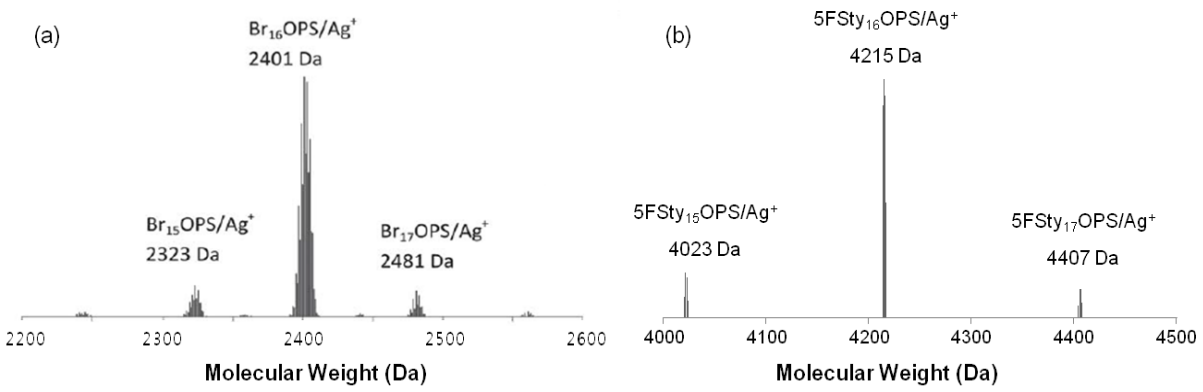

Figure 6.2. MALDI-ToF of spectra of (a) Br_{16}OPS and (b) compound **I**.

The ceramic yield of compound **II** matches well with the theoretical value and we can conclude that all Br groups are converted completely. However, compound **I** shows unexpected behavior, it sublimes, in TGA despite a high molecular weight (4107 g/mol). Based on the results that all Br groups of Br_{16}OPS are completely converted in compounds **I** and **II**, the number of incorporated TPA groups in compounds **III** and **IV** are calculated from the TGA ceramic yields (Table **6.1**). Because the ceramic yields are an average value, we expect that compounds **III** and **IV** consist of mixtures with different numbers of TPA groups.

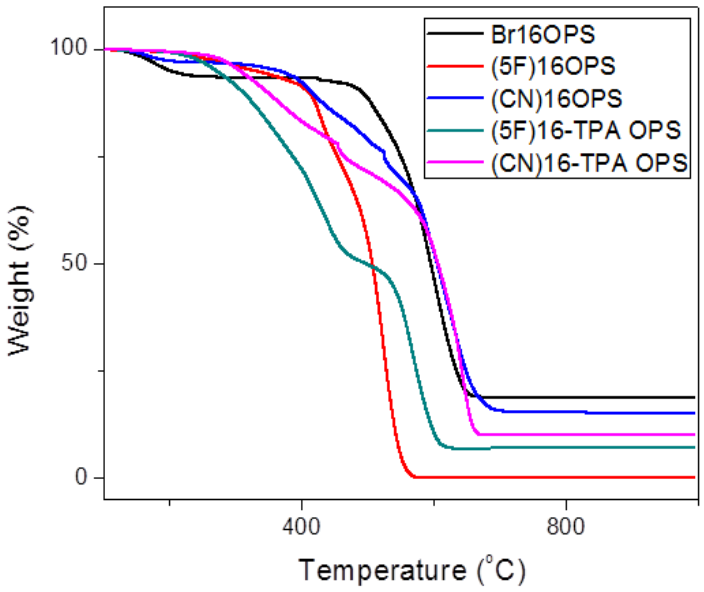

Figure 6.3. TGA of compounds **I** - **IV**.

6.2.2. Photophysical properties of Br_{16}OPS derivatives

Figure **6.4** provides UV-vis absorption and photoluminescence spectra for compounds **I** – **IV** in THF with the photophysical data summarized in Table **6.2**. The absorption spectrum of **IV** consists of two peaks at 305 nm and 362 nm. The first peak at 362 nm corresponds with compound **II** and the second peak matches with compound **III**. This means that the absorption at 305 nm is related to the triphenylamine (TPA) chromophore.

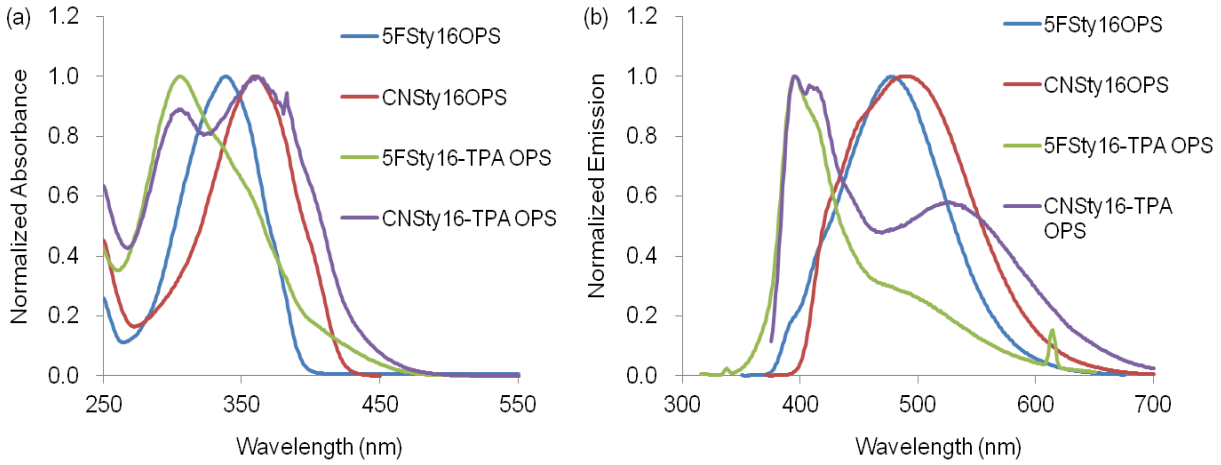

Figure 6.4. (a) UV/vis absorption and (b) photoluminescence spectra of compounds **I-IV** in THF.

Table 6.2. Photophysical data for compounds **I** – **IV** (THF).

	Absorption λ_{max} (nm) (±2 nm)	Emission λ_{max} (nm) (±2 nm)	Φ_{PL} (%)	δ (GM)	δ / group (GM)
$5FSty_{16}OPS$ (**I**)	340	477	14	11	1.3
$CNSty_{16}OPS$ (**II**)	360	487	42	62	7.7
$5FSty_{16}$-TPA OPS (**III**)	305	395	5	46	5.8
$CNSty_{16}$-TPA OPS (**IV**)	305, 362	395, 526	21	26	3.3

The absorption and emission spectra of compounds **III** and **IV** show blue-shifts compared to their parent SQs even though they have electron donating TPA groups, moreover, doubly functionalized SQ compounds have a tendency to be slightly red-shift compared with single functionalized SQs due to the extended excited state conjugation.[16] The reason for this unexpected blue-shift is unclear at present but highlights the unusual photophysical properties of these systems. Moreover, the red shift of absorption edge of the UV-vis spectra of compounds **III** and **IV** indicate reduced bandgap on incorporating TPA groups as discussed below.

Additional interesting features of the emission spectra of compounds **III** and **IV** are broad second peaks. The breadth of these peaks suggests aggregation.[24] Thus, to confirm this aggregation behavior, additional studies were run at more polar solvent, acetonitrile (AN). As shown in Figure **6.5**, the "aggregate peaks" disappear in AN as likely as a result of enhanced solubility. Moreover, it is important to note that compounds **III** and **IV** show 30 ~ 35 nm red shifts in the more polar solvent (AN). These red shifts indicate intramolecular charge transfer (CT) between donor (TPA) and acceptor (F or CN) of push-full chromophores.[25-27]

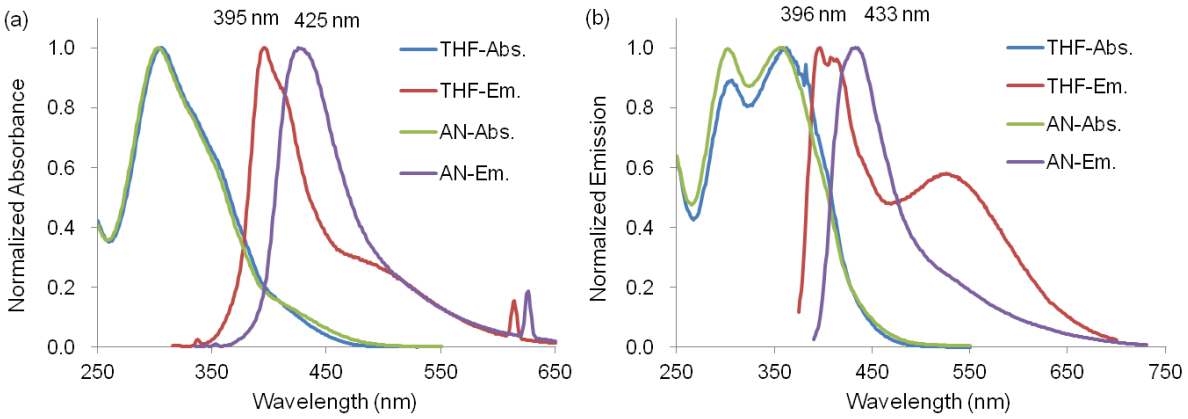

Figure 6.5. UV-vis absorption and PL spectra of (a) compound **III** and (b) **IV** in THF and acetonitrile (AN).

In chapter **5**, we discussed the "aggregate peak" of stilbenevinyl $T_{10/12}$ SQs, suggesting that this behavior arises through formation of interdigitated excimers. In the case of stilbenevinyl SQs, the "aggregate peak" appears only in poor solvents such as hexane or methanol, however, that of compounds **III** and **IV** appear in THF. This implies that the interaction between aggregated SQs of these compounds is stronger than that of stilbenevinyl SQs.

This stronger interaction may be explained by Coulombic force between charged of donor (TPA) and acceptor (F or CN) caused by the intramolecular charge transfer (CT) (Figure **6.6**). This CT behavior is supported by the fluorescent quantum yield (QY) and two photon absorption (TPA) cross section data (Table **6.2**). In general, CT funnels energy away from luminescence and gives rise to low quantum yields. In addition, the TPA cross section values provide a measure of the degree of enhanced dipole-moment. The decrease of QY and increase of TPA cross section of compound **III** indicates CT properties.

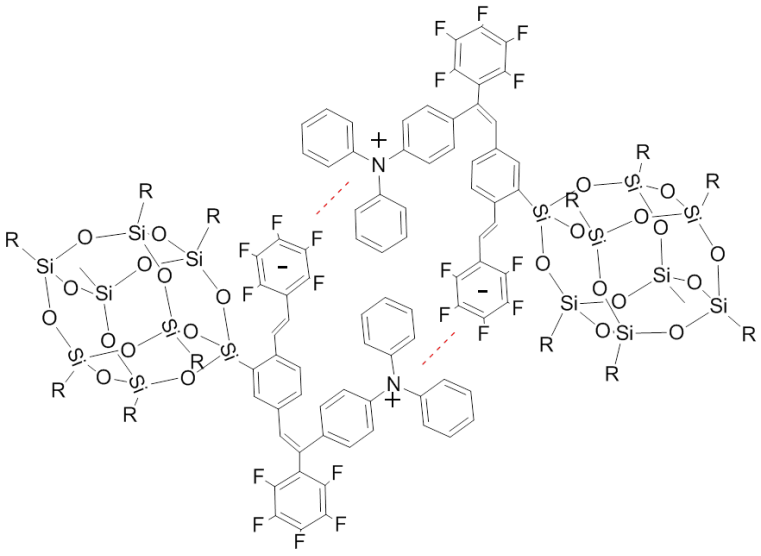

Figure 6.6. Possible aggregation of compound **III**.

6.2.3. Application of $5FSty_{16}OPS$ in Organic photovoltaic (OPV) cells

The literature suggests that the potential electron acceptor materials should have a LUMO that is at least 0.3 or 0.4 eV lower than LUMO of electron donor materials to guarantee charge transfer between donor and acceptor.[28,29] Moreover, since the V_{oc} of the OPV cells is proportional to the difference between the LUMO of acceptor and HOMO of donor,[30] the

appropriate acceptor LUMO energy should be in the range of -3.8 to -3.5 eV in this study because the LUMO energy of P3HT, donor material, is -3.2 eV.

In order to apply compounds **I** - **IV** in OPV cells as electron acceptors, the HOMO and LUMO energy levels were measured by cyclic voltammetry. Figure **6.7** provides an overview of the data measured. As shown in Figure **6.7**, the LUMO energy levels of compounds **I** - **IV** are close to optimal value (-3.6 eV). These results indicate that the introduction of electron withdrawing groups decreases the LUMO energies, on the other hand, electron donating groups raise the HOMOs. Therefore, the bandgap decreases when TPA groups are incorporated in SQs. This result corresponds to the red shift of absorption edge of compound **III** and **IV**. Among the compounds **I** - **IV**, compound **I** was used as an electron acceptor in OPV cells because it is most soluble in chlorobenzene.

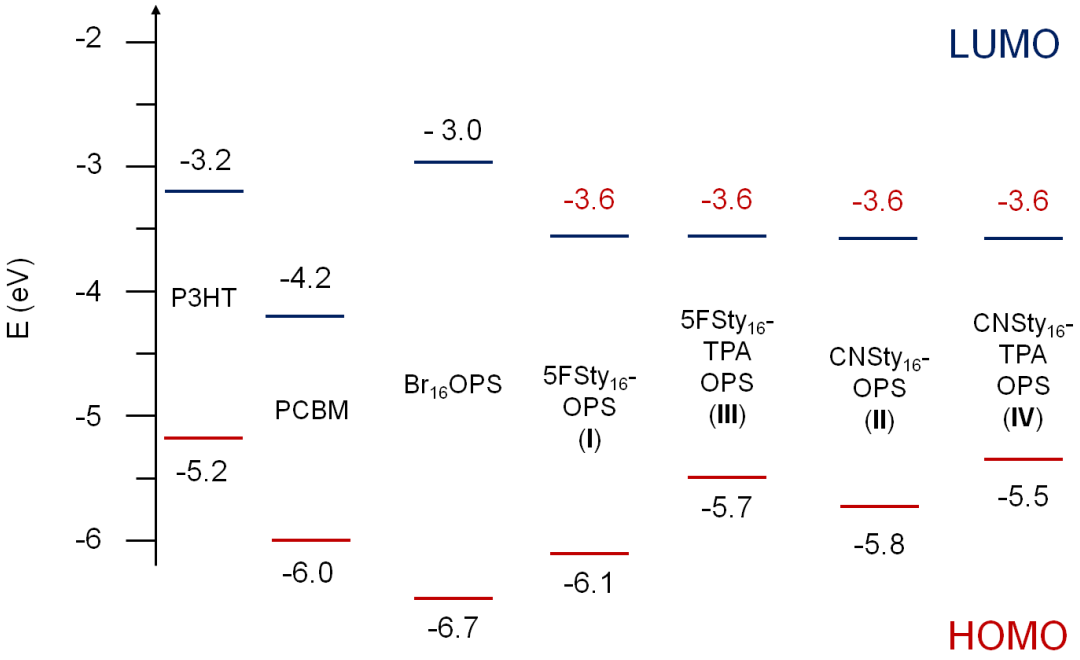

Figure 6.7. HOMO and LUMO energy levels of Br_{16}OPS and compounds **I** - **IV**.

Bulk heterojunction (BHJ) solar cells with the configuration ITO/PEIE/active layer/MoO_3/Ag were fabricated to investigate the photovoltaic properties of SQs (Figure **6.8**). The active layers were prepared using 50 w % of P3HT, electron donor, and other 50 w % of electron acceptor with different ratio of PCBM and compound **I**.

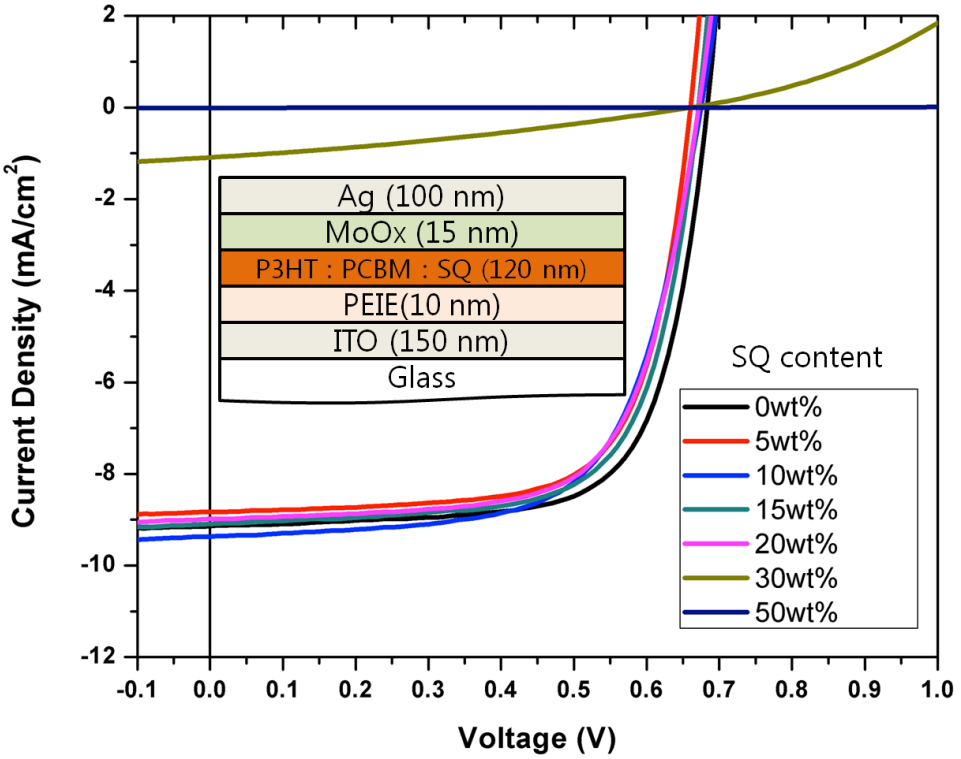

Figure 6.8. *I-V* curves of OPV devices fabricated by mixture of P3HT, PCBM, and compound **I** with the device configuration of glass/ITO/PEIE/active layer/MoO_3/Ag.

Table 6.3. PCE, J_{SC}, V_{OC}, and FF of OPV device prepared by mixture of P3HT, PCBM and compound **I** (SQ).

SQ contents (%)	PCE (%)	J_{SC} (mA/cm^2)	V_{OC} (V)	FF (%)
0	4.1	8.6	0.68	69.5
5	3.9	8.6	0.66	69.4
10	3.8	8.8	0.67	64.6
15	4.1	8.7	0.67	69.2
20	3.5	8.1	0.67	64.1
30	0.4	2.0	0.66	29.3
50	0.0007	0.004	0.60	26.3

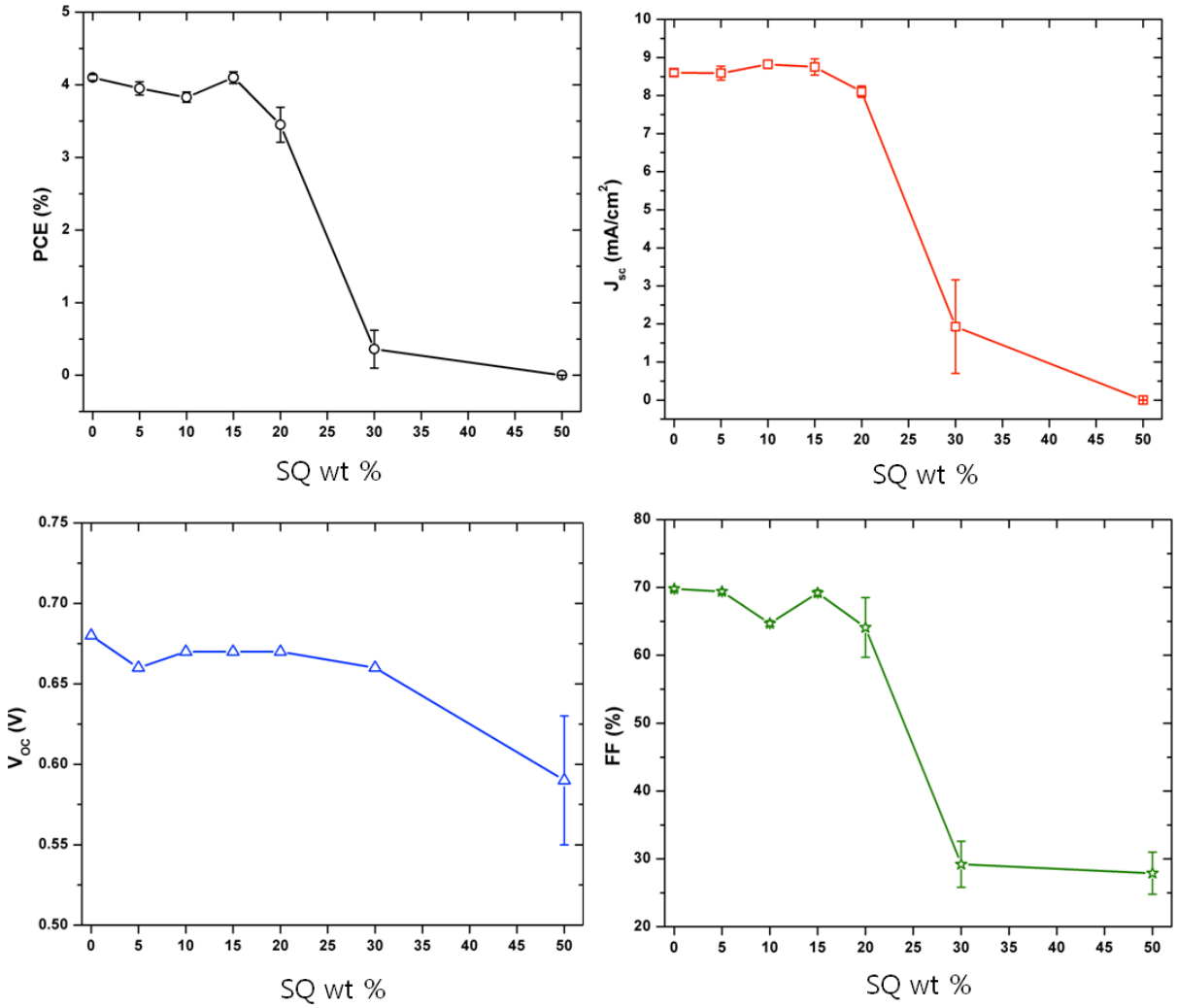

Figure 6.9. PCE, J_{SC}, V_{OC}, and FF of OPV devices depending on the compound **I** contents.

A reference cell made of mixture of P3HT and PCBM showed power conversion efficiency (PCE) of 4.1 ± 0.1 % (Table **6.3**). Compared with reference cell, the device fabricated with 1:1 mixture of P3HT and compound **I** (50 % SQ in Table **6.3**) showed poor power conversion efficiency (PCE) only 0.0007 ± 0.0005 %.

However, when compound **I** is mixed with PCBM, the PCE and other OPV parameters, such as short circuit current (J_{SC}), open circuit voltage (V_{OC}), and file factor (FF), retained similar values to reference cell until the contents of compound **I** is less than 20 % (Figure **6.9** and Table **6.3**). When the content of compound **I** is more than 20 %, the PCE and other OPV parameters dropped dramatically (Figure **6.9**). This result implies that there must be an

interaction between SQs and P3HT or PCBM, otherwise, the PCE would gradually decrease as the SQ content increases. Although further studies are necessary to comprehensively understand the influence of SQs on OPV performance, it is clear that the production cost of OPV cells could be reduced by replacement of PCBM by SQs.

6.3. Conclusions

We have described the synthesis, photophysical properties and photovoltaic performance of functionalized Br_{16}OPS derivatives prepared by Heck coupling reactions. It has been shown that this approach is useful to control LUMO energy of SQs to appropriate levels for electron acceptor in OPV devices fabricated with P3HT donors. The photophysical behaviors of triphenylamine (TPA) incorporated SQs indicate aggregation between polarized partial charge of electron donating groups (D, triphenylamine) and accepting groups (A, pentafluoro or cyano) due to the charge transfer (CT) process through the push-full structure.

The OPV device made from the blend of compound **I** with P3HT showed poor performance with power conversion efficiency (PCE) of 0.0007 %. However, when the PCBM acceptors are partially substituted with compound **I**, the PCE is maintained similar values of the P3HT/PCBM device (about 4 %) if the contents of compound **I** is less than 15 %. Although the influence of compound **I** in OPV device such as morphology and carrier transfer properties is unclear at present, this result implies that the SQs have interaction with P3HT or PCBM.

References Cited:

1. Yu, G.; Gao, J.; Hummelen, J. C.; Wudl, F.; Heeger, A. J.; "Polymer Photovoltaic Cells: Enhanced Efficiencies via a Network of Internal Donor-Acceptor Heterojunctions," *Science*, **1995**, *270*, 1789-1791.
2. Brabec, C. J.; Sariciftci, N. S.; Hummenlen, J. C.; "Plastic Solar Cells," *Adv. Funct. Mater*., **2001**, *11*, 15-26.
3. Li, G.; Shrotriya, V.; Huang, J. S.; Yao, Y.; Moriarty, T.; Emery, K.; Yang, Y.; "High-efficiency solution processable polymer photovoltaic cells by self-organization of polymer blends," *Nat. Mater*., **2005**, *4*, 864-868.

4. Ma, W.; Yang, C.; Gong, X.; Lee, K.; Heeger, A. J.; "Thermally Stable, Efficient Polymer Solar Cells with Nanoscale Control of the Interpenetrating Network Morphology," *Adv. Funct. Mater*., **2005**, *15*, 1617-1622.
5. Kim, Y.; Cook, S.; Tuladhar, S. M.; Choulis, S. A.; Nelson, J.; Durrant, J. R.; Bradley, D. D. C.; Giles, M.; MuCulloch, I.; Ha, C. S.; Ree, M.; "A strong regioregularity effect in self-organizing conjugated polymer films and high-efficiency polythiophene:fullerene solar cells," *Nat. Mater*., **2006**, *5*, 197-203.
6. Peet, J.; Kim, J. Y.; Coates, N. E.; Ma, W. L.; Moses, D.; Heeger, A. J.; Bazan, G. C.; "Efficiency enhancement in low-bandgap polymer solar cells by processing with alkane dithiols," *Nat. Mater*., **2007**, *6*, 497-500.
7. Scharber, M. C.; Muhlbacher, D.; Koppe, M.; Denk, P.; Waldauf, C.; Heeger, A. J.; Brabec, C. J.; "Design Rules for Donors in Bulk-Heterojunction Solar Cells—Towards 10 % Energy-Conversion Efficiency," *Adv. Mater*., **2006**, *18*, 789-794.
8. Bundgaard, D.; Krebs, F. C.; "Low band gap polymers for organic photovoltaics," *Sol. Energy Mater. Sol. Cells*, **2007**, *91*, 954-985.
9. Chirvase, D.; Parisi, J.; Hummelem, J. C.; Dyakonov, V.; "Influence of nanomorphology on the photovoltaic action of polymer–fullerene composites," *Nanotechnology*, **2004**, *15*, 1317-1323.
10. Zhao, X.; Zhan, X.; "Electron transporting semiconducting polymers in organic electronics," *Chem. Soc. Rev*., **2011**, *40*, 3728-3743.
11. Sonar, P.; Lim, J. P. F.; Chan, K. L.; "Organic non-fullerene acceptors for organic photovoltaics," *Energy Environ. Sci*., **2011**, *4*, 1558-1574.
12. Anthony, J. E.; "Small-Molecule, Nonfullerene Acceptors for Polymer Bulk Heterojunction Organic Photovoltaics," *Chem. Mater*., **2011**, *23*, 583-590.
13. Sulaiman, S.; Zhang, J.; Goodson, T.; Laine, R. M.; "Synthesis, characterization and photophysical properties of polyfunctional phenylsilsesquioxanes: $[o\text{-RPhSiO}_{1.5}]_8$, $[2,5\text{-R}_2\text{PhSiO}_{1.5}]_8$, and $[\text{R}_3\text{PhSiO}_{1.5}]_8$. Compounds with the highest number of functional units/unit volume," *J. Mater. Chem*., **2011**, *21*, 11177-11187.
14. Laine, R. M.; Sulaiman, S.; Brick, C.; Roll, M.; Tamaki, R.; Asuncion M. Z.; Neurock, M.; Filhol, J.-S.; Lee, C.-Y.; Zhang, J.; Goodson, T.; Ronchi, M.; Pizzotti, M.; Rand, S. C.; Li,

Y.; "Synthesis and Photophysical Properties of Stilbeneoctasilsesquioxanes. Emission Behavior Coupled with Theoretical Modeling Studies Suggest a 3-D Excited State Involving the Silica Core," *J. Am. Chem. Soc.*, **2010**, *132*, 3708-3722.

15. Roll, M.; Kampf, J. W.; Kim, Y.; Yi, E.; Laine, R. M.; "Nano Building Blocks via Iodination of $[PhSiO_{1.5}]_n$, Forming $[p\text{-}I\text{-}C_6H_4SiO_{1.5}]_n$ (n = 8, 10, 12), and a New Route to High-Surface-Area, Thermally Stable, Microporous Materials via Thermal Elimination of I_2," *J. Am. Chem. Soc.*, **2010**, *132*, 10171-10183.
16. Jung, J. H.; Furgal, J.; Goodson, T.; Mizumo, T.; Schwartz, M.; Chou, K.; Vonet, J.-F.; Laine, R. M.; "3-D Molecular Mixtures of Catalytically Functionalized $[vinylSiO_{1.5}]_{10}$/$[vinylSiO_{1.5}]_{12}$. Photophysical Characterization of Second Generation Derivatives," *Chem. Mater.*, **2012**, *24*, 1883-1895.
17. Sulaiman, S.; Bhaskar, A.; Zhang, J.; Guda, R.; Goodson, T.; Laine, R. M.; "Molecules with Perfect Cubic Symmetry as Nanobuilding Blocks for 3-D Assemblies. Elaboration of Octavinylsilsesquioxane. Unusual Luminescence Shifts May Indicate Extended Conjugation Involving the Silsesquioxane Core," *Chem. Mater.*, **2008**, *20*, 5563-5573.
18. Xiao, S.; Nguyen, M.; Gong, X.; Cao, Y.; Wu, H. B.; Moses, D.; Heeger, A. J.; "Stabilization of Semiconducting Polymers with Silsesquioxane," *Adv. Funct. Mater.*, **2003**, *13*, 25-29.
19. Chan, K. L.; Sonar, P.; Sellinger, A.; "Cubic silsesquioxanes for use in solution processable organic light emitting diodes (OLED)," *J. Mater., Chem.*, **2009**, *19*, 9103-9120.
20. Lo, M. Y.; Zhen, C.; Lauters, M.; Jabbour, G. E.; Sellinger, A.; "Organic−Inorganic Hybrids Based on Pyrene Functionalized Octavinylsilsesquioxane Cores for Application in OLEDs," *J. Am. Chem. Soc.*, **2007**, *129*, 5808-5809.
21. Senkovskyy, V.; Tkachov, R.; Beryozkina, T.; Komber, H.; Oertel, U.; Horecha, M.; Bocharova, V.; Stamm, M.; Gevorgyan, S. A.; Krebs, F. C.; Kiriy, A.; ""Hairy" Poly(3-hexylthiophene) Particles Prepared via Surface-Initiated Kumada Catalyst-Transfer Polycondensation," *J. Am. Chem. Soc.*, **2009**, *131*, 16445-16453.
22. Rathnayake, H.; Binion, J.; Miekee, A.; Scardino, D. J.; Hammer, N. I.; "Perylenediimide functionalized bridged-siloxane nanoparticles for bulk heterojunction organic photovoltaics," *Nanoscale*, **2012**, *4*, 4631-4640.

23. Roll, M. F.; Mathur, P.; Takahashi, K.; kampf, J. W.; Laine, R. M.; "$[PhSiO_{1.5}]_8$ promotes self-bromination to produce $[o\text{-}BrPhSiO_{1.5}]_8$: further bromination gives crystalline $[2,5\text{-}Br_2PhSiO_{1.5}]_8$ with a density of 2.32 g cm^{-3} and a calculated refractive index of 1.7 or the tetraicosa bromo compound $[Br_3PhSiO_{1.5}]_8$," *J. Mater., Chem.*, **2011**, *21*, 11167-11176.
24. Jenekhe, S. A.; Osaheni, J. A.; "Excimers and Exciplexes of Conjugated Polymers," *Science*, **1994**, *265*, 765-768.
25. Luo, M.-H.; Chen, K.-Y.; "Asymmetric perylene bisimide dyes with strong solvatofluorism," *Dyes and Pigments*, **2013**, *99*, 456-464.
26. Kato, S.-I.' Kivala, M.; Schweizer, W. B.; Boudon, C.; Gisselbrecht, J.-P.; Diederich. F.; "Origin of Intense Intramolecular Charge-Transfer Interactions in Nonplanar Push-Pull Chromophores," *Chem. Eur. J*. **2009**, *15*, 8687 – 8691.
27. Seo, J.; Kim, S.; Park, S. Y.; "Strong Solvatochromic Fluorescence from the Intramolecular Charge-Transfer State Created by Excited-State Intramolecular Proton Transfer," *J. Am. Chem. Soc*., **2004**, *126*, 11154–11155.
28. Kim, K. H.; Kang, H.; Nam, S. Y.; Jung, J.; Kim, P. S.; Cho, C. H.; Lee, C.; Yoon, S. C.; Kim, B. J.; "Facile Synthesis of *o*-Xylenyl Fullerene Multiadducts for High Open Circuit Voltage and Efficient Polymer Solar Cells," *Chem. Mater*., **2011**, *23*, 5090-5095.
29. He, Y.; Chen, H.-Y.; Hou, J.; Li, Y.; "Indene−C_{60} Bisadduct: A New Acceptor for High-Performance Polymer Solar Cells," *J. Am. Chem. Soc*., **2010**, *132*, 1377-1382.
30. Lenes, M.; wetzelaer, G-J. A. H.; Kooistra, F. B.; Veenstra, S. C.; Hummelen, J. C.; Blom, P. W. M.; "Fullerene Bisadducts for Enhanced Open-Circuit Voltages and Efficiencies in Polymer Solar Cells," *Adv. Mater*., **2008**, *20*, 2116-2119.

Chapter 7

Synthesis and characterization of hydroxyl terminated silsesquioxanes and their use for cross-linked polyesters

Published in Applied Organometallic Chemistry, **2013**, *27*, pp. 666-672

Abstract

There is continuing interest in the synthesis of polyhydroxy terminated molecular species for diverse applications ranging from photolithographic materials to intermediates in the synthesis of porous, cross-linked polymers as media for molecular separations, drug delivery etc. We describe here the use of $[vinylSiO_{1.5}]_8$ and $[vinylSiO_{1.5}]_{10/12}$ mixtures to synthesize first and second generation acetoxy phenyl compounds via metathesis with *p*-acetoxystyrene (Generation 1, GEN1) or metathesis with *p*-bromostyrene followed by Heck coupling with *p*-acetoxystyrene (Generation 2, GEN2). The resulting acetoxy compounds were then hydrolyzed to produce octa, deca and dodeca-hydroxy GEN1 and GEN2 compounds. These compounds were purified and then reacted with adipic acid chloride to form the first examples of highly cross-linked polyesters based on silsesquioxanes. The coupling products, their hydrolyzed products and the cross-linked polymers were characterized using a variety of spectroscopic methods. In general the observed specific surface areas were less than 5 m^2/g. However, the T_8 GEN1 derivative gave a surface area of 25 m^2/g and was the only crosslinked polymer with a TGA ceramic yield that matched theory for "perfect" cross-linking. This cross-linked polyester has the shortest organic linker between cages and despite the highly flexible C_6 linker provides continuing evidence that it is possible to use the cubic symmetry in these materials to build well ordered 3-D nanocomposite structures.

7.1. Introduction

Polyhedral silsesquioxanes (SQs), with the formulae $[RSiO_{1.5}]_{8,10,12}$, are organic-inorganic hybrid materials that consist of nanometer sized silica cages surrounded by organic functional groups. While the inorganic core provides mechanical stiffness and thermal stability, the organic pendant groups provide solubility in organic solvents and the opportunity for chemical modification. In particular the T_8 SQs have cubic symmetry offering the potential to be used as three dimensional nano-building blocks.[1-14] Such 3-D building blocks may offer nanocomposites and/or nanoporous materials with a range of applications including access to the low dielectric constant interlayer dielectrics for semiconductor interconnects, encapsulants for drug delivery, porous media for hydrogen storage, separation of pollutants or fine chemicals, and as catalyst substrates.[15-24]

The work presented here details our efforts to develop acetoxy and hydroxy terminated nanobuilding blocks based on different vinyl SQs, T_8 and mixtures of T_{10} and T_{12}. Vinyl SQs are easily modified by metathesis and Heck coupling reactions.[25-31] First generation (GEN1) acetoxySQs were prepared by metathesis of the vinyl SQs and *p*-acetoxystyrene, as illustrated by reaction (1) and second generation (GEN2) acetoxySQs were prepared by Heck coupling of *p*-acetoxystyrene with *p*-BrstyrenylSQs as shown in reaction (2). These *p*-acetoxy GEN1 and GEN2 SQs were converted to the *p*-hydroxySQs by mild hydrolysis, reaction (3).

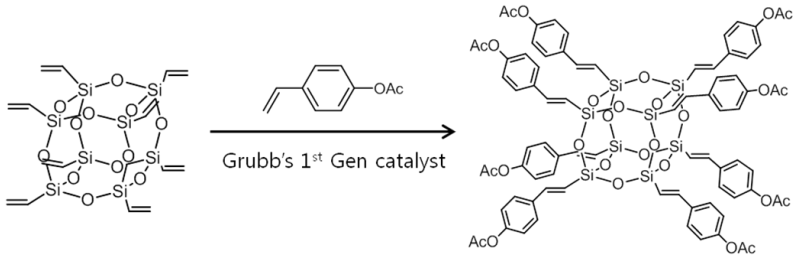

(1)

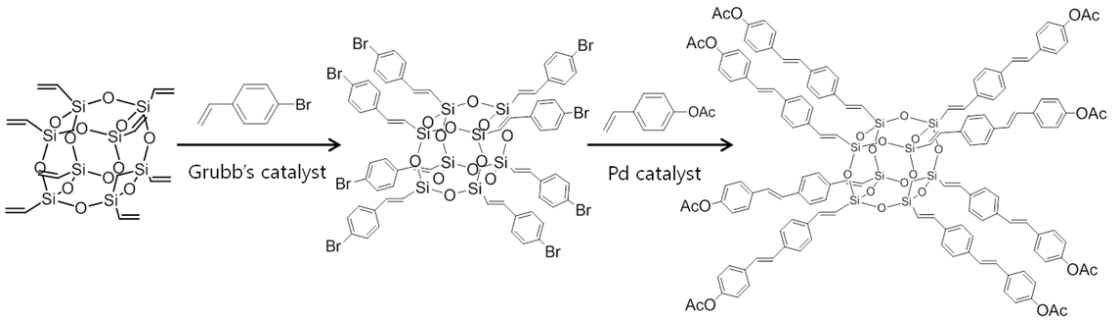

(2)

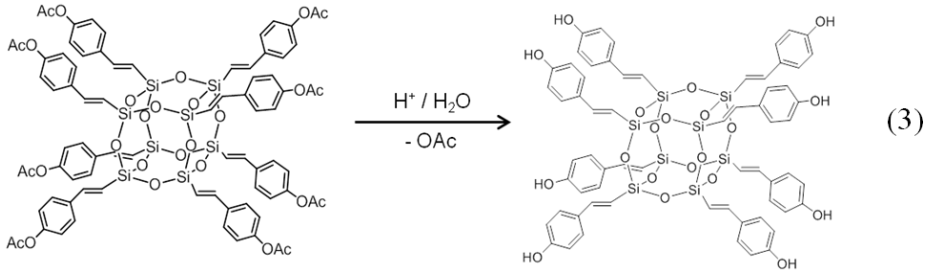

(3)

The *p*-hydroxy GEN1 and GEN2 SQs were reacted with stoichiometric amounts of adipoyl chloride to prepare cross-linked polymers (Scheme **1**) with some limited porosity.

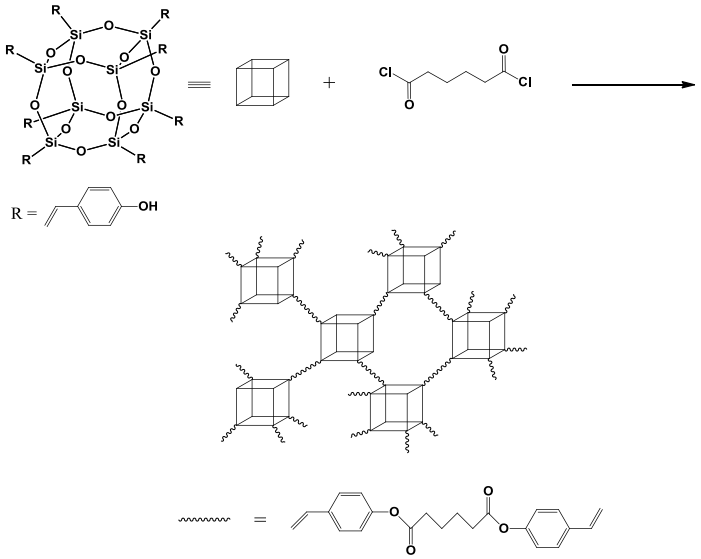

Scheme 7.1. General scheme for reaction of GEN1 Hydroxy T_8 and adipoyl chloride.

The goal of the current work was to develop simple routes to high densities of phenolic groups in small 3-D volumes with the objective of providing simple routes to a wide variety of 3-D polyphenolics for applications as noted above and simply as potential crosslinking agents for polyphenolic resins.

7.2. Results and Discussion

In the following sections, we discuss the synthesis and characterization of various *p*-acetoxy SQs (GEN1 T_8, GEN1 $T_{10/12}$, GEN2 T_8, GEN2 $T_{10/12}$). We then discuss their hydrolysis

to form the corresponding hydroxy SQs and thereafter a first example of their polymerization by reaction with adipoyl chloride to form 3-D cross-linked polyesters.

7.2.1. Synthesis of *p*-acetoxy Silsesquioxanes

Reaction (1) or (2) were used to synthesize four different *p*-acetoxySQs from the vinyl T_8 SQ and $T_{10/12}$ SQs through metathesis and Heck coupling reactions. Vinyl $T_{10/12}$ SQs were prepared by F^- catalyzed rearrangement of polyvinylsilsesquioxane (PVS), $[vinylSiO_{1.5}]_x$, as we recently reported.[30] Vinyl $T_{10/12}$ SQs are a mixture of isomers with the dominant ionizable species being the deca and dodecavinyl compounds. MALDI reveals the presence of a small amount of vinyl T_{14} as well (Figure **7.1**). Because these compounds have similar chemical and physical properties, we have not found a simple method of separating T_{10} from T_{12}. Therefore, it is important to note that vinyl $T_{10/12}$ should be considered to be relatively well defined oligomers rather than distinct molecular species.

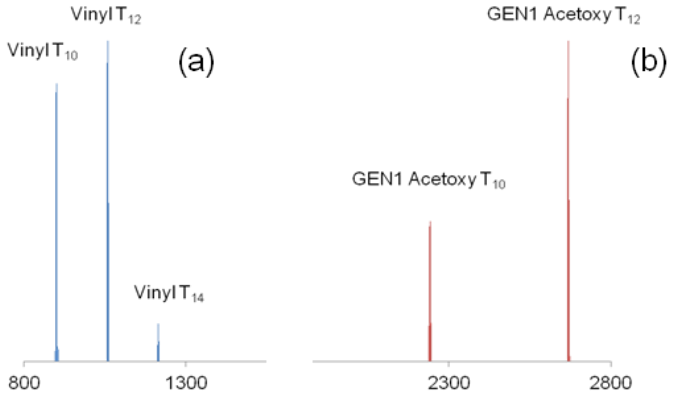

Figure 7.1. MALDI-ToF spectrum of (a) vinyl $T_{10/12}$ and (b) GEN1 *p*-acetoxy $T_{10/12}$.

Table **7.1** summarizes the characterization data for the *p*-acetoxySQs. In general, the GPC, MALDI, TGA data are all in agreement with those expected for the isolated compounds. The narrow molecular weight distribution of these SQ compounds in the GPC indicates that they retain their cage structures. The MALDI-ToF spectrum of GEN1 $T_{10/12}$ *p*-acetoxySQ indicates that this compound is fully substituted. The ^1H NMR spectra of these compounds confirm their complete conversion from their parent material as well.

Table 7.1. Characterization data for *p*-acetoxySQs.

	GPC			m/z (Ag^+ adduct)		TGA		
	Mn	Mw	PDI	Calcd.	MALDI	CY	Theo. CY	$T_{d5\%}$(°C)
GEN1 T_8	2070	2150	1.04	1813.9	1813.5	27.9 %	28.2 %	345
GEN1 $T_{10/12}$	2500	2560	1.02	T_{10}: 2240.4 T_{12}: 2666.9	2240.4 2667.5	28.4 %	28.2 %	345
GEN2 T_8	4080	4270	1.04	2630.9	2629.6	19.2 %	19.1 %	335
GEN2 $T_{10/12}$	4130	4270	1.03	T_{10}: 3261.7 T_{12}: 3892.5	3261.0 3892.3	19.5 %	19.1 %	305

7.2.2. Synthesis of *p*-hydroxy Silsesquioxanes

The *p*-acetoxySQs were gently hydrolyzed with HCl to give the corresponding *p*-hydroxySQs. These reactions were monitored by FTIR until the characteristic νC=O (1760 cm^{-1}) of *p*-acetoxySQs disappeared (Figure **7.2**). Since the synthetic procedures and subsequent characterization are analogous for all *p*-acetoxy SQs, only the hydrolysis of the GEN1 T_8 *p*-acetoxySQ is discussed in further detail.

The FTIR of GEN1 T_8 p-acetoxySQ shows characteristic νO-H (3300 cm^{-1}) and νSi-O (1112 cm^{-1}) bands (Figure **7.2**). FTIR spectra for the corresponding compounds are given in Figure **A3.2**. As expected all the spectra are very similar given the essentially identical chemical and structural compositions.

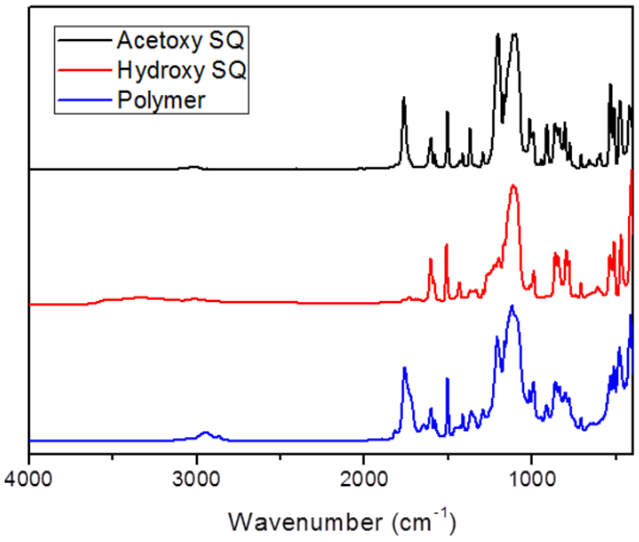

Figure 7.2. FTIR of GEN1 T_8 *p*-acetoxySQ, *p*-hydroxySQ and cross-linked polyester.

MALDI-ToF spectra of the product does not show any unreacted *p*-acetoxy T_8 species (Figure **7.1b**) and no methyl peaks (δ 2.3-2.4 ppm) are seen in the ^{1}H NMR spectrum, indicating that all of the acetoxy groups hydrolyze off (Figure **7.3**). The characterization data for the *p*-hydroxySQs are given in Table **7.2**. Figures **A3.2** to **A3.4** provides similar characterization data for all the other analogs. Again no significant differences are seen or expected.

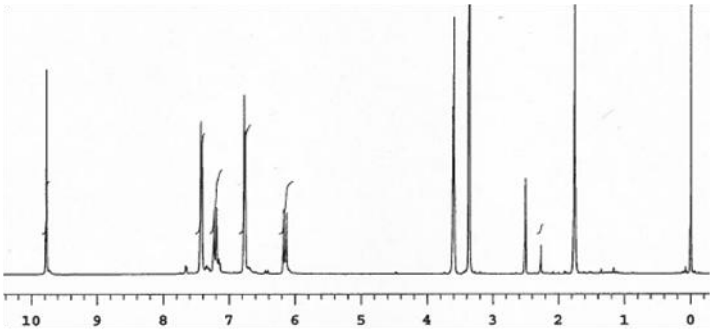

Figure 7.3. ^{1}H NMR (DMSO) of GEN1 T_8 *p*-Hydroxy SQ.

In accord with the NMR, GPC and MALDI-ToF data, the found and calculated ceramic yields of all the compounds are within the error limits of analysis identical again supporting the fact that these compounds are compositionally and structurally identical on a per silicon basis.

Table 7.2. Characterization data for the various *p*-hydroxy SQs.

	GPC			m/z (Ag^+ adduct)		TGA		
	Mn	Mw	PDI	Calcd.	MALDI	CY	Theo. CY	$T_{d5\%}$(°C)
GEN1 T_8	2000	2030	1.01	1477.6	1477.5	34.6 %	35.1 %	235
GEN1 $T_{10/12}$	2240	2300	1.03	T_{10}: 1820.1 T_{12}: 2162.5	1819.4 2162.8	34.4 %	35.1 %	280
GEN2 T_8	3410	3560	1.04	2294.6	2293.1	22.2 %	22.0 %	360
GEN2 $T_{10/12}$	3490	3590	1.03	T_{10}: 2841.3 T_{12}: 3388.0	3261.0 3892.3	22.3 %	22.0 %	345

7.2.3. Polymerization of *p*-hydroxy silsesquioxanes and adipoyl chloride

The *p*-hydroxySQs were reacted with adipoyl chloride in an effort to form cross-linked nanoporous polyesters per Scheme **7.1**. The FTIR spectrum of synthesized polyester showed

characteristic νC=O (1760 cm^{-1}), νC-O (1210 cm^{-1}) and aliphatic νC-H (2950 cm^{-1}) (Figure **7.3**). Figure **7.4** provides the TGA traces for GEN1 T_8 *p*-acetoxySQ, *p*-hydroxySQ and cross-linked polyester. Figure **A3.5**, **A3.6**, **A3.7** provide analogous TGAs for the related compounds. The lower ceramic yields for the polyester compared with *p*-hydroxySQ indicates that adipoyl groups were incorporated into the polymer.

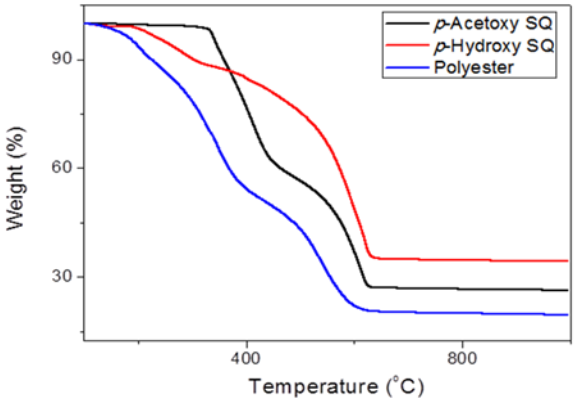

Figure 7.4. TGA of GEN1 T_8 *p*-acetoxySQ, *p*-hydroxySQ and cross-linked polyester (air, 10 °C/min).

Although the exceptional flexibility of the adipate cross-linker would suggest that we should not observe any degree of porosity, Brunauer-Emmett-Teller (BET) specific surface areas (SSAs) were measured. Only one polymeric compound, the GEN1 T_8 polymer, had a surface area of 25 m^2/g (Table **7.3**). Given that this system has the shortest spacer between cages and the highest symmetry, one might infer that there is sufficient restriction of chain motion that ingress and egress of N_2 during the measurements is possible.

One might therefore extend this idea to suggest that while some pores probably exist in the cross-linked systems, they are not easily accessible for N_2 absorption and desorption perhaps because of highly torturous paths. However, there is a simpler explanation. Except the GEN1 T_8 polymer, the ceramic yields of other polymers are lower than the theoretical value based on 100 % conversion to the cross-linked form. This means that excess of adipoyl chloride reacts with *p*-hydroxySQs leading to dangling, unreacted carboxyl groups after water workup. Thus, the cross-link densities are much lower and while there may be extensive porosity, the resulting mesopores are too large to be "seen" by BET.

We could also expect the $T_{10/12}$ SQ polyesters to show lower SSAs than that of GEN1 T_8 SQ. Because the T_{10} and T_{12} cages are larger than T_8 cage, they offer smaller angles between C6 linkers perhaps leading to stronger interactions that reduce pore size. To produce nanoporous materials having high surface areas and to investigate the relationship between the porosity and chemical structure of nano-building blocks, it is necessary to control the reaction conditions to make highly cross-linked nanocomposites with emphasis on using more rigid cross-linkers. Furthermore, it appears likely that high symmetry as found with the T_8 systems will provide better access to nanoporous materials with better controlled cross-link densities and therefore better control of pore size distributions.

Table 7.3. Characterization of cross-linked polyesters.

	TGA			BET SSAs
	CY	Theo. CY	$T_{d5\%}$ (°C)	
GEN1 T_8	26.7 %	26.6 %	260	24 m^2/g
GEN1 $T_{10/12}$	20.7 %	26.6 %	210	5 m^2/g
GEN2 T_8	14.8 %	18.3 %	190	1 m^2/g
GEN2 $T_{10/12}$	15.3 %	18.3 %	200	4 m^2/g

7.3. Conclusions

We have demonstrated the synthesis of a variety of *p*-acetoxy and *p*-hydroxySQs based on T_8 and $T_{10/12}$ vinylSQs as a 3-D nanobuilding blocks. We have begun to explore the application of these *p*-hydroxySQs as precursors to nanoporous polymeric materials by studying their reaction with adipoyl chloride. The crosslinked polyester prepared from GEN1 T_8 SQ exhibited up to 25 m^2/g of BET surface area in spite of the flexible C_6 linker. This comes as a result of the very high symmetry of the SQ coupled with the shortest linker between cages. Moreover, the TGA data suggest that all corners of the cage are fully reacted. The results reported here are in keeping with other recent studies comparing T_8 with T_{10} and T_{12} nanoporous structures.[21] In the near future we anticipate exploring reactions with rigid diacid chlorides and also working with the T_8 amine analogs.[30,31]

References Cited:

1. Voronkov, M.G.; Lavrent'yev, V.I.; "Polyhedral Oligosilsesquioxanes and Their Homo Derivatives," *Top. Curr. Chem*., **1982**, *102*, 199-236.
2. Baney, R.H.; Itoh, M.; Sakakibara, A.; Suzuki, T.; "Silsesquioxanes," *Chem. Rev*., **1995**, *95*, 1409-1430.
3. Loy, D.A.; Shea, K.J.; "Bridged Polysilsesquioxanes. Highly Porous Hybrid Organic-Inorganic Materials," *Chem. Rev*., **1995**, *95*, 1431-1442.
4. Calzaferri, G.; "Silsesquioxanes," in Tailor-made Silicon-Oxygen Compounds, from molecules to materials, Corriu, R. and Jutzi, P. Ed., Friedr. Vieweg & Sohn mbH, Braunshweig/Weisbaden, Germany, **1996**, pp. 149-169.
5. Lichtenhan, J.; "Silsesquioxane-based Polymers," in Polymeric Materials Encyc., Salmon, J.C. Ed., Vol. 10, CRC Press, N.Y., **1996**, pp. 7768-7777.
6. Provatas, A.; Matisons, J.G.; "Synthesis and applications of silsesquioxanes," *Trends Polym. Sci*., **1997**, *5*, 327-333.
7. Li, G.; Wang, L.; Ni, H.; Pittman, C.U.; "Polyhedral Oligomeric Silsesquioxane (POSS) Polymers and Copolymers: A Review," *J. Inorg. Organomet. Polym.*, **2001**, *11*, 123-151.
8. Duchateau, R.; "Incompletely Condensed Silsesquioxanes: Versatile Tools in Developing Silica-Supported Olefin Polymerization Catalysts," *Chem. Rev.*, **2002,** *102*, 3525-3542.
9. Abe, Y.; Gunji, T.; "Oligo- and polysiloxanes" *Prog. Polym. Sci.*, **2004**, *29*, 149-182.
10. Phillips, S H.; Haddad, T. S.; Tomczak, S. J.; "Developments in nanoscience: polyhedral oligomeric silsesquioxane (POSS)-polymers," *Curr. Opin. Solid State Mater. Sci*., **2004**, *8*, 21-29.
11. Laine, R. M.; "Nanobuilding blocks based on the $[OSiO_{1.5}]_x$ (x = 6, 8, 10) octasilsesquioxanes," *J. Mater. Chem*., **2005**, *15*, 3725-3744.
12. Lickiss, P. D.; Rataboul, F.; "Fully Condensed Polyhedral Oligosilsesquioxanes (POSS): From Synthesis to Application," *Adv. Organomet. Chem*., **2008**, *57*, 1-116.
13. Cordes, D. B.; Lickiss, P. D.; Franck, R.; "Recent Developments in the Chemistry of Cubic Polyhedral Oligosilsesquioxanes," *Chem. Rev*., **2010**, *10*, 2081-2173.
14. Laine, R. M.; Roll, M. F.; "Polyhedral Phenylsilsesquioxanes," *Macromolecules*, **2011**, *44*, 1073-1109.

15. Laine, R. M.; Choi, J.; Lee, I.; "Organic–Inorganic Nanocomposites with Completely Defined Interfacial Interactions," *Adv. Mater*., **2001**, *13*, 800.
16. Choi, J.; Kim, S. G.; Laine, R. M.; "Organic/Inorganic Hybrid Epoxy Nanocomposites from Aminophenylsilsesquioxanes," *Macromolecules*, **2004**, *37*, 99.
17. Joshi, M.; Butola, B. S.; "Polymeric Nanocomposites—Polyhedral Oligomeric Silsesquioxanes (POSS) as Hybrid Nanofiller," *J. Macromol. Sci. Polym. Rev*., **2004**, *44*, 389-410.
18. Kim, Y.; Koh, K.; Roll, M. F.; Laine, R. M.; Matzger, A. J.; "Porous Networks Assembled from Octaphenylsilsesquioxane Building Blocks," *Macromolecules*, **2010**, *43*, 6995-7000.
19. Chaikittisilp, W.; Sugawara, A.; Shimojima, A.; Okubo, T.; "Hybrid Porous Materials with High Surface Area Derived from Bromophenylethenyl-Functionalized Cubic Siloxane-Based Building Units," *Chem. Eur. J*., **2010**, *16*, 6006-6014.
20. Chaikittisilp, W.; Kubo, M.; Moteki, T.; Sugawara, A.; Shimojima, A.; Okubo, T.; "Porous Siloxane–Organic Hybrid with Ultrahigh Surface Area through Simultaneous Polymerization–Destruction of Functionalized Cubic Siloxane Cages," *J. Am. Chem. Soc*., **2011**, *133*, 13832-13835.
21. Roll, M. F.; Wampf, J. W.; Kim, Y.; Yi, E.; Laine, R. M.; "Nano Building Blocks via Iodination of $[PhSiO_{1.5}]_n$, Forming $[p\text{-I-}C_6H_4SiO_{1.5}]_n$ (n = 8, 10, 12), and a New Route to High-Surface-Area, Thermally Stable, Microporous Materials via Thermal Elimination of I_2," *J. Am. Chem. Soc*., **2010**, *132*, 10171-10183.
22. Su, R. Q.; Muller, T. E.; Prochazka, J.; Lercher, J. A.; "A New Type of Low-$\varkappa$ Dielectric Films Based on Polysilsesquioxanes," *Adv. Mater*., **2002**, *14*, 1369-1373.
23. Thomas, A.; "Functional Materials: From Hard to Soft Porous Frameworks," *Angew. Chem. Int. Ed*., **2010**, *49*, 8328-8344.
24. Hoffmann, F.; Cornelius, M.; Morell, J.; Frobe, M.; "Silica-Based Mesoporous Organic–Inorganic Hybrid Materials," *Angew. Chem. Int. Ed*., **2006**, *45*, 3216-3251.
25. Marciniec, B.; Pietraszuk, C.; "Synthesis of unsaturated organosilicon compounds via alkene metathesis and metathesis polymerization," *Curr. Org. Chem*., **2003**, *7*, 691-735.

26. Itami, Y.; Barciniec, B.; Kubicki, M.; "Functionalization of octavinylsilsesquioxane by ruthenium-catalyzed silylative coupling versus cross-metathesis," *Chem. Eur. J*., **2004**, *10*, 1239-1248.
27. Feher, F. J.; Soulivong, D.; Eklund, A. G.; Wyndham, K. D.; "Cross-metathesis of alkenes with vinyl-substituted silsesquioxanes and spherosilicates: A new method for synthesizing highly-functionalized Si/O frameworks," *Chem. Commun*., **1997**, 1185-1186.
28. Sellinger, A.; Tamaki, R.; Laine, R. M.; Ueno, K.; Tanabe, H.; Williams, E.; Jabbour, G. E.; "Heck coupling of haloaromatics with octavinylsilsesquioxane: solution processable nanocomposites for application in electroluminescent devices," *Chem. Commun*, **2005**, 3700-3702.
29. Lo, M. Y.; Zhen, C.; Lauters, M.; Jabbour, G. E.; Sellinger, A.; "Organic−Inorganic Hybrids Based on Pyrene Functionalized Octavinylsilsesquioxane Cores for Application in OLEDs," *J. Am. Chem. Soc*., **2007**, *129*, 5808-5809.
30. Sulaiman, S.; Bhaskar, A.; Zhang, J.; Guda, R.; Goodson III, T.; Laine, R. M.; "Molecules with perfect cubic symmetry as nanobuilding blocks for 3-D assemblies. Elaboration of octavinylsilsesquioxane. Unusual luminescence shifts may indicate extended conjugation involving the silsesquioxane core," *Chem. Mater*., **2008**, *20*, 5563-5573.
31. Jung, J. H.; Furgal, J. C.; Goodson III, T.; Mizumo, T.; Schwartz, M.; Chou, K.; Vonet, J.; Laine, R. M.; "3-D Molecular Mixtures of Catalytically Functionalized $[vinylSiO_{1.5}]_{10}/[vinylSiO_{1.5}]_{12}$. Photophysical Characterization of Second Generation Derivatives," *Chem. Mater*., **2012**, *24*, 1883-1895.
32. Harrison, P. G.; Hall, C.; "Preparation and characterization of octasilsesquioxane cage monomers," *Main Group Met. Chem*., **1997**, *20*, 515-529.

Chapter 8

Future work

This dissertation has described synthetic routes to organic/inorganic hybrid beads on a chain (BoC) polymers with SQ molecules in the polymer backbone and functionalization of SQs to offer potential for optoelectronic devices and microporous materials. In Chapter **3**, we discussed synthetic routes to di- or triaminophenyl SQs via fluoride ion catalyzed rearrangement reaction of octaphenylSQs (OPS) and octaaminophenylSQs (OAPS), and their polymerization with diglycidyl ether of bisphenol A (DGEBA) to prepare BoC polymers. Chapter **4** detailed our work on synthesis of conjugated BoC polymers from *p*-octaiodophenylsilsesquioxane (I_8OPS) via Heck and Sonogashira coupling. These polymers, in particular DEB polymers, show unique photophysical behavior supporting electronic communication along the polymer chains and through the cages via the conjugated linkers.

Chapter **5** described the functionalization of deca- and dodecavinylsilsesquioxane to produce second generation compounds via cross-metathesis, and Heck coupling. The novel photophysical properties of these SQs indicate unique 3-D conjugation between the organic tethers and T_{10} and T_{12} SQ molecules. Chapter **6** discussed the synthesis, photophysical properties and photovoltaic performance of functionalized octa(2,5-dibromophenyl)SQ (Br_{16}OPS) derivatives prepared by Heck coupling reactions. Chapter **7** gives a discussion of the synthesis of hydroxyphenyl-terminated SQs and initial studies on their use to prepare microporous, crosslinked polyesters with 25 m^2/g of BET surface area.

We have demonstrated unique photophysical properties in conjugated SQs to support the idea that electron delocalization involving SQ core and conjugated organic tethers can extend to T_{10} and T_{12} SQs, even their BoC polymers. Moreover, we have shown that the HOMO and LUMO energies of conjugated SQs can be adjusted by introduction of electron donating or

withdrawing groups. These properties offer potential for new organic/inorganic hybrid semiconducting materials with tunable optical and electronic properties.

In addition, we have demonstrated three different synthetic routes to BoC polymers. (1) direct polymerization of octafunctional SQs with difunctional monomers (polymer **I** in Chapter **4**), (2) preparation of di- or trifunctional SQs via fluoride ion rearrangement reaction of two different SQs, and polymerization of them with another difunctional monomers (Chapter **3**), (3) synthesis of difunctional SQs through partial modification of octafunctional SQs (monomers **A-C** in Chapter **4**), and polymerization of them (polymer **V - XII** in Chapter **4**).

We found another synthetic method to prepare BoC polymers recently via fluoride rearrangement between SQ molecules and bis(triethoxy)silanes (Scheme **8.1**).[1] In this reaction, bis(triethoxy)silanes act as linker between SQs in BoC polymers. During the fluoride ion rearrangement reaction, both silane groups are incorporated into two different SQs connecting each forming BoC polymers. When the mole ratio of SQ molecules and bis(triethoxy)silane are appropriately controlled, high molecular weight BoC polymers can result.

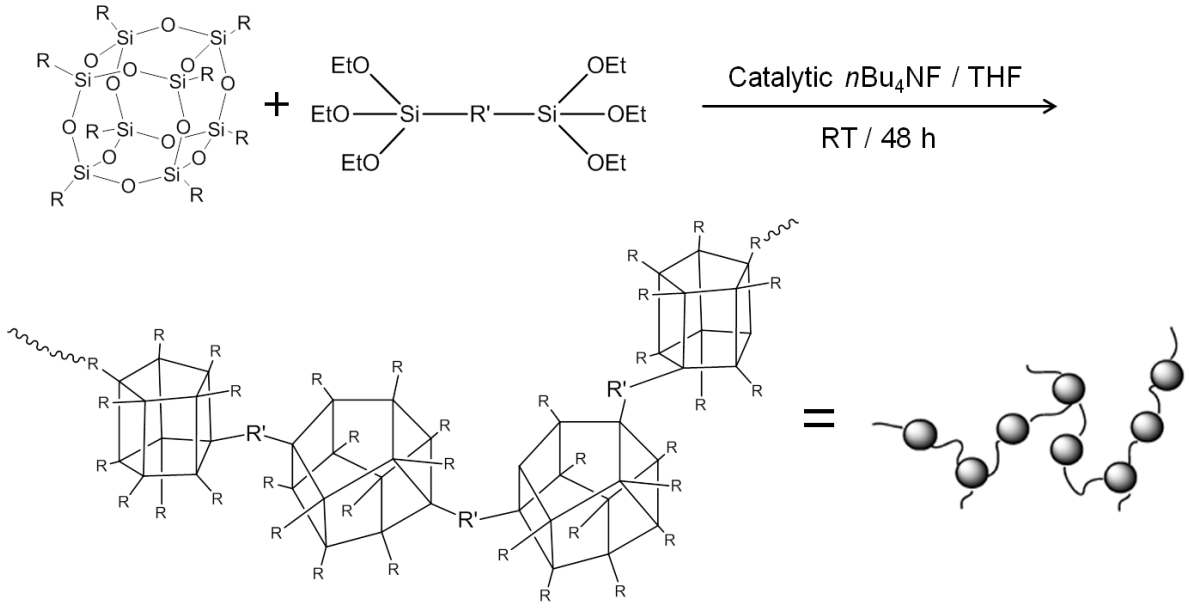

Scheme 8.1. Synthesis of BoC polymers via F^- rearrangement reaction.[1]

Compared with other synthetic routes to BoC polymers, this reaction has a variety of advantages such as it is not necessary to separate difunctional SQs and there is no limit to the

functionality of the SQ molecules' R groups because the organic groups of SQs are not involved in the polymerization reaction. These polymerization methods offer potential for functional hybrid polymers such as optically active polymers and polymeric ionic liquids as discussed below.

Recently, our group has explored synthetic routes to optically active SQ molecules through thiol-ene reaction of vinylSQs and L-cysteine (Scheme **8.2**). These SQs could be polymerized to prepare new hybrid optically active polymers. One of the most important applications of optically active polymers is the chiral separation of racemic compounds by high performance liquid chromatography (HPLC) using the polymers as chiral stationary phases.[2,3]

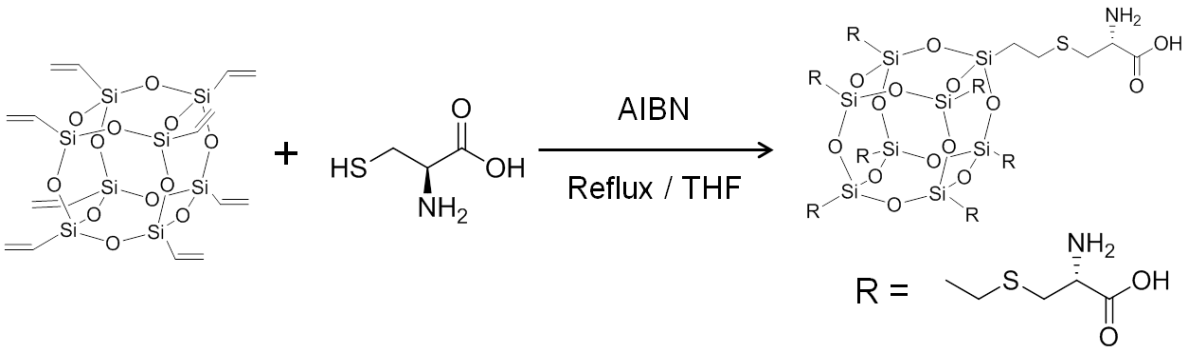

Scheme 8.2. Synthesis of optically active SQs.

Another interesting area for functional hybrid SQ polymers could be polymeric ionic liquids. Ionic liquids (ILs) are nonvolatile salts with melting points below 100 ^{o}C which present good chemical and electrochemical stability, low flammability, and high ionic conductivity.[4-6] Most studies related to ILs are associated with their application in green chemistry as substitutes for volatile organic solvents,[7] however, ILs are being explored for a wide variety of applications including catalysis,[8] porous materials,[9] separation and absorption,[10] and energy harvesting and storage.[11]

Polymeric ionic liquids (PILs) refer to polyelectrolytes having ionic liquid species in each monomer repeating units, thus, PILs present the unique properties of ILs together with the intrinsic polymer properties (Figure **8.1**).[4,5] In particular, due to their high ionic conductivity and wide electrochemical potential window, PILs have been employed as electrolytes for energy storage devices, such as capacitors, fuel cells, and dye sensitized solar cells.[12-14]

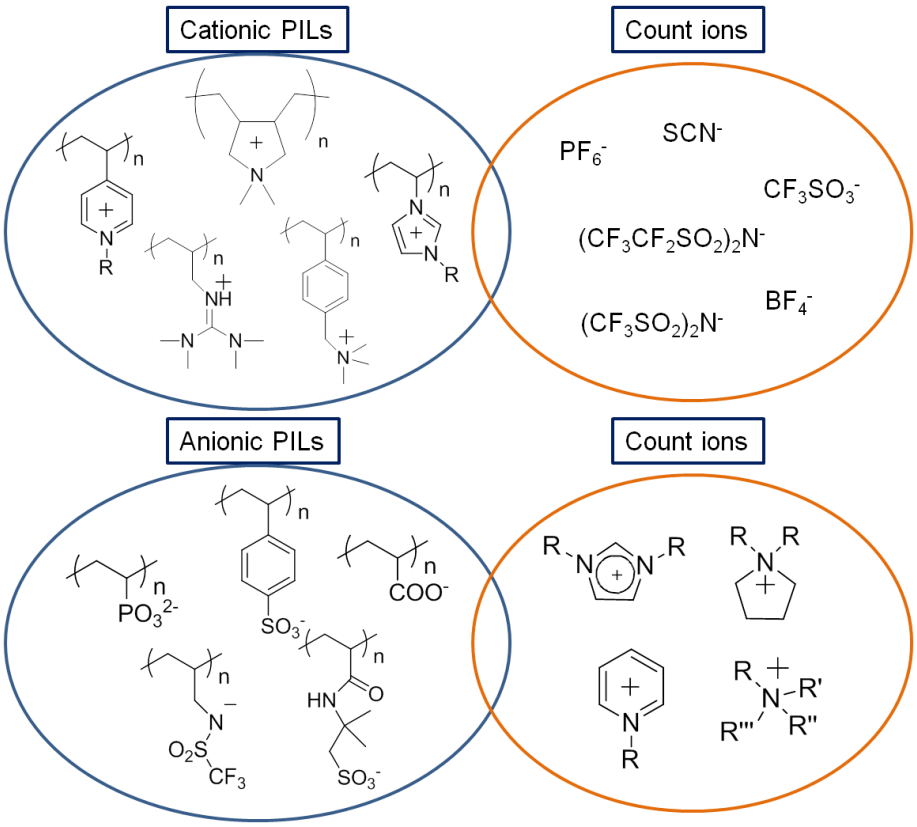

Figure 8.1. Representative chemical structures of polymeric ionic liquids (PILs).[4]

Recently, several research groups developed synthetic routes to SQ molecules with ionic liquid species (Figure **8.2**).[15-17] The authors argued that the rigid SQ cores can play a significant role in decreasing melting point of ILs and enhancement of thermal stability. In addition, introduction of SQs into ILs improve their conductivities. Indeed, Zhang et al. demonstrated the potential applicability of IL functionalized SQs for polymer electrolyte membrane fuel cells.[17] When these new SQs having IL groups are polymerized, the hybrid polymers could provide a new set of PLIs with improved thermal stability, mechanical strength and ionic conductivity.

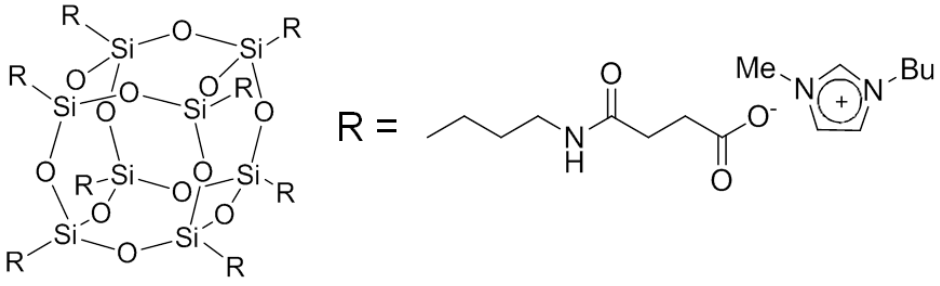

Figure 8.2. Example of SQ molecule with ionic liquid groups.[15]

References Cited:

1. Furgal, J. C.; Jung, J. H.; Laine, R. M.; Unpublished results.
2. Yamamoto, C.; Okamoto, Y.; "Optically Active Polymers for Chiral Separation," *Bull. Chem. Soc. Jpn*., **2004**, *77*, 227-257.
3. Subramanian, G.; "A Practical Approach to Chiral Separations by Liquid Chromatography," VCH, New York, **1994**.
4. Mecerreyes, D.; "Polymeric ionic liquids: Broadening the properties and applications of polyelectrolytes," *Prog. Polym. Sci*., **2011**, *36*, 1629-1648.
5. Yuan, J.; Mecerreyes, D.; Antonietti, M.; "Poly(ionic liquid)s: An update," *Prog. Polym. Sci*., **2013**, *38*, 1009-1036.
6. Tanaka, K.; Chujo, Y.; "Advanced functional materials based on polyhedral oligomeric silsesquioxane (POSS)," *J. Mater. Chem*., **2012**, *22*, 1733-1746.
7. Rogers, R. D.; Seddon, K. R.; Volkov, S.; Green industrial applications of ionic liquids. NATO Science Series II, New York, Springer-Verlag, **2003**, pp 545.
8. Vasile, I. P.; Hardacre, C.; "Catalysis in ionic liquids," *Chem. Rev*., **2007**, *107*, 2615-2665.
9. Yan, F.; Texter, J.; "Solvent-reversible poration in ionic liquid copolymers," *Angew. Chem. Int. Ed*., **2007**, *46*, 2440-2443.
10. Tang, J.; Tang, H.; Sun, W.; Plancher, H.; Radosz, M.; Shen, Y.; "Poly(ionic liquid)s: A new material with enhanced and fast CO2 absorption," *Chem. Commun*, **2005**, 3325-3327.
11. Wishart, J. F.; "Energy applications of ionic liquids," *Energy Environ. Sci*., **2009**, *2*, 956-961.
12. Lu, W.; Fadeev, G. A.; Qi, B.; Smela, E.; Mattes, B. R.; Ding, J.; Spinks, G. M.; Mazurkiewicz, J.; Zhou, D.; Wallace, G. C.; MacFarlane, D.; Forsyth, A. A.; Forsyth, M.; " Use of ionic liquids for p-conjugated polymer electrochemical devices," *Science*, **2002**, *297*, 983-987.
13. Marcilla, R.; Alcaide, F.; Sardon, H.; Pomposo, J. A.; Pozo-Gonzalo, C.; Mecerreyes, D.; "Tailor-made polymer electrolytes based upon ionic liquids and their application in all plastic electrochromic devices," *Electrochem. Commun*., **2006**, *8*, 482-488.
14. Kawano, R.; Katakabe, T.; Shimosawa, H.; Nazeeruddin, M. D.; Gratzel, M.; Matsui, H.; Kitamura, T.; Tanabe, N.; Watanabe, M.; "Solid-state dye-sensitized solar cells using

polymerized ionic liquid electrolyte with platinum-free counter electrode," *Phys. Chem. Chem. Phys*., **2010**, *12*, 1916-1921.

15. Tanaka, K.; Ishiguro, F.; Chujo, Y.; "POSS Ionic Liquid," *J. Am. Chem. Soc*., **2010**, *132*, 17649-17651.
16. Cardiano, P.; Lazzara, G.; Manickam, S.; Mineo, P.; Milioto, S.; Schiavo, S. L.; "POSS-Tetraalkylammonium Salts: A New Class of Ionic Liquids," *Eur. J. Inorg. Chem*., **2012**, 5668-5676.
17. Zhang, F.; Tu, Z.; Yu, J.; Li, H.; Huang, C.; Zhang, H.; "Impregnation of imidazole functionalized polyhedral oligomeric silsesquioxane in polymer electrolyte membrane for elevated temperature fuel cells," *RSC Adv*., **2013**, *3*, 5438-5446.

Appendix 1

Characterization Data of BoC polymers from I_8OPS

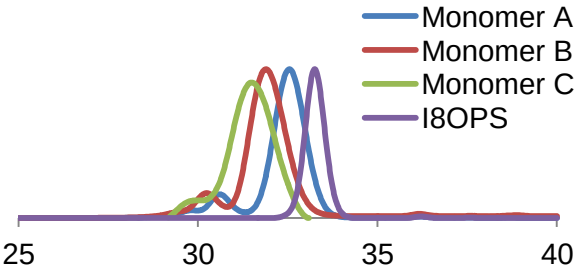

Figure A1.1. GPC traces of Monomer **A**-**C** and I_8OPS for comparison.

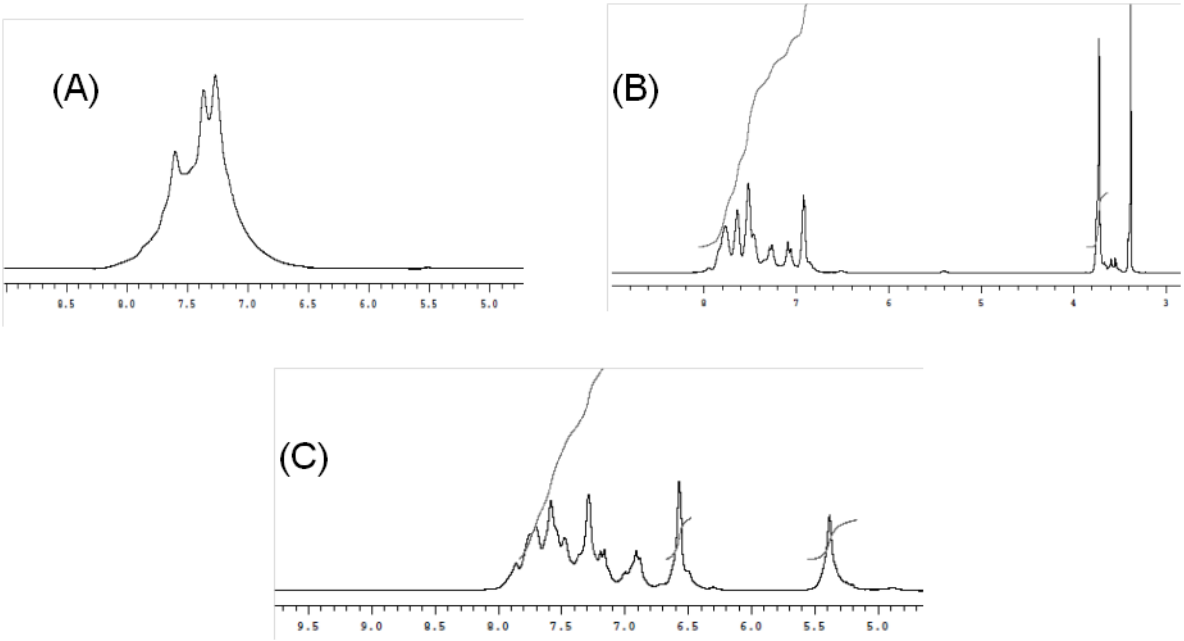

Figure A1.2. ^1H data for monomer **A**-**C**.

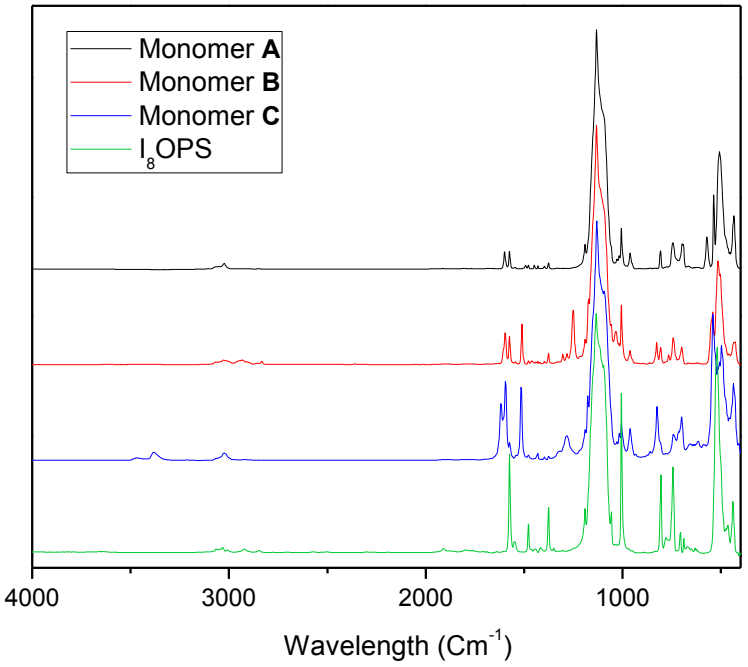

Figure A1.3. FTIR data for monomer **A**-**C** and I_8OPS for comparison.

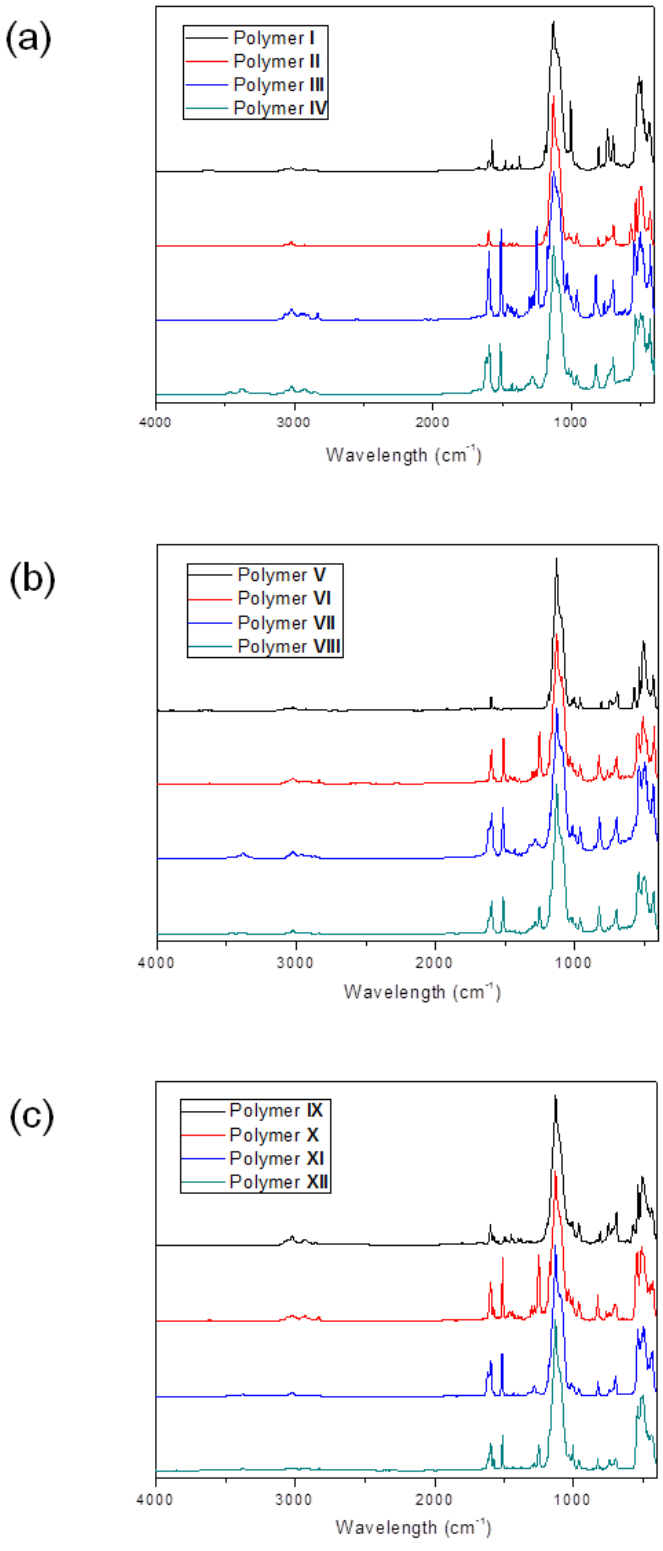

Figure A1.4. FTIR data for (a) polymers **I-IV** (b) polymers **V-VIII** and (c) polymers **IX-XII**.

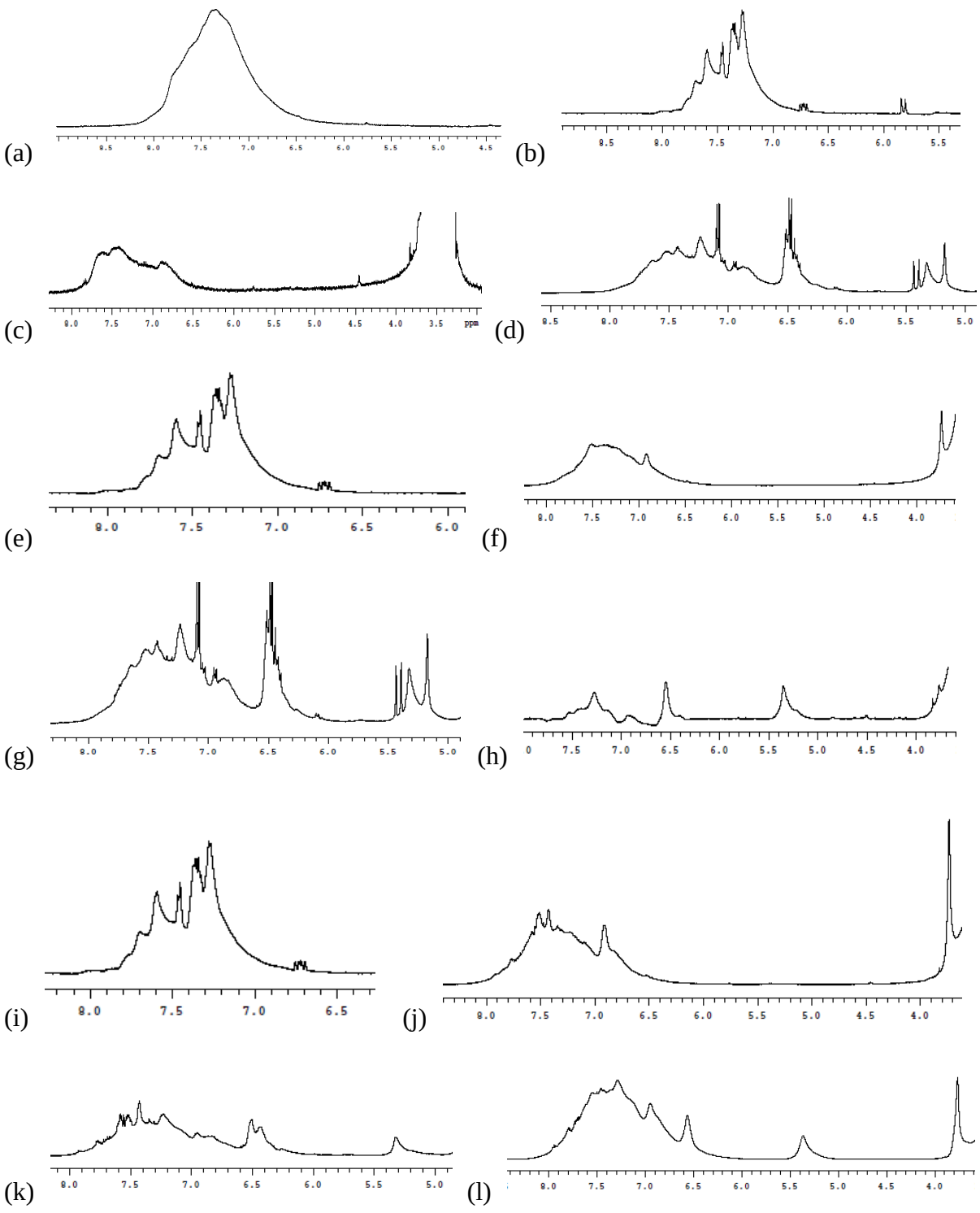

Figure A1.5. ^{1}H-NMR of (a) polymer **I**, (b) polymer **II**, (c) polymer **III**, (d) polymer **IV**, (e) polymer **V**, (f) polymer **VI**, (g) polymer **VII**, (h) polymer **VIII**, (i) polymer **IX**, (j) polymer **X**, (k) polymer **XI** and (l) polymer **XII**.

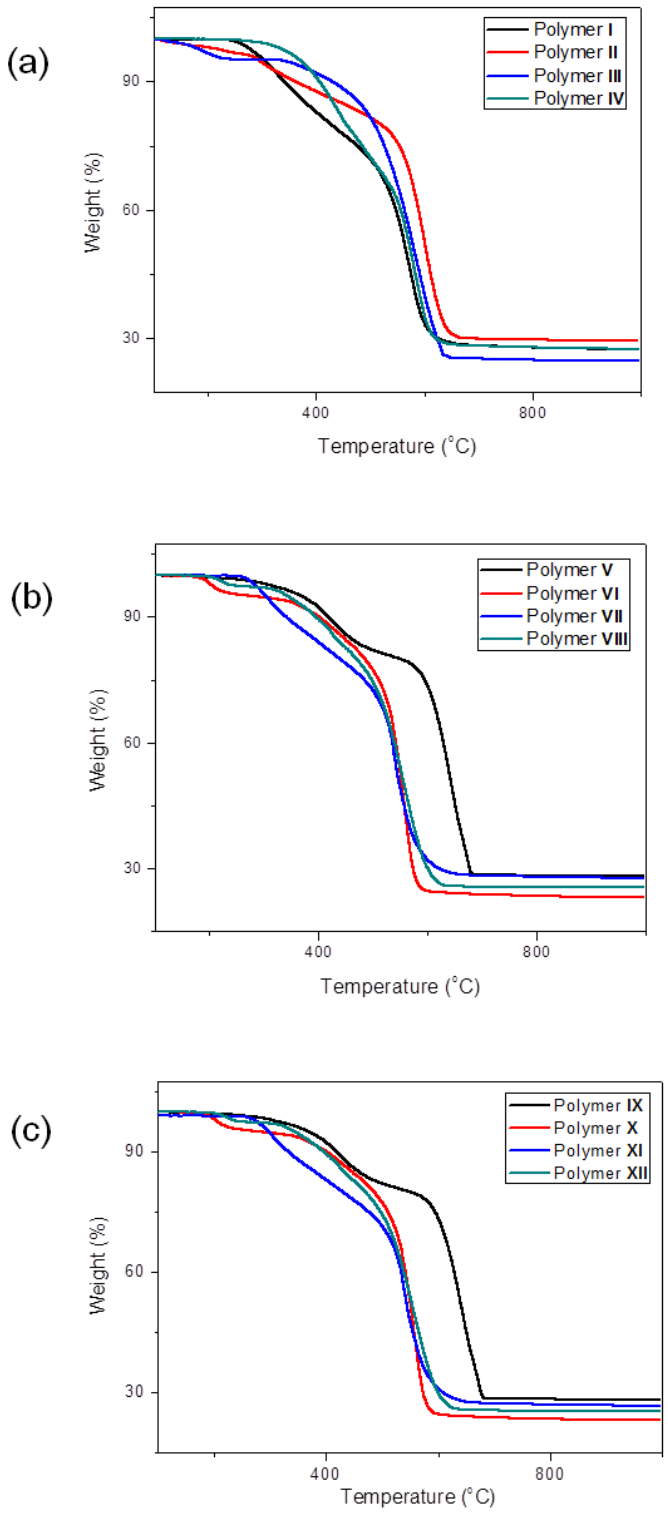

Figure A1.6. TGA for (a) polymers **I-IV** (b) polymers **V-VIII** and (c) polymers **IX-XII** in air (10℃/min).

Appendix 2

Characterization Data of second generation (GEN2) derivatives by functionalization of vinyl $T_{10/12}$ silsesquioxanes

Table A2.1. Characteristic FTIR bands for GEN 1 compounds.

R group	Functional group	Wavenumber (cm^{-1})
Ph	νC-H, νC=C, aromatic νSi-O-Si	3022 1605, 1494 1111
NP	νC-H, νC=C, aromatic νSi-O-Si	3054 1606 1117
MePh	νC-H, aliphatic νC=C, aromatic νSi-O-Si	2997 1609, 1510 1120
MeOPh	νC-H, aliphatic νC=C, aromatic νC-O νSi-O-Si	2999 1605, 1510 1254 1116
CH_2ClPh	νC-H, aliphatic νC=C, aromatic C-H wag (CH_2X) νSi-O-Si	3002 1605, 1510 1266 1117
BrPh	νC=C, aromatic νSi-O-Si	1605, 1485 1120
BiPh	νC-H, νC=C, aromatic νSi-O-Si	3027 1603, 1486 1120

Table A2.2. Characteristic FTIR absorption bands for GEN 2 compounds.

R' group	Functional group	Wavenumber (cm^{-1})
H	νC-H, νC=C, aromatic νSi-O-Si	3024 1601, 1509 1116
Me	νC-H, νC=C, aromatic νC=C, Si-O-Si	3022 1598, 1514 1117
MeO	νC-H, aromatic νC-H, aliphatic νC=C, aromatic νC-O νSi-O-Si	3022 2833 1597, 1513 1251 1110
NH_2	νN-H νC-H, νC=C,aromatic νSi-O-Si	3378 3023 1595, 1516 1111
5F	νC-H, νC=C, aromatic νSi-O-Si νC-F	3025 1521, 1495 1123 1006, 962

Table A2.3. T_m for GEN1 compounds.

R group	DSC	Optical microscopy
Ph (S-Heck)	100 ^oC	100-120^oC
Ph (D-Heck)	100^oC	100-130^oC
Ph (Metathesis)	100^oC	100-120^oC
NP (S-Heck)	130^oC	130-160^oC
NP (D-Heck)	130^oC	130-160^oC
NP (Metathesis)	130^oC	130-160^oC
CH_2ClPh (Metathesis)	150^oC	150-170^oC

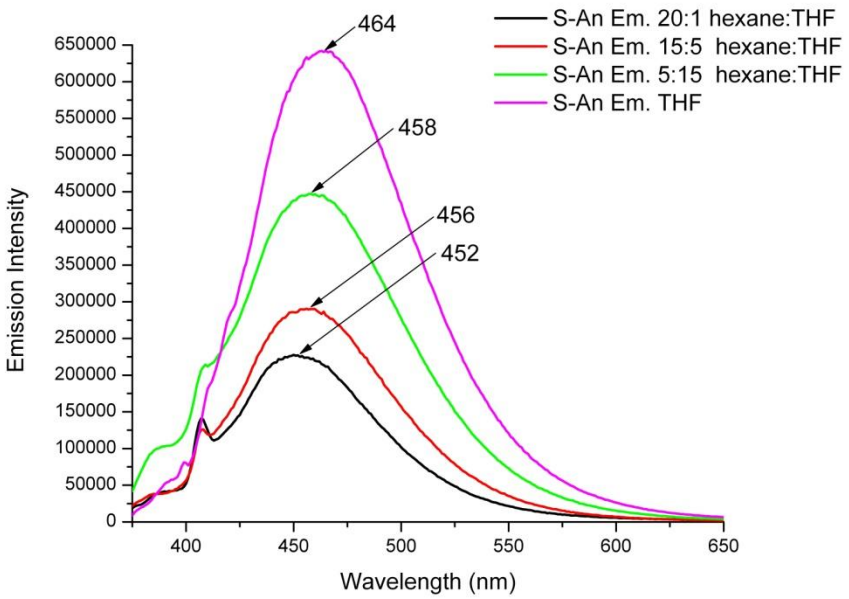

Figure A1.1. Emission spectra of S-anthracene hexane:THF ratio study at constant concentration.

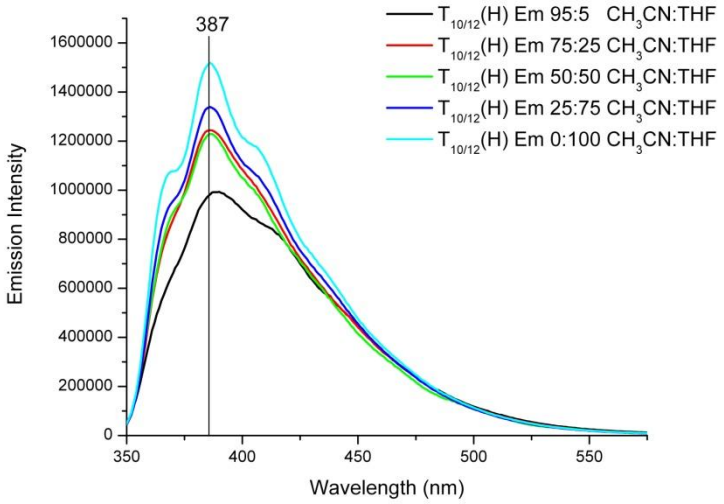

Figure A2.2. Emission spectra of $T_{10/12}$ R = H acetonitrile:THF at 0.86 μM.

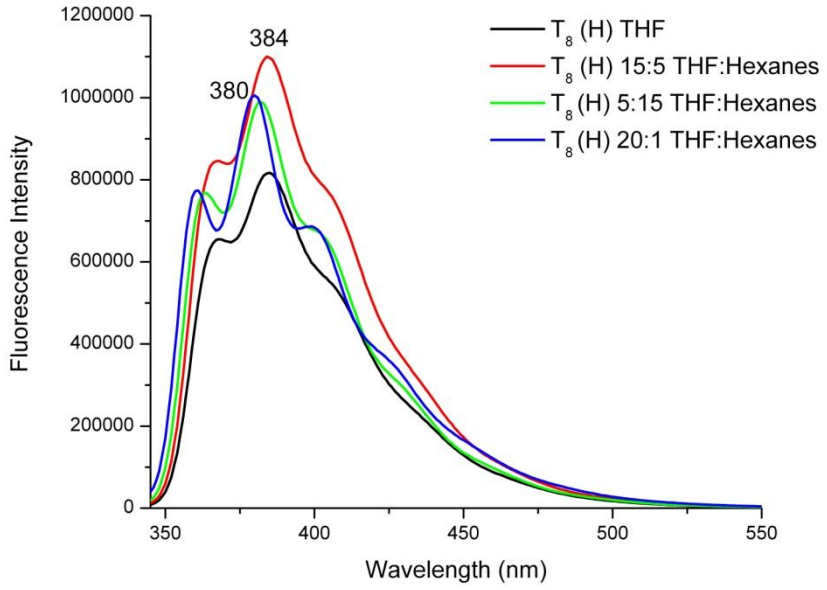

Figure A2.3. Emission spectra of T_8 (H) in hexane:THF at 0.55 μM.

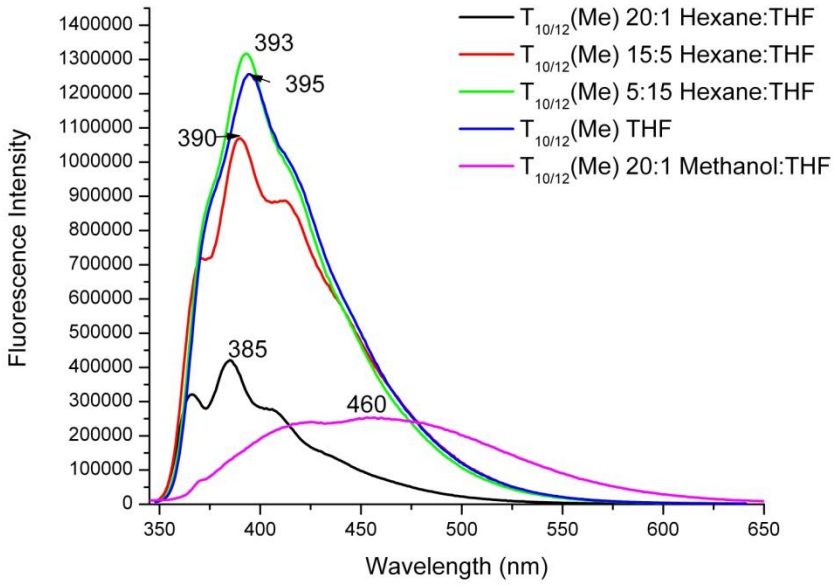

Figure A2.4. Emission spectra of $T_{10/12}$ (Me) in hexane:THF at 0.51 μM.

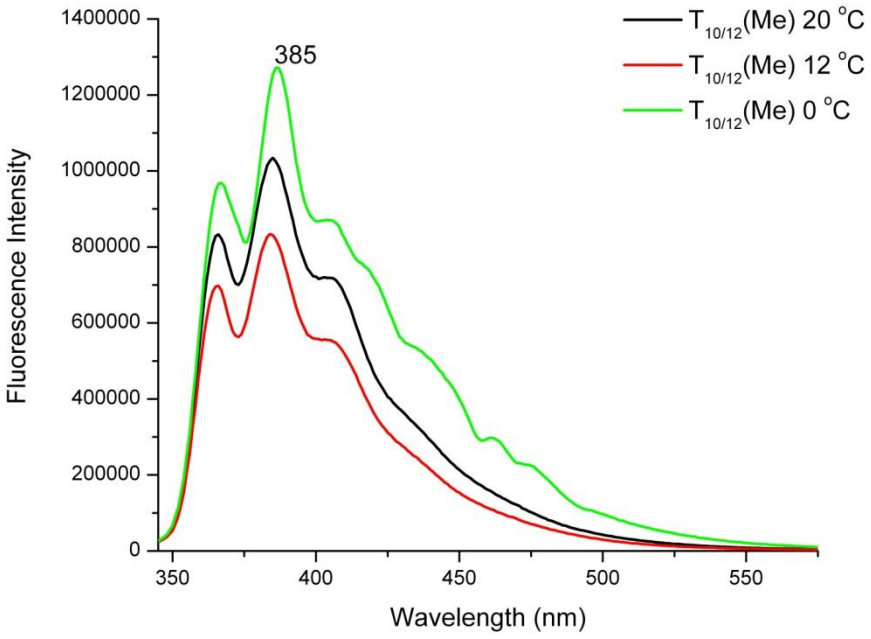

Figure A2.5. Emission spectra of $T_{10/12}$ (Me) in 20:1 hexane:THF at 0.43 μM and selected temperatures.

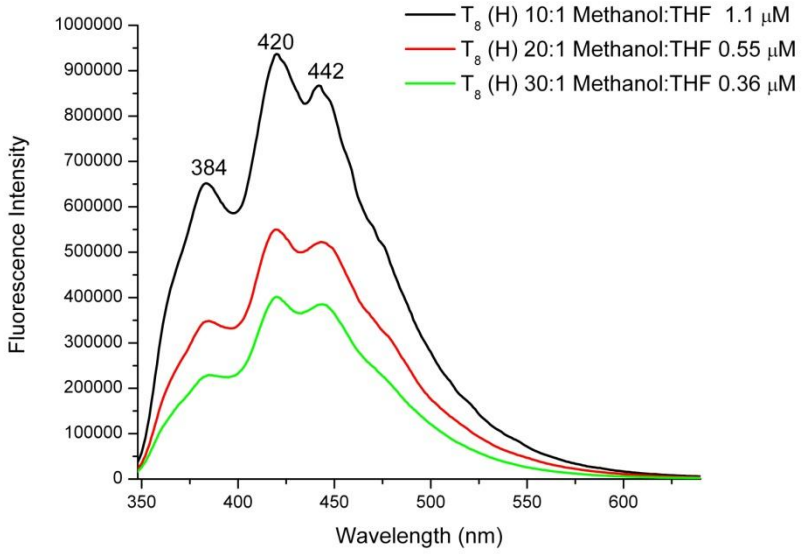

Figure A2.6. Emission spectra of T_8 (H) in MeOH at various concentrations, showing aggregate formation.
[Note that this spectrum is the same as that obtained for $T_{10/12}$ (H) in acetonitrile].

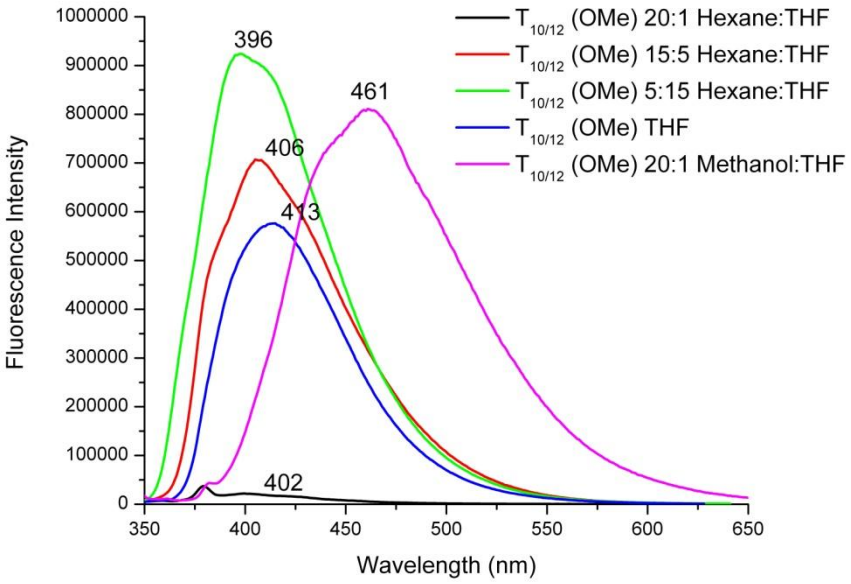

Figure A2.7. Emission spectra of $T_{10/12}$ (OMe) in THF and hexanes at 0.43 μM.

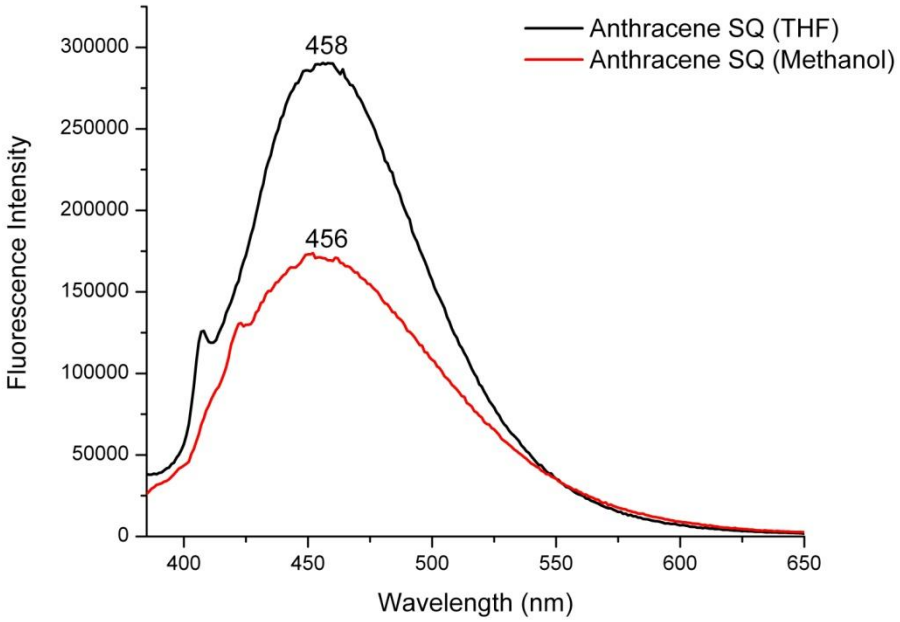

Figure A2.8. Emission spectra of $T_{10/12}$ (S-An) in THF and methanol at 1.0 μM.

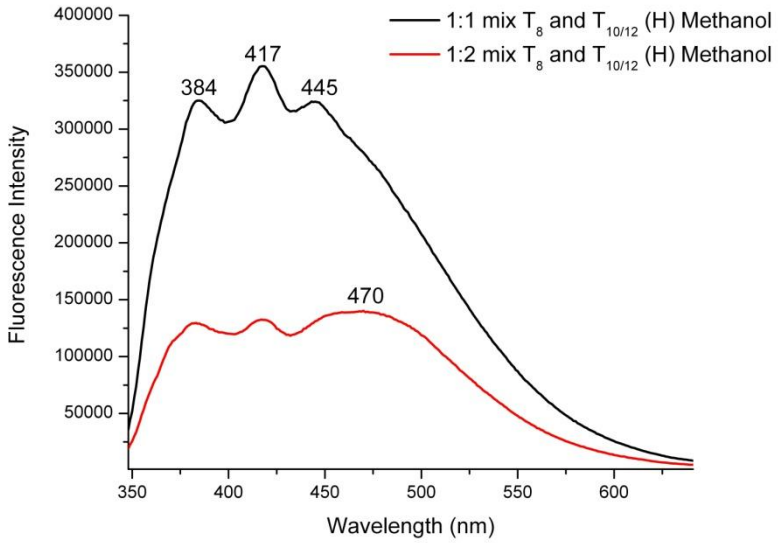

Figure A2.9. Emission spectra of mixed $T_{10/12}$ and T_8 (H) at 10:1 of methanol:THF at 1:1 and 2:1 ratios.

Table A2.4. Molar extinction coefficients per mol of GEN1 and GEN2 compounds.*

	Molar Extinction (ε $M^{-1}cm^{-1}$)
$T_{10/12}$ S-Ph	$1.09x10^5$
$T_{10/12}$ S-Ph	$8.51x10^4$
$T_{10/12}$ S-NP	$1.01x10^4$
$T_{10/12}$ S-NP	$9.62x10^4$
$T_{10/12}$ S-An	$4.20x10^4$
$T_{10/12}$ S-An	$4.81x10^4$
$T_{10/12}$ H	$3.94x10^5$
$T_{10/12}$ Me	$3.77\ x10^5$
$T_{10/12}$ OMe	$4.01\ x10^5$
$T_{10/12}$ NH_2	$4.00\ x10^5$
$T_{10/12}$ C_6F_5	$4.84\ x10^5$
$T_8C_6F_5$	$2.44\ x10^5$

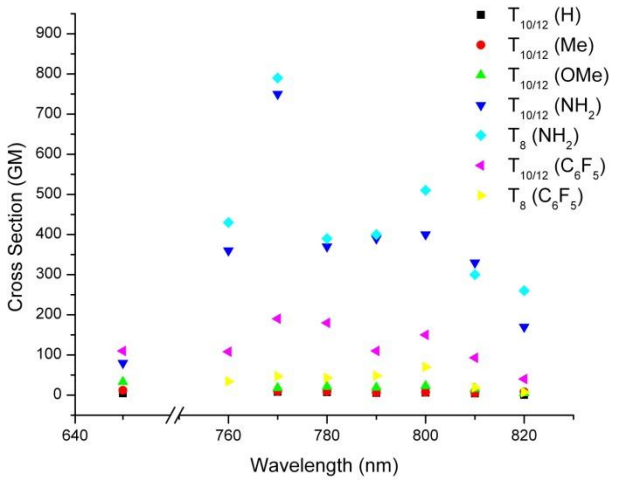

Figure A2.10. Full cage two-photon absorption cross-sections for Gen II compounds. **Note amount of T_{10} and T_{12} cage determined by MALDI to be a 10 to 7 ratio respectively, which was used in calculations for photophysical characterization.*

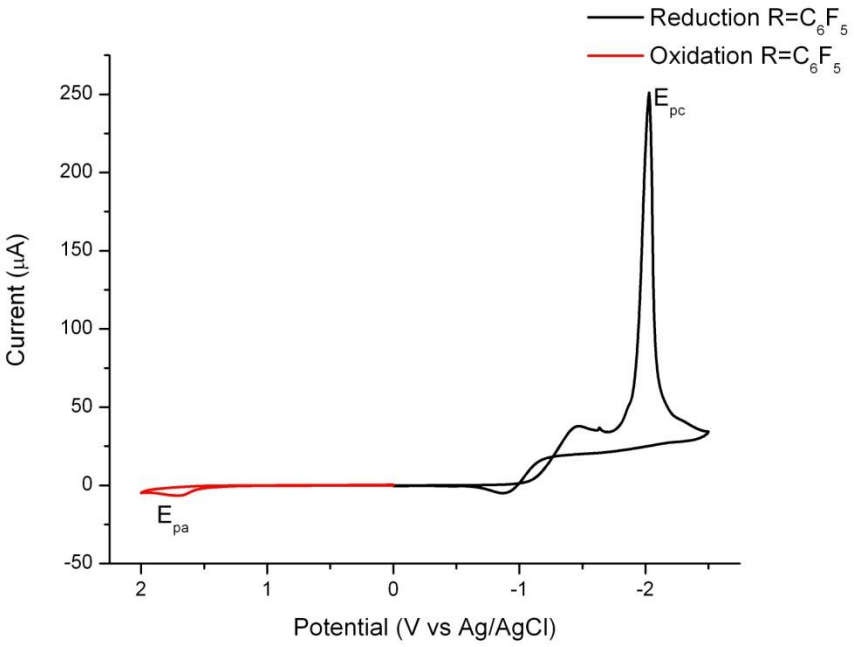

Figure A2.11. Cyclic voltammetry plot for pentafluorophenyl GEN2.

Appendix 3

Characterization Data of hydroxyl terminated silsesquioxanes and their use for cross-linked polyesters

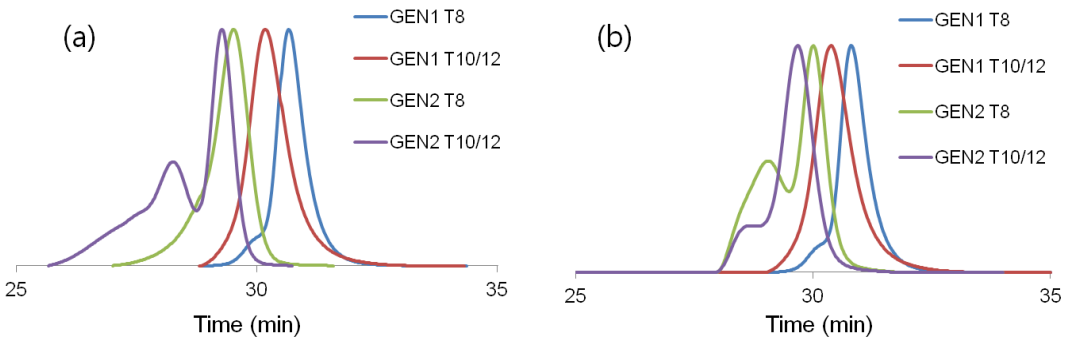

Figure A3.1. GPC data for (a) GEN1/ GEN2 T_8 and $T_{10/12}$ *p*-acetoxy SQs (b) GEN1/ GEN2 T_8 and $T_{10/12}$ *p*-hydroxy SQs.

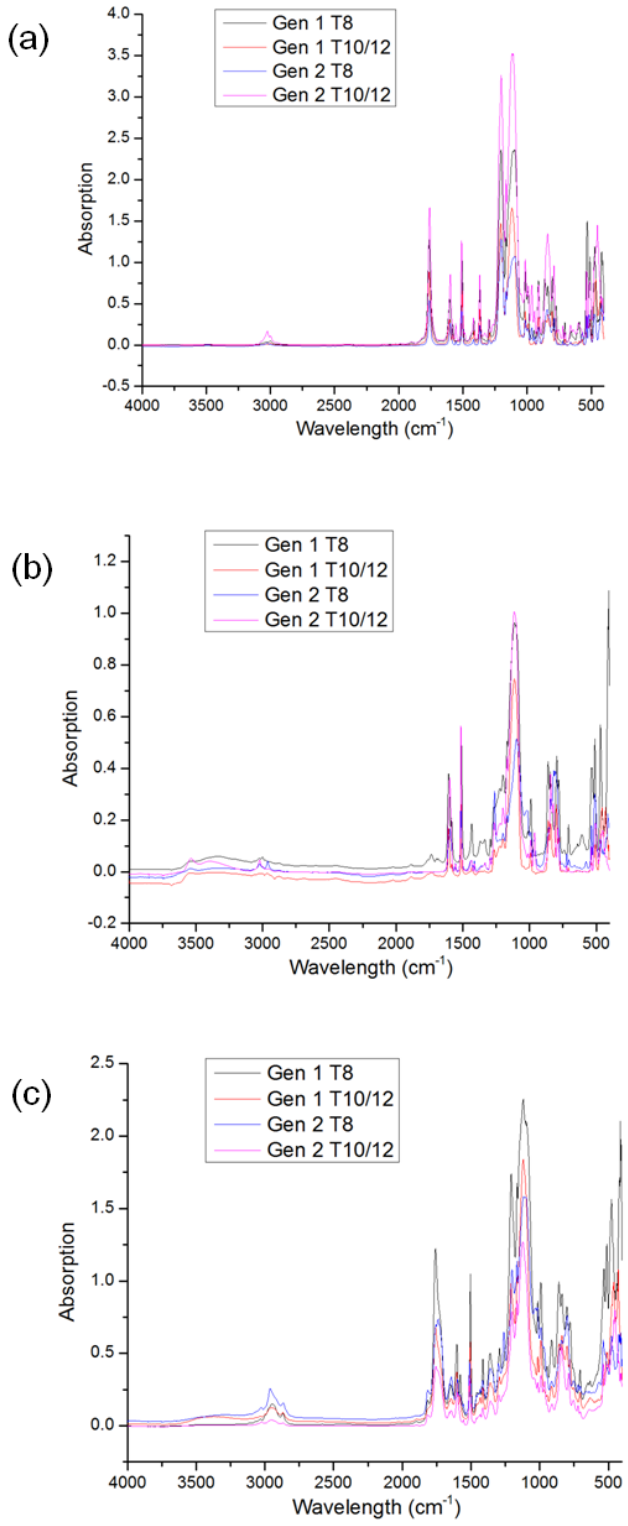

Figure A3.2. FTIR data for the (a) acetoxy, (b) hydroxyl, and (c) polymeric SQs. Note that all the spectra overlap uniformly as expected for the essentially identical chemical and structural compositions.

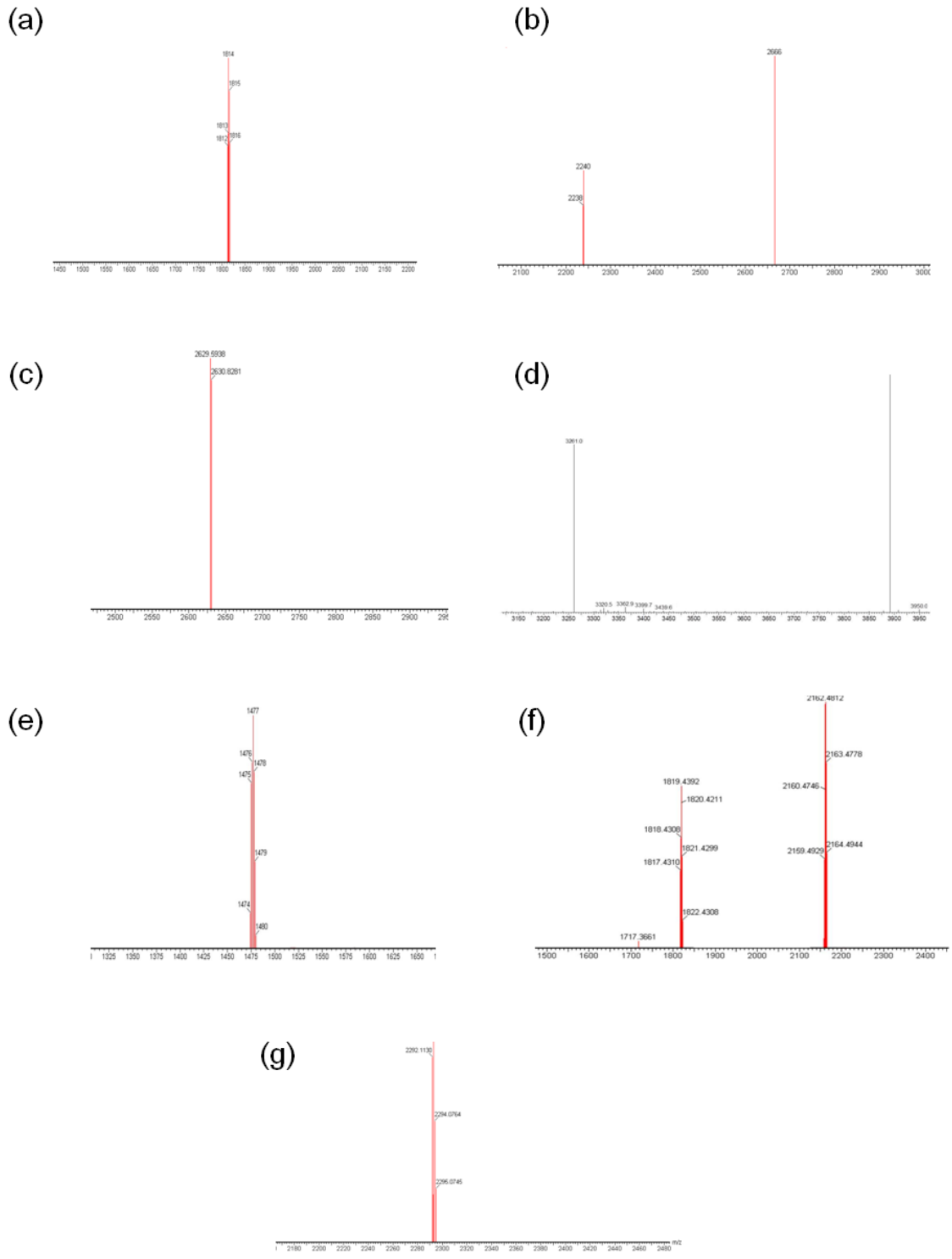

Figure A3.3. MALDI-ToF data for the (a) GEN1 Acetoxy T_8 SQ, (b) GEN1 Acetoxy $T_{10/12}$ SQ, (c) GEN2 Acetoxy T_8 SQ, (d) GEN2 Acetoxy$T_{10/12}$ SQ, (e) GEN1 Hydroxy T_8 SQ, (f) GEN1 Hydroxy $T_{10/12}$ SQ, and (g) GEN2 Hydroxy T_8 SQ.

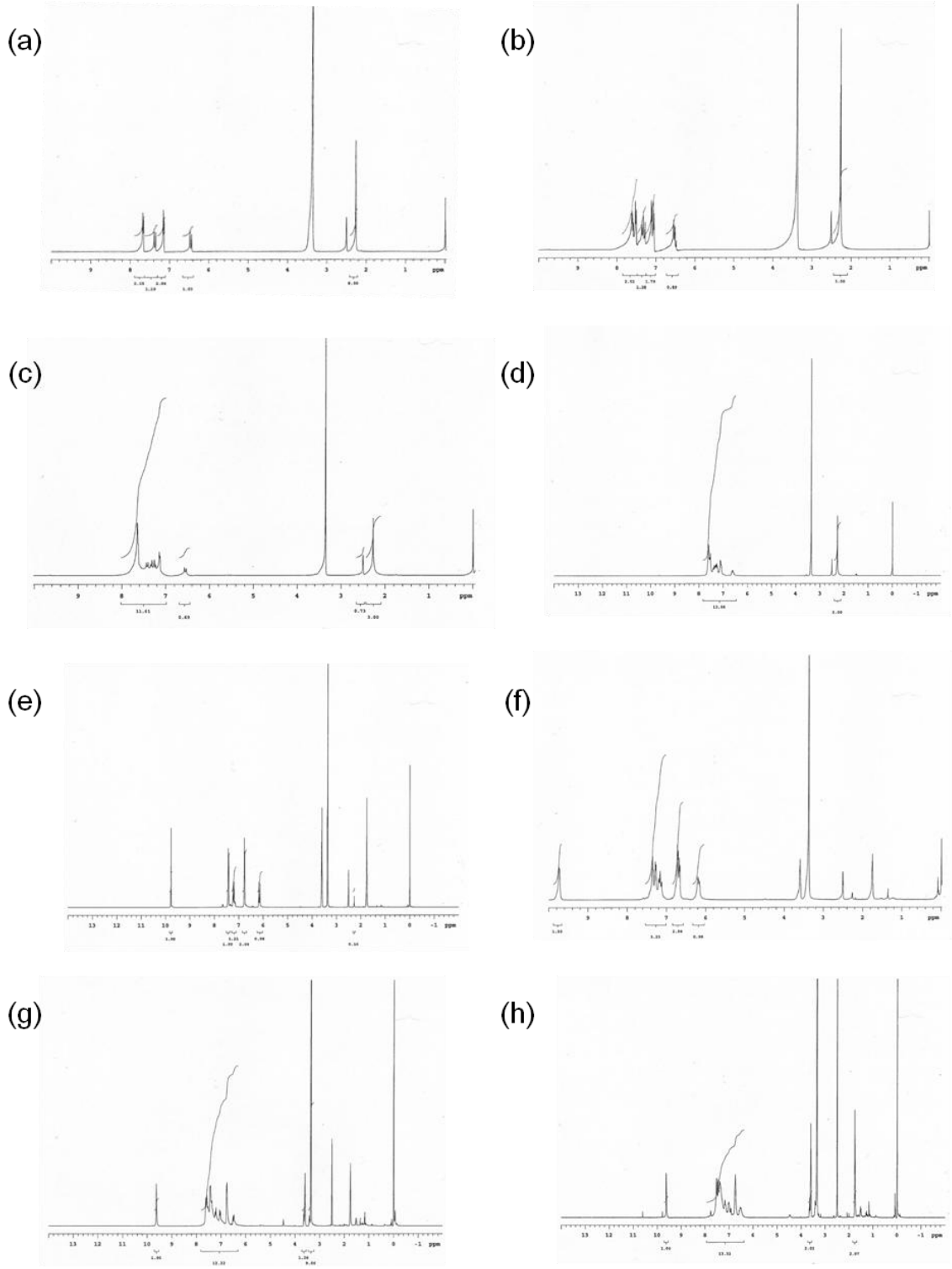

Figure A3.4. ^{1}H data for the (a) GEN1 Acetoxy T_8 SQ, (b) GEN1 Acetoxy $T_{10/12}$ SQ, (c) GEN2 Acetoxy T_8 SQ, (d) GEN2 Acetoxy$T_{10/12}$ SQ, (e) GEN1 Hydroxy T_8 SQ, (f) GEN1 Hydroxy $T_{10/12}$ SQ, (g) GEN2 Hydroxy T_8 SQ (h) GEN2 Hydroxy $T_{10/12}$ SQ.

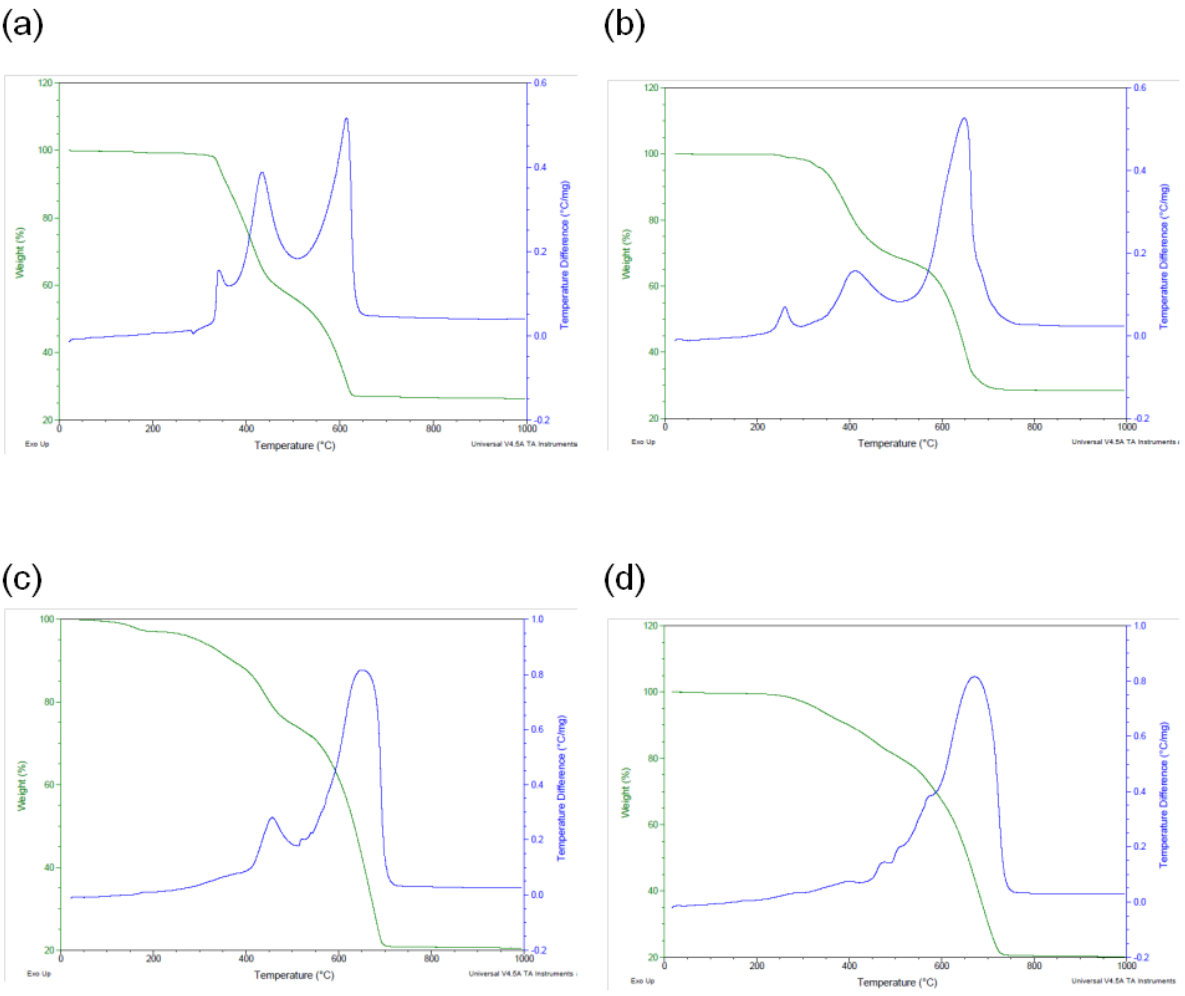

Figure A3.5. TGA for the Acetoxy SQs.
(a) GEN1 Acetoxy T_8 SQ, (b) GEN1 Acetoxy $T_{10/12}$ SQ,
(c) GEN2 Acetoxy T_8 SQ, (d) GEN2 Acetoxy $T_{10/12}$ SQ.

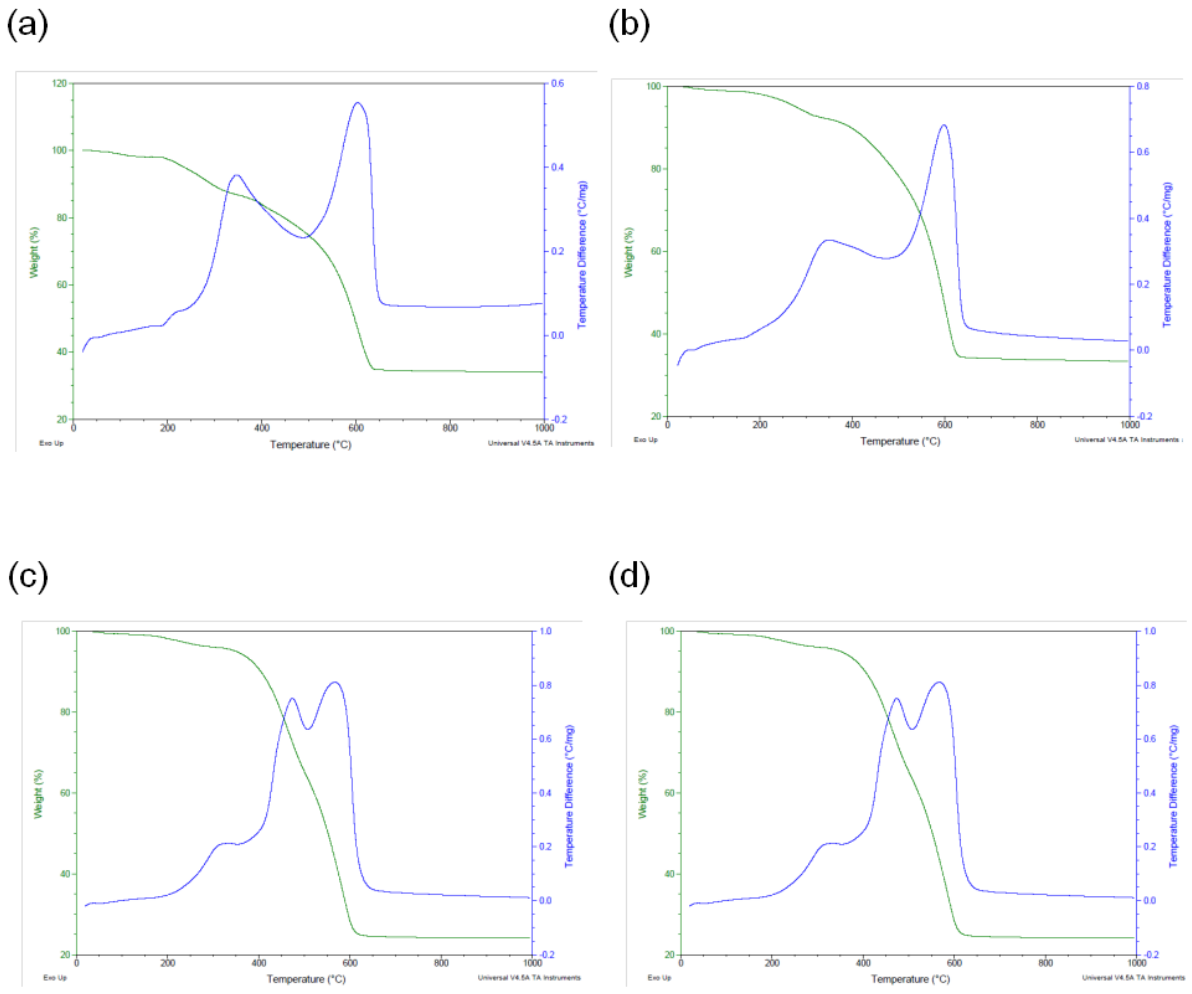

Figure A3.6. TGA for the Hydroxy SQs.
(a) GEN1 Hydroxy T_8 SQ, (b) GEN1 Hydroxy $T_{10/12}$ SQ,
(c) GEN2 Hydroxy T_8 SQ, (d) GEN2 Hydroxy $T_{10/12}$ SQ.

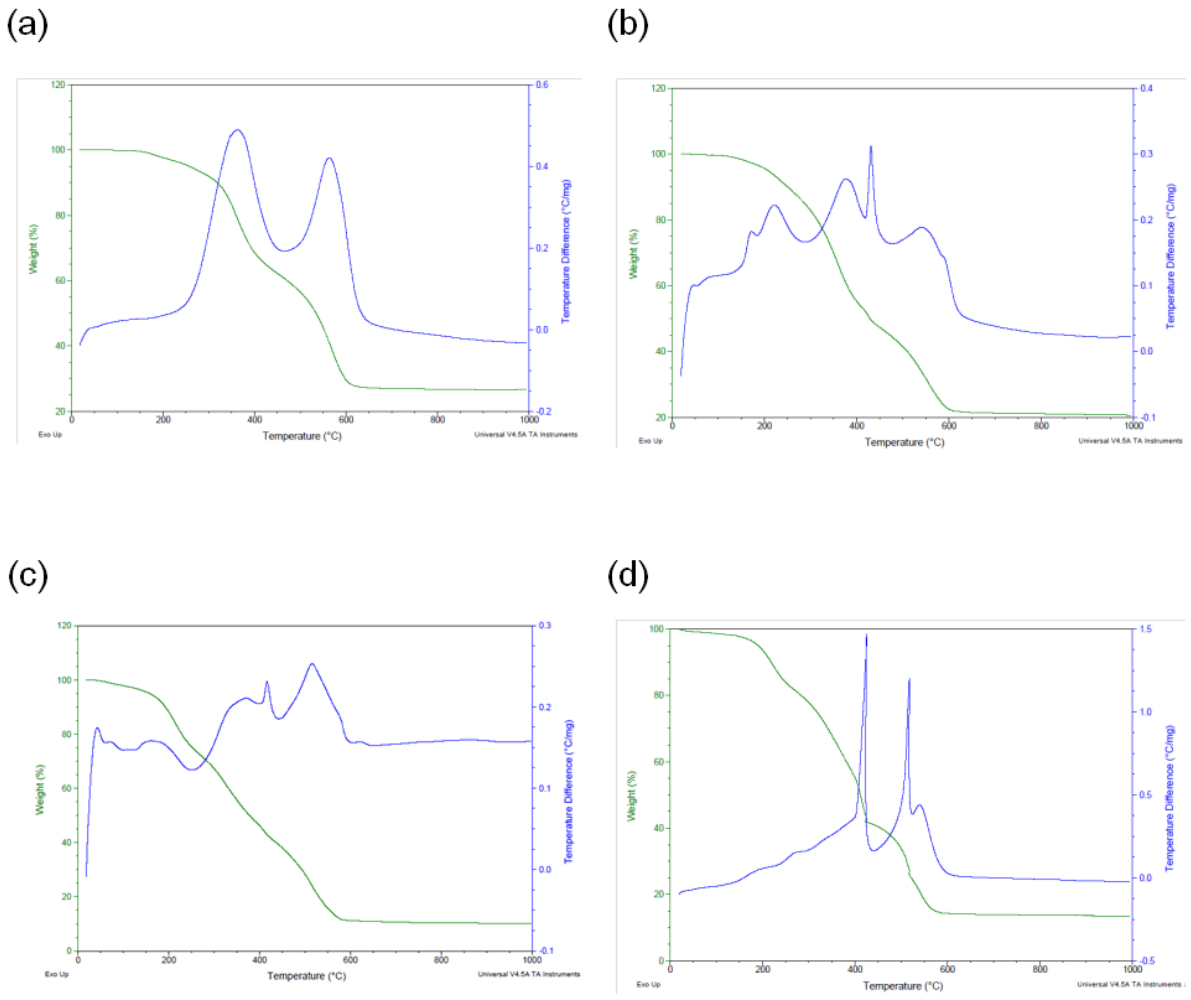

Figure A3.7. TGA for the Polyesters.
(a) Polyester from GEN1 T_8 SQ, (b) Polyester from GEN1 $T_{10/12}$ SQ,
(c) Polyester from GEN2 T_8 SQ, (d) Polyester from GEN2 $T_{10/12}$ SQ.